UNIVERSITÀ
DI PAVIA

Dipartimento di Biologia e Biotecnologie "L. Spallanzani"

Innovative strategies to fight bacterial infections in cystic fibrosis: exploring dispirotripiperazines and bacteriophages as alternative therapeutic options

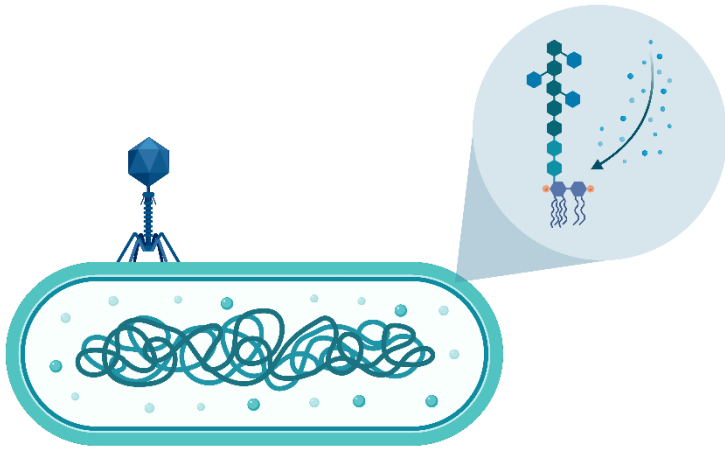

Andrea Bonacorsi

Dottorato di Ricerca in
Genetica, Biologia Molecolare e Cellulare
Ciclo XXXVI – A.A. 2020-2023

UNIVERSITÀ
DI PAVIA

Dipartimento di Biologia e Biotecnologie "L. Spallanzani"

Innovative strategies to fight bacterial infections in cystic fibrosis: exploring dispirotripiperazines and bacteriophages as alternative therapeutic options

Andrea Bonacorsi

Supervised by Prof. Silvia Buroni and Prof. Maria Rosalia Pasca

Dottorato di Ricerca in
Genetica, Biologia Molecolare e Cellulare
Ciclo XXXVI – A.A. 2020-2023

Cover image created with BioRender.com

Table of contents

Abstract

Although quality of life and survival of patients with cystic fibrosis (CF) has been continuously improving, respiratory failure due to pulmonary infections remains the primary cause of mortality in these individuals. *Pseudomonas aeruginosa*, *Burkholderia cenocepacia* and *Staphylococcus aureus* continue to pose significant treatment challenges due to their high levels of antibiotic resistance. Given the lack in antibiotic development, there is an urgent need for alternative therapeutic strategies.

In the first part of this work, the dispirotripiperazine derivative PDSTP, previously investigated as antiviral since it impairs viral adsorption to human cells, was repurposed for the treatment of bacterial infections. Specifically, this compound was characterized for its activity against the adhesion of the CF bacteria to epithelial cells, resulting effective in inhibiting their interaction with human cells. Furthermore, antibiotic adjuvant and biofilm inhibitory potential properties of PDSTP were investigated on *P. aeruginosa* after demonstrating that the compound interacts with the lipopolysaccharide of this bacterium.

In the second part of this study, two siphoviral and one myoviral *P. aeruginosa* bacteriophages were characterized for therapeutic purposes. Genomic analysis of the myoviral phage confirmed its suitability for clinical applications. All the three phages demonstrated stability, a broad host-range and effective bacterial killing. Moreover, phage-resistant *P. aeruginosa* mutants were selected and characterized, suggesting potentially beneficial traits for the treatment of *P. aeruginosa* infections.

Abbreviations

BIM	Bacteriophage-insensitive mutant
CAMHB	Cation-adjusted Mueller-Hinton broth
CCCP	Carbonyl cyanide m-chlorophenylhydrazone
CF	Cystic fibrosis
CFTR	Cystic fibrosis transmembrane conductance regulator
CLSM	Confocal laser scanning microscopy
DiSC(5)	3,3'-Dipropylthiadicarbocyanine iodide
DMEM	Dulbecco's modified Eagle's medium
DPX	Dansyl-polymyxin
EVPL	*Ex vivo* pig lung
HSGAG	Heparan-sulphate glycosaminoglycan
LB	Luria-Bertani broth
LPS	Lipopolysaccharide
MEM	Minimal essential medium
MIC	Minimum inhibitory concentration
MOI	Multiplicity of infection
NPN	N-phenyl-1-naphthylamine
TSB	Tryptic soy broth

1. Introduction

1.1. Cystic fibrosis

Cystic fibrosis (CF) is one of the most common human inherited diseases, affecting a significant number of individuals across the globe. Currently, there are over 100,000 patients worldwide, of which approximately 48,000 in Europe (European Cystic Fibrosis Society, 2022) and 40,000 in the United States (Cystic Fibrosis Foundation, 2022). The incidence of this condition varies depending on the country and ethnic group, with a prevalence of one in 3,000 - 6,000 live births in the Caucasian population (Scotet *et al*., 2020).

CF is an autosomal monogenic disease that is transmitted in a recessive manner and exhibits complete penetrance. The clinical phenotype of this condition is complex and typically characterized by chronic lung infections and inflammation, pancreatic exocrine insufficiency and male infertility (Figure 1.1). These symptoms arise due to the formation of a thick layer of sticky mucus at the epithelial level which impairs the physiological functioning of the affected organs (Shteinberg *et al*., 2021).

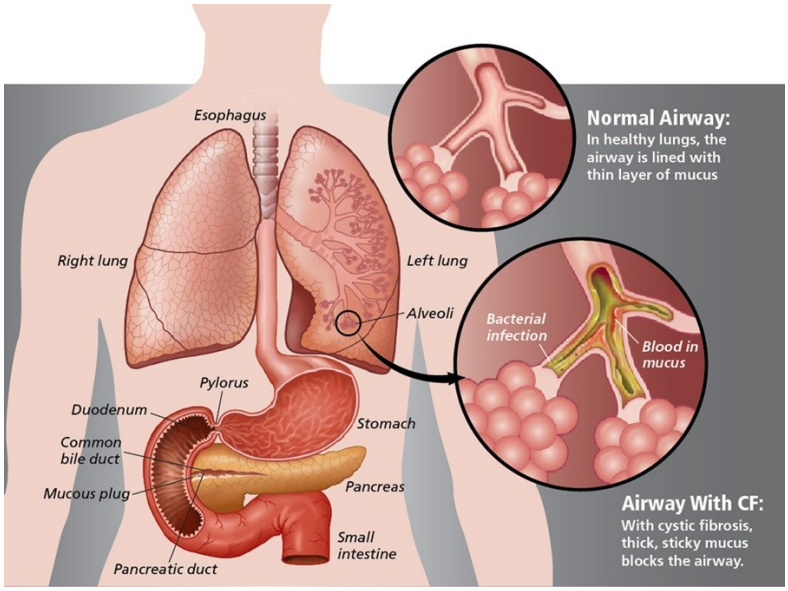

Figure 1.1. Clinical phenotype of CF at the respiratory and gastrointestinal levels. In healthy individuals, the airways are lined with a thin layer of mucus. In CF patients, instead, the airways are obstructed by a thick layer of sticky mucus, leading to chronic pulmonary infections and inflammation. Additionally, abnormal mucus develops in the pancreatic duct, hindering the delivery of digestive enzymes to the duodenum. In certain cases, CF can also result in the obstruction of the common bile duct (Jay Smith, 2023).

1.1.1. CF molecular origin

The molecular origin of CF involves the *Cystic Fibrosis Transmembrane conductance Regulator* (*CFTR*) gene, located on the long arm of chromosome 7 (7q31.2) and consisting of 189.36 kb divided into 27 exons. *CFTR* encodes a chloride and bicarbonate channel of 1480 amino acids which belongs to the ATP-binding cassette transporter family. This channel is expressed at the apical membrane of secretory epithelial cells and plays a crucial role in maintaining a thin mucus layer above the epithelia. Mutations in *CFTR* impair the function of the channel, resulting in the formation of the aforementioned thick, sticky mucus layer (Kerem *et al*., 1989; Shteinberg *et al*., 2021).

CF is a multi-allelic disease, with over 2,000 variants identified to date. Among these, more than 700 variants are recognized as disease-causing according to the CFTR2 database (www.cftr2.org). Pathogenic mutations can be classified into six classes (I to VI), each characterized by a specific defect (Figure 1.2). Class I mutations result in the production of truncated CFTR due to premature stop codons. Class II mutations lead to misfolded CFTR, preventing its proper trafficking to the apical membrane. Class III mutations cause CFTR to be unresponsive to chemical signalling, resulting in its failure to open. Class IV mutations reduce the anion conductance of CFTR. Class V mutations decrease the amount of CFTR due to promoter or splicing defects. Class VI mutations lead to unstable CFTR with a short half-life. Intuitively, different mutations are associated with variations in disease severity (Rowe *et al*., 2005).

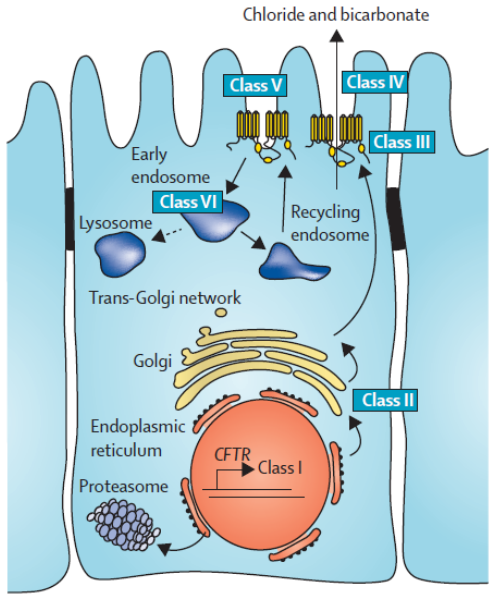

Figure 1.2. Classification of CF mutations. Class I, defects in CFTR synthesis. Class II, defects in CFTR maturation. Class III, defects in CFTR gating. Class IV, defects in CFTR conductance. Class V, reduced amount of CFTR. Class VI, reduced CFTR stability (Shteinberg *et al*., 2021).

Although there are more than 700 known disease-causing variants in *CFTR,* most of CF patients are homozygous or heterozygous for the deletion of the phenylalanine at position 508 (Phe508del mutation). This specific mutation is present in approximately 85.5% of individuals with CF in the USA (Cystic Fibrosis Foundation, 2022) and 80.7% of individuals with CF in Europe (European Cystic Fibrosis Society, 2022). The Phe508del mutation leads to the misfolding of CFTR, resulting in its premature degradation within the endoplasmic reticulum. As a consequence, this mutation is classified as a class II mutation (Cheng *et al*., 1990).

1.1.2. CF clinical management

While a cure for CF is currently unavailable, significant progresses have been made in the clinical management of CF patients. Antibiotic therapy and DNase treatment are effective in addressing lung infections, while mucus airway clearance techniques are essential for improving lung function. In addition, pancreatic enzyme supplementation is provided to ensure a proper digestion. These interventions have collectively contributed to significant improvements in the quality of life for CF patients, ultimately extending their life expectancy (Shteinberg *et al*., 2021). Indeed, individuals with CF can live beyond 50 years of age nowadays (Cystic Fibrosis Foundation, 2022; European Cystic Fibrosis Society, 2022). This is particularly remarkable since CF was a fatal disease in early childhood during 1935, when the disease was firstly described. Furthermore, the introduction of small-molecule CFTR modulators has revolutionized the treatment of these patients by correcting structural and functional abnormalities of specific mutated CFTR proteins, resulting in improved pulmonary function and reduced rates of exacerbation. As a result, the health of CF patients is further improved (Jia and Taylor-Cousar, 2023). Noteworthy, a significant milestone in improving CFTR activity for CF patients with one or two Phe508del mutations was the introduction of a combination therapy consisting of elexacaftor and tezacaftor, which are correctors that increase CFTR concentration at the cell surface, along with ivacaftor, a potentiator that promotes CFTR opening (Taylor-Cousar *et al*., 2019).

1.1.3. CF airway pathophysiology

At the airway level, CFTR is involved in the hydration of the airway surface liquid (ASL) which is a thin layer of fluid that covers the surface of the airway epithelium. The ASL is essential for proper ciliary function and antimicrobial activity. In individuals with dysfunctional CFTR, chloride transport is impaired, leading to increased absorption of sodium ions by epithelial cells. Consequently, water is absorbed from the epithelium, causing dehydration of the ASL and the accumulation of sticky mucus.

This abnormal mucus hinders mucociliary clearance which is the primary defence mechanism of the airways, involved in the removal of inhaled particles and pathogens trapped in the mucus through ciliary beating. As a result, impaired clearance promotes the establishment of chronic bacterial infections, leading to sustained inflammation in the airways (Figure 1.3). Over time, this chronic inflammation progressively damages the lungs and eventually results in respiratory failure (Randell and Boucher, 2006). This is particularly relevant as respiratory failure is the leading cause of mortality in CF patients, responsible for 56.8% of CF-related deaths in Europe (European Cystic Fibrosis Society, 2022) and 44.4% of CF-related deaths in the United States (Cystic Fibrosis Foundation, 2022).

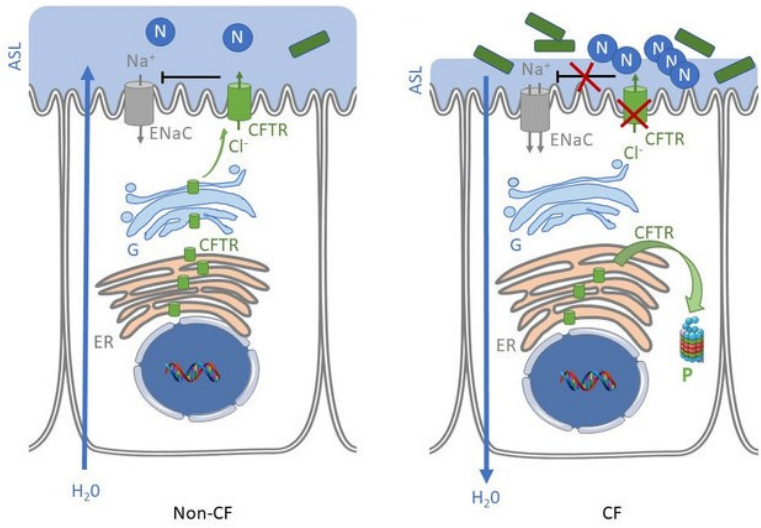

Figure 1.3. Non-CF and CF airway epithelial cells. In non-pathological conditions (non-CF, on the left), CFTR reaches the surface of airway epithelial cells (ER: endoplasmic reticulum; G: Golgi apparatus), where it regulates the hydration of the airway surface liquid (ASL) by secreting chloride and downregulating the activity of the epithelial sodium channel (ENaC), thereby maintaining the proper balance of ions and water in the airway. In pathological conditions associated with CF (CF, on the right), CFTR with the Phe508del mutation is retained in the ER and degraded by the proteasome (P), leading to an imbalance of ionic permeability and water absorption through epithelial cells. The impaired CFTR function leads to the accumulation of sticky mucus that impairs the mucociliary clearance, with neutrophil (N) and bacteria accumulation (green rectangles) in the airways. These infections trigger chronic inflammation that eventually causes respiratory failure (Philippe and Urbach, 2018).

1.2. CF airway infections

Chronic upper and lower airway infections are hallmarks of CF, with rhinosinusitis and lung infections being prominent examples. Because of dysfunctional mucociliary clearance in people with CF, chronic bacterial infections develop and persist throughout the life of these patients (Randell and Boucher, 2006).

Classical bacterial pathogens found in CF airways include *Pseudomonas aeruginosa*, *Staphylococcus aureus*, species belonging to the *Burkholderia cepacia* complex, *Haemophilus influenzae*, *Achromobacter* species and *Stenotrophomonas maltophilia* (Thornton and Parkins, 2023). In particular, *S. aureus* and *H. influenzae* are the most prevalent bacteria during infancy and early childhood, while *P. aeruginosa* and other pathogens, including species of the *B. cepacia* complex, are acquired later in life (Figure 1.4) (Cystic Fibrosis Foundation, 2022; European Cystic Fibrosis Society, 2022).

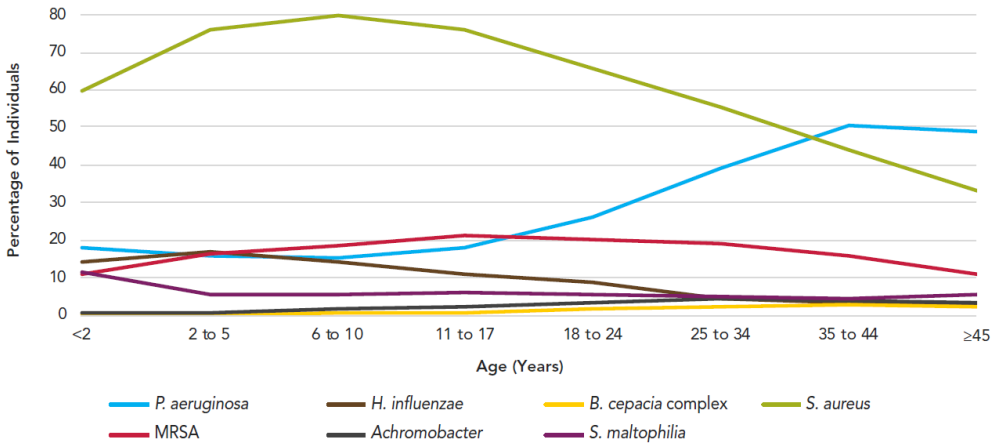

Figure 1.4. Prevalence of respiratory bacteria in CF patients by age group in the United States (Cystic Fibrosis Foundation, 2022).

1.3. *Pseudomonas aeruginosa*

Pseudomonas aeruginosa is a rod-shaped, opportunistic, Gram-negative bacterium that causes several acute and chronic infections, especially in CF patients and immunocompromised individuals. Being motile and widely distributed, this bacterium can disseminate and thrive in many environments such as soil and water, increasing the risk of exposure and consequently leading to a high incidence of infections (Qin *et al*., 2022). In the context of CF, *P. aeruginosa* represents the prevalent bacterial pathogen and the predominant cause of morbidity and mortality in adult patients. However, the percentage of individuals with a positive culture for this bacterium is declining over time, likely attributable to improved infection prevention measures and the implementation of antibiotic eradication strategies at the time of initial acquisition (Mogayzel *et al*., 2014).

1.3.1. *P. aeruginosa* pathogenesis and virulence factors

P. aeruginosa is commonly acquired by CF patients during childhood, primarily from environmental sources. However, patient-to-patient transmission of this bacterium has been described (Stapleton *et al*., 2021). Being characterized by a large genome ranging from approximately 5.5 to 7 Mbp, *P. aeruginosa* exhibits remarkable versatility, allowing it to thrive in several hostile niches within the human body. Indeed, this bacterium is equipped with an arsenal of virulence factors, including the lipopolysaccharide, adhesins for bacterial colonization, secretion systems for delivering effector proteins and toxins, siderophores for iron chelation and quorum-sensing for bacterial communication and biofilm formation (Figure 1.5) (Liao *et al*., 2022).

Once acquired by CF patients, *P. aeruginosa* pili facilitate the adhesion of the bacterium to airway epithelial cells (Feldman *et al*., 1998). Following bacterial adhesion, the bacterium downregulates genes associated with the production of flagella (Mahenthiralingam *et al*., 1994), while upregulating genes involved in mucoidy (Pedersen, 1992), biofilm formation (Ryder *et al*., 2007) and antibiotic resistance (Pitt *et al*., 2003). These adaptive behaviours serve as primary mechanisms employed by *P. aeruginosa* to evade the host immune system and counteract antibiotic treatment.

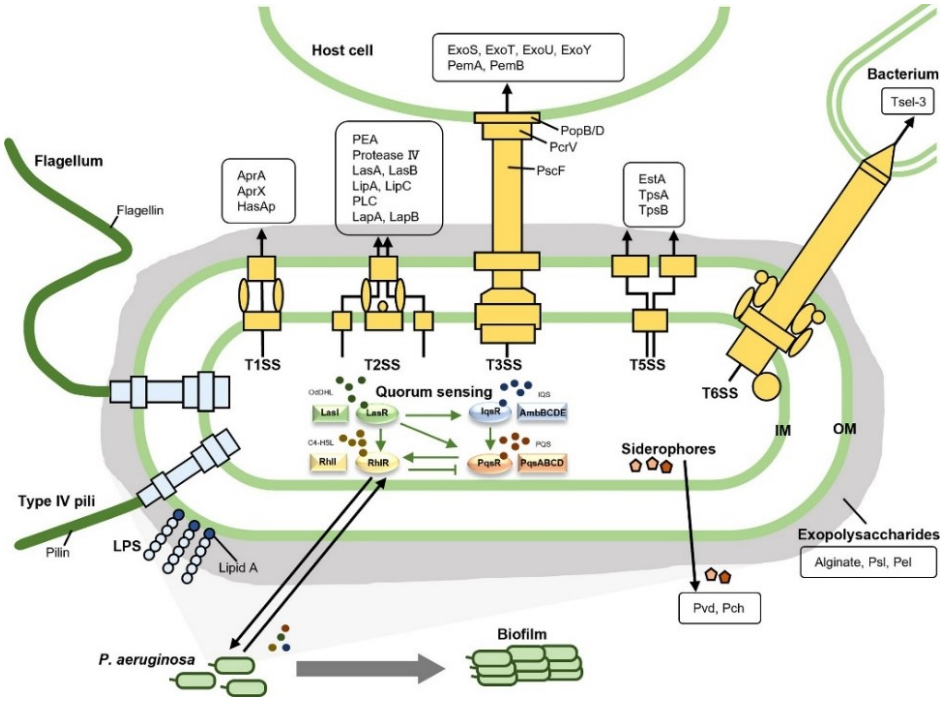

Figure 1.5. *P. aeruginosa* virulence factors, including bacterial surface structures (type IV pili, flagella and lipopolysaccharide), secretion systems (T1SS, T2SS, T3SS, T5SS and T6SS that deliver effector proteins and toxins) and bacterial cell-to-cell interactions (quorum-sensing, also fundamental for biofilm formation) (Liao *et al*., 2022).

1.3.1.1. Lipopolysaccharide

The lipopolysaccharide (LPS) is the primary structural component of the external leaflet of the outer membrane of Gram-negative bacteria. The LPS consists of three main constituents: lipid A, core oligosaccharide and O-antigen (Figure 1.6) (Huszczynski *et al*., 2019).

The lipid A is an acylated and phosphorylated glucosamine disaccharide, constituting the hydrophobic portion of the LPS (Huszczynski *et al*., 2019). The arrangement of lipid A molecules in the outer membrane is highly compact, creating a barrier that restricts the diffusion of small hydrophobic molecules (Nikaido, 2023). The lipid A is associated with potent endotoxic properties which elicit strong innate immune responses in human hosts. Upon interaction with immune cells, lipid A activates signalling pathways that lead to the production of proinflammatory cytokines such as TNF-α and IL-1β (Sebastian-Valverde and Pasinetti, 2020).

The core oligosaccharide constitutes the hydrophilic portion of the LPS and is covalently linked to the lipid A. It can be further divided in inner and outer core, each exhibiting distinct structural features. The inner core generally contains 3-deoxy-D-manno-oct-2-ulosonic acid (Kdo) which is attached to heptose residues. These heptose residues can undergo phosphorylation and/or chemical modification. On the other hand, the outer core typically contains hexoses and hexosamines, including glucose, galactosamine and L-rhamnose (Huszczynski *et al*., 2019). In *P. aeruginosa*, the core oligosaccharide undergoes significant phosphorylation, resulting in an overall increase in the negative charge of the bacterial cell membrane. This increased negative charge facilitates interactions with divalent cations, such as calcium and magnesium ions, promoting membrane stability (Nikaido, 2023).

The O-antigen is a hydrophilic polysaccharide composed from a few to hundreds of sugar residues that can be covalently linked to the core oligosaccharide. LPS that presents the O-antigen is defined as “capped”, while LPS lacking O-antigen is defined as “uncapped” (Huszczynski *et al*., 2019). The O-antigen, along with the core oligosaccharide, lead to a drastic decrease in membrane permeability to lipophilic compounds (Nikaido, 2023). Noteworthy, the presence of the O-antigen in *P. aeruginosa* exhibits protective effects against phagocytosis and opsonization (Engels *et al*., 1985). Furthermore, the long chains of O-specific antigen, one of the two *P. aeruginosa* O-antigens, play a role in serum resistance by impairing the complement system (Kintz *et al*., 2008).

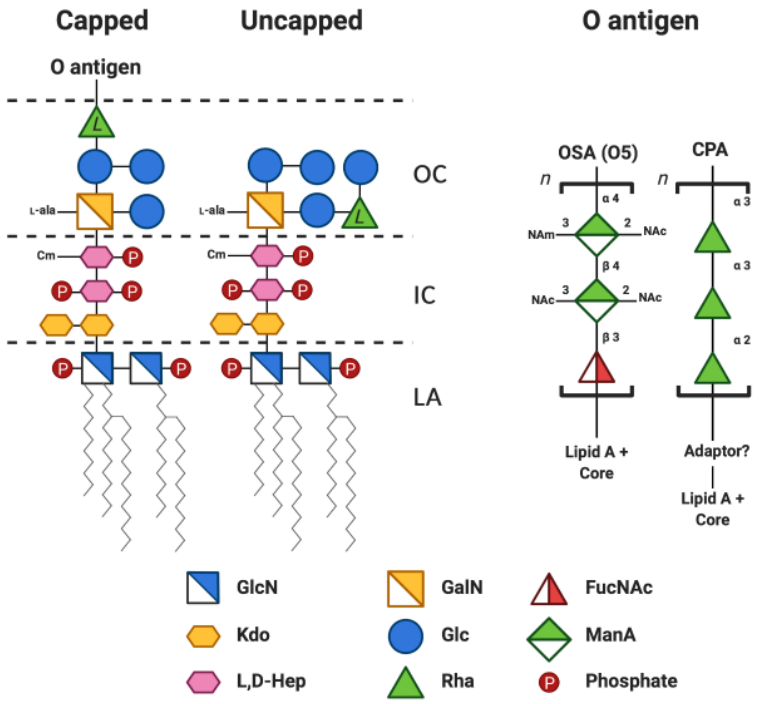

Figure 1.6. Chemical structure of *P. aeruginosa* PA01 LPS. The lipid A (LA) – core (divided in inner and outer core, IC and OC) can be capped with an O-antigen. This bacterium can produce two O-antigens: the common polysaccharide antigen (CPA) and the O-specific antigen (OSA). GlcN, glucosamine; GalN, galactosamine; FucNAc, N-acetyl-D-fucosamine Kdo; 3-deoxy-D-manno-oct-2-ulosonic acid; Glc, glucose; ManA, manuronic acid; L,D-Hep, L-glycero-D-manno-heptose; Rha, rhamnose; Cm, 7-O-carbamoylation; L-ala, 2-L-alanylation; NAm, N-amidino; NAc, N-acetyl; n, variable number of repeats (Huszczynski *et al*., 2019).

1.3.1.2. Bacterial adhesins

The initial step in *P. aeruginosa* pathogenesis involves its adhesion to the host. This bacterium achieves this through specific surface appendages such as pili and flagella (Liao *et al*., 2022).

On one hand, *P. aeruginosa* type IV pili, composed by pilin monomers, play a central role in various bacteria processing, including twitching and swarming motility, adhesion, biofilm formation and exchange of bacterial DNA. In particular, the transfer of DNA can be problematic from a clinical perspective when it involves the acquisition of antibiotic resistance genes (Burrows, 2012). On the other hand, *P. aeruginosa* flagella, which are hairlike appendages formed by flagellins, contribute to motility, adhesion and biofilm formation (Dasgupta *et al*., 2004). Since flagella can elicit the activation of the host immune response, *P. aeruginosa* downregulates the genes involved in their biosynthesis after colonizing the airways of CF patients (Feuillet *et al*., 2006).

1.3.1.3. Secretion systems

Bacterial secretion systems are protein complexes located on bacterial surface, responsible for the secretion of effector proteins. Specifically, *P. aeruginosa* secretion systems release virulence factors involved in adhesion, invasion, heme acquisition, biofilm formation and cytotoxicity (Liao *et al*., 2022).

In *P. aeruginosa*, six types of secretion systems have been identified, referred to as T1SS to T6SS. The type 1 secretion system (T1SS) is responsible for secreting alkaline proteases (AprA and AprX) and hemophores (HasAp) which are involved in immune evasion and heme acquisition. In particular, the alkaline protease AprA degrades complement components, IFN-γ and TNF-α, thereby impairing host immunity (Bleves *et al*., 2010). The type 2 secretion system (T2SS) delivers extracellular toxins, including proteases (protease IV), lipases (LipA and LipC), phospholipases (PLC), phosphatases (LapA and LapB), as well as elastases (LasA and LasB) and exotoxin A (PEA). These toxins interfere with the host immune response and lead to tissue damage (Ball *et al*., 2012). Elastases, in particular, play a significant role in respiratory infections as they degrade elastin, an important component of the pulmonary tissue, thereby impairing lung function (Kessler *et al*., 1998). The type 3 secretion system (T3SS) is a needle-like protein complex that injects effector proteins, including ExoS, ExoT, ExoU, ExoY, PemA and PemB, into host cells. These effectors disrupt the actin cytoskeleton, resulting in impaired cell-to-cell adhesion, cytotoxicity and apoptosis. The severity of infection is directly correlated with the presence of T3SS, making it one of the most important virulence factors in *P. aeruginosa* (Horna and Ruiz, 2021). The type 4 secretion system (T4SS) includes pili that are involved in horizontal gene transfer, as previously mentioned. The type 5 secretion system (T5SS) releases virulence factors involved in bacterial pathogenicity and biofilm formation such as EstA, TpsA and TpsB. In particular, EstA promotes the expression of rhamnolipids which facilitates biofilm formation, while Tps proteins are β-barrel outer membrane proteins responsible for secreting molecules involved in bacterial adhesion and immune evasion (Henderson *et al*., 2004). Finally, the type 6 secretion system (T6SS) is involved in the digestion of the peptidoglycan of bacterial competitors through the release of effectors such as Tse1-3 (Russell *et al*., 2011). Additionally, T6SS delivers PldS and PldB into host cells, promoting bacterial endocytosis (Jiang *et al*., 2014).

1.3.1.4. Siderophores

Siderophores are iron-chelating molecules that bacteria secrete to scavenge iron, essential for bacterial growth, especially under conditions of iron limitation in the host (Liao *et al*., 2022). *P. aeruginosa* produces two siderophores, pyoverdine (Pvd) and pyochelin (Pch), which are able to sequester Fe^{3+} ions from transferrin and lactoferrin (Cornelis, 2010).

1.3.1.5. Quorum-sensing

Quorum-sensing is a cell-to-cell communication process that enables bacteria to regulate and coordinate gene expression according to bacterial cell density. This intricate communication system relies on the production and detection of specific signal molecules called autoinducers which are secreted into the surrounding environment. These autoinducers are recognized by specific receptors, triggering a cascade of signalling events that ultimately lead to the activation of various virulence factors, including biofilm formation (Liao *et al*., 2022).

P. aeruginosa employs *Las*, *Rhl*, *Iqs* and *Psq* quorum-sensing pathways, along with the corresponding autoinducers OdDHL, C4-HSL, IQS and PQS, to orchestrate cellular communication. These pathways are involved in the release of virulence factors, including alkaline proteases, lipases, elastases, exotoxin A, rhamnolipids and pyocyanin, besides activating intracellular pathways promoting biofilm formation (Lee and Zhang, 2015; Li *et al*., 2022a).

1.3.1.6. Bacterial biofilm and exopolysaccharides

Bacterial biofilms are complex communities of bacteria adhered to both living (biotic) and non-living (abiotic) surfaces, embedded in a self-produced matrix. This matrix consists of exopolysaccharides, proteins and extracellular DNA, contributing to the structural integrity of the biofilm. The formation of biofilm confers several advantages to bacteria, including resistance to environmental stresses (e.g., desiccation and oxidizing agents), nutrient deficiency and antibiotic treatment. Moreover, biofilms serve as a protective shield against the host immune system, especially opsonization and phagocytosis. Interestingly, bacteria within biofilms exhibit resistance levels ranging from 10 to 1000 times higher than their planktonic counterpart, primarily due to the reduced antibiotic penetration into the biofilm matrix. In addition, as biofilm matures, a small subpopulation of bacteria undergoes differentiation into slow-growing, metabolically inactive persister cells, characterized by tolerance to antibiotic treatments (Liao *et al*., 2022).

P. aeruginosa produces the exopolysaccharides alginate, Psl and Pel. Specifically, strains isolated from CF patients predominately secrete alginate, while Psl and Pel are primary produced by environmental strains (Franklin *et al*., 2011). Alginate is composed of D-mannuronic and L-glucuronic acids and plays a significant role in *P. aeruginosa* pathogenesis. Firstly, alginate facilitates bacterial adhesion to mucins in the respiratory tract, contributing to bacterial colonization (Mann and Wozniak, 2012). Furthermore, this exopolysaccharide protects the bacterium from both phagocytosis and reactive oxygen species (Leid *et al*., 2005).

These properties also make alginate an essential component during biofilm maturation. This is particularly relevant since, after colonization of the airways of CF patients, *P. aeruginosa* switches from non-mucoid to mucoid phenotype, characterized by the overproduction of alginate. This transition leads to the establishment of chronic infections that are difficult to treat. As anticipated, bacteria residing within biofilms exhibit increased resistance to antibiotics: one example is the inactivation of aminoglycosides which lose their effectiveness upon binding to alginate (Goltermann and Tolker-Nielsen, 2017).

1.3.2. *P. aeruginosa* antibiotic resistance

P. aeruginosa is known for its extensive resistance to a wide range of antibiotics, making challenging to treat it effectively. This bacterium exhibits resistance to aminoglycosides, β-lactams, quinolones and cationic antimicrobial peptides (Pang *et al*., 2019). Aminoglycosides antibiotics, including amikacin, gentamycin and tobramycin, interfere with bacterial protein synthesis by binding to the 30S ribosomal subunit. β-lactams antibiotics such as carbapenems, cephalosporins and penicillins impair bacterial cell wall biosynthesis by binding to penicillin-binding proteins which are crucial for cell wall formation. Quinolone antibiotics, including ciprofloxacin and levofloxacin, interfere with bacterial DNA replication by inhibiting DNA gyrase and topoisomerase IV, enzymes that are essential for DNA unwinding and DNA replication. Finally, cationic antimicrobial peptides like polymyxin B and E (colistin) disrupt bacterial cell membranes, causing leakage and ultimately leading to cell death (Pang *et al*., 2019).

Interestingly, hydrophilic β-lactams and quinolones are able to enter bacterial cells though porins which are water-filled channels in the outer membrane, while aminoglycosides and polymyxins promote their own uptake into bacterial cells after interaction with LPS molecules. Specifically, polymyxins interact electrostatically with phosphate groups of lipid A and core oligosaccharide, enabling self-diffusion across the outer membrane (Lambert, 2002).

P. aeruginosa antibiotic resistance can be classified into three distinct types: intrinsic, acquired and adaptive (Pang *et al*., 2019). The classification is determined by the specific mechanism underlying the resistance (Figure 1.7).

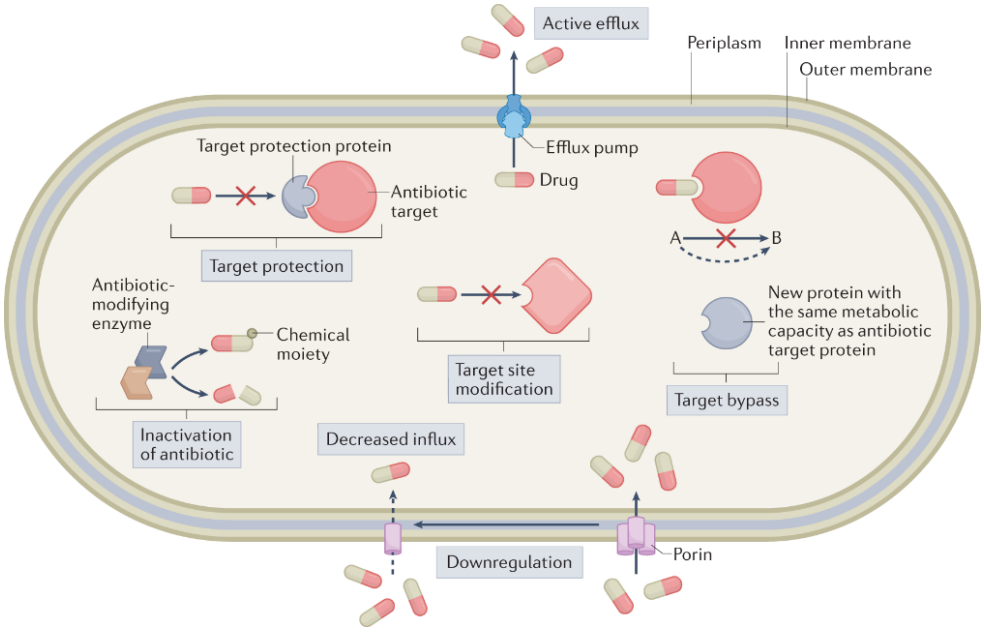

Figure 1.7. Examples of antibiotic resistance mechanisms. Efflux pumps can actively expel antibiotics. Downregulation of porins can lead to a decreased antibiotic influx. Antibiotic-modifying enzymes can attach chemical moieties to antibiotics, resulting in their inactivation. The antibiotic target can be protected by specific proteins that bind to the target site; additionally, spontaneous mutations can contribute to antibiotic resistance by modifying the target site. Target bypass involves the emergence of a new protein that shows redundancy with the antibiotic target, without being inhibited by the antibiotic (Darby *et al*., 2023).

1.3.2.1. Intrinsic antibiotic resistance

P. aeruginosa shows intrinsic antibiotic resistance attributed to multiple factors, including the low permeability of its outer membrane, the expression of efflux pumps responsible for expelling antimicrobials and the synthesis of antibiotic-inactivating enzymes (Pang *et al*., 2019).

The outer membrane of *P. aeruginosa* is known to have limited permeability, especially when it comes to antibiotics. However, there are specific porins that facilitates antibiotic diffusion across this membrane. For instance, OprD allows the entry of carbapenems. It is worth noting that mutations or downregulation of the gene encoding this porin can lead to an increased resistance of *P. aeruginosa* to this particular class of antibiotic (Li *et al*., 2012). In addition, this bacterium can develop resistance to polymyxins through mutations that decrease the negative charge of its LPS (Hancock, 1997).

Efflux pumps in *P. aeruginosa* are involved in the expulsion of various toxic compounds, including antibiotics, from the cell. Specifically, efflux pumps belonging to the resistance-nodulation-division (RND) family contribute significantly to antibiotic resistance in this bacterium (Li and Nikaido, 2009). For instance, MexAB-OprM is responsible for efficiently expelling both β-lactams and quinolones, while MexXY-OprM effectively pumps out aminoglycosides. As a consequence, mutations that lead to overexpression of these efflux systems contribute to bacterial antibiotic resistance (Masuda *et al*., 2000). Although efflux pumps inhibitors such as phenylalanine arginyl β-naphthylamide are able to counter the activity of these pumps (Askoura *et al*., 2011), their use in clinics is forbidden because of their toxicity.

P. aeruginosa possesses the capability to produce antibiotic-modifying enzymes that impair the activity of antibiotics. Among these enzymes, the most important ones produced by this bacterium are the β-lactamases which inactivate β-lactam antibiotics by hydrolysing the β-lactam ring (Wright, 2005). Interestingly, certain *P. aeruginosa* clinical isolates can produce extended-spectrum β-lactamases that break down a broad range of β-lactam antibiotics, including cephalosporins and penicillins (Rawat and Nair, 2010). However, β-lactam antibiotics can be combined with β-lactamase inhibitors such as clavulanate, sulbactam and tazobactam to treat patients. Another example of antibiotic modification in *P. aeruginosa* is the enzymatic modification of aminoglycosides, primarily targeting the amino and glycoside groups, resulting in their inactivation (Drawz and Bonomo, 2010).

1.3.2.2. Acquired antibiotic resistance

P. aeruginosa can acquire antibiotic resistance through spontaneous mutations in its genetic material and acquisition of resistance genes through horizontal gene transfer (Pang *et al*., 2019).

Spontaneous mutations play a significant role in the development of antibiotic resistance in *P. aeruginosa*. In addition to mutations involved in reduced antibiotic uptake, overexpression of efflux pumps and upregulation of genes encoding antibiotic-inactivating enzymes, as previously mentioned, mutations can directly modify the target of the antibiotic, further contributing to bacterial antibiotic resistance.

For instance, mutations in genes encoding DNA gyrase and topoisomerase IV can lead to reduced susceptibility to quinolones (Bruchmann *et al*., 2013). Similarly, mutations in genes encoding the 30S ribosomal subunit can confer resistance to aminoglycosides (El'Garch *et al*., 2007). In the case of β-lactams, mutations in genes encoding penicillin-binding proteins can result in resistance (Moyá *et al*., 2012). Lastly, mutations in genes encoding LPS components can lead to resistance to polymyxins (Hancock, 1997).

Horizontal gene transfer (HGT) is a process that enables the exchange of genetic material among different organisms. HGT can occur through several mechanisms, including transformation, conjugation and transduction. Transformation involves the uptake of free DNA from the environment, conjugation is related to direct exchange of plasmid DNA and transduction utilizes bacteriophages for DNA transfer. Plasmids, transposons and bacteriophages are known vectors of antibiotic resistance genes which can be transferred through HGT (Arber, 2014). *P. aeruginosa*, for instance, has been reported to acquire resistance genes for aminoglycosides and β-lactams through HGT (Poole, 2011).

1.3.2.3. Adaptive antibiotic resistance

Bacterial adaptive antibiotic resistance arises as a result of transient modifications in gene expression triggered by host-related stimuli, ultimately leading to a decreased bacterial sensitivity to antibiotics. These phenotypic variations are reversible upon removal of the specific stimulus. The adaptive antibiotic resistance mechanisms in the case of *P. aeruginosa* are biofilm formation and persister cell differentiation which are associated to chronic infection and contribute to a poor prognosis in CF patients (Pang *et al*., 2019).

As anticipated, bacteria within biofilms exhibit reduced susceptibility to antibiotics compared to the planktonic counterparts, primarily due to lower antibiotic penetration (Pang *et al*., 2019). Remarkably, antibiotic susceptibility restores upon the disruption of the biofilm, indicating that biofilm-associated resistance is independent of genetic mutations (Walters *et al*., 2003). Similarly, persister cells are not genetically resistant to antibiotics but show tolerance to high concentrations of antibiotics by entering a dormant state (Pang *et al*., 2019). Once antibiotics are removed, persister cells resume growth and repopulate biofilms, thereby contributing to the persistence of chronic infections (Maisonneuve and Gerdes, 2014). Interestingly, *P. aeruginosa* strains isolated from CF patients are generally characterized by a higher proportion of persister cells compared to wild-type strains (Mulcahy *et al*., 2010).

1.3.3. *P. aeruginosa* antibiotic treatment

The global standards of care for CF patients include eradication of acute *P. aeruginosa* infections. Typically, a combination of an aminoglycoside and a β-lactam is administered through inhaled, oral or intravenous routes to effectively eradicate this bacterium in most CF patients (Langton Hewer and Smyth, 2014). However, there are some cases where antibiotic eradication therapy fails, leading to the establishment of chronic infections, associated with a rapid decline in lung function and premature death in individuals with CF (Pamukcu *et al*., 1995). In such cases, the focus shifts to long-term suppression using inhaled antibiotics, especially tobramycin (Smith *et al*., 2018). Other antibiotics utilized in clinics for the treatment *of P. aeruginosa* infections include amikacin, ceftazidime, ciprofloxacin, colistin and meropenem (Li and Schneider-Futschik, 2023).

1.4. *Burkholderia cenocepacia*

Burkholderia cenocepacia is a rod-shaped, opportunistic, Gram-negative bacterium belonging to the *B. cepacia* complex (Bcc). This complex comprises 24 closely related species, commonly found in various natural habitats such as soil and water, where they can disseminate using their flagella. *Burkholderia* species represent an important clinical threat, especially to CF and immunocompromised individuals (Rojas-Rojas *et al*., 2019).

In 2021, only 1.4% of CF patients were infected with Bcc species in the United States (Cystic Fibrosis Foundation, 2022). Historically, *B. cenocepacia* was the most commonly encountered Bcc species in CF. However, more recent trends indicate a shift, with *B. multivorans* emerging as a more prevalent species. This change can likely be attributed to the implementation of improved infection prevention measures (Govan *et al*., 2007). Nevertheless, *B. cenocepacia* infections are feared by individuals with CF due to their association with rapid decline in lung function and high mortality, generally caused by necrotizing pneumonia with bloodstream infections, known as “cepacia syndrome” (Daccò *et al*., 2023). To worsen this scenario, CF patients infected with *B. cenocepacia* are generally excluded from transplantation listing because of poor outcomes after lung transplantation (Mitchell and Glanville, 2021).

1.4.1. *Burkholderia cenocepacia* pathogenesis and virulence factors

As an environmental bacterium, *B. cenocepacia* can be acquired from several sources, but it can also be transmitted from patient-to-patient (LiPuma *et al*., 1990). Due to its versatile genome of up to 9 Mbp, subdivided into three circular chromosomes and one plasmid (Figure 1.8), *B. cenocepacia* is highly adaptable to changing environments, also within the human body (Rojas-Rojas *et al*., 2019). In fact, *B. cenocepacia* is equipped with numerous virulence factors, including LPS, pili, secretion systems, extracellular proteases, quorum-sensing and the ability to form biofilms (Figure 1.8) (Thornton and Parkins, 2023). Interestingly, the predominant focus of research on this particular bacterium was on the molecular pathogenesis of epidemic clones belonging to the electrophoretic type 12 lineage, especially *B. cenocepacia* J2315 which caused outbreaks in CF population in Canada, the United Kingdom and Europe (Drevinek and Mahenthiralingam, 2010). Additionally, another well characterized strain is *B. cenocepacia* K56-2, clonally related to *B. cenocepacia* J2315 (Mahenthiralingam *et al*., 2000).

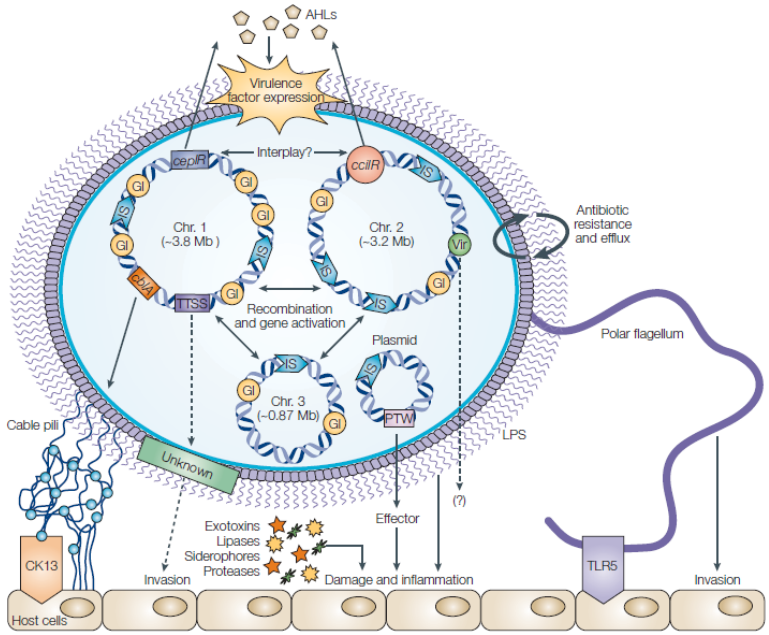

Figure 1.8. *B. cenocepacia* genomic structure and main virulence factors. This bacterium possesses three circular chromosomes and one plasmid, all of which contain insertion sequences (IS). Moreover, chromosomes present genomic islands (GI). Pili and adhesins (light blue circles) allow bacterial adhesion to host-cell receptors such as intermediate filament protein cytokeratin 13 (CK13). T3SS may have a role in invasion of the host cells. *B. cenocepacia* produces extracellular toxins, lipases, siderophores and proteases, contributing to tissue damage and inflammation, along with T4SS PTW and LPS. T4SS Vir system requires further investigation. The polar flagellum is involved in host cell invasion and flagellins are recognized by Toll-like receptor 5 (TLR5), triggering the activation of the host immune response. Regulation of virulence factors expression is governed by the quorum-sensing systems *cepIR* and *ccilR*, mediated by acyl-homoserine lactose (AHLs) (Mahenthiralingam *et al*., 2005).

1.4.1.1. Lipopolysaccharide

Just like *P. aeruginosa*, the LPS of *B. cenocepacia* is composed of lipid A, core oligosaccharide and O-antigen. Also in this case, not all the *B. cenocepacia* strains produce the O-antigen. Specifically, *B. cenocepacia* K56-2 produces the O-antigen through to the expression of glycosyltransferase WbxE (Ortega *et al*., 2005). In this strain, the presence of the O-antigen is associated with increased resistance to serum-mediated killing (Ortega *et al*., 2005) and cationic antimicrobial peptides (Loutet *et al*., 2006). In contrast, *B. cenocepacia* J2315 presents an insertion sequence within the *wbxE* gene, leading to the truncation of the glycosyltransferase and impairing the formation of complete LPS (Ortega *et al*., 2005). As is characteristic of LPS, *B. cenocepacia* LPS elicits a robust innate immune response (Bamford *et al*., 2007) and impairs opsonization and phagocytosis (Saldías *et al*., 2009).

1.4.1.2. Bacterial adhesins

B. cenocepacia exhibits various cell envelope structures, including flagella and pili which are involved in host-pathogen interactions and allow DNA exchange through conjugation. Interestingly, *B. cenocepacia* upregulates flagellar genes when incubated in CF sputum. This upregulation is essential for the progression of the infection and is in contrast with *P. aeruginosa* behaviour (Drevinek *et al*., 2008). Indeed, deletion of genes encoding the primary flagellin subunit results in a non-motile strain with impaired virulence *in vivo* (Urban *et al*., 2004). On the other hand, pili are involved in damage of the pulmonary tissue (Cheung *et al*., 2007).

1.4.1.3. Secretion systems

B. cenocepacia utilizes secretion systems to release effector proteins that play fundamental roles in bacterial pathogenesis. Among these secretion systems, the T3SS is essential for the virulence of the bacterium and its survival *in vivo* (Tomich *et al*., 2003). Additionally, *B. cenocepacia* possesses two T4SSs, involved in intracellular survival and replication within epithelial cells and macrophages (Sajjan *et al*., 2008), as well as plasmid mobilization (Zhang *et al*., 2009). Furthermore, similarly to the T3SS, T6SS is associated with bacterial virulence and mutants lacking functional T6SS show reduced pathogenicity *in vivo* (Hunt *et al*., 2004).

1.4.1.4. Siderophore

B. cenocepacia can produce two different siderophores, namely ornibactin and pyochelin which are involved in chelating and acquiring iron (Thomas, 2007). Among these siderophores, ornibactin is the primary one produced by this bacterium, necessary for its virulence *in vivo* (Visser *et al*., 2004). Notably, *B. cenocepacia* can enzymatically degrade ferritin, a host-produced protein responsible for storing iron, thereby releasing it (Whitby *et al*., 2006). Degradation of ferritin is particularly important during lung infections in individuals with CF since ferritin concentrations are significantly higher in the lungs of CF patients compare to healthy individuals, making iron accessible to this bacterium (Stites *et al*., 1999; Whitby *et al*., 2006).

1.4.1.5. Quorum-sensing

B. cenocepacia intraspecies communication depends primarily on two quorum-sensing systems, *cepIR* and *cciIR*, which are mediated by specific acyl-homoserine lactone (AHL) autoinducers. These systems are involved in various bacterial processes, including motility (Lewenza *et al*., 2002), biofilm formation (Tomlin *et al*., 2005), *in vivo* virulence (Sokol *et al*., 2003), as well as the production of siderophores, proteases and lipases (Lewenza *et al*., 1999). Interestingly, *cepIR* and *cciIR* show functional overlap by sharing multiple gene targets, even though they do so in an agonistic manner (O'Grady *et al*., 2009). In addition, this bacterium possesses an AHL-independent quorum-sensing system based on the *B. cenocepacia* diffusible signal factor (Deng *et al*., 2009) and another based on the molecule valdiazen (Jenul *et al*., 2018).

1.4.1.6. Bacterial biofilm and exopolysaccharides

Biofilm formation in *B. cenocepacia* serves as an important defence mechanism, providing protection against the host immune system and antibiotic treatments. In the lungs of CF patients, *B. cenocepacia* has the ability to form biofilms, often in association with *P. aeruginosa* (Tomlin *et al*., 2001). Interestingly, these two bacteria can communicate within the biofilm, potentially regulating some of their virulence factors during CF lung infections (Lewenza *et al*., 2002). In addition, biofilm formation also leads to the differentiation of a small bacterial population into antibiotic-tolerant persister cells (Van Acker *et al*., 2014).

B. cenocepacia biofilm formation is influenced by the synthesis of exopolysaccharides, especially during CF respiratory infections (Conway *et al*., 2004). Unlike *P. aeruginosa*, where alginate production is typically associated with the establishment of chronic lungs infections, not all *B. cenocepacia* strains chronically infecting the pulmonary tissue of CF patients produce exopolysaccharides. This includes strains like *B. cenocepacia* J2315 and K56-2 (Zlosnik *et al*., 2008).

However, for those strains that do synthetize exopolysaccharides, they contribute to the persistence of the bacterium within the CF lungs (Conway *et al*., 2004).

1.4.2. *B. cenocepacia* antibiotic resistance

B. cenocepacia represents a significant treatment challenge mainly due to its high intrinsic resistance to antibiotics currently used in clinics. This bacterium is resistant to aminoglycosides, β-lactams, phenicols, quinolones, tetracyclines and antimicrobial peptides (Scoffone *et al*., 2017). Similarly to *P. aeruginosa*, antibiotic resistance of *B. cenocepacia* can be classified into intrinsic, acquired and adaptive antibiotic resistance (Figure 1.6).

1.4.2.1. Intrinsic antibiotic resistance

B. cenocepacia intrinsic antibiotic resistance is attributed to different factors, including reduced permeability of its cell envelope, presence of efflux pumps and enzymes that hydrolyse or modify antibiotics (Scoffone *et al*., 2017).

The cell envelope of *B. cenocepacia* plays a significant role in limiting the diffusion of both hydrophilic and hydrophobic antibiotics, primarily due to the LPS, as previously described (Nikaido, 2023). Interestingly, the net negative charge of the LPS of this bacterium is reduced because of the substitution of phosphate groups with 4-amino-4-deoxy-L-arabinose in both lipid A and core oligosaccharide structures. This modification confers resistance to antimicrobial peptides, including polymyxin B (Olaitan *et al*., 2014). Indeed, when the core oligosaccharide is removed from the LPS, *B. cenocepacia* becomes more susceptible to this antibiotic (Ortega *et al*., 2009). In addition, porins are also involved in reduced membrane permeability to antibiotics. In fact, *B. cenocepacia* strains isolated from CF patients and resistant to β-lactams are characterized by a decreased porin content (Aronoff, 1988).

Efflux pumps play an important role in the resistance of *B. cenocepacia* to antibiotics. Similarly to *P. aeruginosa*, the RND efflux pump family is the major contributor to antibiotic resistance in this bacterium (Scoffone *et al*., 2017). For instance, RND-3 pump expels ciprofloxacin and tobramycin, while RND-4 pump confers resistance to ciprofloxacin, tobramycin, minocycline and chloramphenicol. These efflux pumps are activated particularly during planktonic growth of *B. cenocepacia*. Furthermore, only when biofilms are formed, RND-8 and RND-9 pumps expel tobramycin (Buroni *et al*., 2014). Interestingly, in cases where *B. cenocepacia* establishes chronic infections in the respiratory tract of CF patients, there is an upregulation of the RND-4 pump, highlighting its importance during CF infections (Mira *et al*., 2011).

B. cenocepacia expresses antibiotic-inactivating enzymes, especially β-lactamases (Scoffone *et al*., 2017). In particular, this bacterium produces AmpC which hydrolyses extended-spectrum cephalosporins (Bush and Fisher, 2011) and PenB which is a broad-spectrum carbapenemase (Poirel *et al*., 2009).

1.4.2.2. Acquired antibiotic resistance

The acquired antibiotic resistance observed in *B. cenocepacia* arises from spontaneous mutations in its genetic material. These mutations can lead to a reduction in the negative charge of the LPS or an increase in the expression of efflux pumps and enzymes that inactivate antibiotics. Although it is not a major mechanism of resistance in this bacterium, drug target modification can also occur (Scoffone *et al*., 2017). For instance, point mutations in the gene encoding the DNA gyrase subunit A can confer resistance to levofloxacin (Tseng *et al*., 2014). In addition to mutations-driven resistance, *B. cenocepacia* can acquire antibiotic resistance genes through conjugation and transduction (Scoffone *et al*., 2017).

1.4.2.3. Adaptive antibiotic resistance

In *B. cenocepacia*, adaptive antibiotic resistance is attributed to biofilm formation and persister cells differentiation which are associated with the establishment of chronic infections. In such cases, resistance to antibiotics is primarily caused by decreased antibiotic diffusion within the biofilm matrix and tolerance to antimicrobial compounds, respectively (Scoffone *et al*., 2017).

1.4.3. *B. cenocepacia* antibiotic treatment

B. cenocepacia represents a major threat to CF patients not only due to its extensive resistance to a broad range of antibiotics, but also due to the lack of an established treatment strategy to eradicate the chronic infections of this bacterium (Regan and Bhatt, 2019). Unfortunately, the limited number of individuals with CF infected with *B. cenocepacia* has resulted in insufficient funding for the identification of new drugs (Salsgiver *et al*., 2016). Despite these challenges, there are case reports where eradication treatment was successful. For instance, a treatment regimen involving a two-week intravenous administration of ceftazidime, tobramycin and temocillin, followed by three months of inhaled tobramycin, resulted in the complete eradication of *B. cenocepacia* in two children (Kitt *et al*., 2016). However, there are many questions that remain unanswered, including the optimal duration of the therapy, the effectiveness of single versus multiple antibiotic therapies and the lack of correlation between *in vitro* and *in vivo* susceptibility data (Gautam *et al*., 2015).

1.5. *Staphylococcus aureus*

Staphylococcus aureus is an opportunistic, Gram-positive coccus that is commonly found as a commensal in the nasal cavities and skin of around 30% of healthy individuals. However, the widespread presence of this bacterium, even from an early age, can lead to the establishment of chronic infections in individuals with CF and compromised immune system (Goss and Muhlebach, 2011). In CF patients, *S. aureus* is frequently the first pathogen detected, with a prevalence of approximately 60% in infants under the age of 2 and around 80% in children across the United States (Figure 1.4). Although the incidence tends to decrease with age (Figure 1.4), the impact remains significant, as *S. aureus* infections are associated with increased lung inflammation and impaired lung function (Zemanick and Hoffman, 2016).

S. aureus is characterized by a relatively small genome of about 3 Mbp, yet it can rapidly adapt to hostile host niches, including the airways of CF individuals. The most important adaptations of *S. aureus* include biofilm formation, which protects bacteria from both the host immune system and antibiotic therapy (Waters *et al*., 2016), and the emergence of small colony variants (SCVs), which are phenotypic variations characterized by the formation of small, slow-growing colonies on agar plates (Yagci *et al*., 2013). SCVs arise from mutations in metabolic genes, leading to nutritional deficiencies and reduced growth rates. This altered phenotype confers resistance to antibiotics and allows bacteria to persist within host tissues. Interestingly, SCVs frequently adopt an intracellular lifestyle by invading host cell, further protecting *S. aureus* from the immune system and antibiotics (Yagci *et al*., 2013).

In individuals with CF, prophylactic and suppressive antibiotic treatments of *S. aureus* infections are challenging due to antibiotic resistance. Of particular concern is the emergence of methicillin-resistant *S. aureus* (MRSA) which is associated with worsened lung function and increased mortality in CF patients (Rumpf *et al*., 2021). The resistance to this β-lactamase-resistant penicillin arose after its clinical use in the 1960s and resulted from acquisition of the *mecA* gene (Akil and Muhlebach, 2018). This gene encodes the penicillin-binding protein 2a (PBP2a), a modified form of a penicillin-binding protein. PBP2a has a reduced affinity for methicillin, allowing it to function even in the presence of this antibiotic, without impairing cell wall biosynthesis (Chambers, 1997). However, *mecA*-independent resistance mechanisms have been described in certain MRSA strains (Hryniewicz and Garbacz, 2017).

The clinical impact of prophylactic and suppressive antibiotic therapies for methicillin-sensitive *S. aureus* in CF patients remains uncertain (Rosenfeld *et al*., 2020). In addition, anti-staphylococcal treatment has been associated with increased prevalence of *P. aeruginosa* (Ratjen *et al*., 2001). In contrast, given the detrimental effects of chronic MRSA infections in individuals with CF, eradication therapy is generally recommended, showing decreased rates of persistence and reduced frequency of exacerbations (Dolce *et al*., 2019). Several antibiotics are commonly used in clinical settings to treat *S. aureus* infections in CF patients, including trimethoprim/sulfamethoxazole, rifampicin, vancomycin and linezolid (Lo *et al*., 2022).

1.6. Alternative treatments to fight bacterial infections

Given the limited progress in the development of new antibiotics and the increasing threat of infections with antibiotic-resistant strains, there is an urgent need to develop alternative therapeutic strategies, including the repurposing of existing drugs. Among these approaches, antivirulence strategies are particularly promising as they are aimed at interfering with bacterial virulence factors, thereby impairing bacterial pathogenesis without killing the bacteria. As a consequence, antivirulence strategies may exert a lower selective pressure and reduce the likelihood of resistance development compared to conventional antibiotics. Examples of antivirulence treatments include targeting bacterial surface structures (e.g. LPS, flagella and pili) preventing bacterial attachment to and invasion of the host, disruption of secretion systems (e.g. *P. aeruginosa* T3SS), neutralization of secreted virulence factors (e.g. siderophores, toxins, exopolysaccharides, etc.) and inhibition of quorum-sensing and biofilm formation (Liao *et al*., 2022). However, strategies for direct bacterial killing remain essential. Currently, the most encouraging approaches in this context are bacteriophages and antimicrobial peptides (Qin *et al*., 2022). Furthermore, considering combination therapy is essential. This approach involves the combination of existing and novel antimicrobials with compounds that increase membrane permeability, inhibit efflux pumps or impair signalling pathways connected to antibiotic resistance (Wang *et al*., 2020).

As mentioned earlier, CFTR modulators are revolutionizing the treatment of CF, improving mucus hydration and mucociliary clearance, thereby leading to an improved bacterial elimination (Hisert *et al*., 2017). However, structural lung damage and consequent chronic airway infections still persist (Ribeiro *et al*., 2023; Thornton and Parkins, 2023). For instance, a clinical study showed that modulators initially caused a decline in the abundance of *P. aeruginosa* in the lungs of CF patients, but eventually led to a rebound effect (Harris *et al*., 2020). RECOVER (https://classic.clinicaltrials.gov/ct2/show/NCT04602468) and PROMISE (https://classic.clinicaltrials.gov/ct2/show/NCT04038047) clinical studies are currently evaluating the impact of CFTR modulators on bacterial infections. These studies are expected to be completed in July and October 2024, respectively. Considering the persistent bacterial infections upon CFTR therapy and the fact that some CF patients are not eligible for this therapy due to their *CFTR* mutations, age or intolerance to the treatment, it remains crucial to address bacterial infections treatment (Ribeiro *et al*., 2023). It is worth noting that there is evidence suggesting that modulators possess mild antimicrobial properties. For instance, the potentiator ivacaftor may inhibit DNA replication due to the presence of a quinoline ring (Reznikov *et al*., 2014). In addition, it can synergize with tobramycin against *S. aureus* and with ciprofloxacin against *P. aeruginosa* (Payne *et al*., 2017; Cho *et al*., 2019).

1.7. The dispirotripiperazine derivative PDSTP

PDSTP, an abbreviation for 3,3'-(2-methyl-5-nitropyrimidine-4,6-diyl)3,12-bis-6,9-diaza-diazoniadispiro [5.2.5.2] hexadecane tetrachloride dihydrochloride, is non-toxic dispirotripiperazine derivative of 965 g/mol synthetized by our collaborator Dr. Vadim Makarov of the Federal Research Centre "Fundamentals of Biotechnology" of the Russia Academy of Sciences (Moscow, Russia). Dispirotripiperazines are tricyclic molecules that possess two shared atoms, known as spiro atoms, belonging to the dispiro compounds. In the case of dispirotripiperazines, the spiro atoms are two quaternary positively charged nitrogen atoms (Egorova *et al*., 2021). Specifically, PDSTP contains two of this molecular scaffold, resulting in a total of four reactive nitrogens (Schmidtke *et al*., 2002) (Figure 1.9).

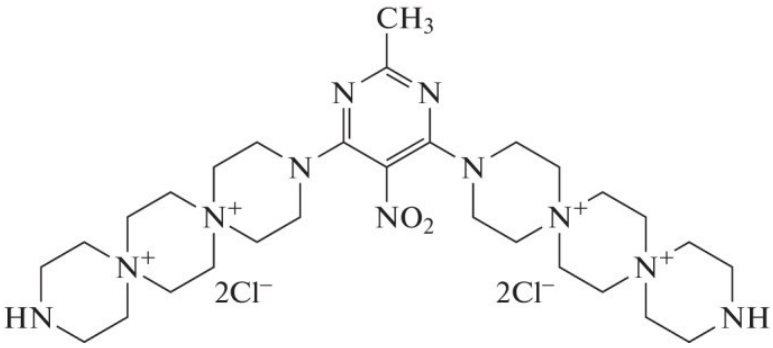

Figure 1.9. Molecular structure of PDSTP, characterized by four quaternary positively charged nitrogens (Makarov and Popov, 2022).

Historically, the dispirotripiperazine scaffold has been investigated as antiviral due to its ability to impair viral adsorption to negatively charged heparan-sulphate glycosaminoglycans (HSGAGs) expressed at the surface of human cells. The mechanism of action of dispirotripiperazine-based compounds involves the saturation of HSGAGs though electrostatic interactions, thus preventing the interaction of viruses with this host-cell receptor (Schmidtke *et al*., 2002).

1.7.1. Heparan-sulphate proteoglycans

Heparan-sulphate proteoglycans (HSPGs) represent one of the most important constituents of the extracellular matrix and are present on the surface of human cells (Bishop *et al*., 2007). HSPGs are composed of one or more HSGAGs, which are long linear polysaccharides consisting of repeated disaccharides units, covalently attached to a core protein (Figure 1.10A) (Sarrazin *et al*., 2011). The negatively charged nature of HSPGs arises from the presence of carboxylic and sulphate groups (Sarrazin *et al*., 2011). HSPGs can be classified into two groups, syndecans and glypicans, based on their core protein (Figure 1.10B). In particular, syndecans are transmembrane proteins anchored to the cell membrane through a hydrophobic domain (Poulain and Yost, 2015). On the other hand, glypicans are connected to the plasma membrane through a glycosylphosphatidylinositol linkage (Iozzo and Schaefer, 2015). The principal disaccharide unit consists of glucuronic acid and N-acetylglucosamine, while the minor component is composed of 2-O-sulphated glucuronic acid or 6-O-sulfated glucosamine, with the possibility of sulphation at the N-position of glucosamine (Figure 1.10C).

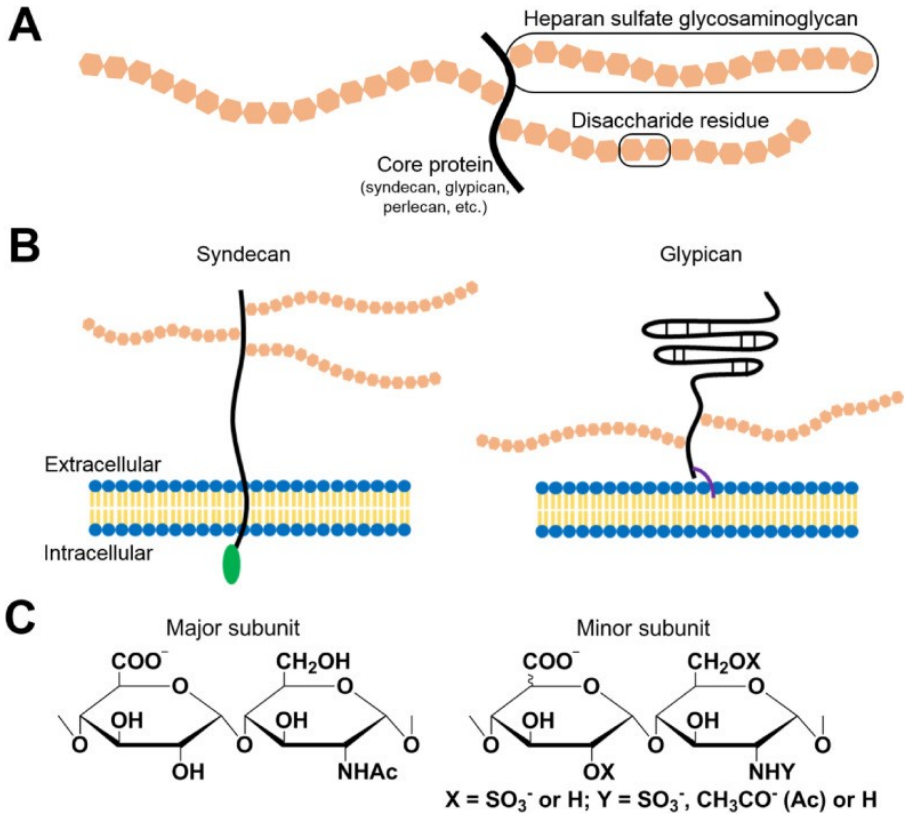

Figure 1.10. HSPGs consist of HSGAGs chains which are, in turn, composed by repeated disaccharide residues, connected to a core protein (A). Syndecans and glypicans are the two main classes of HSPGs (B). Chemical structure of the major and minor disaccharide subunits composing the HSGAGs (C) (Egorova *et al*., 2021).

HSPGs are involved in a diverse array of biological functions such as cell proliferation, differentiation, migration and adhesion. They also contribute to the organization and integrity of the extracellular matrix, inflammation and wound healing. This is due to the interactions of HSPGs with a vast repertoire of ligands (more than 300). Among these ligands there are growth factors, chemokines and cytokines. Importantly, HSPGs are implicated in different pathological processes such as cancer and neurodegenerative disorders, where dysregulation of HSPGs-mediated signalling pathways can contribute to disease pathogenesis and progression (Sarrazin *et al*., 2011).

Several viruses have evolved to specifically recognize HSPGs, either as receptors or attachment factors, allowing their attachment to host cells. Examples of such viruses include herpes simplex virus (HSV) (Shukla and Spear, 2001), human papillomavirus (HPV) (Giroglou *et al*., 2001), human immunodeficiency virus (HIV) (Connell and Lortat-Jacob, 2013) and hepatitis viruses (Barth *et al*., 2003; Leistner *et al*., 2008; Kalia *et al*., 2009).

In addition to viruses, bacteria also have the ability to interact with this host-cell receptor. Specifically, *P. aeruginosa* binds to heparan-sulphate chains through bacterial adhesins, especially flagella (Bucior *et al*., 2012). This interaction becomes particularly significant in the context of epithelia injury. For instance, when the airway epithelium is damaged, polarized epithelial cells dedifferentiate and upregulate the expression of HSPGs on their apical surface, promoting *P. aeruginosa* adhesion (Bartlett and Park, 2011). Furthermore, an increased expression of syndecan-1, the most common HSPG of epithelia, has been observed in bronchial epithelial cells exposed to glucocorticoids, facilitating *P. aeruginosa* adhesion. This effect is particularly relevant in patients who receive recurrent inhalation of corticosteroids, as it may be associated with the increased risk of pneumonia reported in these individuals (Liu *et al*., 2021a). However, other bacteria have been demonstrated to bind to heparan-sulphate chains, including *B. cenocepacia* (Martin *et al*., 2019) and *S. aureus* (Liang *et al*., 1992).

HSGAGs can be targeted by different drug classes aimed at preventing the adhesion of pathogens, including GAG mimetics that compete with endogenous GAGs, enzymes that modify or hydrolyse HSGAGs, as well as cationic compounds that interact with the negative charges of HSGAGs (Weiss *et al*., 2017). In particular, PDSTP belongs to the class of cationic molecules and interacts with two negatively charged sulphate groups located in adjacent saccharide residues (Makarov and Popov, 2022).

1.7.2. PDSTP properties and activity

PDSTP toxicity has been extensively investigated, showing a non-cytotoxic profile in both *in vitro* and *in vivo* studies. This is consistent with the size and charge characteristics of the compound which prevent its entry into human cells (Egorova *et al*., 2021).

PDSTP exhibited a good antiviral activity *in vitro* when tested against HSV-1 (Schmidtke *et al*., 2002) and both HIV-1 and HIV-2 (Novoselova *et al*., 2017). Furthermore, this compound prevented the death of a herpetic encephalitis mouse model when utilized in combination with acyclovir (Novoselova *et al*., 2019), was more effective compared to acyclovir when used to treat a guinea pig model of genital herpes (Novoselova *et al*., 2020), reduced both corneal lesions and viral infection course in a rabbit model of herpes simplex epithelial keratitis (Alimbarova *et al*., 2022) and prevented severe viral pneumonia induced by SARS-CoV-2 in a Syrian hamster infection model (Makarov and Popov, 2022).

In conclusion, it is worth mentioning that PDSTP may possess anti-inflammatory properties. This hypothesis arises from the characterization of prospidine, a dispirotripiperazine derivative that inhibited the production of proinflammatory cytokines in the context of rheumatoid arthritis (Benenson *et al*., 1986; Nemtsov *et al*., 1998). By sharing the same molecular scaffold, it is likely that PDSTP also prevents the production of those cytokines.

1.8. Bacteriophages

Bacteriophages (or phages) are natural predators of bacteria. They are the most abundant and diverse entities on Earth, with an estimated number of 10^{31} phages in the biosphere (Hendrix, 2002). Phages have been found in every biome inhabited by bacteria, including the human gastrointestinal tract (Shkoporov *et al*., 2018), where they affect human physiology, as well as the deep oceans (Nigro *et al*., 2017).

Phages were initially discovered in 1915 by the English bacteriologist Frederick Twort and, shortly after, in 1917, the French microbiologist Felix d'Herelle described their bacteriolytic properties. In 1919, d'Herelle successfully utilized phages to treat bacterial dysentery in children, marking the beginning of phage therapy for both human and animal bacterial infections. The first phage therapy programs were established in Georgia and Poland, and they continue to operate today. However, with the discovery of penicillin by Alexander Fleming in 1928, the use of phages for treating bacterial infections was overshadowed, especially in the Western world. In recent years, there has been a significant increase in interest to phage therapy, particularly due to its potential in combating antibiotic-resistant bacteria (Summers, 2012).

1.8.1. Bacteriophage biology

Phages generally have a double-stranded DNA genome, but single-stranded DNA, double-stranded RNA and single-stranded RNA phage genomes have been described. Their genetic material ranges in size from approximately 2,500 bp to over 540 kbp. Genomes are enclosed within a capsid that can be polyhedral, filamentous or pleomorphic, and can be attached to a tail (Dion *et al*., 2020). The majority of described phages possess a double-stranded DNA genome packed into a tailed icosahedral capsid, belonging to the *Caudovirales* order. This order comprises different families, including *Myoviridae*, *Siphoviridae* and *Podoviridae* (Figure 1.11). The diameter of the capsid of *Caudovirales* phages typically ranges from 45 to 185 nm, while their tail can be either contractile (*Myoviridae*) or non-contractile (*Siphoviridae* and *Podoviridae*) (Ackermann, 2007).

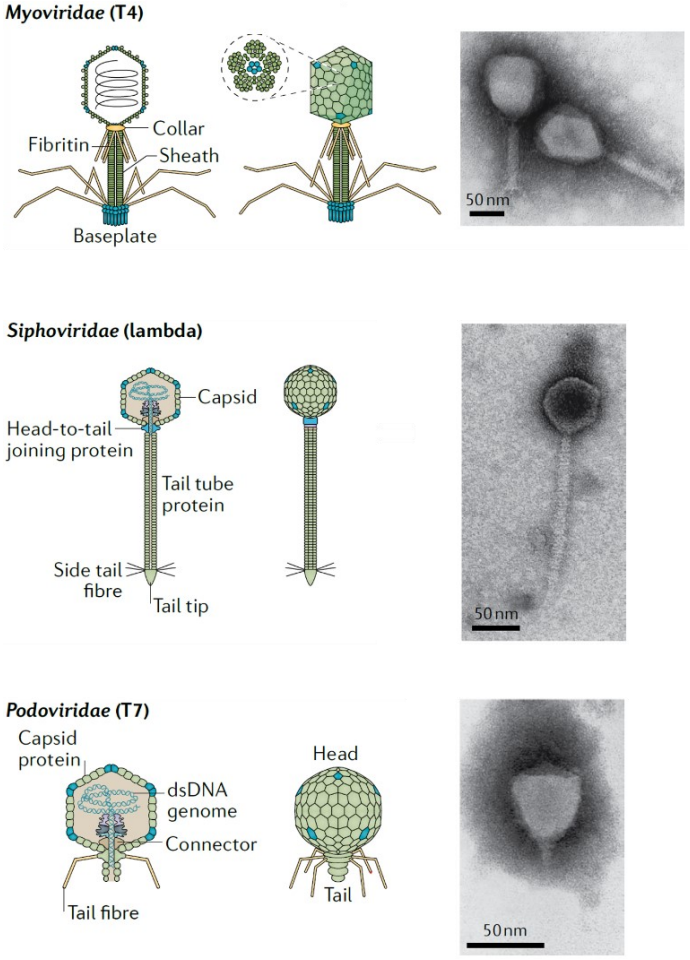

Figure 1.11. Schematic representations and transmission electron micrographs depicting *Myoviridae*, *Siphoviridae* and *Podoviridae* phages which belong to the *Caudovirales* order. T4 phage represents the *Myoviridae* family, while phage lambda and T7 represent the *Siphoviridae* and *Podoviridae* families, respectively (Dion *et al*., 2020).

Phages have undergone co-evolution with bacteria for over 3 billion years, resulting in their high specificity for their host. This species-specificity is a trait that is shared with eukaryotic viruses. Additionally, phages exhibit other shared characteristics such as replication within the host by exploiting its machinery, as well as possessing relatively small genomes, as mentioned earlier (Strathdee *et al*., 2023).

Phages can be classified as lytic (virulent) or lysogenic (temperate) (Figure 1.12). The initial stage of phage infection involves the recognition of receptors on the surface of bacterial cells by receptor binding proteins located at either the tip of the tail or the baseplate. Subsequently, the phage genome is injected from the capsid into the cytoplasm (Strathdee *et al*., 2023).

The lytic cycle is characterized by a sequential program involving the expression of early phage genes responsible for genome replication, followed by late phage gene expression involving structural and assembly components. This culminates in the assembly of virions and subsequent lysis of the bacterial host, releasing the phage progeny. Phages can also undergo a lysogenic cycle, wherein their genomes integrate within the bacterial host chromosome, leading also to the silencing of lytic genes. Integrated phages are known as "prophages", while bacterial cells containing an integrated prophage are referred as "lysogens". However, under specific conditions, the prophage can be induced, excised from the bacterial chromosome and enter the lytic cycle. The occurrence of lysogeny varies depending on the phage, host and environmental conditions, ranging from a low percentage to the majority of infections. Since lytic phages have a higher frequency of lysing bacterial cells compared to lysogenic phages, lytic phages are more suitable for clinical applications. Nevertheless, lysogenic phages can be genetically engineered to be strictly lytic (Strathdee *et al*., 2023).

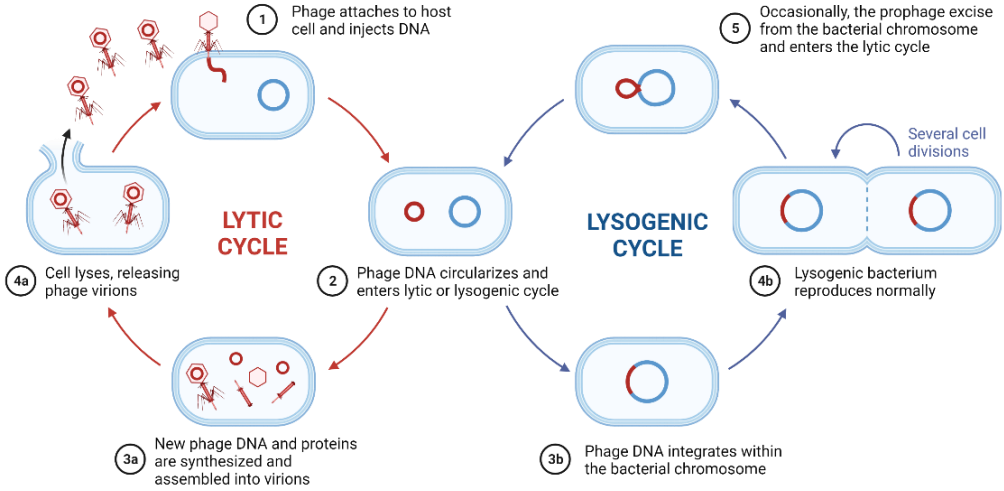

Figure 1.12. Lytic and lysogenic cycles of phages. Upon phage attachment and DNA injection into the host cell, the phage DNA circularizes and can enter either lytic or lysogenic cycle. In the lytic cycle, the phage takes control of the host's machinery to replicate its genetic material, assemble new virions and ultimately cause bacterial lysis, releasing the phage progeny. On the other hand, during the lysogenic cycle, the phage DNA integrates into the bacterial chromosome. The prophage becomes a stable part of the bacterial genome and is inherited as the bacterial cells replicate. However, under certain circumstances, the prophage can be induced to excise from the bacterial chromosome, entering the lytic cycle (BioRender.com).

The phage lytic cycle is characterized by three important parameters which are adsorption kinetics, latent period and burst size. The adsorption kinetics is related to the process by which phages bind to their bacterial cell receptor. The latent period of a phage refers to the time interval between phage infection of a bacterial cell and the release of the phage progeny. Finally, the burst size is the number of new virions that are released from an infected bacterial cell after its lysis (Strathdee *et al*., 2023).

1.8.2. Bacteriophage therapy

Phage therapy is a therapeutic approach that utilizes phages to treat bacterial infections. There are many advantages related to clinical applications of phages. Besides their species-specificity which allows to avoid killing of bacteria belonging to the normal microbiota, phages can infect and lyse not only antibiotic-resistant strains, but also persister cells. Furthermore, phages can eradicate the biofilm of biofilm-forming bacteria by both killing bacteria within the biofilm and degrading its matrix, possibly promoting the access of antibiotics to the deeper regions of the biofilm (Strathdee *et al*., 2023).

Phages intended for clinical use are commonly isolated from the environment. As mentioned previously, phages can be found in any niche where bacteria exist. One important source for isolation of phages with therapeutic potential is wastewater. Indeed, wastewater serves as a fertile environment for the proliferation and interaction of bacteria, providing a reservoir for phages that naturally infect and control bacterial populations (Clokie *et al*., 2011).

Following isolation, phages require an extensive characterization before their clinical use. Specifically, phages must be demonstrated to be lytic, effective and devoid of genes associated with potential side effects. In particular, whole-genome sequencing allows to exclude the presence of genes associated with antimicrobial resistance, toxins and virulence factors (Philipson *et al*., 2018). Particularly important is the determination of the host range which refers to the range of bacterial species or strains that a phage is capable of infecting. The host range is primarily determined by the specific receptor on the bacterial surface recognized by the phage and should ideally be broad. Prior to clinical application, phages need to be propagated on a well-characterized host and purified to minimize endotoxin levels. The propagating strain should have no integrated prophages to avoid contamination with prophage-derived particles. Interestingly, multiple phages can be combined into phage cocktails to broaden the host range, thus enhancing treatment efficacy. To facilitate this, the establishment of phage banks becomes crucial for clinical use, potentially allowing personalized medicine where specific phages can be selected based on the individual's bacterial infection profile (Strathdee *et al*., 2023).

Once phages have been extensively characterized, they can be administered to patients. Phage therapy relies on various routes of administration, including both parenteral and non-parenteral routes, with an increasing trend towards intravenous administration. A recent comprehensive review has shown the safety and tolerability of phage administration, regardless administration route (Liu *et al*., 2021b). However, it is important to note that the immune system of the patient may be activated in response to phages, potentially compromising their efficacy. Therefore, it is fundamental to conduct both pharmacokinetic and pharmacodynamic studies to optimize the route of administration and understand the role of pre-existing or induced adaptive immune responses (Dąbrowska and Abedon, 2019). In the case of CF infections, phages are generally administered by inhalation, although the stability after nebulisation needs to be assessed (Wang *et al*., 2021).

Currently, most of the research on phage therapy is focused on pulmonary infections and the sterilization of infected implanted medical devices, including vascular and orthopaedic devices. Furthermore, a growing number of clinical trials are ongoing in Europe, Australia and the UK, where the efficacy of environmental phages in treating multidrug-resistant bacterial infections is being evaluated, according to ClinicalTrials.gov.

In addition to the phage therapy programs in Georgia and Poland, established programs are now available in the United States, France, Belgium and Sweden. Furthermore, the UK has recently announced its consideration of compassionate-use of phages. It is important to develop standardized phage therapy protocols for clinical applications and this is the direction that Europe and Australia are pursuing (Strathdee *et al*., 2023).

1.8.3. Bacteriophage resistance in bacteria

Similar to antibiotics, phages exert strong selective pressure on their bacterial hosts, driving the evolution of resistance. This process can lead to the emergence of bacteria that are resistant to phage therapy, ultimately resulting in therapy failure (Wang *et al*., 2023a).

Over a span of more than 3 billion years, co-evolution between bacteria and phages has led to the development of several defence mechanisms in bacteria. These mechanisms include inhibition of phage adsorption, genome injection, replication and assembly (Figure 1.13). Simultaneously, phages have also developed multiple strategies to counteract these bacterial defences (Wang *et al*., 2023a).

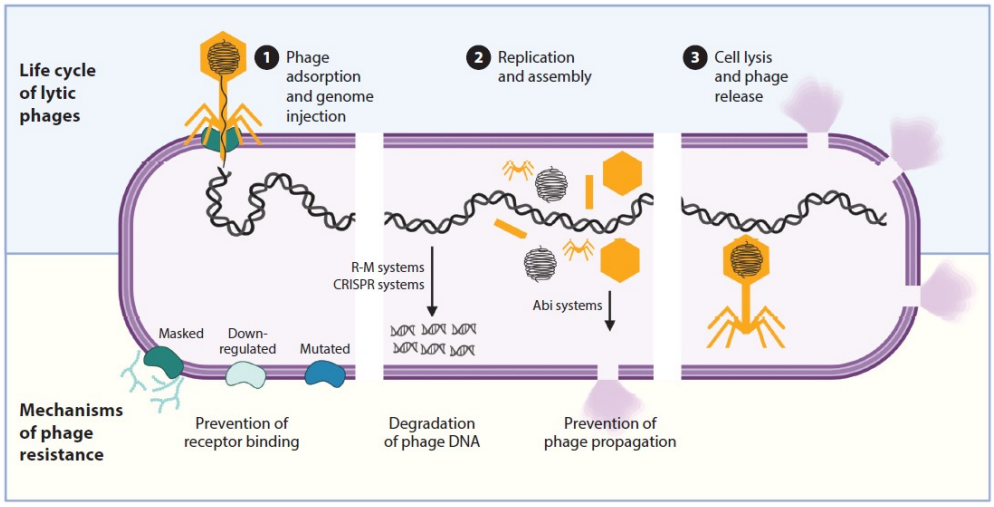

Figure 1.13. Life cycle of lytic phages and examples of mechanisms of phage resistance, including prevention of receptor binding by receptor masking, downregulation or mutation, degradation of phage DNA by restriction-modification (R-M) and CRISPR-Cas systems, and prevention of phage propagation by the abortive infection (Abi) system (Oromí-Bosch *et al*., 2023).

As a primary defence mechanism, bacteria can prevent phage adsorption by modifying surface phage receptors, including LPS, outer membrane proteins, flagella and pili. For instance, bacteria can mutate, downregulate or mask these receptors. In particular, receptors can be shielded by masking proteins or extracellular polymeric substances (Oechslin, 2018). In addition, bacteria residing within biofilms are further protected against phage infection (Wong *et al*., 2021).

Once a phage successfully adsorbs to the bacterial receptor and injects its genome into the cell, bacteria have the ability to degrade the phage genome, thus preventing phage replication. Similarly to Eukaryotic organisms, bacteria possess both innate and adaptive immunity. Bacterial innate immunity relies on restriction-modification (R-M) systems that recognize specific modified sequences in the phage genome and cleave them. Indeed, nucleic acid modifications, such as DNA methylation, allow bacteria to distinguish between self (methylated) and nonself-DNA (unmethylated) (Bernheim and Sorek, 2020). On the other hand, bacterial adaptive immunity relies on CRISPR-Cas systems that cleave specific DNA/RNA phage sequences based on short-phage derived DNA sequences present in the bacterial genome. These sequences derive from previous interactions with similar phages. The presence of the protospacer adjacent motif (PAM) near the sequence recognized by the CRISPR-Cas complex helps to avoid autoimmunity as it is absent in the bacterial genome (Westra *et al*., 2012).

In the event that a phage manages to replicate within the bacterial host, phage-specific components can be detected and trigger the activation of abortive infection (Abi) systems. These systems induce bacterial cell death, thereby preventing the production of phage progeny and safeguarding uninfected cells. Unlike the previous examples which were related to bacterial protection at the individual cell level, the Abi system confers protection at the population level, allowing the bacterial population to survive through the sacrifice of individual cells (Lopatina *et al*., 2020).

Simultaneously, phages undergo evolutionary changes to overcome bacterial resistance. For instance, they can evolve to utilize different receptors or develop the ability to cleave masking proteins and extracellular polymeric substances, enabling them to gain access to bacterial cell receptors (Labrie *et al*., 2010). Moreover, phages can modify their genetic material to evade recognition by R-M systems, mutate the PAM sequence to impair CRISPR-Cas activity and even synthetize proteins that disable these defence systems (Hampton *et al*., 2020).

1.8.4. How to minimize bacterial resistance to phages

To overcome phage resistance in bacteria, the strategy primarily involves the selection of highly effective phages, maximizing the rate of phage killing across different strains of the bacterial target. Specifically, phages should be characterized by rapid and strong adsorption to their receptors, a short latent period and a large burst size (Strathdee *et al*., 2023).

Highly efficient phages that recognize different receptors can be combined into phage cocktails. This approach broadens the host range of the phage and minimizes the emergence of phage-resistant bacteria. By employing this method, bacteria would need to evolve rescuing mutations for multiple receptors simultaneously, a process that occurs with lower probabilities (Abedon *et al*., 2021).

Interestingly, phage evolution can be exploited to counter bacterial resistance. Phage training, also known as phage preadaptation, involves the training of the phage population to anticipate and overcome phage resistance that may develop in bacteria through the accumulation of mutations. Phage training can be achieved *in vitro* either by propagating viruses for serial rounds of infection on a non-evolving host (Morello *et al*., 2011) or co-evolving the phages with the host for several passages (Borin *et al*., 2021).

For instance, propagating phages with a non-evolving clinical isolate of *P. aeruginosa* resulted in trained phages that evolved to kill the bacterium with significantly higher efficiency *in vivo*, compared to non-trained phages (Morello *et al*., 2011). Interestingly, phage training has been used to update commercial phage cocktails against emerging epidemiological bacterial strains (Ujmajuridze *et al*., 2018).

Another strategy in combating bacterial resistance is through phage engineering, a technique employed to expand the phage host range, reduce bacterial resistance to phages, increase phage safety and improve their stability (Pires *et al*., 2016). For instance, phage engineering was used to genetically modify two *Mycobacterium abscessus* temperate phages into strictly lytic phages which, along with a natural lytic phage, were used to treat a 15-years-old CF patients infected with drug-resistant *M. abscessus*. In this case, the resulting lytic phages showed increased killing activity against the bacterium, resulting in clinical improvements (Dedrick *et al*., 2019). Remarkably, this was the first successful phage therapy employing engineered phages. In addition, phages can be engineered to express biofilm-degrading enzymes (Lu and Collins, 2007) or molecules that inhibit quorum-sensing (Pei and Lamas-Samanamud, 2014).

However, bacterial resistance to phages is inevitable. As a consequence, one interesting approach involves driving bacterial evolution toward favourable trade-offs. This means that bacteria may develop resistance to phage infections but at the cost of impaired bacterial fitness. Moreover, bacterial resistance can be connected to antibiotic potentiation and resensitization. For instance, the phage OMKO1 recognizes as receptor the outer membrane porin M of *P. aeruginosa* which is a component of the MexAB and MexXY efflux pump systems. Mutations in these efflux pumps can compromise the export of antibiotics from the bacterial cell, leading to increased susceptibility to antibiotics (Chan *et al*., 2016). However, some phages may drive bacterial evolution towards deleterious trade-ups, including increasing bacterial resistance to antibiotics. For instance, phages T6 and U115 interact with Tsx porins in *Escherichia coli* which are involved in diffusion of the antibiotic albicidin across bacterial membranes. Mutations in Tsx conferred resistance to both the phages and albicidin (Kortright *et al*., 2021). This illustrates the need for a thorough characterization of phages before considering them for therapeutic applications.

2. Aim of the work

The objective of this work was to explore innovative alternative therapeutic strategies for treating bacterial infections in cystic fibrosis (CF) patients. Specifically, our focus was on addressing the challenges posed by the antibiotic-resistant pathogens *Pseudomonas aeruginosa*, *Burkholderia cenocepacia* and *Staphylococcus aureus*. The first part of our investigation was centered on the evaluation on the dispirotripiperazine derivative PDSTP as a potential treatment option. This particular compound, characterized by a non-toxic nature, has been extensively investigated for its antiviral activity, involving the inhibition of viral adsorption to heparan-sulphate glycosaminoglycans on the surface of human cells (Schmidtke *et al*., 2002). Given that CF bacteria adhere to this specific host cell receptor (Bucior *et al*., 2012; Martin *et al*., 2019; Liang *et al*., 1992), the efficacy of PDSTP in inhibiting the adhesion of these pathogens to human epithelial cells was evaluated. Subsequently, after confirming that PDSTP interacted with *P. aeruginosa*, our investigation focused towards identifying the molecular target of the compound, as well as at exploring the potential of PDSTP as an antibiotic adjuvant and an inhibitor of biofilm formation in this bacterium.

The second part of this study is related to the research conducted during my time in the laboratory of Prof. Sarah Vreugde at the University of Adelaide (Adelaide, South Australia). Specifically, it involved the characterization of three bacteriophages targeting *P. aeruginosa* for their therapeutic potential, with a focus on their lytic activity against both planktonic and biofilm-embedded bacteria. Furthermore, this work aimed at understanding the impact of mutations conferring phage resistance on bacterial growth, biofilm formation and antibiotic susceptibility, potentially identifying advantageous traits for the treatment of *P. aeruginosa* infections.

Overall, this work focused on developing novel approaches to combat bacterial infections in CF patients, particularly those caused by difficult-to-treat antibiotic-resistant pathogens.

3. Materials and methods

3.1. Bacterial strains, growth conditions, antibiotics and compounds

Pseudomonas aeruginosa PA01 reference strain (laboratory collection), isogenic GFP-expressing *P. aeruginosa* PA01 strain (Crabbé *et al*., 2017), 18 *P. aeruginosa* CF clinical isolates BT2, BT72, BST44, NN2, NN83, NN84, RP73, RP74, SG2 (Alcalá-Franco *et al*., 2012), C450, C452, C453, C457, C458, C459, C460, C462 and C464 (Department of Otorhinolaryngology, Academic Medical Centre, Amsterdam, The Netherlands) and 9 non-CF isolates from patients affected by chronic rhinosinusitis C392, C394, C405, C419, C423, C427, C430, C433 and C440 (Department of Otolaryngology, Head and Neck Surgery, University of Adelaide at The Queen Elizabeth Hospital, Woodville, South Australia) were grown in tryptic soy broth (TSB; BD) at 37°C (200 rpm). *Burkholderia cenocepacia* K56-2, J2315 (laboratory collection) and MH1K ΔOAg (Hanuszkiewicz *et al*., 2014) were grown in Luria-Bertani (LB; BD) broth at 37°C (200 rpm). Methicillin-sensitive *Staphylococcus aureus* ATCC 25923 (laboratory collection) was grown in TSB at 37°C (200 rpm). Minimum inhibitory concentration determination and antibiotic combination susceptibility assay were performed in cation-adjusted Mueller-Hinton broth (CAMHB; BD). The synthetic cystic fibrosis sputum medium (SCFM) was prepared as previously described and supplemented with 0.1% casamino acids (Harrington *et al*., 2021).

Used antibiotics were amikacin (Sigma-Aldrich), ceftazidime (Sigma-Aldrich), ciprofloxacin (Sigma-Aldrich), colistin (Sigma-Aldrich), meropenem (Venus Pharma GmbH) and tobramycin (Sigma-Aldrich); ciprofloxacin was dissolved in 0.1N NaOH, while the other antibiotics were dissolved in water. PDSTP (Schmidtke *et al*., 2002), heparin (Sigma-Aldrich), heparinase III (Sigma-Aldrich) and dansyl-polymyxin (DPX; Sigma-Aldrich) were dissolved in water. N-phenyl-1-naphthylamine (NPN; Sigma-Aldrich) was dissolved in acetone. 3,3'-Dipropylthiadicarbocyanine iodide (DiSC3(5); Sigma-Aldrich) and carbonyl cyanide *m*-chlorophenylhydrazone (CCCP; Sigma-Aldrich) were dissolved in dimethyl sulfoxide (DMSO).

3.2. Human pulmonary epithelial cell cultures

Human pulmonary epithelial cells were cultured in 75 cm^2 flasks either in Dulbecco's modified Eagle's medium (DMEM; Euroclone) supplemented with 10% fetal bovine serum (FBS), 0.1 mM non-essential amino acids, 100 U/mL penicillin and 0.1 mg/mL streptomycin or minimal essential medium (MEM; Euroclone) supplemented with 10% FBS, 2 mM glutamine, 100 U/mL penicillin and 0.1 mg/mL streptomycin, at 37°C in 5% CO_2.

Specifically, A549 cells (Giard *et al*., 1973) were grown in DMEM, while 16HBE14o- (Cozens *et al*., 1994) and CFBE41o- (carrying the biallelic Phe508del mutation) (Bruscia *et al*., 2002) were cultured in MEM.

3.3. Minimum inhibitory concentration determination

According to the EUCAST guidelines (Wiegand *et al*., 2008), the minimum inhibitory concentrations (MICs) were determined in CAMHB using the broth microdilution method. Two-fold serial dilutions of the antibiotic (or compound) were prepared into a U-bottom 96-well plate. Bacteria were collected during the mid-log phase of growth and diluted to have approximately 5 x 10^5 CFU/mL. The culture was inoculated into the 96-well plate and subsequently incubated at 37°C for 24 hours. After the incubation, 30 µL of 0.01% resazurin were added to each well and the plate was further incubated at 37°C for four hours. Aerobic respiration of metabolically active bacterial cells reduces blue resazurin to pink resorufin, allowing visual determination of the MICs.

3.4. Quantification of the adhesion by plate counting

Adhesion assays were performed by plate counting as previously described (Berlutti *et al*., 2008), with modifications. Approximately 1.5 x 10^5 cells per well were seeded in a 24-well tissue culture plate in medium without antibiotics and incubated for 48 hours. After two days, confluent monolayers were infected with mid-log phase bacteria, resuspended in medium without antibiotics, at a multiplicity of infection (MOI) of 10 bacteria per human cell. At the time of the infection, PDSTP (and/or heparin) was added at the desired concentration in duplicate, while two wells were not treated (control). After two hours of incubation at 4°C, monolayers were gently washed three times with phosphate-buffered saline (PBS) to remove non-adherent bacteria and lysed with 1% Triton. Cell lysates were diluted and plated to enumerate adhered bacteria. The percentage of bacterial adhesion to human cells was calculated as:

$$\frac{CFUs/mL\ of\ adhered\ bacteria}{CFUs/mL\ of\ inoculated\ bacteria}\ x\ 100$$

The percentage of bacterial adhesion to human cells was then normalized to the untreated sample, set at 100%.

To investigate the mechanism of action of the compound, PDSTP pretreatments were performed as follows. Pretreatment of bacterial cells: incubation of bacteria with 50 µg/mL of PDSTP for 30 minutes at 4°C (gentle shaking). Pretreatment of human cells: incubation of pulmonary epithelial cells with 100 µg/mL of PDSTP for one hour at room temperature (a high concentration of the compound was used to saturate heparan-sulphate glycosaminoglycans). After PDSTP pretreatment, both bacteria and human cells were washed three times with PBS to remove the excess of the compound.

To cleave the heparan-sulphate chains, human cells were pretreated with 100 mU of heparinase III (which hydrolyses the glycosidic bond between N-acetylglucosamine and glucuronic acid) for two hours at 37°C in 5% CO_2.

3.5. Quantification of the adhesion by ImageStream Flow Cytometry

After incubating the infected monolayers (MOI = 100) with an isogenic GFP-expressing *P. aeruginosa* PA01 strain for two hours at 4°C and washing them four times with pre-chilled PBS to remove non-adherent bacteria, quantification of the adhesion was performed by ImageStream Flow Cytometry. Briefly, human cells were gently detached from the 24-well tissue culture plate with a cell scraper, washed by centrifugation at 4°C with 1 mL of Dulbecco's PBS (D-PBS; devoid of Ca^{2+} and Mg^{2+}) and resuspended in 50 µL of D-PBS to obtain a final concentration of approximately 2 x 10^7 cells/mL. Until the analysis at the Amnis ImageStreamX MkII (Cytek), samples were kept on ice.

For each sample, 10,000 events were acquired at 40x magnification (NA = 0.75; core size 10 µm) with 488 nm laser excitation (100 mW). Brightfield images were collected in channel 04, cells with adhered bacteria in channel 02 (480-560 nm channel width, 528/65 bandpass) and channel 06 (745-800 nm width, 762/35 bandpass) was used for scatterplot detection. D-PBS was used in all measurements.

Acquisition was performed by Inspire software (Amnis, version 1.3) with the following gating strategy: focused cells linear gate G1 (GradientRMS_Ch04) and selecting single cells square gate G2 (AspectRatio_Ch04/Area_Ch04).

Data analysis was made using Amnis IDEAS software (version 6.2): focused cells gate ("GradientRMS_Ch04" feature), single cells gate ("AspectRatio_Ch04"/"Area_Ch04" features) and finally custom "BactCount" features were applied for quantification. "BactCount" feature was created as follows: a custom "BactCount" mask was created (PeakM02,Ch02,Bright24.5) and the "SpotCount" feature was applied on this mask.

3.6. PDSTP binding assay

PDSTP binding assay was performed as follows. P*. aeruginosa* PA01 was grown in TSB, collected during the mid-log phase of growth, washed and resuspended in pre-chilled PBS. Subsequently, bacteria were incubated with 100 µg/mL of PDSTP for 30 minutes at 4°C. The excess of PDSTP was removed by washing the bacteria with pre-chilled PBS twice. The compound was eluted from the surface of the bacteria by resuspending them in 300 mM sodium chloride. After centrifugation, the presence of PDSTP was detected spectrophotometrically in the supernatant. Indeed, this compound absorbs light at λ = 370 nm. The calibration curve was obtained by plotting the absorbance values against different concentrations of PDSTP, ranging from 1 to 100 µg/mL.

3.7. Phase-contrast microscopy analysis

Phase-contrast microscopy analysis was performed as previously described (Pellegrini *et al*., 2022). *P. aeruginosa* PA01 was grown in TSB and 5 µL of the bacterial culture at an OD_{600} of approximately 0.5 were seeded on agar pads (Young *et al*., 2011) with or without 50 µg/mL of PDSTP. Agar pads were then placed onto a cover glass-dish in an environmental microscope incubator set at 37°C. Phase-contrast imaging was performed using a Leica DMi8 widefield microscope, equipped with a 100x oil immersion objective (Leica HC PL Fluotar 100x/1.32 OIL PH3), a Leica DFC9000 sCMOS camera and driven by Leica LASX software.

3.8. Dansyl-polymyxin binding assay

The dansyl-polymyxin (DPX) binding assay was performed as previously described (Akhoundsadegh *et al*., 2019), with modifications. *P. aeruginosa* PA01 was grown in TSB, collected during the mid-log phase of growth, washed once and resuspended in a solution of 5 mM HEPES (pH 7.2). To define the amount of DPX needed for lipopolysaccharide (LPS) saturation on whole cells, bacteria were diluted 1:10 in the same buffer (OD_{600} = 0.05) and 100 µL were transferred to a quartz cuvette. Fluorescence was measured using a Cary Eclipse fluorescence spectrometer (Agilent) (excitation and emission wavelengths of 340 and 500 nm, respectively) after multiple additions of 1 µL of DPX (100 µM), until the maximum fluorescence signal was reached. Then, to assess the interaction of PDSTP with the LPS on bacterial surface, DPX displacement assay was performed. A concentration of DPX that gave 90% saturation was added to the bacterial suspension (OD_{600} = 0.05) and 0.5 µL of PDSTP (1 mM) were added before each measurement, recording the progressive decrease in fluorescence. The assay was repeated using colistin as control. Inhibition graphs were obtained plotting fluorescence reduction against PDSTP or colistin concentrations. The concentration of compound causing the 50% decrease in fluorescence (I_{50}) was then extrapolated.

3.9. Lipopolysaccharide extraction

LPS extraction was performed as follows (Marolda *et al*., 2006). Bacteria were grown on agar plates, collected and suspended in 2 mL of PBS to an OD_{600} of approximately 2. 1.5 mL of the bacterial suspension were centrifuged at 10,000 *x g* for one minute, the bacterial pellet was resuspended in 150 µL of lysis buffer (0.5 M Tris-HCl pH 6.8, 2% sodium dodecyl sulphate and 4% β-mercaptoethanol) and incubated at 95°C for 10 minutes. 10 µL of 20 mg/mL proteinase K were added, samples were vortexed and incubated overnight at 60°C to digest proteins. 150 µL of pre-warmed (70°C) 90% phenol solution were added and, after vortexing, samples were incubated at 70°C for 15 minutes to extract digested and residual undigested proteins. After 10 minutes of incubation on ice to help the separation of the aqueous and phenolic phases, samples were centrifuged at 10,000 *x g* for 10 minutes to further separate them. 100 µL of the clear aqueous phase (top phase) were transferred in a clean tube, making sure not to transfer the white interface containing proteins. 10 volumes of ethyl ether saturated with Tris-EDTA were added to the aqueous phase and vigorously mixed. In this way, the ether removed phenol traces in the samples. Samples were centrifuged at 10,000 *x g* for one minute and the ether phase was removed by aspiration. Finally, purified LPS solutions were stored at -20°C.

3.10. Lipopolysaccharide staining with silver nitrate (silver stain)

Before the staining, sodium dodecyl sulphate (SDS) polyacrylamide gel was prepared and LPS was separated into its components (Marolda *et al*., 2006). The running gel was prepared with a 18% acrylamide solution supplemented with ammonium persulfate (APS) and tetramethylethylenediamine (TEMED) to catalyse the polymerization. When TEMED was added, the solution was immediately poured on the casting gel unit. A layer of 0.1% SDS was added to prevent air from interacting with the gel which was left polymerize for at least 20 minutes. After polymerization of the running gel, a layer of a 4.5% acrylamide solution supplemented with APS and TEMED was added and, after a 10-well gel comb was applied, it was let polymerize for at least 20 minutes. Once the gel was ready, the gel apparatus was assembled and cathode buffer (100 mM Tris-HCl pH 8.25, 100 mM of tricine and 0.1% SDS) and anode buffer (200 mM Tris-HCl pH 8.9) were added to the upper and lower chambers, respectively. LPS samples were supplemented with loading dye (0.187 M Tris-HCl pH 6.8, 6% SDS, 30% glycerol, 0.03% bromophenol blue and 15% β-mercaptoethanol), incubated at 95°C for 5 minutes and loaded on the gel. LPS was separated into its components by running the electrophoresis at 35 mA until the dye reached the bottom of the gel.

LPS silver stain was performed as previously described (Marolda *et al*., 2006). Silver stain protocol is particularly sensitive to metals dissolved in water. Consequently, milli-Q deionized water was used during the entire procedure. In addition, glass containers were used in every step. Briefly, the gel was soaked overnight in 200 mL of fixing solution (25% isopropanol and 7% acetic acid). The following day, the gel was incubated with 200 mL of oxidizing solution (0.7% periodic acid and 2.7% isopropanol) for 5 minutes. After discarding this solution, the gel was washed with 500 mL of water for one hour, changing the water every 15 minutes. The staining solution (19 mL of 100 mM NaOH, 0.7 mL of NH_4OH concentrated solution, 3.3 mL of 20% $AgNO_3$ and 77 mL of water) was added for 15 minutes. The gel was washed with water for 45 minutes, changing the water every 15 minutes. The developing solution (0.005% citric acid and 0.019% formaldehyde) was added until yellow or brown bands appeared (generally between 5 to 15 minutes). Finally, stop solution (0.35% acetic acid) was added and pictures of the gel were acquired.

3.11. Antibiotic combination susceptibility assay

Antibiotic combination susceptibility assay was performed in CAMHB as follows. Two-fold serial dilutions of antibiotics were prepared into a U-bottom 96-well plate. Bacteria were collected during the mid-log phase of growth and diluted to have approximately 5 x 10^5 CFU/mL. The culture was divided into two subcultures and one of them was supplemented with PDSTP at the desired concentration. Subcultures were inoculated into the 96-well plate and subsequently incubated at 37°C for 24 hours. After the incubation, 30 µL of 0.01% resazurin were added to each well and the plate was further incubated at 37°C for four hours, allowing visual determination of the MICs.

3.12. Time-killing assay by plate counting

Time-killing assays were performed in TSB using the broth microdilution method (Jayathilaka *et al*., 2021). An overnight liquid bacterial culture was diluted 1:100 in fresh medium and incubated at 37°C (200 rpm). At an OD_{600} of approximately 0.35 (about 1 x 10^8 CFU/mL), the culture was divided into four subcultures. One subculture was not treated (control), the second one was supplemented with PDSTP at sub-inhibitory concentrations, the third one was treated with the antibiotic at a concentration equivalent to a half of the MIC and the last one was supplemented with both PDSTP and the antibiotic. Subcultures were further incubated at 37°C (200 rpm). At 0, 1, 2, 3, 4, 5 and 24 hours, the OD_{600} was measured and bacterial viable count was evaluated by plating dilutions of collected aliquots to calculate the respective number of CFU/mL.

In these experiments, synergy was defined as a ≥ 2 log10 decrease in CFU/mL of the subculture treated with the combination after 5 hours, compared to the most active compound (CLSI, 1999).

3.13. High-throughput time-killing assay with the plate reader

The time-killing assay procedure was modified, obtaining a high-throughput protocol using the plate reader. Overnight bacterial cultures in TSB were diluted 1:100 in fresh medium and incubated at 37°C (200 rpm). At an OD_{600} of approximately 0.35, 200 µL/well of bacterial cultures were inoculated into a U-bottom 96-well plate. Bacterial cultures were supplemented with PDSTP at sub-inhibitory concentrations, antibiotic at an appropriate concentration, or their combination, in duplicate. One well was not treated (control). Assays were carried out using a CLARIOstar microplate reader (BMG Labtech) at 37°C, measuring the OD_{600} of the cultures every 15 minutes for 24 hours. A custom plate mode program was set up to perform these experiments, including 90 cycles of 900 seconds each (orbital shaking at 300 rpm, with 3 mm of diameter) with shaking before each reading, both to increase the oxygenation and maintain bacteria in suspension.

3.14. *In vivo* analysis of PDSTP and ceftazidime combination

PDSTP and ceftazidime combination was tested *in vivo* employing a *Galleria mellonella* infection model (Benthall *et al*., 2015). Larvae were purchased from a provider located in Pavia and were grouped according to their weight (at least 10 per group). Larvae were inoculated with either a lethal dose (10^4 CFU) of mid-log phase *P. aeruginosa* PA01 or physiological saline (control), with an injection volume of 10 µL. After two hours of incubation at 30°C, in the dark, control and infected larvae were administered with 10 µL of physiological saline (control), PDSTP (6.25 mg/kg), ceftazidime (5 mg/kg) or a combination of them. Larvae were subsequently incubated under the same conditions for three days. Larval viability was registered after 24, 48 and 72 hours. Specifically, larval death was assessed by considering the lack of movement after tactile stimulus.

3.15. N-phenyl-1-naphthylamine assay

N-phenyl-1-naphthylamine (NPN) assay was performed as previously described (Helander and Mattila-Sandholm, 2000), with modifications. A flat-bottom 96-well black plate was prepared as follows: two wells were filled with 50 µL of 5 mM HEPES buffer (pH 7.2) (control), while 50 µL of PDSTP and EDTA were added to two different wells to have a final concentration of 10 µg/mL and 5 mM, respectively. EDTA was the positive control since it permeabilizes bacterial membranes. An overnight *P. aeruginosa* PA01 culture was diluted 1:100 into 10 mL of fresh medium and was incubated at 37°C (200 rpm). Once the culture reached an OD_{600} of approximately 0.5, it was centrifuged at 4400 rpm for 10 minutes and the pellet was resuspended in 5 mL of 5 mM HEPES (pH 7.2). Subsequently, NPN was added to have a final concentration of 10 µM. 150 µL of the culture were then inoculated into each well and fluorescence intensity was detected with a GloMax Discover microplate reader (Promega) at specific time points (0, 5, 10, 15, 30 and 60 minutes) utilizing an excitation wavelength of 350 nm and an emission wavelength of 420 nm.

3.16. Depolarization assay

3,3'-Dipropylthiadicarbocyanine iodide (DiSC3(5)) assay was performed as previously described (Buttress *et al*., 2022), with modifications. An overnight *P. aeruginosa* PA01 culture in TSB was diluted 1:100 in 10 mL of fresh medium and incubated at 37°C (200 rpm). Once the culture reached an OD_{600} of approximately 0.5, it was centrifuged at 4400 rpm for 10 minutes and the pellet was washed and resuspended in a solution of 5 mM HEPES (pH 7.2) and 5 mM glucose. Bacteria were diluted to about 10^7 CFU/mL and two aliquots of 3 mL were prepared. 0.5 mg/mL of bovine serum albumin were added to each aliquot, while 1 mM of EDTA was added to one of them to increase bacterial membrane permeability to DiSC3(5). Both aliquots were then supplemented with 0.8 µM of DiSC3(5). Bacteria were incubated at 37°C for 15 minutes (200 rpm). After the incubation, 100 µL of bacteria were transferred into a U-bottom 96-well plate. Initial fluorescence intensity was detected with a CLARIOstar microplate reader (BMG Labtech) by utilizing an excitation wavelength of 622 nm and an emission wavelength of 670 nm. Subsequently, the compounds were added. Specifically, PDSTP was added at a concentration of 1, 10, 20, 50 and 100 µg/mL, carbonyl cyanide m-chlorophenyl hydrazone (CCCP) was supplemented at a concentration of 10 and 30 µM, and colistin was added at a concentration of 1, 5 and 10 µg/mL. One well was the control without EDTA, while another well was the control with EDTA. A custom plate mode program was set up to perform these experiments, detecting fluorescence intensity every two minutes for 30 minutes with shaking (100 rpm) before each reading.

3.17. *In vitro* biofilm inhibition test by crystal violet assay and confocal laser scanning microscopy

In vitro biofilm inhibition test in U-bottom 96-well plate was performed as follows (Pellegrini *et al*., 2022). An overnight bacterial culture grown in TSB was diluted in fresh medium to an OD_{600} of approximately 0.05 (about 1×10^8 CFU/mL). 200 µL of the culture were inoculated into the U-bottom 96-well plate and incubated for two hours at 37°C. After the incubation, the culture containing planktonic bacteria was removed and replaced with 200 µL of fresh medium with or without 50 µg/mL of PDSTP. Subsequently, the plate was incubated for 20 hours at 37°C. Finally, biofilm biomass was quantified by crystal violet staining.

For the confocal laser scanning microscopy, an overnight bacterial culture grown in TSB was diluted in fresh medium to an OD_{600} of approximately 0.05. Bacteria were inoculated into the four-well chambered coverslip µ-Slide Glass Bottom (Ibidi) for two hours at 37°C. After the incubation, the culture containing non-adhered bacteria was removed and replaced with fresh TSB medium with or without 25-50 µg/mL of PDSTP. After overnight incubation, the supernatant was removed, biofilms were washed with PBS twice and stained with 1 µM Syto9. Biofilms were visualized with a Leica TCS SP8 confocal microscope, equipped with a 63x oil immersion objective (HC Pl Apo CS2 63x oil/1.4, Leica). A 488 nm laser line was used to excite Syto9 and the emission was collected between 500 and 550 nm. Three snapshots were acquired at different positions in the confocal field of each chamber. The Z-slices were obtained every 0.3 µm. For visualization and processing of images, ImageJ was employed. Thickness, biomass, roughness coefficient and biofilm distribution were analyzed using the COMSTAT2 software (Heydorn *et al*., 2000).

3.18. *Ex vivo* pig lung dissection, infection and bacterial count determination

Pig lungs were supplied by a local butcher. *Ex vivo* pig lung (EVPL) tissue was dissected on the day of arrival to collect the bronchioles, as previously described (Heydorn *et al*., 2000). EVPL was sterilized by UV light and square pieces were placed into a 24-well plate with UV-sterilized 0.8% agarose pads.

An overnight bacterial culture grown in TSB was diluted to an OD_{600} of approximately 0.05. 2 µL of the culture were spotted onto the tissue, while 2 µL of SCFM were spotted onto the tissue as negative control. To further mimic the CF lung environment, 500 µL SCFM were supplemented to each well. The 24-well plate was incubated statically for two hours at 37°C. After the incubation, the medium was removed and replaced with 500 µL of fresh SCFM with or without 25-50 µg/mL of PDSTP. Ciprofloxacin (0.06 µg/mL) was used as positive control. The 24-well plate was incubated overnight at 37°C. The following day, tissues were removed from the wells, washed with 500 µL of PBS and transferred in homogenization tubes (Fisherbrand) containing 5 mm glass beads (Merck) and 500 µL of PBS. Minilys Homogenizer (Bertin) was used to homogenize samples for 20 seconds at 15 m/s. Tissue homogenates were serially diluted and plated to calculate the number of CFU/mL.

3.19. Wastewater processing for phage isolation

Wastewater samples were collected in Glenelg (South Australia), stored at 4°C and processed in two days (Camens *et al*., 2021). Aliquots of 50 mL were centrifuged at 4400 rpm for 10 minutes at 4°C and supernatants were filtered (0.22 µm filter) to remove bacteria. Filtered wastewater aliquots were stored at 4°C for further use.

3.20. Phage screening and isolation

To screen for the presence of *P. aeruginosa* PA01 phages, the double layer agar method was performed (Camens *et al*., 2021). 100 µL of filtered wastewater samples were mixed with 100 µL of an overnight *P. aeruginosa* PA01 culture and 4 mL of molten 0.4% TSA. The mixture was then poured onto a 1.5% TSA plate and incubated overnight at 37°C. Following overnight incubation, phage plaques were picked with a cotton swab and collected into vials containing sodium magnesium buffer (SM buffer) (50 mM Tris-HCl pH 7.5, 100 mM NaCl, 8 mM MgSO4, 0.01% gelatine).

3.21. Phage propagation

A small-scale propagation of phages was first performed (Camens *et al*., 2021). *P. aeruginosa* PA01 was grown in 5 mL of TSB**,** infected during the log-phase of growth with 100 µL of the phage and incubated overnight at 37°C (200 rpm). After overnight incubation, the mixture was centrifuged at 4400 rpm for 10 minutes, the supernatant was filtered to remove bacteria and phage titration was performed (see below) prior to large-scale propagation.

For large-scale phage propagation (Camens *et al*., 2021), *P. aeruginosa* PA01 was grown in 50 mL of TSB, infected during the log-phase of growth with phages at a MOI of 1 phage per bacterial cell and incubated overnight at 37°C (200 rpm). After overnight incubation, the mixture was treated as described for the small-scale propagation, followed by phage titration.

3.22. Phage titration

The number of PFUs/mL was determined using the double layer agar spot method (Camens *et al*., 2021). 100 µL of an overnight *P. aeruginosa* PA01 culture were mixed with 4 mL of molten 0.4% TSA and poured onto a 1.5% TSA plate. Phages were diluted in SM buffer, spotted in triplicate on the agar plate and incubated overnight at 37°C. The following day, plaques were counted and the phage titer was calculated.

3.23. Phage morphology

Transmission electron microscopy was performed to determine the phage morphology, using a modified protocol (Ackermann, 2009). 5 µL of the phage stock (approximately 1 x 10^{10} PFU/mL) were placed on the coated side of a carbon/formvar grid (ProSciTech) and incubated for two minutes at room temperature. After the incubation, the grid was washed twice with water, 5 µL of the negative stain 2% uranyl acetate were added and the grid was incubated for one minute at room temperature. Stain excess was removed and samples were analysed by a FEI Tecnai G2 Spirit 120 kV TEM (FEI Technologies).

3.24. Phage DNA extraction

Phage DNA extraction was performed using the Phage DNA Isolation Kit (Norgen Biotek Corp), following the instructions of the manufacturer. Briefly, 1 mL of the phage stock (approximately 1 x 10^{10} PFU/mL) was treated with 20 U of RNase-free DNase I at room temperature for 15 minutes, followed by inactivation of the enzyme by incubation at 75°C for 5 minutes. In this way, bacterial DNA was degraded. 500 µL of Lysis Buffer B were added and samples were vortexed for 10 seconds. 4 µL of 20 mg/mL proteinase K were added and incubated at 55°C for 30 minutes to increase DNA yield. Samples were incubated at 65°C for 15 minutes, mixing them a few times during incubation. 320 µL of isopropanol were added and samples were mixed to precipitate the DNA. The lysate was applied to the column and centrifuged for one minute at 8000 rpm. The column was washed three times with 400 µL of Wash Solution A and centrifuged for one minute at 8000 rpm. To completely dry the column, a spin for two minutes at 14,000 rpm was performed. Finally, DNA was eluted adding 75 µL of Elution Buffer B to the column and centrifuging for one minute at 8000 rpm.

3.25. Phage genome sequencing, assembly and annotation

The Rapid Barcoding Kit (Oxford Nanopore Technology, SQK-RBK 110.96) was used to sequence the phage genome on Oxford Nanopore Technologies R9.4.1 MinION flowcells with 50 ng of DNA. Base-calling was done with the Guppy software v 6.2.11 in super accuracy mode, with the 'dna_r9.4.1_450bps_sup.cfg' file as configuration.

Phage genome assembly was conducted with Spae (https://github.com/linsalrob/spae). Namely, reads were filtered with Filtlong v0.2.1 (https://github.com/rrwick/Filtlong) keep all reads over 1000 bp. All reads were then assembled with Flye v2.9.2 (Kolmogorov *et al*., 2019), polished with Medaka v1.7.0 (https://github.com/nanoporetech/medaka) and reoriented to begin with the large terminase subunit with Dnaapler (https://github.com/gbouras13/dnaapler).

Phage genome annotation was conducted with Pharokka v1.2.0 (Bouras *et al*., 2023). Coding sequences (CDS) were predicted with PHANOTATE v1.5 (McNair *et al*. 2019), tRNAs with tRNAscan-SE 2.0 (Chan *et al*., 2021), tmRNAs with Aragorn (Laslett and Canback, 2004) and CRISPRs with CRT (Bland *et al*., 2007). Functional annotation was generated by matching each CDS to the PHROGs (Terzian *et al*., 2021), VFDB (Chen *et al*., 2005) and CARD (Alcock *et al*., 2020) databases using MMseqs2 v13.45111 (Steinegger and Söding, 2017). Contigs were assigned their closest hit in the INPHARED database (Cook *et al*., 2021) using Mash v2.3 (Ondov *et al*., 2016).

3.26. Phage stability (pH, temperature and storage condition)

Phage stability was determined in a wide range of pH values (3, 4, 5, 6, 7, 8, 9, 10, 11 and 12), temperatures (4, 30, 37, 40, 50, 60, 70 and 80°C) and storage conditions (-80°C, -20°C, 4°C and room temperature) (Camens *et al*., 2021). For pH stability, the phage stock (approximately 1 x 10^{10} PFU/mL) was diluted 1:10 in SM buffer adjusted at different pH values, subsequently incubated at room temperature for one hour. For temperature stability, aliquots of the phage stock (approximately 1 x 10^{9} PFU/mL) were incubated at different temperatures for one hour. For phage stability in different storage conditions, aliquots of the phage stock (approximately 1 x 10^{10} PFU/mL) were incubated at -80°C, -20°C, 4°C and room temperature for 4 months. Phage titers were determined using the double layer agar spot method.

3.27. Phage adsorption assay

Phage adsorption was performed as previously described (Wannasrichan *et al*., 2022), with modifications. P*. aeruginosa* PA01 was grown in TSB, infected during the mid-log phase of growth with the phage at a MOI of 0.01 phages per bacterial cell and incubated at 37°C. Every 2.5 minutes for 30 minutes, aliquots of the infected culture were collected, centrifuged at 15,000 rpm for two minutes and the number of PFU/mL in the supernatant was determined by the double layer agar spot method. The percentage of unadsorbed phage, for each time point, was normalized on time 0, set at 100%.

3.28. One-step growth curve

One-step growth curve was performed according to the following modified protocol (Wannasrichan *et al*., 2022). P*. aeruginosa* PA01 was grown in TSB, infected during the mid-log phase of growth with the phage at a MOI of 0.01 phages per bacterial cell and incubated at 37°C for 10 minutes. The culture was centrifuged at 4400 rpm for 5 minutes, the pellet was resuspended in fresh medium and incubated at 37°C (200 rpm). Every 10 minutes for 80 minutes, aliquots were collected, centrifuged at 12,000 rpm for 5 minutes and the number of PFU/mL in the supernatant was determined by double layer agar spot method. The burst size was calculated as follows:

$$Burst\ size = \frac{PFUs/mL\ after\ the\ burst}{Initial\ PFUs/mL}$$

3.29. Phage host range determination

The host range of the phage was determined using the double layer agar spot method (Camens *et al*., 2021). 100 µL of an overnight *P. aeruginosa* culture were mixed with 4 mL of molten 0.4% TSA and poured onto 1.5% TSA plates. Phages (approximately 1 x 10^{10} PFU/mL) were diluted in SM buffer, spotted in triplicate on the top layer and incubated overnight at 37°C. After overnight incubation, bacterial strains were classified as sensitive (clear lysis), semi-sensitive (partial lysis) and non-sensitive (no lysis).

3.30. Inhibition assay

Inhibition assay was performed as follows (Hon *et al*., 2022). *P. aeruginosa* PA01 was grown in TSB, infected during the early-log phase of growth with the phage at a MOI of 0, 0.1, 1 and 10 phages per bacterial cell, and incubated at 37°C (200 rpm). Every 30 minutes for 300 minutes (5 hours), the OD_{600} was measured.

3.31. Biofilm formation and biofilm eradication assays

Biofilm formation assay was performed as previously described (Camens *et al*., 2021). 1.0 McFarland bacterial suspension in 0.9% saline was diluted 1:15 in TSB and 150 µL of the resulting suspension were inoculated in a U-bottom 96-well plate. One lane was filled with 150 µL of TSB (control). The plate was incubated for 24 hours at 37°C. After the incubation, biofilm formation was evaluated by crystal violet staining.

For biofilm eradication assay (Camens *et al*., 2021), after the incubation of the plate for 24 hours at 37°C, supernatants were aspired and wells were gently washed with saline three times to remove all the planktonic bacteria. Phages were diluted in 180 µL of TSB to achieve 1 x 10^7, 1 x 10^8 and 1 x 10^9 PFUs and applied to the biofilms in six replicates. One lane was filled with 180 µL of TSB (untreated samples). The plate was incubated for 24 hours at 37°C and biofilm eradication was evaluated by crystal violet staining.

3.32. Isolation of phage-insensitive mutants (BIMs)

The isolation of phage-resistant *P. aeruginosa* PA01 mutants was performed according to the following protocol (Wannasrichan *et al*., 2022), with modifications. P*. aeruginosa* PA01 was grown in TSB, infected during the mid-log phase of growth with the phage at a MOI of 100 phages per bacterial cell and incubated at room temperature for 10 minutes. 100 µL of the infected culture were plated on a 1.5% TSA plate and incubated overnight at 37°C. After overnight incubation, single colonies were isolated at least three times. The double layer agar spot method was used to confirm phage resistance.

3.33. Growth curve

Growth curve was performed as follows. Overnight *P. aeruginosa* cultures were diluted 1:100 in TSB, 200 µL were inoculated into a flat-bottom 96-well plate in triplicate and incubated at 37°C (80 rpm). The OD_{600} was measured every 15 minutes for 720 minutes (12 hours) using SPECTROstar Nano (BMG LABTECH).

3.34. Graphical representations and statistical analyses

GraphPad Prism version 10.0 was employed for generating graphical representations and conducting statistical analyses. Graphical representations depict mean values alongside their corresponding standard deviation. Group differences were assessed using the Student's *t t*est, one-way ANOVA or the Log-rank (Mantel-Cox) test. Statistical significance was established at a threshold of $p < 0.05$.

4. Results

Pt. I: Antivirulence and antibiotic potentiation properties of the dispirotripiperazine derivative PDSTP

4.1. PDSTP has a negligible inhibitory activity against *P. aeruginosa*, *B. cenocepacia* and *S. aureus* growth

The inhibitory activity of PDSTP was tested by broth microdilution method in CAMHB and TSB or LB against *P. aeruginosa* PA01 and nine CF clinical isolates, *B. cenocepacia* K56-2 and J2315, and *S. aureus* ATCC 25923. Considering the size and positive charge of PDSTP, the compound should not be able to enter bacterial cells (Egorova *et al*., 2021). Indeed, PDSTP showed a negligible inhibitory effect on the growth of all strains (Table 4.1).

Table 4.1. Minimum inhibitory concentrations of PDSTP for *P. aeruginosa* PA01 and nine CF clinical isolates, *B. cenocepacia* K56-2 and J2315, and *S. aureus* ATCC 25923 in CAMHB and TSB (for *P. aeruginosa* and *S. aureus*) or LB (for *B. cenocepacia*).

Bacterial strain	CAMHB (μg/mL)	TSB or LB (μg/mL)
P. aeruginosa PA01	64	256
P. aeruginosa BST44	256	512
P. aeruginosa SG2	128	256
P. aeruginosa NN2	64	256
P. aeruginosa NN83	32	128
P. aeruginosa NN84	64	256
P. aeruginosa RP73	512	> 512
P. aeruginosa RP74	512	512
P. aeruginosa BT2	32	256
P. aeruginosa BT72	32	128
B. cenocepacia K56-2	> 512	> 512
B. cenocepacia J2315	> 512	> 512
S. aureus ATCC 25923	32	512

4.2. PDSTP impairs *P. aeruginosa*, *B. cenocepacia* and *S. aureus* adhesion to human pulmonary epithelial cells

To investigate the potential antiadhesive properties of PDSTP, adhesion assays by plate counting were performed. Prior to these experiments, the MIC of PDSTP for *P. aeruginosa* PA01 was determined in the growing media of human cells and corresponded to 64 and 128 μg/mL in DMEM and MEM, respectively. Indeed, PDSTP partially impaired bacterial growth when adhesion assays were performed at 37°C. Consequently, infected monolayers were incubated at 4°C to arrest bacterial growth (Berlutti *et al*., 2008), thus avoiding PDSTP-mediated growth impairment, even when the compound was present at high concentrations (data not shown). The adhesion of *P. aeruginosa* PA01 to A549 lung epithelial cells was impaired in a dose-dependent manner when increasing concentrations of PDSTP, ranging from 1 to 400 μg/mL, were administered. Remarkably, a significant reduction in bacterial adhesion of 41.4%, compared to the control, was already observed when cells were treated with 10 μg/mL of the compound. Moreover, nearly complete inhibition of bacterial adhesion was achieved with 400 μg/mL of compound, resulting in a 95.9% reduction, compared to the control (Figure 4.1).

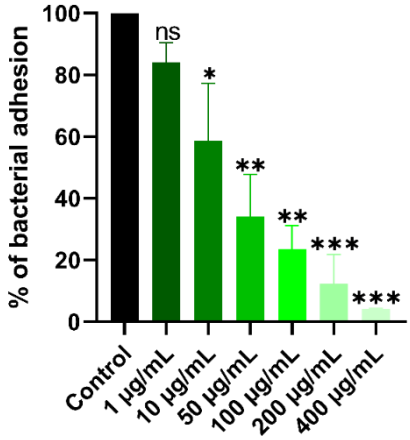

Figure 4.1. Differential adhesion abilities of *P. aeruginosa* PA01 to A549 cells treated with 1 to 400 μg/mL of PDSTP. The experiment was performed twice, each time in duplicate. Statistically significant differences are indicated (One-way ANOVA test; ns, not significant; *, $p < 0.05$; **, $p < 0.005$; ***, $p < 0.0005$).

At a concentration of 50 μg/mL, PDSTP also affected the adhesion of *P. aeruginosa* PA01 to the 16HBE14o- (with functional CFTR) and CFBE41o- (without functional CFTR) bronchial cell lines, resulting in a reduction of bacterial adhesion of 60.6 and 54.3%, respectively, compared to the control (Figure 4.2).

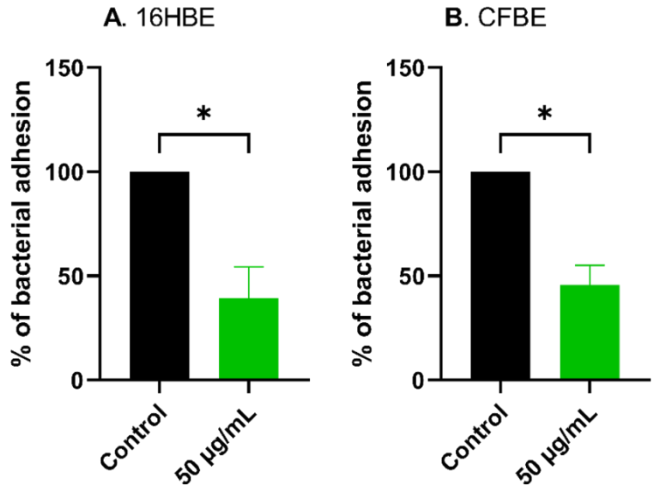

Figure 4.2. Differential adhesion abilities of *P. aeruginosa* PA01 to 16HBE14o- (A) and CFBE41o- (B) cells treated with 50 μg/mL of PDSTP. The experiment was performed twice, each time in duplicate. Statistically significant differences are indicated (Student's *t* test; *, $p < 0.05$).

The antiadhesive activity of PDSTP was evaluated on two hypermucoid *P. aeruginosa* strains derived from the same CF patient but isolated 15 years apart: BT2 (an early isolate) and BT72 (a late isolate). Interestingly, the BT2 strain exhibited a higher level of adhesion to the A549 cell line compared to the BT72 strain (data not shown), a characteristic previously described in longitudinal studies (Hawdon *et al*., 2010). As shown in Figure 4.3A, when treated with 50 and 200 μg/mL of PDSTP, *P. aeruginosa* BT2 adhesion was 22.5 and 7.5% of that observed in the control, respectively. The adhesion of *P. aeruginosa* BT72, instead, was unaffected by 50 μg/mL of PDSTP but, when the concentration of the compound was increased to 200 μg/mL, it resulted in a 65.8% reduction in bacterial adhesion, compared to the control (Figure 4.3B).

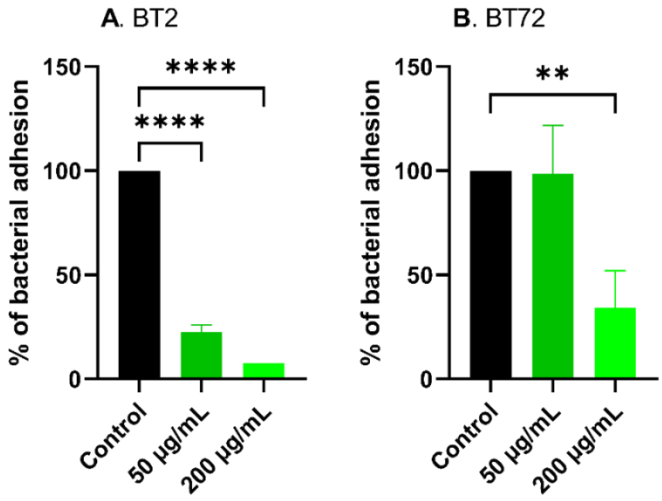

Figure 4.3. Differential adhesion abilities of *P. aeruginosa* BT2 (A) and BT72 (B) to A549 cells treated with 50 and 200 µg/mL of PDSTP. The experiment was performed twice, each time in duplicate. Statistically significant differences are indicated (One-way ANOVA test; **, $p < 0.01$; ****, $p < 0.0001$).

To validate and further characterize the antiadhesive properties of PDSTP, bacterial adhesion was also quantified by imaging flow cytometry. When treated with 50 µg/mL of PDSTP, the adhesion of GFP-expressing *P. aeruginosa* PA01 to A549 cells was reduced of 67.9%, compared to the control (Figure 4.4). This is consistent with the 65.8% reduction in bacterial adhesion reported in Figure 4.1, when the same concentration of the compound was used during adhesion assays by plating adhered bacteria.

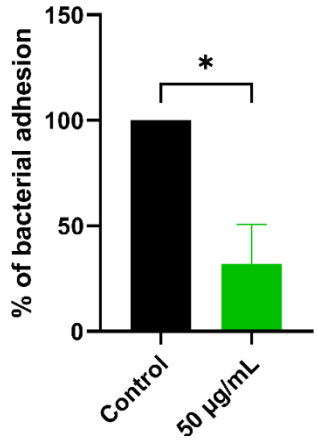

Figure 4.4. Differential adhesion abilities of GFP-expressing *P. aeruginosa* PA01 to A549 cells treated with 50 µg/mL of PDSTP. The experiment was performed twice, each time in duplicate. Statistically significant differences are indicated (Student's *t* test; *, $p < 0.05$).

Imagin flow cytometry also allows to perform software-based analyses of fluorescent spots of single-cell images (Figure 4.5).

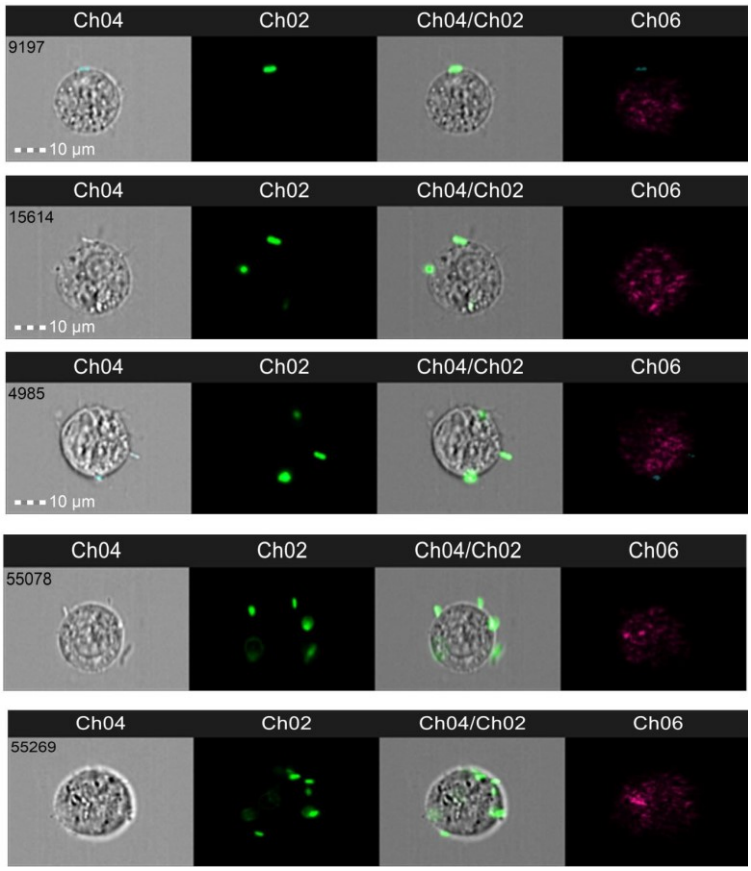

Figure 4.5. Representative images of A549 cells infected with GFP-expressing *P. aeruginosa* PA01. Ch04: bright field. Ch02: GFP fluorescence. Ch04/Ch02: superimposition of bright field and fluorescence channels. Ch06: dark field side scatter. Pictures were acquired at 40x magnification using Amnis ImageStreamX Mk II (Cytek).

The software counted the number of fluorescent spots, corresponding to adhered *P. aeruginosa* PA01 bacteria, for each human cell. Data were represented in terms of number of events, i.e., the number of human cells with 1, 2 to 3, 4 to 6 or > 7 adhered bacteria, on a total of 10,000 acquisitions. The majority of control human cells interacted with only one bacterium, with a proportional decrease in the number of events involving a higher number of bacteria. The same trend was observed for cells treated with 50 µg/mL of PDSTP, but with fewer events because of impaired bacterial adhesion (Figure 4.6).

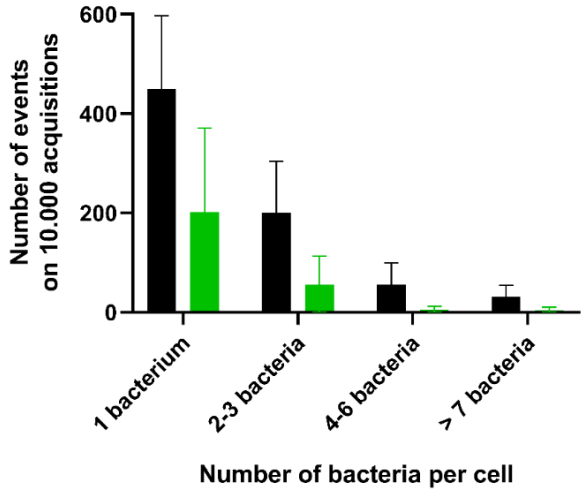

Figure 4.6. Events showing the number of adhered *P. aeruginosa* PA01 bacteria per A549 cell on a total of 10,000 acquisitions of the control (black column) and treatment with 50 μg/mL of PDSTP (green column).

Moreover, when the events were normalized on the total number of human cells with at least one adhered bacterium, it was observed that the compound especially affected multiple bacterial adhesion (Figure 4.7).

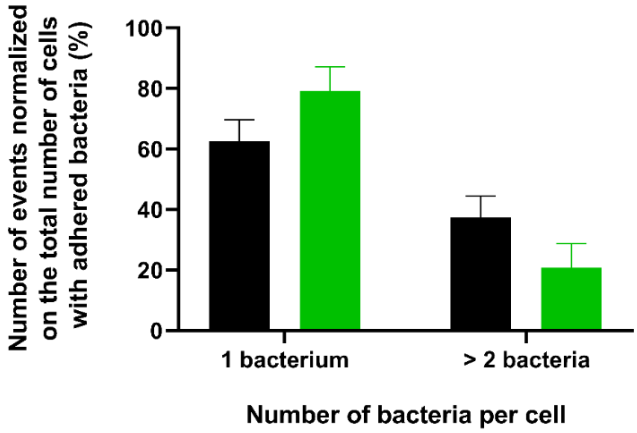

Figure 4.7. Events of adhered *P. aeruginosa* PA01 bacteria per A549 cell on a total of 10,000 acquisitions normalized on the total number of human cells with at least one adhered bacterium of the control (black column) and treatment with 50 μg/mL of the PDSTP (green column), expressed in percentage.

The antiadhesive activity of PDSTP was subsequently explored on *B. cenocepacia*, another Gram-negative bacterium. Specifically, the activity of the compound was tested against the hypervirulent strains *B. cenocepacia* K56-2 and J2315. PDSTP resulted to be ineffective against the K56-2 strain, even at high concentrations (200 µg/mL) (Figure 4.8A). However, the compound was active against the J2315 strain, reducing the adhesion of 60.8 and 76.4% when treated with 50 and 200 µg/mL, respectively, compared to the control (Figure 4.8B).

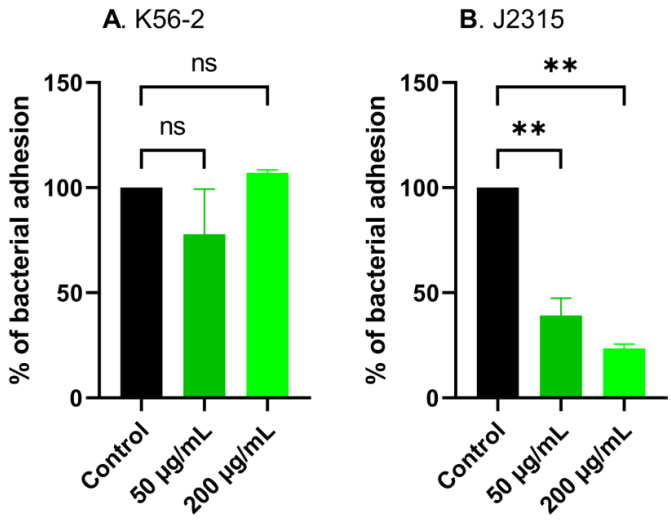

Figure 4.8. Differential adhesion abilities of *B. cenocepacia* K56-2 (A) and J2315 (B) to A549 cells treated with 50 and 200 µg/mL of PDSTP. The experiment was performed twice, each time in duplicate. Statistically significant differences are indicated (One-way ANOVA test; ns, not significant; **, $p < 0.05$).

Finally, the antiadhesive properties of PDSTP were investigated on *S. aureus*, a Gram-positive bacterium. The adhesion of *S. aureus* ATCC 25923 to A549 cells was impaired when treated with 50 and 200 µg/mL of the compound. In particular, adhesion was 20.8 and 8.8% of that observed in the control, respectively (Figure 4.9).

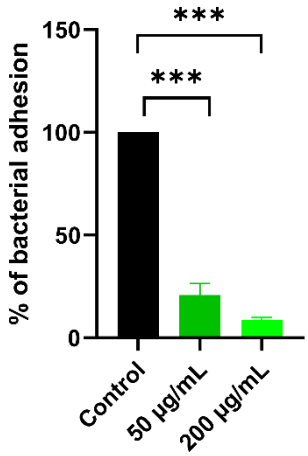

Figure 4.9. Differential adhesion abilities of *S. aureus* ATCC 25923 to A549 cells treated with 50 and 200 µg/mL of PDSTP. The experiment was performed twice, each time in duplicate. Statistically significant differences are indicated (One-way ANOVA test; ***, $p < 0.0005$).

4.3. PDSTP interacts with both human and bacterial cells

To evaluate the mechanism of action of the compound, adhesion assays were performed subsequent to PDSTP pretreatment. In particular, pretreatment was administered to *P. aeruginosa* PA01 at a concentration of 50 µg/mL, to A549 cells at a concentration of 100 µg/mL to saturate heparan-sulphate glycosaminoglycans (HSGAGs), and to both simultaneously. As illustrated in Figure 4.10, pretreatment of *P. aeruginosa* PA01 resulted in a 2.2-fold increase in its adhesion to human cells, compared to the control. This suggests an interaction between PDSTP and bacterial cells since they are washed after the pretreatment, removing non-interacting PDSTP. Considering that PDSTP should not be able to enter bacterial cells (Egorova *et al*., 2021), it is reasonable to hypothesize that the compound interacts with the outer membrane of the bacterium, increasing its positive net charge. This, in turn, may promote electrostatic interactions with negative charges present on the surface of human cells, increasing the adhesion of *P. aeruginosa* PA01 to A549 cells. Furthermore, A549 pretreatment did not lead to a significant reduction in bacterial adhesion to human cells, compared to the control. Finally, double pretreatment resulted in a 62.1% reduction in bacterial adhesion, compared to the control, which is comparable to the adhesion impairment achieved through a standard PDSTP treatment. This may be due to electrostatic repulsion between PDSTP molecules bound to bacteria and those bound to human cells. Given this result, it seems that the antiadhesive properties of PDSTP depend on the interaction of the compound with both bacteria and human cells.

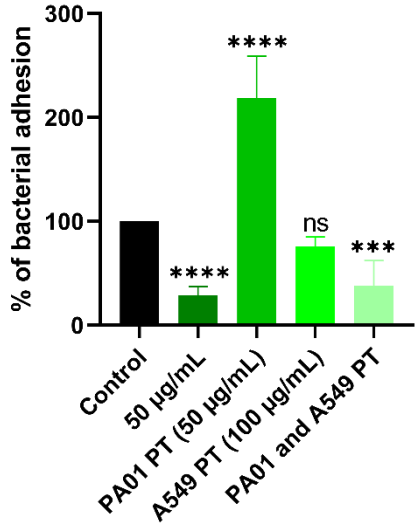

Figure 4.10. Differential adhesion abilities of *P. aeruginosa* PA01 to A549 cells subsequent to PDSTP pretreatment (PT) of the bacteria (50 µg/mL), human cells (100 µg/mL) and both simultaneously. The experiment was performed three times, each time in duplicate. Statistically significant differences are indicated (One-way ANOVA test; ns, not significant; ***, $p = 0.0005$; ****, $p < 0.0001$).

4.4. The mechanism of action of PDSTP does not appear to involve HSGAGs

In the context of viral infections, PDSTP impairs viral adsorption to negatively charged HSGAGs expressed on the surface of human cells by saturating them though electrostatic interactions. This prevents viruses from interacting with this host-cell receptor, thereby avoiding viral infections (Egorova *et al*., 2021). Besides viruses, also bacteria possess the ability to interact with HSGAGs: this has been shown for *P. aeruginosa* (Bucior *et al*., 2012), *B. cenocepacia* (Martin *et al*., 2019) and *S. aureus* (Liang *et al*., 1992). Since PDSTP inhibits the adhesion of these bacteria to human cells (Figures 4.1, 4.3, 4.8 and 4.9), it is plausible to speculate that PDSTP may exhibit a similar mode of action during bacterial infections as it does against viruses. To investigate this hypothesis, adhesion assays were performed using heparin, a structural analogue of heparan-sulphates (Liu and Thorp, 2002). A549 cells were treated with 50 µg/mL PDSTP, 50 µg/mL of heparin and a combination of both compounds (50 µg/mL each). When compared to the control, heparin alone did not affect *P. aeruginosa* PA01 adhesion to human cells, as well as PDSTP and heparin in combination (Figure 4.11). Indeed, the excess of heparin scavenged PDSTP, allowing bacteria to interact with HSGAGs and, consequently, adhere to human cells.

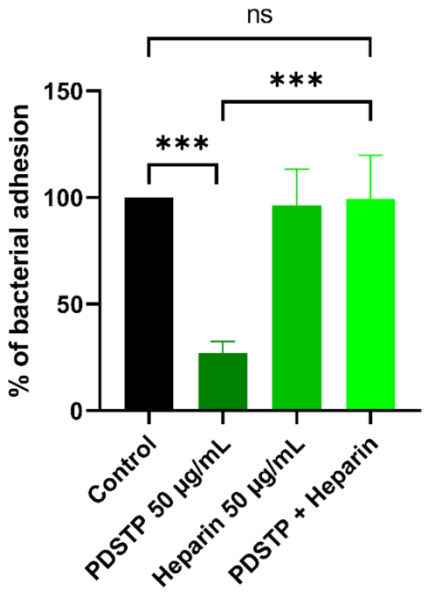

Figure 4.11. Differential adhesion abilities of *P. aeruginosa* PA01 to A549 cells treated with PDSTP (50 µg/mL), heparin (50 µg/mL) and a combination of PDSTP and heparin (50 µg/mL each). The experiment was performed three times, each time in duplicate. Statistically significant differences are indicated (One-way ANOVA test; ns, not significant; ***, $p < 0.001$).

To further evaluate this assumption, adhesion assays were performed after heparinase pretreatment of human cells. Indeed, heparinase hydrolyses the glycosidic bond between N-acetylglucosamine and glucuronic acid, cleaving the HS chains of HSGAGs (Dong *et al*., 2012). In this way, PDSTP can no longer bind to this host-cell receptor. Unexpectedly, *P. aeruginosa* PA01 adhered to both untreated and heparinase-pretreated A549 cells in the same manner. Moreover, treatment with 50 and 200 µg/mL of PDSTP showed the same adhesion impairment trend to cells treated or not with heparinase (Figure 4.12). This experiment was also performed with the CFBE41o- cell line, showing a similar pattern as observed with A549 cells (data not shown). The same result was obtained when using another bacterium, *B. cenocepacia* J2315 (data not shown).

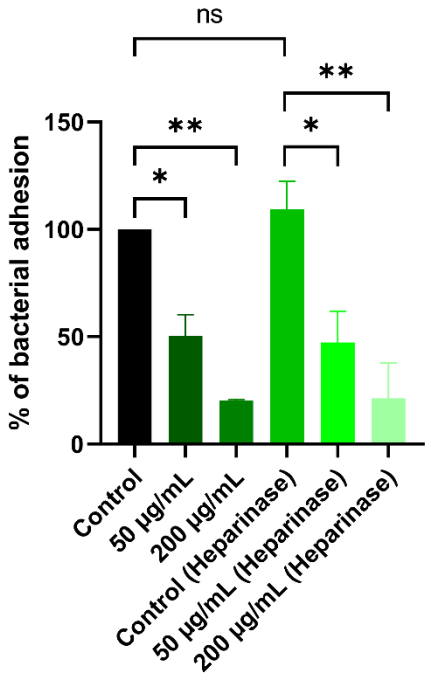

Figure 4.12. Differential adhesion abilities of *P. aeruginosa* PA01 to A549 cells treated with 50 and 200 µg/mL of PDSTP following pre-treatment of the human cells with heparinase III which cleaves the heparan-sulphates. The experiment was performed twice, each time in duplicate. Statistically significant differences are indicated (One-way ANOVA test; ns, not significant; *, $p < 0.05$; **, $p < 0.005$).

Adhesion assays to cells pretreated with heparinase were also performed after pretreatment of *P. aeruginosa* PA01 with PDSTP. Pretreatment of the bacterium resulted in a significant increase in its adhesion to human cells, compared to the control, as previously described (Figure 4.10). However, when heparinase pretreated A549 cells were challenged with *P. aeruginosa* PA01 pretreated with PDSTP, the adhesion of the bacterium was identical to that of the control, i.e., human cells pretreated with heparinase and challenged with *P. aeruginosa* (Figure 4.13).

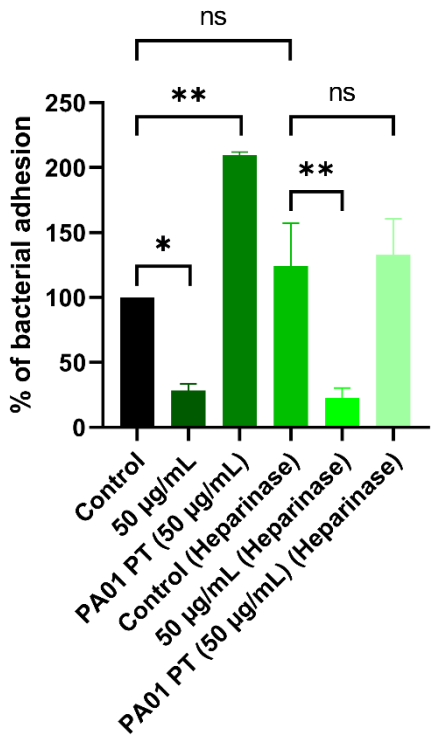

Figure 4.13. Differential adhesion abilities of *P. aeruginosa* PA01 treated and pretreated (PT) with 50 µg/mL of PDSTP following A549 cell pretreatment with heparinase III. The experiment was performed twice, each time in duplicate. Statistically significant differences are indicated (One-way ANOVA test; ns, not significant; *, $p < 0.05$; **, $p < 0.01$).

P. aeruginosa has evolved to recognize HSGAGs as host-cell receptors (Bucior *et al*., 2012). However, they are not the only receptors involved in the adhesion of this bacterium to human cells (de Bentzmann *et al*., 1996). Considering the obtained results, it is likely that HSGAGs are not the primary receptors mediating bacterial adhesion, as their cleavage did not affect it, neither in the presence nor in the absence of PDSTP. This implies that the mechanism of action of the compound is different for bacterial infections compared to those of viruses. Finally, a possible explanation for the reduced adhesive capabilities of *P. aeruginosa* PA01 pretreated with PDSTP and infecting heparinase-pretreated A549 cells is that the negative charges of HSGAGs become particularly important when the bacterium is saturated by positively charged PDSTP, promoting interactions between the bacterium and human cells. Consequently, cleavage of these receptors results in reduced bacterial adhesion to human cells.

4.5. PDSTP interacts with the lipopolysaccharide of Gram-negative bacteria

Considering that PDSTP interacts with bacterial cells (Figure 4.10) and is positively charged (Egorova *et al*., 2021), it is plausible that electrostatic forces play a role in the interaction between PDSTP and *P. aeruginosa* PA01. To explore this hypothesis, PDSTP binding assays were performed. Specifically, bacteria were treated with PDSTP and then washed to remove non-interacting PDSTP. Subsequently, interacting PDSTP was displaced from the surface of the bacterium using an excess of sodium chloride and detected through spectrophotometry at λ = 370 nm in the supernatant. This result implies that electrostatic interactions are involved in this process (Figure 4.14). Furthermore, a calibration curve was used to extrapolate the concentration of bound PDSTP (y = 0.01x + 0.0109 R^2 = 0.9995). This allowed not only to estimate the percentage of interacting PDSTP, corresponding to approximately 2.12%, but also the number of molecules of the compound interacting with a single bacterial cell, through the Avogadro's number and the CFU/mL, which corresponded to about 4.35 x 10^7 PDSTP molecules per bacterium.

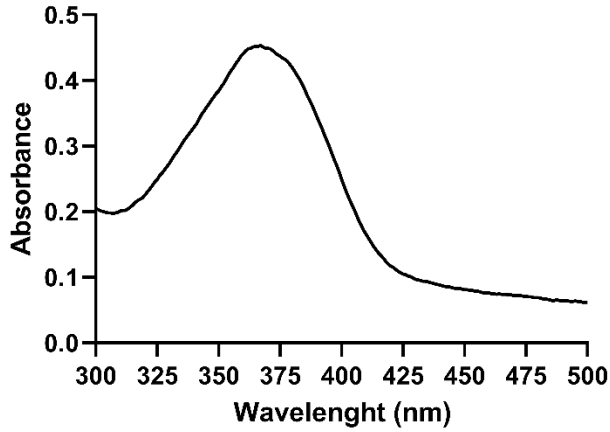

Figure 4.14. PDSTP binding assay of *P. aeruginosa* PA01. PDSTP absorbs light at λ = 370 nm, allowing its detection spectrophotometrically. The experiment was performed three times. Data from a single representative experiment are reported.

To further characterize the interaction between PDSTP and the outer membrane of *P. aeruginosa* PA01, a phase-contrast microscopy analysis was performed. Upon treatment with 50 μg/mL of PDSTP, there was an alteration in the morphology of the bacterium, transitioning from a rod-shaped to a more spherical shape (Figure 4.15), providing visual evidence of the interaction of the compound with the bacterial outer membrane.

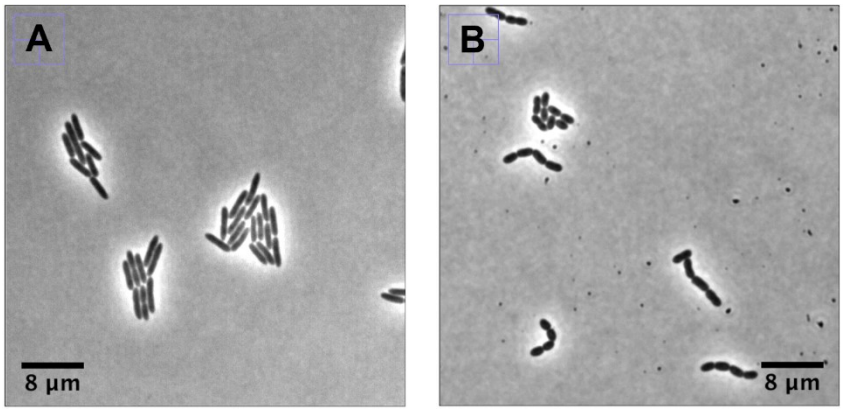

Figure 4.15. Representative phase-contrast micrographs of *P. aeruginosa* PA01 untreated (A) and treated with 50 µg/mL of PDSTP (B). The experiment was performed twice.

The lipopolysaccharide (LPS) is the primary structural component of the external leaflet of the outer membrane of Gram-negative bacteria. The core oligosaccharide and the O-antigen of *P. aeruginosa* LPS carry negative charges due to the presence of phosphate groups (Huszczynski *et al*., 2019). Given that PDSTP interacts with the outer membrane of the bacterium through electrostatic interactions, it is reasonable that these may occur between the compound and the LPS. To investigate this possibility, dansyl-polymyxin (DPX) binding assays were performed on *P. aeruginosa* PA01. DPX is a fluorescent dye that shows a strong increase in fluorescence upon binding to the LPS. Therefore, the displacement of DPX correlates with a decrease in fluorescence intensity (Akhoundsadegh *et al*., 2019). By increasing PDSTP concentration from 0 to 115 µM, there was a dose-dependent reduction in DPX fluorescence (Figure 4.16A). The same trend was observed by displacing DPX with colistin, used as a positive control due to its analogy with DPX (Akhoundsadegh *et al*., 2019) (Figure 4.16B). The I_{50}, representing the concentration required for 50% displacement of DPX, provides insights into the relative affinity of a specific compound for LPS. For PDSTP, the I_{50} value corresponded to 18.09 µM (17 µg/mL), while for colistin it was 23.91 µM (28 µg/mL). Consequently, PDSTP showed a higher relative affinity for LPS compared to colistin. This experimental outcome validates the interaction between PDSTP and LPS. Furthermore, since DPX interacts with the negative charges of both lipid A and core-oligosaccharide in *P. aeruginosa* PA01 (Moore *et al*., 1986), PDSTP-mediated displacement of DPX implies that the compound recognizes those negative charges with higher affinity.

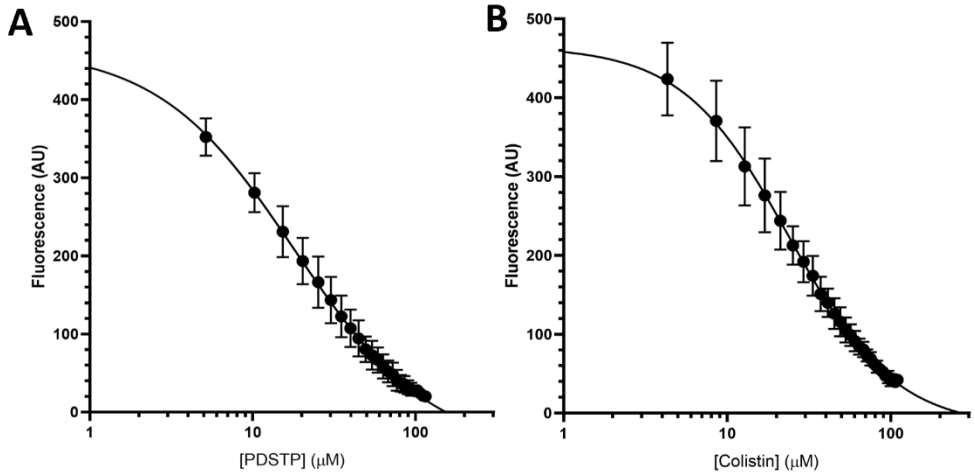

Figure 4.16. Dansyl-polymyxin binding assays on *P. aeruginosa* PA01. LPS displacement was assessed for PDSTP (A) and colistin (B) as a positive control. The experiment was performed four times.

As previously described, when the antiadhesive properties of PDSTP were evaluated on *B. cenocepacia*, the compound resulted to be ineffective against the K56-2 strain but active against the J2315 strain (Figure 4.8). This disparity may be due to differences in the structure of their LPS. According to the literature, *B. cenocepacia* K56-2 produces the O-antigen through to the expression of glycosyltransferase WbxE, whereas *B. cenocepacia* J2315 carries an insertion sequence within the *wbxE* gene, impairing the formation of the O-antigen (Ortega *et al*., 2005). Consequently, the presence of the O-antigen in the K56-2 strain may be associated with its resistance to PDSTP. To explore this assumption, *B. cenocepacia* MH1K ΔOAg and an O-antigen producing strain of *B. cenocepacia* J2315 were employed. In detail, *B. cenocepacia* MH1K ΔOAg is a deletion mutant of the K56-2 strain, lacking a portion of the O-antigen gene cluster and therefore incapable of producing the O-antigen (Hanuszkiewicz *et al*., 2014). On the other hand, *B. cenocepacia* J2315 was transformed with the pXO4 plasmid which derives from the cloning of the *wbxE* gene into the pSCRhaB3 plasmid, allowing the production of the O-antigen (Ortega *et al*., 2005).

The LPS structures of these strains were confirmed by separating the components of purified LPS using SDS polyacrylamide gel electrophoresis and silver-staining. In particular, the LPS profiles of *B. cenocepacia* J2315, J2315 carrying the empty pSCRhaB3 plasmid, J2315 bearing the pXO4 plasmid, K56-2 and MH1K ΔOAg were analysed. Upon silver staining, LPS components appeared as typical ladder-like bands. Specifically, both *B. cenocepacia* J2315 and J2315 carrying the empty pSCRhaB3 plasmid showed the same LPS profile, characterized by three bands corresponding to the lipid A-core oligosaccharide. In contrast, the J2315 strain bearing the pXO4 plasmid had a smaller lipid A-core oligosaccharide compared to the other J2315 LPS, represented by just one band, but produced an O-antigen of eleven bands. On the other hand, *B. cenocepacia* K56-2 had a LPS characterized by a lipid A-core oligosaccharide consisting of two bands and an O-antigen with eleven bands. Differences in number and size of LPS components may be attributed to genomic diversity between the two *B. cenocepacia* strains, although they are closely related. Finally, *B. cenocepacia* MH1K ΔOAg lacked the O-antigen and showed a lipid A-core oligosaccharide with two bands, even though it appeared to be different in size compared to that of the K56-2 strain (Figure 4.17).

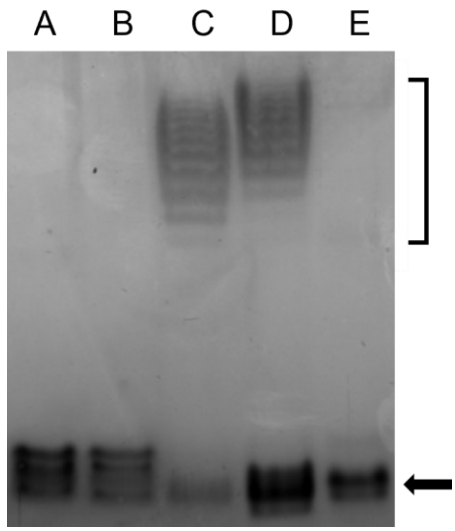

Figure 4.17. Electrophoretic profiles of LPS extracted from *B. cenocepacia* J2315 (A), J2315 carrying either the empty pSCRhaB3 plasmid (B) or the pXO4 plasmid (C), K56-2 (D) and MH1K ΔOAg (E). LPS components appears as ladder-like bands. The bracket indicates the O-antigen, while the arrow shows the lipid A-core oligosaccharide. The experiment was performed twice.

After confirming the LPS structures of the strains, adhesion assays were performed. As illustrated in Figure 4.18, the antiadhesive activity of PDSTP was restored using the *B. cenocepacia* K56-2 strain that does not produce the O-antigen (MH1K ΔOAg), resulting in a 58.1% reduction in bacterial adhesion to A549 cells, compared to the control.

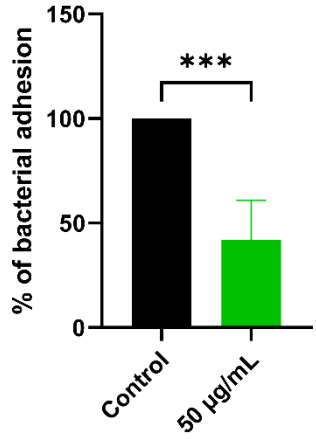

Figure 4.18. Differential adhesion abilities of *B. cenocepacia* MH1K ΔOAg to A549 cells treated with 50 µg/mL of PDSTP. The experiment was performed four times, each time in duplicate. Statistically significant differences are indicated (Student's *t* test; ***, $p < 0.001$).

In the complementary experiment, the adhesion of *B. cenocepacia* J2315 bearing the empty pSCRhaB3 plasmid to A549 cells was affected when treated with 50 and 200 µg/mL, showing a reduction of 59.2 and 64.4%, respectively, compared to the control. This is consistent with the reduction in bacterial adhesion previously observed for wild-type *B. cenocepacia* J2315 (Figure 4.8). However, when *B. cenocepacia* J2315 produced the O-antigen (bearing the pXO4 plasmid), it exhibited resistance to PDSTP, even at high concentrations (200 µg/mL) (Figure 4.19).

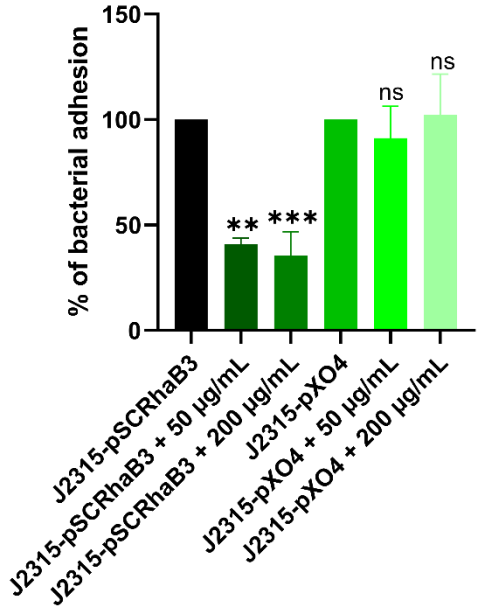

Figure 4.19. Differential adhesion abilities of *B. cenocepacia* J2315 carrying either the empty pSCRhaB3 plasmid or the pSCRhaB3 plasmid bearing the gene encoding the glycosyltransferase WbxE (pXO4 plasmid) to A549 cells treated with 50 and 200 µg/mL of PDSTP. The experiment was performed twice, each time in duplicate. Statistically significant differences are indicated (One-way ANOVA test; ns, not significant; **, $p < 0.005$; ***, $p < 0.001$).

According to the literature, *P. aeruginosa* PA01 LPS presents a complete LPS with the O-antigen (Sadovskaya *et al*., 1998). As shown in Figure 4.20, this was validated also for the strain used in these experiments. In particular, *P. aeruginosa* PA01 had an LPS characterized by a lipid A-core oligosaccharide consisting of eight bands and an O-antigen with eleven bands.

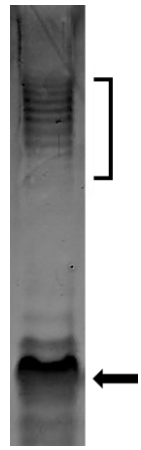

Figure 4.20. Electrophoretic profile of LPS extracted from *P. aeruginosa* PA01. LPS components appear as ladder-like bands. The bracket indicates the O-antigen, while the arrow shows the lipid A-core oligosaccharide. The experiment was performed twice.

This is interesting because, differently from O-antigen producing *B. cenocepacia* K56-2 (Figure 4.8), *P. aeruginosa* PA01 resulted sensitive to PDSTP antiadhesive activity (Figures 4.1 and 4.2).

Since PDSTP interacts with the negative charges of both lipid A and core-oligosaccharide, PDSTP-mediated resistance may be ascribed to the O-antigen shielding of the compound in *B. cenocepacia*. In contrast, the presence of O-antigen does not confer resistance to PDSTP in *P. aeruginosa* PA01.

4.6. PDSTP potentiates the activity of antibiotics against *P. aeruginosa*

Combination therapy involves the use of antibiotics in conjunction with compounds that either increase their intracellular concentration or allow the overcoming of antibiotic resistance (Wang *et al*., 2020). To evaluate whether PDSTP potentiates the activity of antibiotics currently employed for treating *P. aeruginosa* infections, antibiotic combination susceptibility assays were performed. Specifically, antibiotics with different mechanisms of action were selected, including amikacin, ceftazidime, ciprofloxacin, colistin, meropenem and tobramycin. These antibiotics were then combined with PDSTP and tested against the *P. aeruginosa* PA01 strain. For these experiments, the compound was administered at a concentration of 25 μg/mL which corresponds to approximately half of the MIC in CAMHB (Table 4.1). As indicated in Table 4.2, combination of PDSTP with the tested antibiotics resulted in a reduction of the MICs, ranging from 2 to 128-fold. In particular, PDSTP did not lead to a significant increase in the efficacy of tobramycin (2-fold decrease in the MIC), while an adjuvant activity was observed for the other antimicrobials, especially ceftazidime (128-fold decrease in the MIC).

Table 4.2. Minimum inhibitory concentrations in CAMHB of six antibiotics and those of their combinations with PDSTP against the *P. aeruginosa* PA01 strain.

P. aeruginosa PA01	Susceptible	Intermediate	Resistant	MIC	MIC + PDSTP	Fold reduction
Amikacin	≤ 16 µg/mL	32 µg/mL	≥ 64 µg/mL	4 µg/mL	1 µg/mL	4x
Tobramycin	≤ 4 µg/mL	8 µg/mL	≥ 16 µg/mL	0.5 µg/mL	0.25 µg/mL	2x
Ceftazidime	≤ 8 µg/mL	16 µg/mL	≥ 32 µg/mL	2 µg/mL	0.0156 µg/mL	128x
Meropenem	≤ 2 µg/mL	4 µg/mL	≥ 8 µg/mL	1 µg/mL	0.0625 µg/mL	16x
Ciprofloxacin	≤ 0.5 µg/mL	1 µg/mL	≥ 2 µg/mL	0.125 µg/mL	0.0078 µg/mL	16x
Colistin	-	≤ 2 µg/mL	≥ 4 µg/mL	1 µg/mL	0.0625 µg/mL	16x

MIC breakpoints used to classify *P. aeruginosa* as susceptible, intermediate or resistant to antibiotics are reported. MIC values classifying the bacterium as susceptible are depicted in green, those related to intermediate antibiotic profiles are reported in orange and those corresponding to resistant antibiotic profiles are indicated in red. The respective fold reduction is shown. The experiment was performed three times.

Subsequently, antibiotic combination susceptibility assays were performed on nine strains of multidrug-resistant *P. aeruginosa* isolated from CF patients (BST44, SG2, NN2, NN83, NN84, RP73, RP74, BT2 and BT72), focusing on those antimicrobials that exhibited an intermediate or resistant profile according to the Clinical and Laboratory Standard Institute (CLSI) guidelines (CLSI, 2020). Also for these experiments, PDSTP was administered at a concentration of approximately half of the MIC determined for each bacterium in CAMHB (Table 4.1), i.e., 100 µg/mL for BST44, 50 µg/mL for SG2, 25 µg/mL for NN2,15 µg/mL for NN83, 25 µg/mL for NN84, 200 µg/mL for RP73 and 200 µg/mL for RP74. As reported in Table 4.3, combination of PDSTP with the tested antibiotics resulted in an overall increased activity. For ciprofloxacin and tobramycin, the MIC reduction did not go beyond 2-fold for each strain. Amikacin only resulted in a 4-fold decrease in the MIC against the SG2 strain. Similar to the PA01 strain (Table 4.2), combination of PDSTP with ceftazidime showed the most significant effect, resulting in a substantial reduction in the MICs of all the isolates, up to 128-fold. Lastly, meropenem combined with PDSTP showed a significantly increased activity against each tested strain, up to 32-fold, confirming the promising combination between the compound and β-lactams. In general, all the tested clinical isolates displayed resistance to at least two antibiotics. Two strains were even resistant to four antimicrobials (NN84 and RP74). In most cases, PDSTP was effective at resensitizing the clinical isolates that exhibited a resistant antibiotic profile, particularly against meropenem (4/4 strains), ceftazidime (6/7 strains) and amikacin (4/6 strain), while one isolate showed partial resensitization from a resistant to an intermediate antibiotic profile (amikacin for RP73).

Table 4.3. Minimum inhibitory concentrations in CAMHB of five antibiotics and those of their combinations with PDSTP against seven multidrug-resistant *P. aeruginosa* isolated from CF patients.

		BST44	SG2	NN2	NN83	NN84	RP73	RP74
Amikacin	MIC		64 µg/mL	32 µg/mL	256 µg/mL	32 µg/mL	64 µg/mL	32 µg/mL
	MIC + PDSTP		16 µg/mL	16 µg/mL	128 µg/mL	16 µg/mL	32 µg/mL	16 µg/mL
	Fold reduction		4x	2x	2x	2x	2x	2x
Tobramycin	MIC		8 µg/mL	>256 µg/mL	>256 µg/mL			
	MIC + PDSTP		4 µg/mL	>256 µg/mL	>256 µg/mL			
	Fold reduction		2x					
Ceftazidime	MIC	16 µg/mL	128 µg/mL	16 µg/mL	32 µg/mL	16 µg/mL	32 µg/mL	128 µg/mL
	MIC + PDSTP	1 µg/mL	2 µg/mL	0.125 µg/mL	4 µg/mL	0.5 µg/mL	4 µg/mL	32 µg/mL
	Fold reduction	16x	64x	128x	8x	32x	8x	4x
Meropenem	MIC	16 µg/mL				32 µg/mL	16 µg/mL	16 µg/mL
	MIC + PDSTP	1 µg/mL				1 µg/mL	1 µg/mL	2 µg/mL
	Fold reduction	16x				32x	16x	8x
Ciprofloxacin	MIC					4 µg/mL		16 µg/mL
	MIC + PDSTP					2 µg/mL		8 µg/mL
	Fold reduction					2x		2x

MIC breakpoints used to classify *P. aeruginosa* as susceptible, intermediate or resistant to antibiotics are reported. MIC values classifying the bacterium as susceptible are depicted in green, those related to intermediate antibiotic profiles are reported in orange and those corresponding to resistant antibiotic profiles are indicated in red. The respective fold reduction is shown. The experiment was performed at least three times.

Results

To better investigate the effectiveness of the combinations, time-killing assay were performed in TSB using *P. aeruginosa* PA01. When tobramycin (1 μg/mL), ciprofloxacin (0.0625 μg/mL), ceftazidime (1 μg/mL) and colistin (1 μg/mL) at concentrations equal to half of the respective MIC in TSB (data not shown) were combined with 50 and 200 μg/mL of PDSTP, a significant reduction in bacterial viability was observed, compared to the best treatment with only antibiotics or PDSTP, particularly during the initial hours of treatment. As expected, combinations with 200 μg/mL of PDSTP showed a greater activity compared to those with 50 μg/mL. Specifically, the combination of tobramycin with 50 and 200 μg/mL of PDSTP resulted in a reduction in bacterial viability of up to 3.48 and 4.45 logs in CFU/mL, respectively. On the other hand, 50 and 200 μg/mL of PDSTP combined with ciprofloxacin reduced bacterial viability by up to 2.78 and 4.54 logs, respectively. Since the reductions in CFU/mL after five hours of treatment exceeded 2 logs compared to the most effective individual compound, these combinations were defined as synergistic at the lowest tested concentration of PDSTP. Conversely, the combination of PDSTP with either ceftazidime or colistin did not exhibit synergy, with reductions in CFU/mL of up to 0.72-1.89 logs for ceftazidime and 1.43-1.42 logs for colistin. Interestingly, when 50 μg/mL of PDSTP were administered in combination with the antibiotics, bacterial viability after 24 hours was comparable to the growth control for tobramycin, ciprofloxacin and colistin, and with the antibiotic treatment alone for ceftazidime. In contrast, when antimicrobials were combined with 200 μg/mL of PDSTP, the CFU/mL after 24 hours were significantly lower for each antibiotic except for colistin, especially for ceftazidime (Figure 4.21).

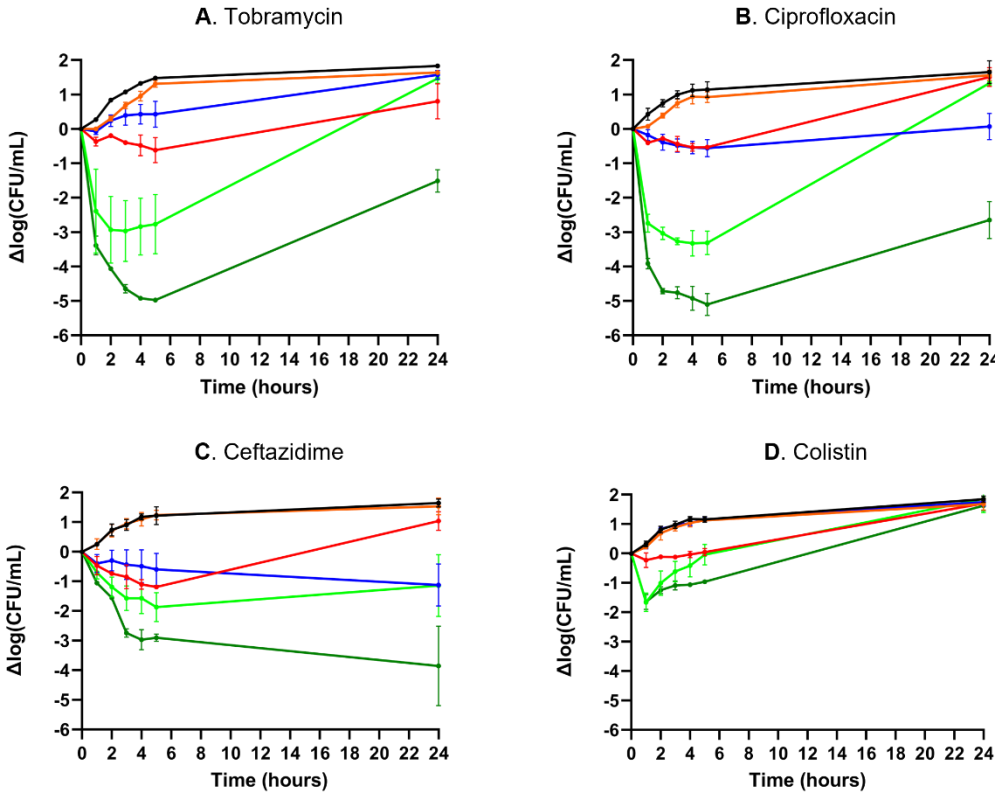

Figure 4.21. Time-killing assays of *P. aeruginosa* PA01 treated with tobramycin (A), ciprofloxacin (B), ceftazidime (C) and colistin (D) combined with 50 and 200 μg/mL of PDSTP. Data are represented in terms of difference in CFU/mL on a logarithmic scale. Black line, untreated sample; orange line, treatment with 50 μg/mL of PDSTP; red line, treatment with 200 μg/mL of PDSTP; blue line, treatment with a concentration equivalent to ½ MIC of the antibiotic; light green line, combination of 50 μg/mL of PDSTP with the antibiotic; dark green line, combination of 200 μg/mL of PDSTP with the antimicrobial. The experiment was performed twice.

Results

To validate the results observed with the PA01 strain (Figure 4.21), time-killing assays were performed in TSB using a plate reader. This allowed to evaluate the efficacy of the same PDSTP-antibiotic combinations against the nine CF clinical isolates of *P. aeruginosa*. In this case, bacterial growth was monitored for 24 hours by measuring the OD_{600}, considering the fair correlation between CFU reduction and OD_{600} variations observed in the time-killing experiments with the PA01 strain (Figure 4.22).

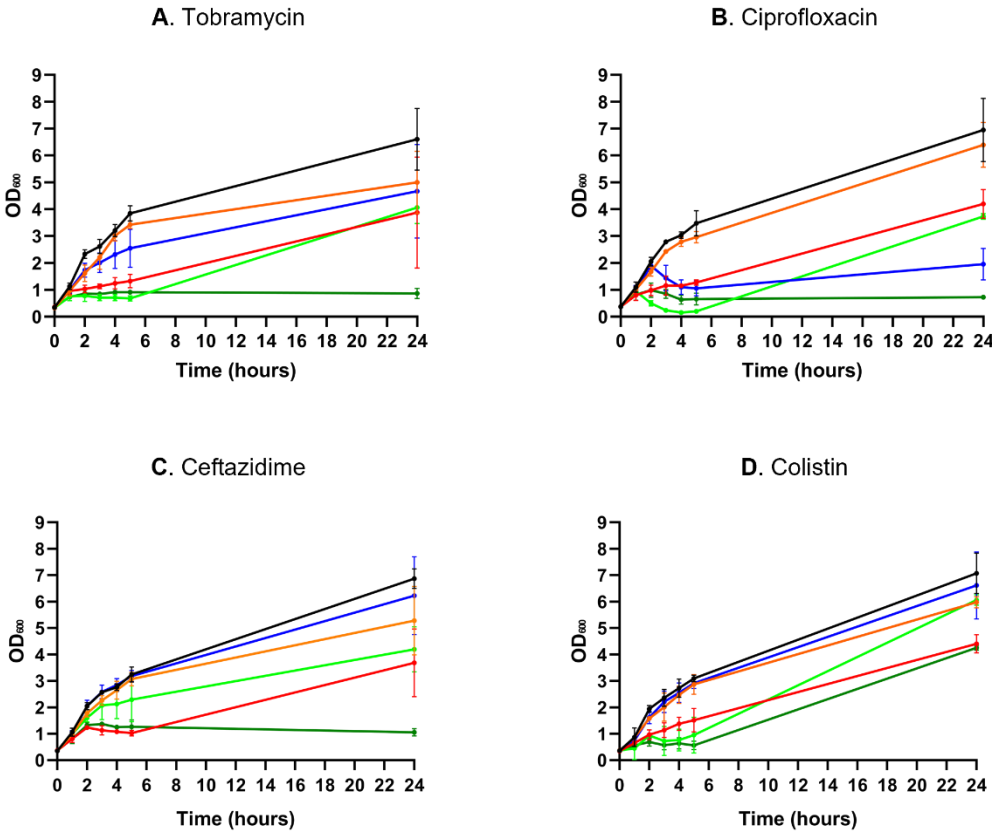

Figure 4.22. Time-killing assays of *P. aeruginosa* PA01 treated with tobramycin (A), ciprofloxacin (B), ceftazidime (C) and colistin (D) combined with 50 and 200 µg/mL of PDSTP. Data are represented in terms of variation of OD_{600}. Black line, untreated sample; orange line, treatment with 50 µg/mL of PDSTP; red line, treatment with 200 µg/mL of PDSTP; blue line, treatment with a concentration equal to ½ MIC of the antibiotic; light green line, combination of 50 µg/mL of PDSTP with the antibiotic; dark green line, combination of 200 µg/mL of PDSTP with the antimicrobial. The experiment was performed twice.

Prior to these experiments, the MIC values of the four antibiotics against the nine *P. aeruginosa* CF clinical isolates were determined (Table 4.4).

Table 4.4. Minimum inhibitory concentrations of ceftazidime, tobramycin, ciprofloxacin and colistin against the nine *P. aeruginosa* CF clinical isolates in TSB.

		BST44	SG2	NN2	NN83	NN84	RP73	RP74	BT2	BT72
MIC (µg/mL)	Ceftazidime	8	64	8	16	16	16	64	4	8
	Tobramycin	8	16	>256	>256	16	32	4	1	4
	Ciprofloxacin	0.25	0.25	1	1	4	1	4	1	0.25
	Colistin	2	0.125	0.5	1	2	2	0.0625	2	1

For these experiments, the concentrations of PDSTP and antibiotics varied for each strain to avoid complete growth inhibition with the monotherapy (Table 4.5). In most cases, these concentrations were approximately half of the MIC values (for ceftazidime, tobramycin and ciprofloxacin, while colistin concentrations were equal to the MIC) (Table 4.4). In this assay, bacterial growth was considered completely inhibited when the increase in OD_{600} did not go beyond 0.3.

Table 4.5. Concentrations of ceftazidime, tobramycin, ciprofloxacin, colistin and PDSTP used in time-killing assays for each of the nine *P. aeruginosa* CF clinical isolates.

	BST44	SG2	NN2	NN83	NN84	RP73	RP74	BT2	BT72
Ceftazidime (µg/mL)	4	32	2	8	12	16	32	1	0.5
Tobramycin (µg/mL)	2	16	32	32	8	8	1	0.75	4
Ciprofloxacin (µg/mL)	0.0156	0.125	0.25	0.25	2	0.25	1	0.0312	0.0312
Colistin (µg/mL)	2	0.125	0.5	1	2	2	0.0625	2	1
PDSTP (µg/mL)	200	200	200	100	200	200	200	200	150

Overall, combination therapies resulted in a significant inhibition of bacterial growth, except for the RP73 and RP74 strains, for which PDSTP failed to synergize with any of the four antibiotics (Figures 4.23-4.26). Therefore, these two strains were considered resistant to the enhancing antibiotic activity of PDSTP. The most promising outcomes were achieved with the combination of PDSTP with ceftazidime which led to complete inhibition of bacterial growth for 24 hours in all *P. aeruginosa* strains, including the highly resistant SG2 strain (Figure 4.23).

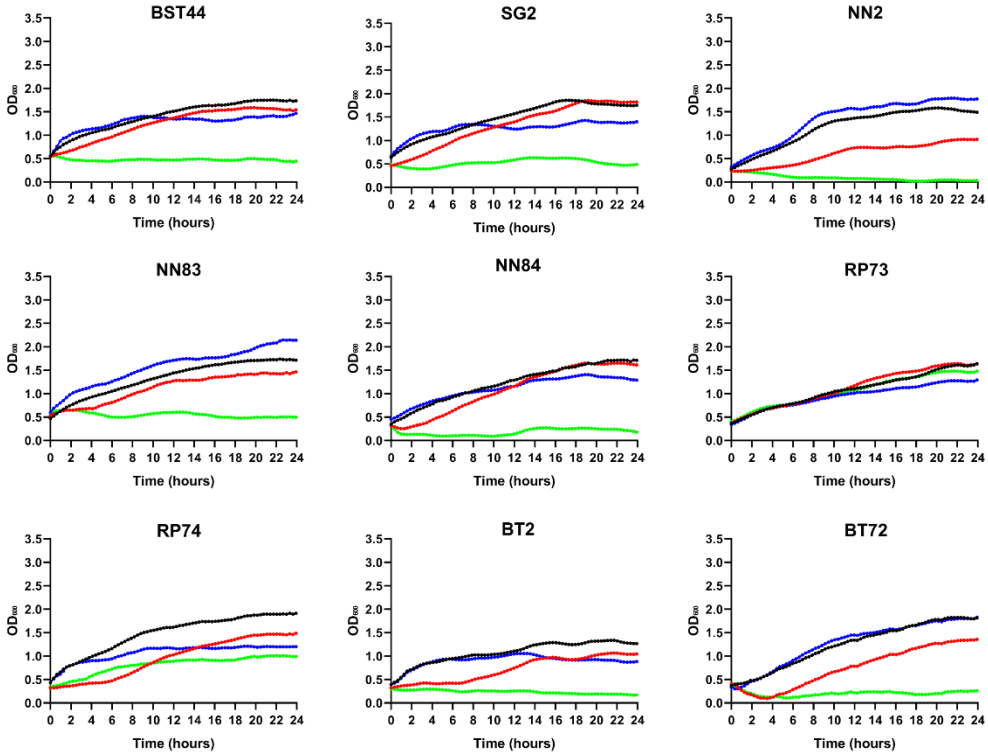

Figure 4.23. Time-killing assays of *P. aeruginosa* CF clinical isolates treated with ceftazidime combined with PDSTP. Data are represented in terms of variation of OD_{600}. Black line, untreated sample; red line, treatment with sub-inhibitory concentrations of PDSTP; blue line, treatment with sub-inhibitory concentrations of ceftazidime; light green line, combination of PDSTP with the antibiotic. The experiment was performed twice, each time in duplicate.

Conversely, the combination with tobramycin exhibited varying efficacy, resulting in 24-hour growth inhibition for the SG2, NN84, BT2 and BT72 strains, but in only 6-hour inhibition for the BST44 strain (Figure 4.24). Additionally, PDSTP could not revert the tobramycin-resistant phenotype of the NN2 and NN83 strains, as previously indicated by antibiotic combination susceptibility testing (Table 4.3).

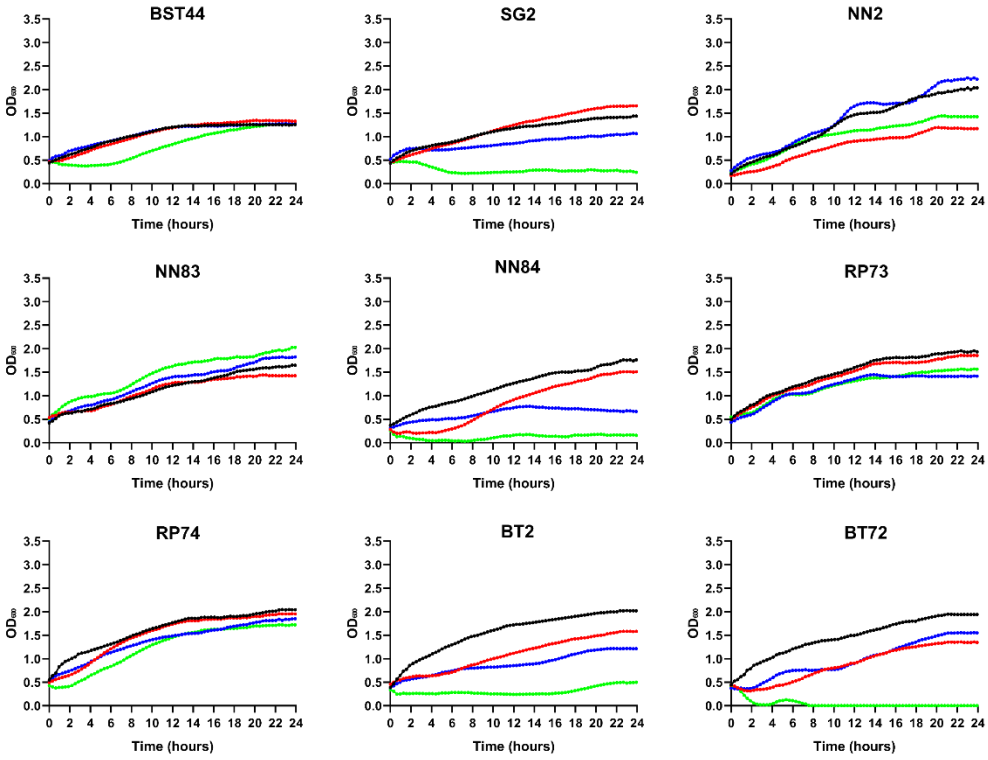

Figure 4.24. Time-killing assays of *P. aeruginosa* CF clinical isolates treated with tobramycin combined with PDSTP. Data are represented in terms of variation of OD_{600}. Black line, untreated sample; red line, treatment with sub-inhibitory concentrations of PDSTP; blue line, treatment with sub-inhibitory concentrations of tobramycin; light green line, combination of PDSTP with the antibiotic. The experiment was performed twice, each time in duplicate.

The combination of PDSTP with ciprofloxacin demonstrated a prolonged inhibitory effect against each strain, though complete growth inhibition was observed only for NN2, NN84, BT2 and BT72 (Figure 4.25).

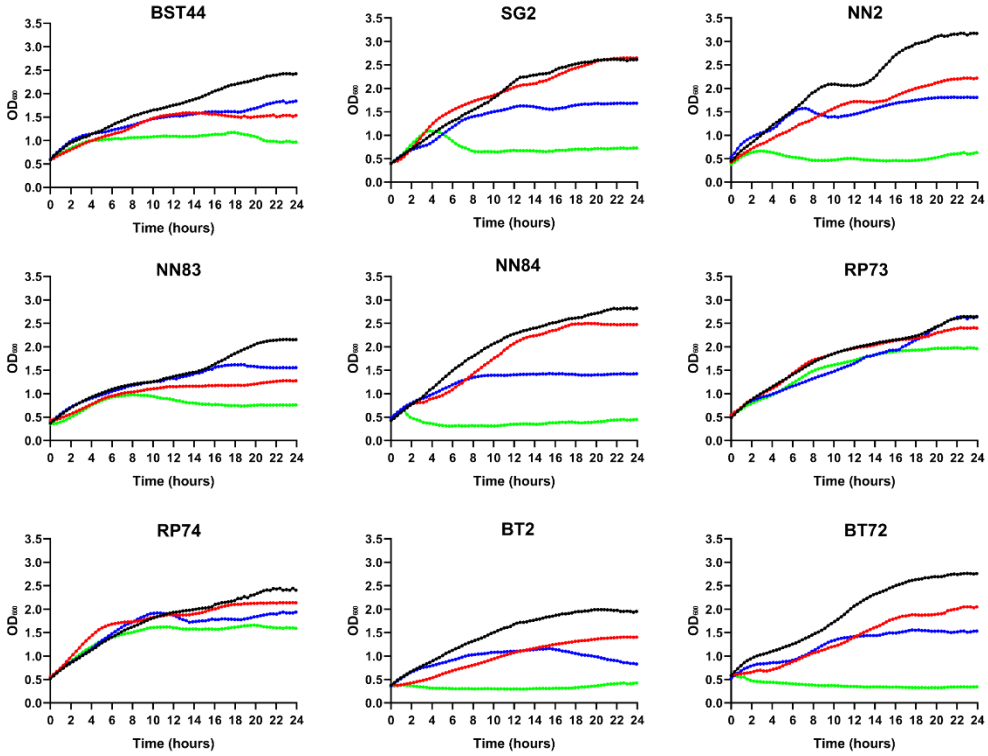

Figure 4.25. Time-killing assays of *P. aeruginosa* CF clinical isolates treated with ciprofloxacin combined with PDSTP. Data are represented in terms of variation of OD_{600}. Black line, untreated sample; red line, treatment with sub-inhibitory concentrations of PDSTP; blue line, treatment with sub-inhibitory concentrations of ciprofloxacin; light green line, combination of PDSTP with the antibiotic. The experiment was performed twice, each time in duplicate.

As previously observed with the PA01 strain (Figures 4.21 and 4.22), colistin was the least effective antibiotic against *P. aeruginosa*. In fact, even when used at a concentration equal to the MIC, its combination with PDSTP only led to long-term inhibition in the NN84 strain, while a 10-hour inhibition was observed for BST44, NN2, NN83, BT2 and BT72. The SG2 strain showed insensitivity to this combination (Figure 4.26).

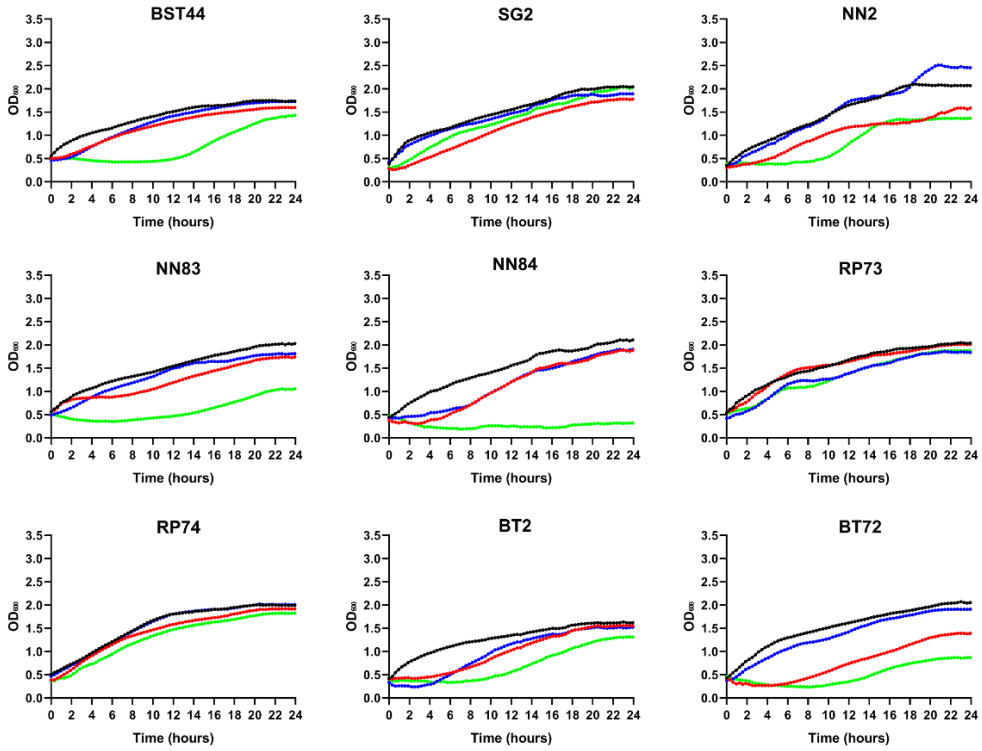

Figure 4.26. Time-killing assays of *P. aeruginosa* CF clinical isolates treated with colistin combined with PDSTP. Data are represented in terms of variation of OD_{600}. Black line, untreated sample; red line, treatment with sub-inhibitory concentrations of PDSTP; blue line, treatment with sub-inhibitory concentrations of colistin; light green line, combination of PDSTP with the antibiotic. The experiment was performed twice, each time in duplicate.

In summary, the results from the time-killing assays validated those obtained from antibiotic combination susceptibility testing, confirming the efficacy of PDSTP as an enhancer of various classes of clinically relevant antibiotics against *P. aeruginosa*.

Results

To validate the efficacy observed *in vitro* of the combination of PDSTP with ceftazidime, a *Galleria mellonella* infection model was employed. The concentrations of ceftazidime (5 mg/kg) and PDSTP (6.25 mg/kg) used in this assay were non-toxic to *G. mellonella* (data not shown). Inoculation with 10^4 CFU of *P. aeruginosa* PA01 resulted in 100% larval mortality in the untreated group (data not shown), as well as in the groups treated with physiological saline and PDSTP at 24 hours post-inoculation (Figure 4.27). Conversely, treatment with ceftazidime alone led to 25% survival after 48 hours. Notably, the combination treatment with PDSTP exhibited a statistically significant increase in larval viability compared to the antibiotic alone, reaching up to 47% survival at 48 hours (Figure 4.27). This validates the *in vitro* activity observed for the PDSTP-ceftazidime combination.

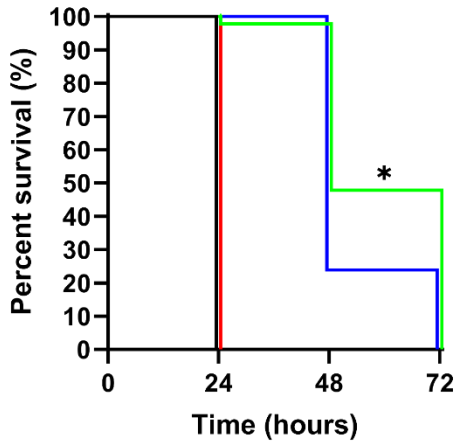

Figure 4.27. Kaplan-Meier survival curve of *G. mellonella* infected with *P. aeruginosa* PA01 and treated with physiological saline (black line), PDSTP (red line), ceftazidime (blue line) or the combination of PDSTP with ceftazidime (green line). The experiment was performed three times. Statistically significant differences are indicated (Log-rank test; *, $p < 0.05$).

4.7. PDSTP antibiotic potentiation relies on membrane depolarization

The antibiotic potentiation activity of PDSTP may be ascribed to the impairment of the outer membrane permeability of *P. aeruginosa*, following treatment with the compound. Indeed, the disruption of membrane integrity may promote the access of antibiotics to the periplasmic space and, subsequently, to the cytoplasm. To evaluate this possibility, N-phenyl-1-naphthylamine (NPN) assays were performed. NPN is a hydrophobic dye that fluoresces strongly in a hydrophobic environment, but weakly in a hydrophilic environment. Therefore, when NPN is incubated with intact bacterial cells, it does not emit fluorescence, but it does so when it is stabilised inside damaged bacterial membranes (Helander and Mattila-Sandholm, 2000). *P. aeruginosa* PA01 was treated with 10 µg/mL of PDSTP (since higher concentrations led to partial bacterial growth impairment in these experimental conditions) or 5 mM of EDTA, a well-characterized membrane-permeabilizing agent used as a positive control (Helander and Mattila-Sandholm, 2000). Thereafter, 10 µM of NPN was added and fluorescence was measured over time. As shown in Figure 4.28, the fluorescence of bacteria treated with PDSTP remained the same as that of the control, while those treated with EDTA showed an increase in fluorescence, compared to the control, over time. In detail, EDTA treatment resulted in an immediate increase in the fluorescence, reaching a plateau already at time 0. This result demonstrates that PDSTP does not potentiate antibiotics through the disruption of membrane integrity.

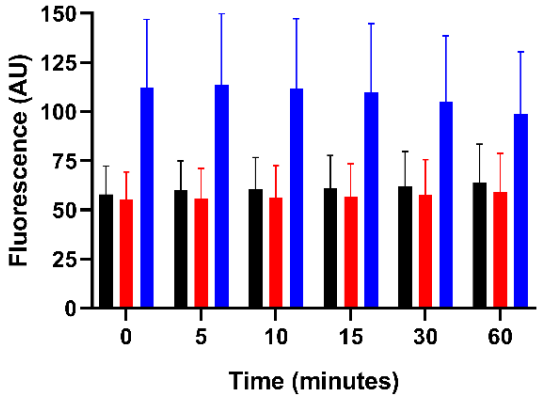

Figure 4.28. NPN assay of *P. aeruginosa* PA01 treated with 10 µg/mL of PDSTP (red column) and 5 mM EDTA (blue column), compared to the control (black column). The experiment was performed twice, each time in duplicate.

Another mechanism that may be involved in PDSTP-mediated antibiotic potentiation is related to membrane depolarization. Indeed, when the membrane potential is disrupted, proton-gradient dependent efflux pumps are inactivated. If the inactivated efflux pumps recognize specific antibiotics as substrates, they will not be able to expel them, thereby increasing their activities (Borselli *et al*., 2016). Interestingly, all the PDSTP-potentiated antibiotics (amikacin, ceftazidime, ciprofloxacin, colistin, meropenem and tobramycin) are substrates of *P. aeruginosa* efflux pumps (Lorusso *et al*., 2022). To explore this hypothesis, depolarization assays using DiSC3(5), an abbreviation for 3,3'-dipropylthiadicarbocyanine iodide, were performed. DiSC3(5) is a fluorescent dye that strongly fluoresces when the membrane potential is impaired and moves from the inner bacterial membrane to the medium (Buttress *et al*., 2022). *P. aeruginosa* PA01 was incubated with DiSC3(5) and then treated with increasing concentrations of PDSTP (1 to 100 µg/mL), carbonyl cyanide m-chlorophenylhydrazone (CCCP) (10 and 30 µM), an uncoupling agent dissipating the proton motive force used as a positive control, and colistin (1 to 10 µg/mL), used as a second positive control due to its membrane-destabilizing properties (French *et al*., 2020). Fluorescence was measured over time. As illustrated in Figure 4.29A, the fluorescence of bacteria treated with PDSTP increased over time in a dose-dependent manner, reaching a plateau. This trend was similar to that observed when bacteria were treated with colistin, both in terms of curve shape and fluorescence intensity (Figure 4.29B). In the case of CCCP, a dose-dependent increase in the fluorescence was observed but, unlike the other curves, the maximum fluorescence was reached immediately (Figure 4.29C). Any decrease in fluorescence may be attributed to adsorption of DiSC3(5) to the 96-well plate. Interestingly, both colistin and CCCP are active against the inner bacterial membrane. Conversely, given that PDSTP should not be able to enter bacterial cells (Egorova *et al*., 2021), its activity appears to be directed at the outer bacterial membrane. This result provides evidence that PDSTP potentiates antibiotics through membrane depolarization and subsequent efflux pumps inhibition.

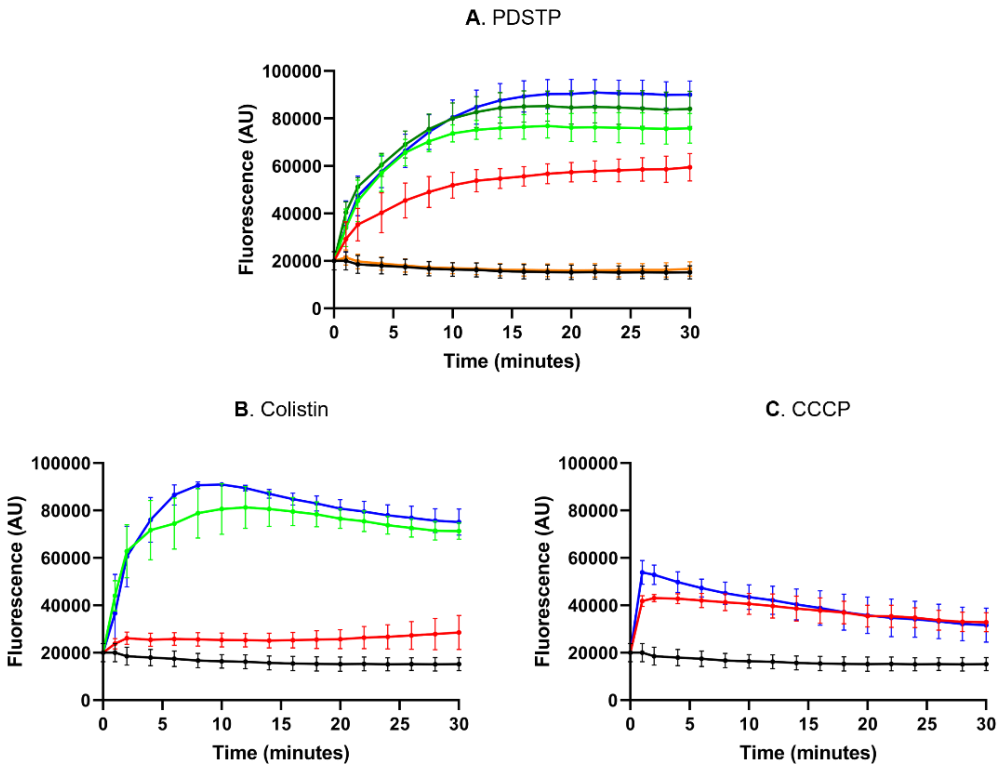

Figure 4.29. Depolarization assay of *P. aeruginosa* PA01 treated with PDSTP (A) (orange line, 1 μg/mL; red line, 10 μg/mL; light green line, 20 μg/mL; dark green line, 50 μg/mL; blue line, 100 μg/mL), colistin (B) (red line, 1 μg/mL; light green line, 5 μg/mL; blue line, 10 μg/mL) and CCCP (C) (red line, 10 μM; blue line, 30 μM). The experiment was performed three times, each time in duplicate.

4.8. PDSTP inhibits *P. aeruginosa* biofilm formation *in vitro* and in *an ex* vivo pig lung model

To investigate the impact of PDSTP on biofilm formation in *P. aeruginosa* PA01 and two clinical isolates, NN2 and SG2, *in vitro* biofilm inhibition assays were performed. Initially, crystal violet assays revealed that 50 μg/mL of PDSTP (or 25 μg/mL for SG2 due to growth inhibition at 50 μg/mL in these experimental conditions) significantly reduced the biofilm biomass, compared to the respective untreated controls, after 24 hours (Figure 4.30).

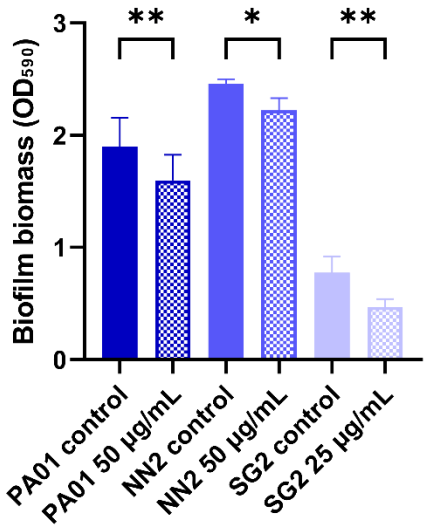

Figure 4.30. Biofilm inhibition assays of *P. aeruginosa* PA01, NN2 and SG2 treated with 25 or 50 µg/mL of PDSTP. The experiment was performed three times, each time in six replicates. Statistically significant differences are indicated (Student's *t* test; *, $p < 0.05$; **, $p < 0.01$).

To further evaluate PDSTP antibiofilm activity, confocal laser scanning microscopy (CLSM) was employed. Specifically, the biofilm formed by the PA01 strain appeared thick and uniform. In contrast, NN2 formed a thicker biofilm, while that of SG2 was heterogeneous, characterized by bacterial aggregates. PDSTP treatment resulted in a visible impairment of biofilm formation for all strains, with a reduction in biofilm biomass. Subsequent analysis using COMSTAT2 indicated that the compound significantly reduced both average biofilm thickness and biomass, while simultaneously increasing roughness, indicating alterations in biofilm structure (Figure 4.31).

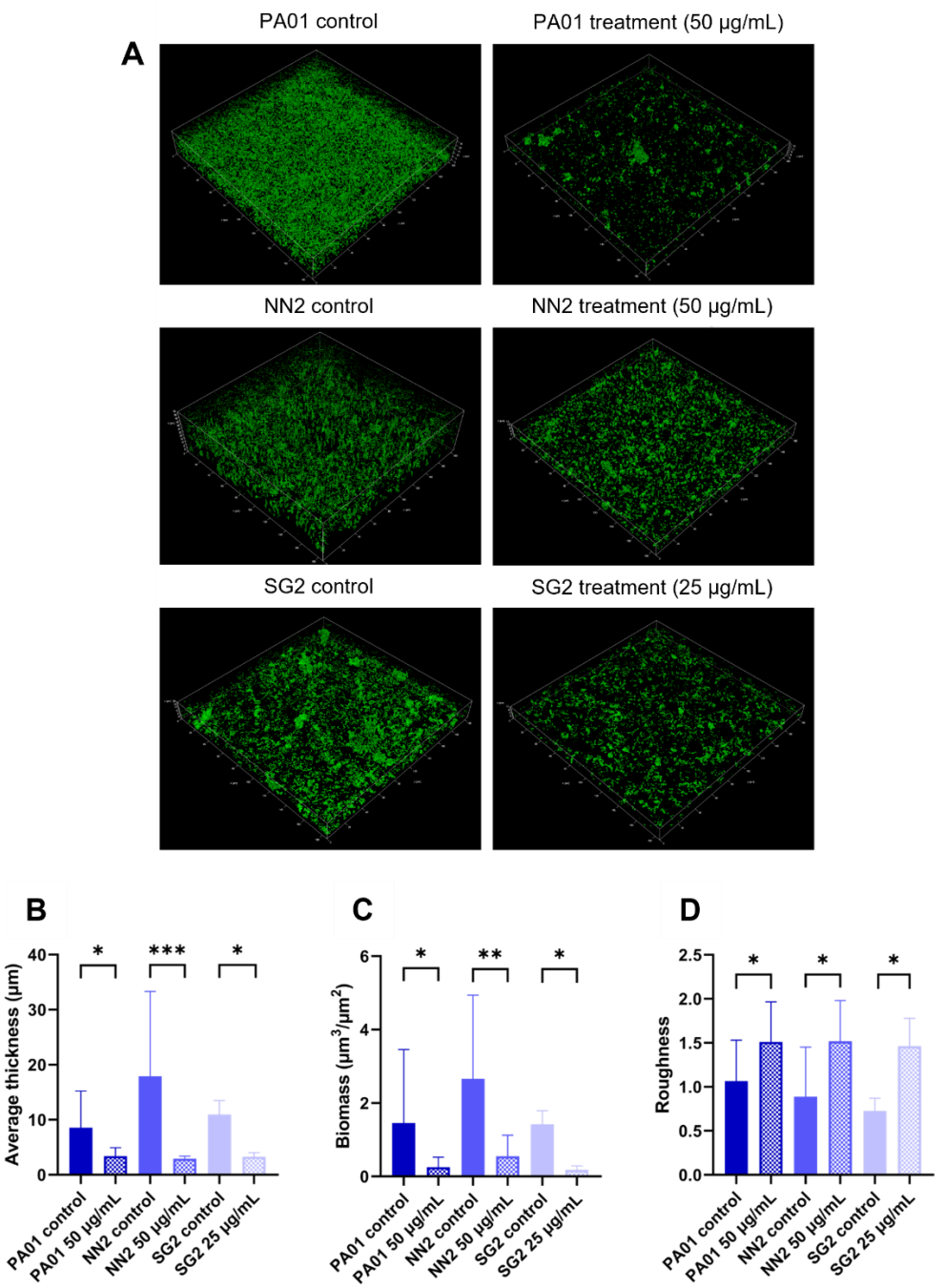

Figure 4.31. CLSM images (400x magnification) of the biofilms formed by *P. aeruginosa* PA01, NN2 and SG2 following treatment with 25 or 50 µg/mL of PDSTP (A). COMSTAT2 analysis of biofilm properties, including average thickness (B), biomass (C) and roughness (D). The experiment was performed three times. Statistically significant differences are indicated (Student's *t* test; *, $p < 0.05$; **, $p < 0.01$; ***, $p < 0.001$).

To validate the antibiofilm properties of PDSTP, an *ex vivo* pig lung (EVPL) tissue model, embedded in SCFM which better simulates the CF lung environment, was employed. Similarly to the previous analyses, PDSTP treatment resulted in impaired biofilm formation across the tested strains. Indeed, the CFU/mL recovered from biofilms were significantly lower when treated with PDSTP, compared to the respective untreated controls. The reduction in CFU/mL was similar to that achieved with ciprofloxacin (0.06 µg/mL), used as a positive control (Figure 4.32).

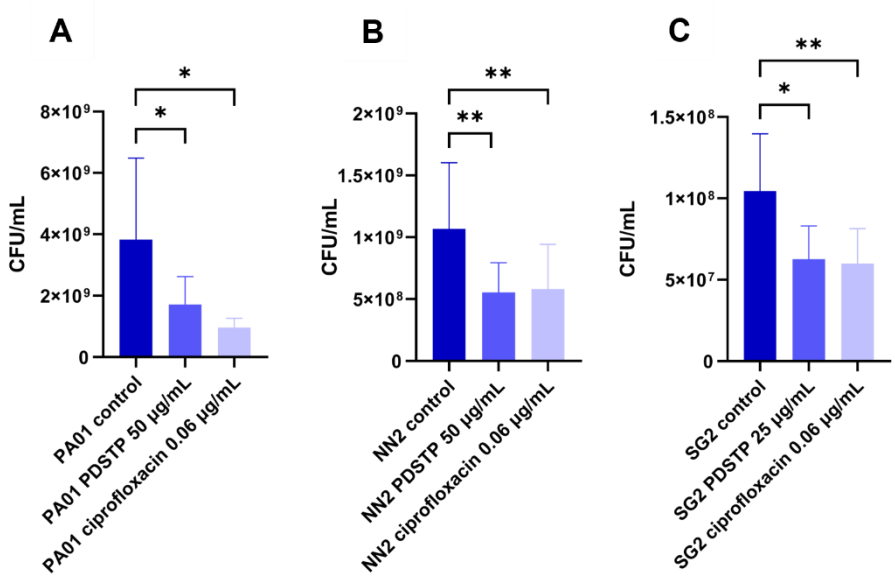

Figure 4.32. Biofilm inhibition assays of *P. aeruginosa* PA01 (A), NN2 (B) and SG2 (C) treated with 25 or 50 µg/mL of PDSTP or 0.06 µg/mL of ciprofloxacin as a positive control, represented as the CFU/mL recovered from pig lung tissue. The experiment was performed three times. Statistically significant differences are indicated (One-way ANOVA test; *, $p < 0.05$; **, $p < 0.01$).

Finally, CLSM was employed to visualize *P. aeruginosa* PA01 biofilm stained with Syto9 on lung tissue fragments. In this case as well, PDSTP (50 µg/mL) impaired biofilm formation and COMSTAT2 analysis confirmed a significant reduction in biofilm biomass due to the treatment which is comparable to that with ciprofloxacin (0.06 µg/mL) (Figure 4.33).

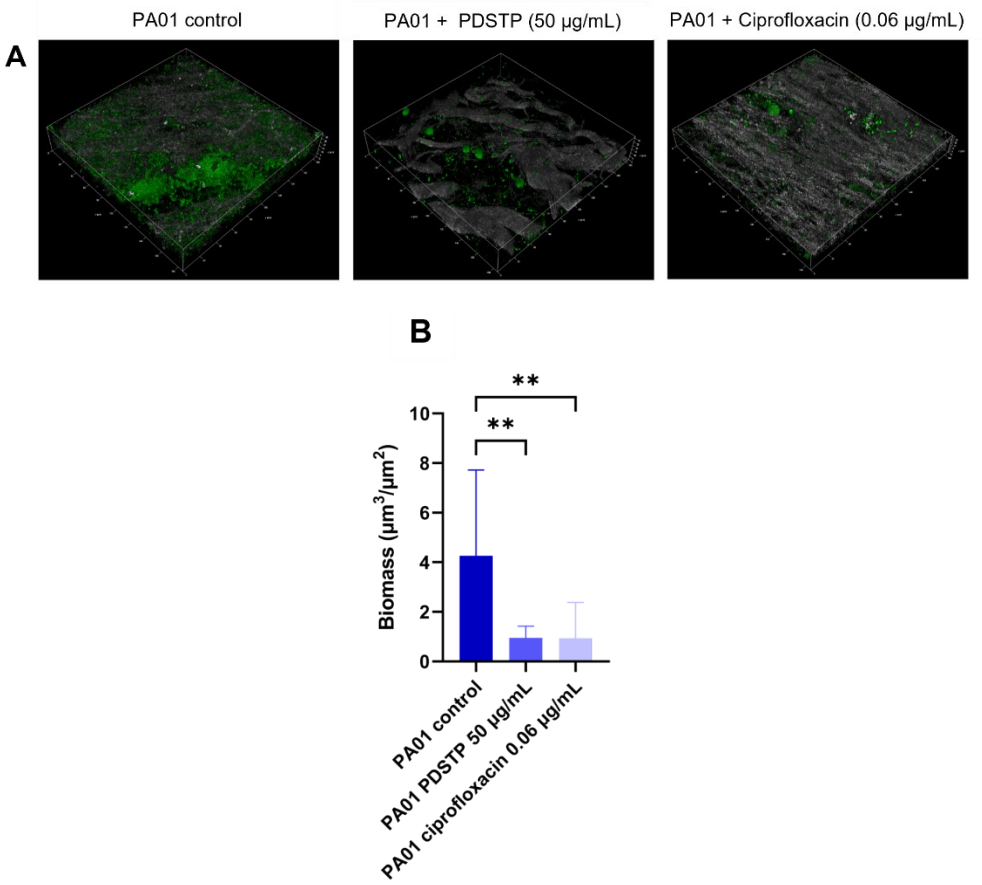

Figure 4.33. CLSM images (400x magnification) of the biofilm formed by *P. aeruginosa* PA01 on EVPL following treatment with 50 µg/mL of PDSTP and 0.06 µg/mL of ciprofloxacin as a positive control (A). COMSTAT2 analysis of biofilm biomass (B). The experiment was performed three times. Statistically significant differences are indicated (One-way ANOVA test; **, $p < 0.005$).

Pt. II: Characterization of *P. aeruginosa* bacteriophages and bacteriophage-resistant mutants

4.9. Three newly isolated phages belonging to the *Caudovirales* order

Three phages named PA48, PA49 and PA50 were isolated from wastewater using as a host *P. aeruginosa* PA01 and selected based on different plaque morphologies. Specifically, plaques of these phages had a clear area at the centre and a diameter of about 1.5 - 2 mm. In addition, PA48 and PA50 had an entire edge, while PA49 had an undulate edge (data not shown). Transmission electron microscopy analysis showed that PA48 and PA50 belong to the *Siphoviridae* family, while PA49 belongs to the *Myoviridae* family (Figure 4.34), following the classification according to the International Committee on Taxonomy of Viruses (ICTV). In particular, the two siphoviral phages had a capsid with an average height and width of 92.6 and 61.5 nm, respectively, while their tails measured approximately 154.3 nm in length. In contrast, the myoviral phage showed average dimensions of 121.7 nm in height, 106.9 nm in width and a tail spanning 186.7 nm. *Myoviridae* and *Siphoviridae* phages belong to the *Caudovirales* order and are characterized by a double-stranded DNA genome enclosed within an icosahedral capsid, attached to a long tail. The tail of *Siphoviridae* phages is non-contractile, while that of *Myoviridae* phages is contractile (Dion *et al*., 2020).

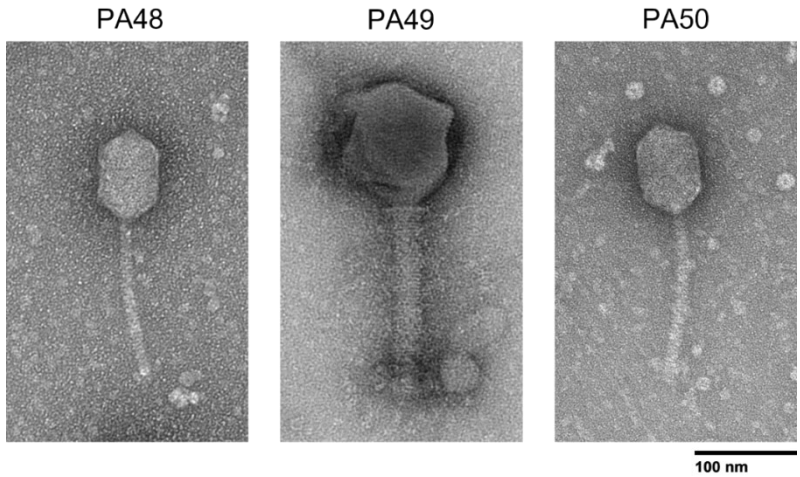

Figure 4.34. Transmission electron micrographs of PA48, PA49 and PA50. PA48 and PA50 have a siphoviral morphotype, while PA49 shows a myoviral morphology. All of them are characterized by an icosahedral head attached to a tail which is non-contractile for PA48 and PA50, and contractile for PA49.

4.10. Genomic analysis of PA49 shows its compatibility with clinical application

Whole-genome sequencing using the Nanopore platform, followed by genome assembly and bioinformatics characterization, confirmed that PA49 has a double-stranded DNA genome (274 kbp) and belongs to the *Myoviridae* family. As listed in Table 4.6, PA49 possesses 411 genes, 321 (78.1%) of which have unknown function. Although there is a significant lack of genomic information, this phage is compatible with clinical applications. Indeed, PA49 does not possess genes involved in integration and excision, excluding the possibility of being lysogenic. Furthermore, this phage does not carry genes encoding neither virulence factors nor antibiotic resistances according to the Virulence Factor Database (VFDB) and the Comprehensive Antibiotic Resistance Database (CARD), respectively. Unfortunately, PA48 and PA50 could not be sequenced properly with the Nanopore platform. This was probably due to base modifications, resulting in low-quality reads which were not compatible with genome assembly and annotation (Nielsen *et al*., 2023). As a consequence, these genomes will be sequenced using the Illumina platform. However, all the three phages were further characterized.

Table 4.6. Category and respective number of genes out of 411 total genes in PA49 genome. The category "Other" includes gene with diverse ungrouped but known functions, i.e., genes encoding a metal-dependent phosphohydrolase, a thymidylate kinase, a transglycosylase and an UvsX-like recombinase.

Category	Count
Connector	0
DNA, RNA and nucleotide metabolism	31
Head and packaging	39
Integration and excision	0
Lysis	1
Moron, auxiliary metabolic gene and host takeover	2
Other	4
Tail	9
Transcription regulation	0
Unknown function	321
tRNAs	4
CRISPRs	0
tmRNAs	0
VFDB_Virulence_Factors	0
CARD_AMR_Genes	0

4.11. Phages withstand a wide range of pH values, temperatures and storage conditions

PA48, PA49 and PA50 withstood a wide range of pH values. Indeed, their viability was not affected from pH 3 to 11. Only at a very alkaline pH, i.e., pH 12, all of them were inactivated (Figure 4.35).

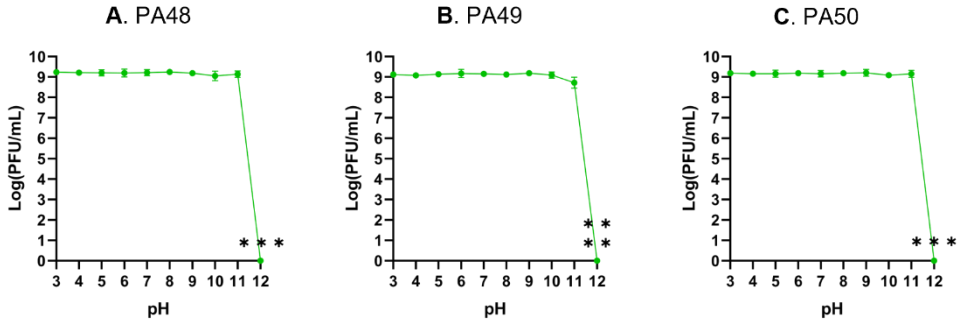

Figure 4.35. PA48 (A), PA49 (B) and PA50 (C) stabilities at different pH values. The experiment was performed three times. Statistically significant differences are indicated (Student's *t* test; ***, $p < 0.0005$; ****, $p < 0.0001$).

Furthermore, phages were viable after incubation in a wide range of temperatures. Specifically, PA48 and PA50 were more resistant to higher temperatures compared to PA49, showing partial phage inactivation at 70°C (PFU/mL reduction of 57 and 22%, respectively) and complete inactivation at 80°C. On the other hand, PA49 viability was already affected at a temperature of 60°C (22% PFU/mL reduction), while it was completely inactivated at 70°C (Figure 4.36).

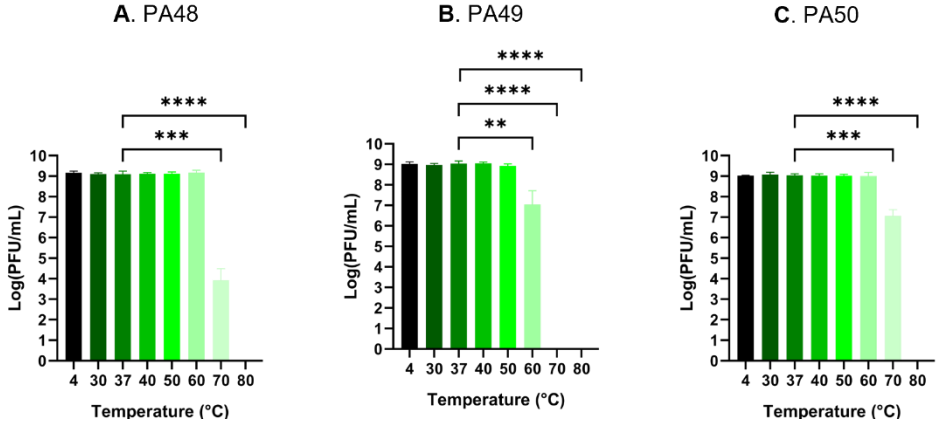

Figure 4.36. PA48 (A), PA49 (B) and PA50 (C) stabilities at different temperatures. The experiment was performed three times. Statistically significant differences are indicated (Student's *t* test; **, $p < 0.01$; ***, $p < 0.0005$; ****, $p < 0.0001$).

Finally, all the phages were stable under different storage conditions (-80°C, -20°C, 4°C and room temperature), over a period of four months, being the PFU/mL all comparable (Figure 4.37).

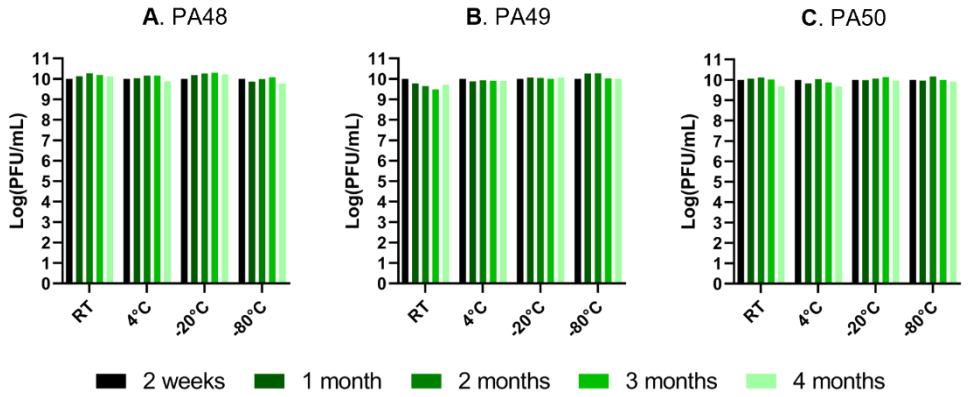

Figure 4.37. PA48 (A), PA49 (B) and PA50 (C) stabilities under different storage conditions. This experiment was performed once. Colour legend is shown below the graphics.

4.12. The two siphoviral phages display a different phage cycle profile compared to the myoviral phage

To characterize the phage cycle, adsorption and one-step growth assays were performed using *P. aeruginosa* PA01 as host. PA48 and PA50 had a different adsorption profile compared to PA49. In particular, a low percentage of both siphoviral phages adsorbed onto host cells (maximum adsorption after 7.5 minutes of 24.5 and 27.3%, respectively), while more than 50% of the myoviral phage already adsorbed onto bacterial cells after 2.5 minutes, reaching 90% after 10 minutes (Figure 4.38).

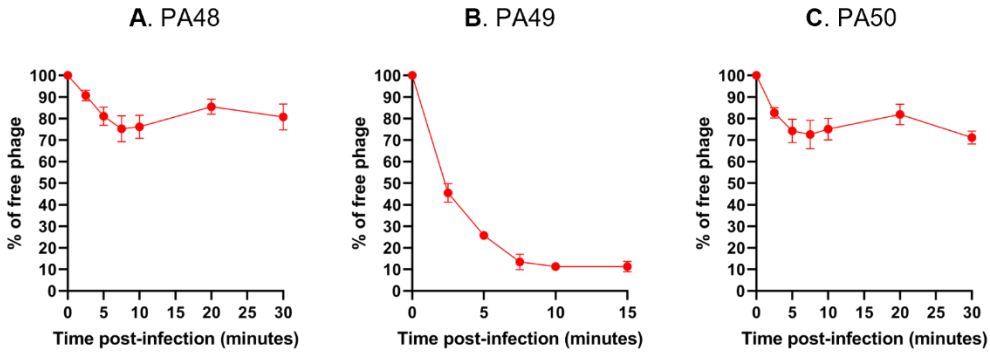

Figure 4.38. PA48 (A), PA49 (B) and PA50 (C) adsorption assay using *P. aeruginosa* PA01 as host. This experiment was performed three times.

Also in the case of one-step growth curves, both latent period and burst size of PA48 and PA50 were similar, in contrast with those of PA49. Specifically, siphoviral phages needed approximately 40 minutes to replicate their genomes inside the host cell, synthetize their proteins and assemble them into new virion particles, subsequently released through bacterial lysis (Figure 4.39). The burst size of PA48 and PA50, i.e., the number of released virions per infected cell, was about 6.9 and 6.5, respectively. On the other hand, the myoviral phage had latent period of approximately 10 minutes which is significantly shorter compared to the other phages (Figure 4.39). In addition, the burst size was about 445.5 which is significantly higher compared to PA48 and PA50.

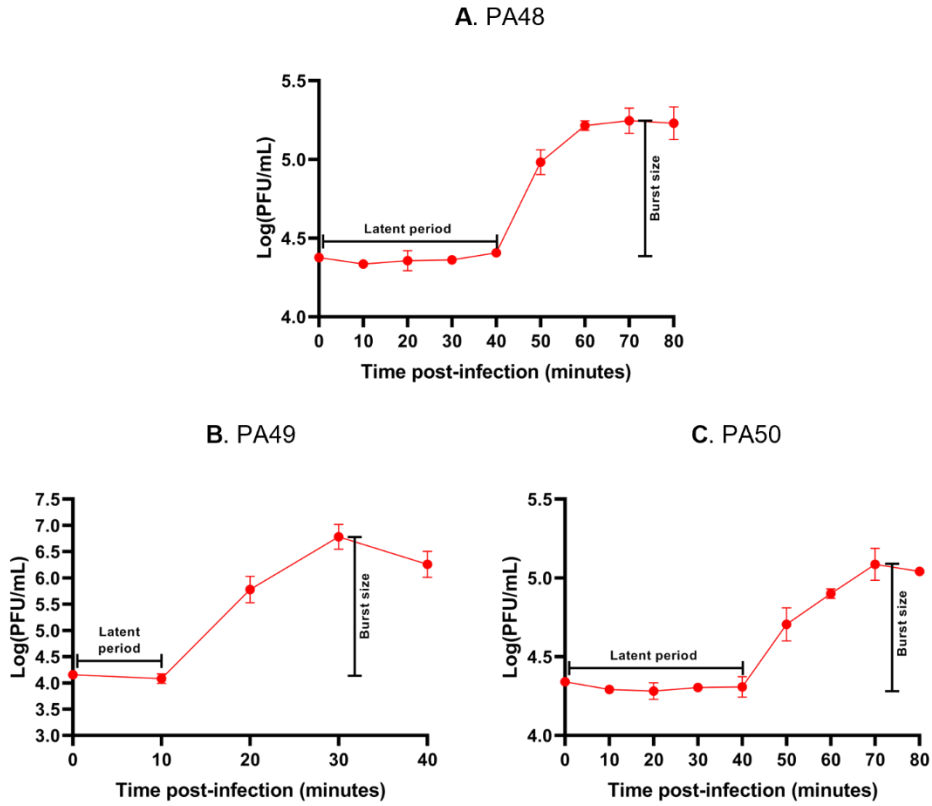

Figure 4.39 PA48 (A), PA49 (B) and PA50 (C) one-step growth assay using *P. aeruginosa* PA01 as host. These experiments were performed three times.

4.13. Phages show a broad host range

To characterize the microbiological activity of phages, their host range was first determined. Specifically, phage lytic properties were tested on *P. aeruginosa* PA01, 9 *P. aeruginosa* CF clinical isolates (C450, C452, C453, C457, C458, C459, C460, C462 and C464) and 9 *P. aeruginosa* non-CF clinical isolates from patients affected by chronic rhinosinusitis (C392, C394, C405, C419, C423, C427, C430, C433 and C440). PA48 lysed 12 out of these 19 strains (63%), PA49 lysed 16 of them (84%) and PA50 lysed 11 of them (58%), indicating that PA50 had the narrowest host range, while PA49 had the broadest one. However, all phages showed a broad host range. Furthermore, 11 strains (PA01, C450, C457, C459, C460, C392, C394, C423, C427, C430 and C440) (58%) were lysed by all the three phages, one strain (C464) (5%) was lysed by PA48 and PA49 and 4 strains (C462, C405, C419 and C433) (21%) were lysed only by PA49. Interestingly, 3 strains (C452, C453 and C458) (16%) were not lysed by any phage (Figure 4.40).

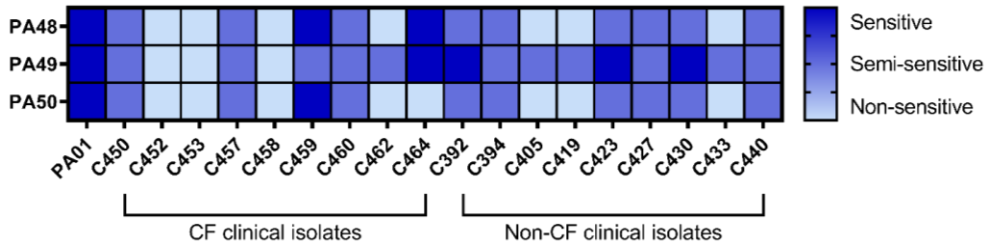

Figure 4.40. PA48, PA49 and PA50 host range determination employing 19 strains which include *P. aeruginosa* PA01, 9 clinical isolates from CF patients and 9 clinical isolates from patients with chronic rhinosinusitis. Colours associated to sensitive (clear lysis), semi-sensitive (partial lysis) and non-sensitive (no lysis) strains are shown in the legend on the right. This experiment was performed three times, each time in triplicate.

4.14. Phages efficiently lyse planktonic *P. aeruginosa*

To evaluate the killing activity of PA48, PA49 and PA50 against *P. aeruginosa* PA01, bacterial growth in the presence of the phages at different MOI (0, 0.1, 1 and 10 phages per bacterial cell) was followed by measuring the OD_{600}, every 30 minutes, up to 300 minutes (5 hours). As expected, the higher the MOI, the greater the lytic activity (Figure 4.41). Siphoviral phages impaired bacterial growth later compared to the myoviral one, which is consistent with their lower adsorption onto host cells (Figure 4.38), longer latent period and lower burst size (Figure 4.39). However, all phages efficiently suppressed *P. aeruginosa* PA01 growth.

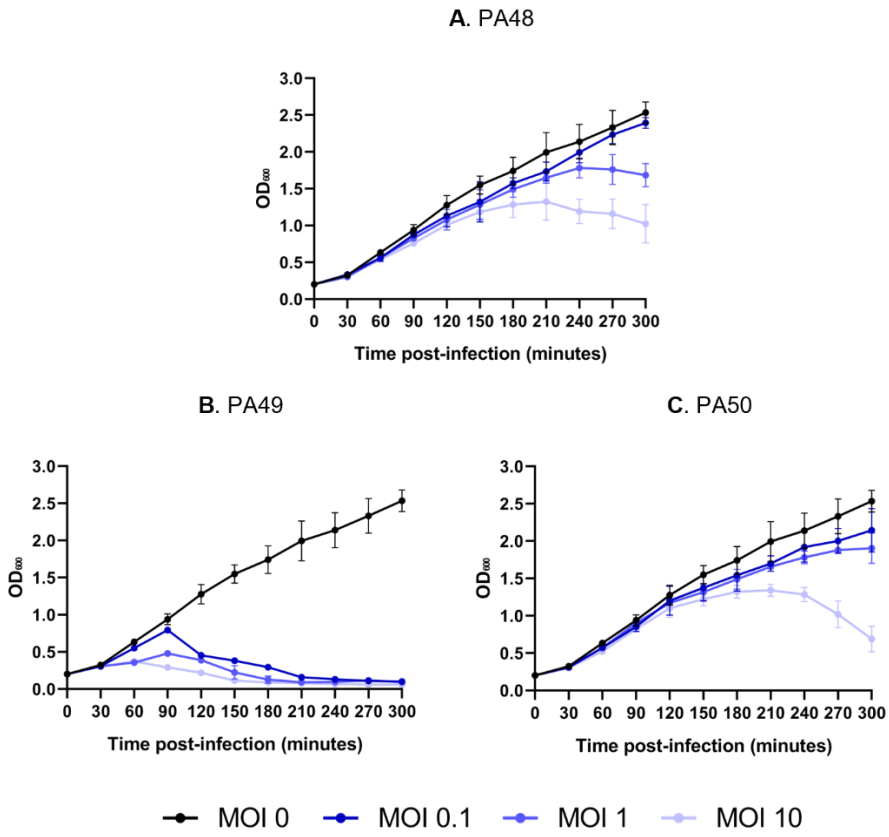

Figure 4.41. PA48 (A), PA49 (B) and PA50 (C) killing activity against planktonic *P. aeruginosa* PA01. Bacteria were infected with phages at different MOI (0, 0.1, 1 and 10 phages per bacterial cell) and their growth was followed by monitoring the OD_{600}. Colour legend is shown below the graphics. These experiments were performed three times.

4.15. Phages efficiently eradicate *P. aeruginosa* biofilms

To further characterize the microbiological activity of phages, different concentrations of PA48, PA49 and PA50 (1 x 10^7, 1 x 10^8 and 1 x 10^9 PFU) were tested against *P. aeruginosa* mature biofilms and biofilm eradication was assessed by crystal violet staining. In particular, five strains were employed to perform these experiments, including *P. aeruginosa* PA01, two CF clinical isolates (C450 and C457) and two non-CF strains (C423 and C430). Clinical isolates were chosen based on biofilm biomass, i.e., one strain per group (CF and non-CF) producing more biofilm (C457 and C423) and another one producing less biofilm (C450 and C430) (data not shown). In particular, PA48 and PA50 were tested against the higher biofilm producers C457 and C423, while PA49 was tested on all the strains since it showed better killing activity against planktonic *P. aeruginosa* PA01 (Figure 4.41).

As reported in Figure 4.42, there was an overall dose-dependent decrease in biofilm biomass when biofilms were treated with increasing concentrations of phages. These decreases were statistically significant in most cases, especially at higher phage concentrations. In just one case, which is C423 biofilms treated with PA48, the biofilm biomass decrease was not significant even at high concentrations (1 x 10^9 PFU). Increasing the phage concentration is likely to impair C423 biofilms. In addition, dose-dependency was not appreciated in the case of PA01 infected by PA50 and C423 infected by PA49. This could be due to the achievement of maximum eradication activity of phages already at a concentration of 1 x 10^7 PFU. Decreasing the phage concentration may allow to appreciate the dose-dependency. Maximum eradications for PA48, PA49 and PA50 were, respectively, 64% (1 x 10^9 PFU against PA01), 71% (1 x 10^8 PFU against C423) and 70% (1 x 10^8 PFU against PA01) decrease in biofilm biomass.

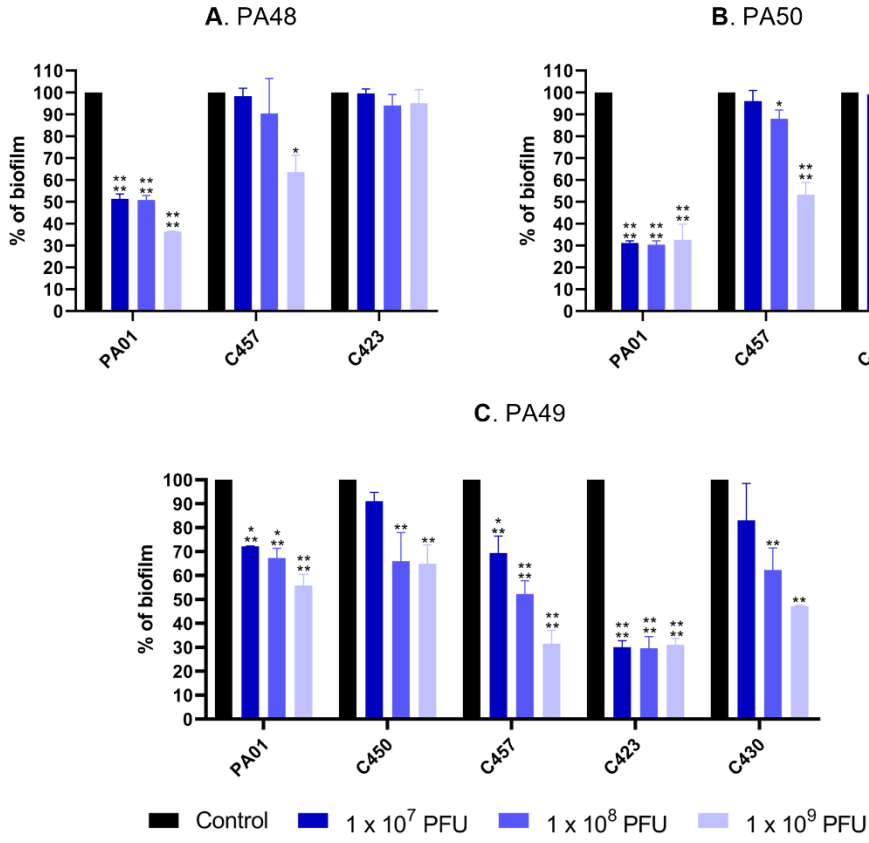

Figure 4.42. PA48 (A), PA50 (B) and PA49 (C) biofilm eradication activity against *P. aeruginosa* PA01, C450, C457, C423 and C430 biofilms treated with increasing concentrations of phages (1 x 10^7, 1 x 10^8 and 1 x 10^9 PFU.) Colour legend is shown below the graphics. These experiments were performed three times, each time in six replicates. Statistically significant differences are indicated (One-way ANOVA test; *, $p < 0.05$; **, $p < 0.005$; ***, $p < 0.0005$; ****, $p < 0.0001$).

4.16. Phages can be employed to select *P. aeruginosa* bacteriophage-insensitive mutants

Phages were employed to select *P. aeruginosa* PA01 bacteriophage-insensitive mutants (BIMs). Specifically, PA49 and PA18 (a lytic *Myoviridae* phage previously characterized in the lab; data not yet published) were used. PA48 and PA50 were excluded since their genomic characterization was lacking. 9 BIMs were selected by PA18 and 10 BIMs were selected by PA49 (Figure 4.43). After isolation, BIMs were confirmed to be resistant to the selecting phage by double layer agar spot method. In addition, their sensitivity for the other phages was tested and *P. aeruginosa* PA01 was used as control. As expected, BIMs were resistant to the respective selecting phage, i.e., BIMs selected by PA18 were resistant to PA18 and BIMs selected by PA49 were resistant to PA49, while *P. aeruginosa* PA01 was sensitive to all phages. Interestingly, PA18 BIMs were all sensitive to PA48, PA49 and PA50, while PA49 BIMs were all resistant to these three phages, but sensitive to PA18 (Figure 4.43). This may be due to the fact that PA48, PA49 and PA50 recognize the same host receptor, which may be different from that recognized by PA18.

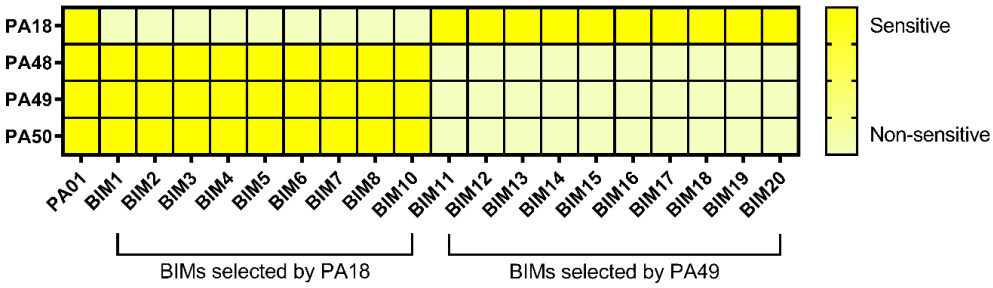

Figure 4.43. Sensitivity to PA18, PA48, PA49 and PA50 of BIMs selected by PA18 and PA49, along with *P. aeruginosa* PA01 as control. Colours associated to sensitive (clear lysis) and non-sensitive (no lysis) strains are shown in the legend on the right. This experiment was performed three times, each time in triplicate.

4.17. Evolutionary trade-off to counter phage infection may influence both growth and biofilm formation of the BIMs

Bacterial resistance to phages typically results in physiological changes that may lead to a reduced bacterial fitness and increased antibiotic susceptibility (Hasan and Ahn, 2022). Consequently, the two panels of BIMs (PA18 BIMs and PA49 BIMs) were first analysed by monitoring their growth, measuring the OD_{600}, every 15 minutes, up to 720 minutes (12 hours). Most of the BIMs selected by PA18 (BIM1, 2, 3, 6, 7, 8 and 10) (77.8%) did not show any growth defects compared to *P. aeruginosa* PA01. In contrast, BIM4 and 5 showed a significant decrease in bacterial growth compared to the control (Figure 4.44).

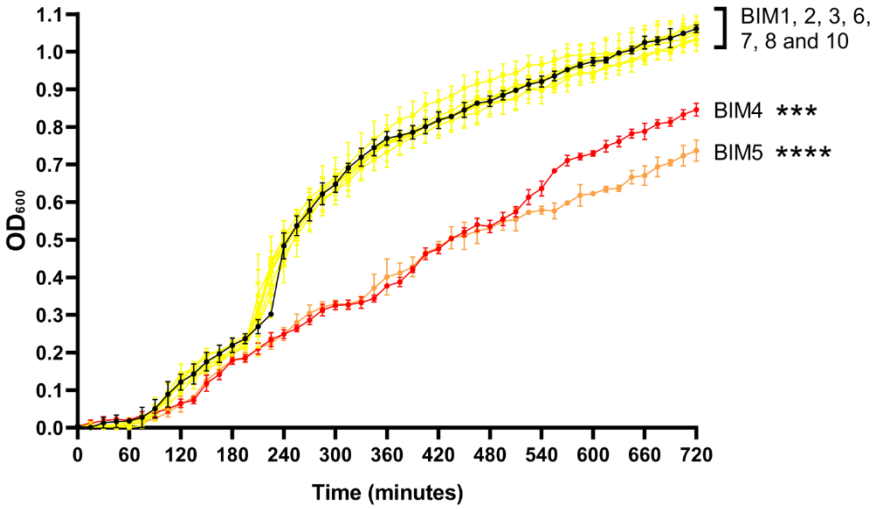

Figure 4.44. Growth curves of BIMs selected by PA18, along with *P. aeruginosa* PA01 as a control (black curve). Growth curves of BIMs with equal statistical significance are represented with the same colour. This experiment was performed three times, each time in triplicate. Statistically significant differences are indicated (Student's *t* test; ***, $p < 0.001$; ****, $p < 0.0001$).

In the case of BIMs selected by PA49, half of them (BIM15, 17, 18, 19 and 20) did not show any growth defects compared to *P. aeruginosa* PA01. On the other hand, BIMs 11, 12, 13, 14 and 16 grew significantly slower compared to the control (Figure 4.45).

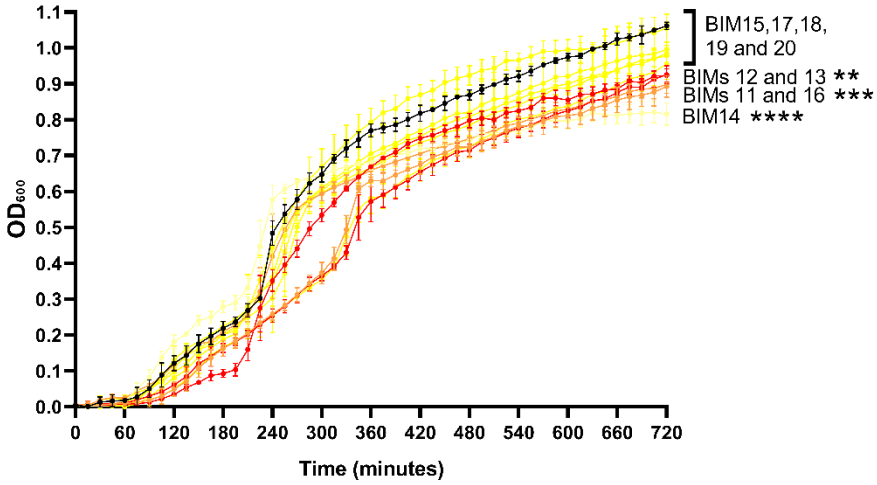

Figure 4.45. Growth curves of BIMs selected by PA49, along with *P. aeruginosa* PA01 as a control (black curve). Growth curves of BIMs with equal statistical significance are represented with the same colour. This experiment was performed three times, each time in triplicate. Statistically significant differences are indicated (Student's *t* test; **, $p < 0.01$; ***, $p < 0.001$; ****, $p < 0.0001$).

To further investigate the extent to which phage resistance causes reduced bacterial fitness, the biofilm formation abilities of the BIMs were analyzed by crystal violet staining. As reported in Figure 4.46, six PA18 BIMs (BIM1, 2, 3, 5, 6 and 8) (67%) produced a significantly higher biofilm biomass compared to *P. aeruginosa* PA01, while biofilm formation abilities of BIM4, 7 and 10 (33%) were not affected. Specifically, biofilm increase ranged from 24 (BIM1) to 51% (BIM5), with an average of 32%. In contrast, nine PA49 BIMs (BIM11, 12, 14, 15, 16, 17, 18, 19 and 20) (90%) resulted significantly impaired in their production of biofilm compared to the control, while BIM13 produced as much biofilm as *P. aeruginosa* PA01. In particular, biofilm decrease ranged from 75 (BIM18) to 91% (BIM11), with an average of 83%.

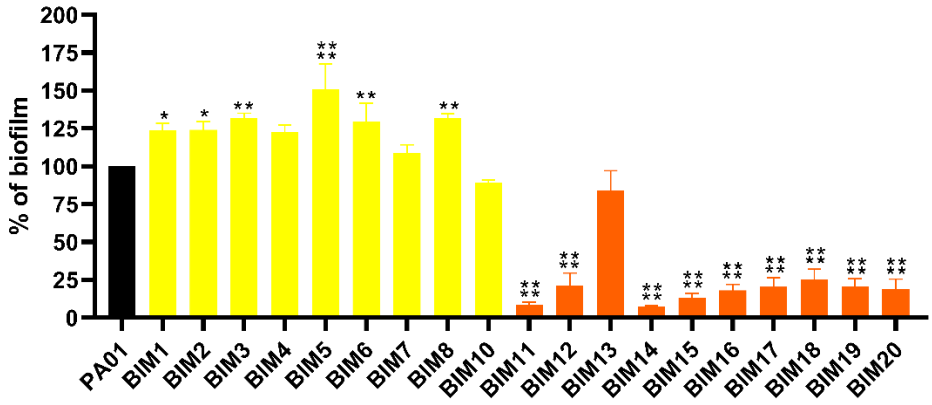

Figure 4.46. Biofilm formation abilities of both PA18 (yellow column) and PA49 (orange column) BIMs compared to the control *P. aeruginosa* PA01 (black column). This experiment was performed three times, each time in six replicates. Statistically significant differences are indicated (Student's *t* test; *, $p < 0.05$; **, $p < 0.005$; ****, $p < 0.0001$).

4.18. Evolutionary trade-off may also influence antibiotic susceptibility of the BIMs

As previously mentioned, bacterial resistance to phages may also result in increased antibiotic susceptibility. To investigate this aspect, the MICs of different antibiotics currently used to treat *P. aeruginosa* infections were determined against six PA18 BIMs (BIM1, 3, 4, 5, 7 and 10), six PA49 BIMs (BIM11, 12, 13, 14, 15 and 19) and *P. aeruginosa* PA01. These BIMs were selected because they displayed different growth and biofilm formation properties. Tested antibiotics were chosen based on different mechanisms of action: tobramycin, ciprofloxacin, ceftazidime, meropenem and colistin. As reported in Table 4.7, PA18 BIMs were slightly more susceptible to at least two antibiotics compared to *P. aeruginosa* PA01 (2-fold decrease in the MIC). In contrast, BIM4 and 5 were mildly less susceptible to ceftazidime and meropenem compared to *P. aeruginosa* PA01 (2-fold increase in the MIC). However, the MIC of colistin against all the BIMs was significantly lower compared to the reference strain, ranging from 4- to 16-fold reductions.

Table 4.7. MIC values of tobramycin, ciprofloxacin, ceftazidime, meropenem and colistin against the BIMs selected by PA18 and *P. aeruginosa* PA01. The MIC fold reduction or increase is indicated in brackets. This experiment was performed three times, each time in duplicate.

Bacterial strain	Tobramycin	Ciprofloxacin	Ceftazidime	Meropenem	Colistin
***P. aeruginosa* PA01**	**1 µg/mL**	**0.125 µg/mL**	**4 µg/mL**	**2 µg/mL**	**8 µg/mL**
BIM 1	1 µg/mL	0.125 µg/mL	2 µg/mL (2-fold reduction)	2 µg/mL	2 µg/mL (4-fold reduction)
BIM 3	1 µg/mL	0.125 µg/mL	2 µg/mL (2-fold reduction)	2 µg/mL	2 µg/mL (4-fold reduction)
BIM 4	0.5 µg/mL (2-fold reduction)	0.0625 µg/mL (2-fold reduction)	8 µg/mL (2-fold increase)	4 µg/mL (2-fold increase)	1 µg/mL (8-fold reduction)
BIM 5	0.5 µg/mL (2-fold reduction)	0.0625 µg/mL (2-fold reduction)	8 µg/mL (2-fold increase)	4 µg/mL (2-fold increase)	0.5 µg/mL (16-fold reduction)
BIM 7	0.5 µg/mL (2-fold reduction)	0.0625 µg/mL (2-fold reduction)	2 µg/mL (2-fold reduction)	2 µg/mL	2 µg/mL (4-fold reduction)
BIM 10	1 µg/mL	0.0625 µg/mL (2-fold reduction)	2 µg/mL (2-fold reduction)	2 µg/mL	2 µg/mL (4-fold reduction)

On the other hand, PA49 BIMs also showed a slightly higher susceptibility to at least two antibiotics compared to *P. aeruginosa* PA01 (2-fold decrease in the MIC). Unlike PA18 BIMs, no PA49 BIM was less susceptible to any antibiotic tested. Also in this case, BIMs resulted to be more susceptible especially to colistin, ranging from 2- to 4-fold reductions in the MIC values (Table 4.8).

Table 4.8. MIC values of tobramycin, ciprofloxacin, ceftazidime, meropenem and colistin against the BIMs selected by PA49 and *P. aeruginosa* PA01. The MIC fold reduction is indicated in brackets. This experiment was performed three times, each time in duplicate.

Bacterial strain	Tobramycin	Ciprofloxacin	Ceftazidime	Meropenem	Colistin
***P. aeruginosa* PA01**	**1 µg/mL**	**0.125 µg/mL**	**4 µg/mL**	**2 µg/mL**	**8 µg/mL**
BIM 11	1 µg/mL	0.0625 µg/mL (2-fold reduction)	2 µg/mL (2-fold reduction)	2 µg/mL	2 µg/mL (4-fold reduction)
BIM 12	1 µg/mL	0.0625 µg/mL (2-fold reduction)	2 µg/mL (2-fold reduction)	2 µg/mL	4 µg/mL (2-fold reduction)
BIM 13	1 µg/mL	0.125 µg/mL	4 µg/mL	2 µg/mL	2 µg/mL (4-fold reduction)
BIM 14	0.5 µg/mL (2-fold reduction)	0.0625 µg/mL (2-fold reduction)	2 µg/mL (2-fold reduction)	2 µg/mL	4 µg/mL (2-fold reduction)
BIM 15	1 µg/mL	0.125 µg/mL	2 µg/mL (2-fold reduction)	2 µg/mL	4 µg/mL (2-fold reduction)
BIM 19	1 µg/mL	0.125 µg/mL	2 µg/mL (2-fold reduction)	2 µg/mL	4 µg/mL (2-fold reduction)

5. Discussion and future perspectives

Infections caused by antibiotic-resistant strains of *Pseudomonas aeruginosa*, *Burkholderia cenocepacia* and *Staphylococcus aureus* represent a significant threat to patients with cystic fibrosis (CF) and those who are immunocompromised (Qin *et al*., 2022; Rojas-Rojas *et al*., 2019; Goss and Muhlebach, 2011). Given the risk of infection by these antibiotic-resistant strains and the limited progress in developing new antibiotics, there is an urgent need to explore alternative therapeutic strategies, also considering drug repurposing and combination therapy (Liao *et al*., 2022; Wang *et al*., 2020).

The dispirotripiperazine derivative PDSTP is a non-toxic compound with a positive net charge that prevents both *in vitro* and *in vivo* infections caused by different viruses (Schmidtke *et al*., 2002; Makarov and Popov, 2022). Its mechanism of action involves impairing viral adsorption to negatively charged heparan-sulphate glycosaminoglycans (HSGAGs) expressed on the surface of human cells by saturating them though electrostatic interactions (Egorova *et al*., 2021). Considering that *P. aeruginosa*, *B.* cenocepacia and *S. aureus* also adhere to HSGAGs (Bucior *et al*., 2012; Martin *et al*., 2019; Liang *et al*., 1992), the aim of the first part of this work was to investigate the potential activity of PDSTP in treating the infections caused by these bacteria, thereby repurposing this compound.

To begin with, PDSTP was shown to have a negligible inhibitory activity on the growth of *P. aeruginosa* PA01 and nine CF clinical isolates, *B. cenocepacia* K56-2 and J2315, and *S. aureus* ATCC 25923. This is consistent with the size and positive charge of the compound which prevent its entry into bacterial cells (Egorova *et al*., 2021). Indeed, the high molecular weight of PDSTP prevents its diffusion through porins, while its high polarity makes its diffusion across the lipid bilayer unlikely (O'Shea and Moser, 2008).

The compound was then tested against *P. aeruginosa* PA01 adhesion to various pulmonary epithelial cell lines, including a CF cell line, resulting to be highly effective at very low concentrations which were more than 50 times lower than the 50% cytotoxic concentration (Schmidtke *et al*., 2002). Furthermore, when tested against hypermucoid *P. aeruginosa* BT2 and BT72 clinical isolates, PDSTP maintained its antiadhesive activity. Imaging flow cytometry validated these results, highlighting that PDSTP treatment particularly affected the adhesion of multiple bacteria to human cells, probably by reducing the accessibility of human cell surface receptors.

Focusing on the current research on antiadhesive molecules against *P. aeruginosa*, PDSTP offers some advantages compared to other approaches such as natural extracts (Ahmed *et al*., 2014; Molina Bertrán *et al*., 2022) and glycoclusters (Malinovská *et al*., 2019). In fact, PDSTP was extensively characterized *in vivo* as an antiviral agent, demonstrating non-cytotoxicity, effectiveness at low concentrations and a broad therapeutic index. Conversely, natural extracts and glycoclusters often necessitate very high concentrations *in vitro*, typically in the range of mg/mL, limiting their *in vivo* application.

Pretreatment of *P. aeruginosa* PA01 with PDSTP prior to adhesion assays resulted in an increase in bacterial adhesion, providing the first evidence that the compound interacts with this bacterium, likely involving its outer membrane due to the molecular structure of PDSTP. On the other hand, pretreatment of both bacteria and human cells with the compound led to a reduction in bacterial adhesion comparable to a standard PDSTP treatment, suggesting that the mechanism of action involved in PDSTP-mediated impairment of bacterial adhesion may be due to electrostatic repulsion between PDSTP molecules bound to bacteria and those bound to human cells.

A preliminary study of the mechanism involved in PDSTP-mediated impairment of bacterial adhesion was conducted. Specifically, the presence of heparin, a structural analogue of heparan-sulphates (Liu and Thorp, 2002), during adhesion assays restored the normal adhesive capabilities of *P. aeruginosa* PA01 by sequestering PDSTP. This result highlights the high affinity of the compound for HSGAGs and suggests a potential involvement of these surface receptors in PDSTP antiadhesive activity, similar to its action during viral adsorption. However, when human cells were pretreated with heparinase, an enzyme that cleaves heparan sulphate chains (Dong *et al*., 2012), *P. aeruginosa* PA01 adhered to both untreated and heparinase-pretreated A549 cells in the same manner, even when PDSTP was administered. This experiment was also performed using another cell line, CFBE41o-, and another bacterium, *B. cenocepacia* J2315, showing the same result. These findings suggest that HSGAGs are not the primary receptors mediating bacterial adhesion, implying that the mechanism of action of PDSTP differs between bacterial and viral infections.

The involvement of HSGAGs in PDSTP antiadhesive properties will be further explored through adhesion assays using A549 cells lacking these host cell receptors. Specifically, the expression of the *β-1,3-glucuronyltransferase 3* gene will be knocked-down as it plays a crucial role in HSGAGs biosynthesis (Martin *et al*., 2019).

The interaction between PDSTP and *P. aeruginosa* PA01 was also investigated. Preliminary analyses showed that this interaction relies on electrostatic forces and mediates the transitioning of the bacterium from a rod-shape to a spherical shape. Subsequently, it was demonstrated that the molecular target of the compound was the lipopolysaccharide (LPS) present on the external leaflet of the outer membrane of *P. aeruginosa* PA01. Indeed, PDSTP displaced the dansyl-polymyxin (DPX) from the LPS, targeting the negative charges of both lipid A and core-oligosaccharide (Moore *et al*., 1986).

Interestingly, the O-antigen of *B. cenocepacia* K56-2 prevented the interaction of PDSTP with lipid A and core-oligosaccharide. In fact, a strain of *B. cenocepacia* incapable of producing the O-antigen (MH1K ΔOAg) (Hanuszkiewicz *et al*., 2014) resulted to be sensitive to the antiadhesive properties of the compound, while a strain of *B. cenocepacia* J2315 transformed with a plasmid allowing the production of the O-antigen (J2315-pXO4) (Ortega *et al*., 2005) exhibited resistance to the antiadhesive activity of PDSTP. However, the O-antigen shielding activity of the compound depends on the bacterial strain since *P. aeruginosa* PA01 was sensitive to the compound even though it produces the O-antigen. This could be attributed to differences in the O-antigen composition between *P. aeruginosa* PA01 and *B. cenocepacia* K56-2. Indeed, although both LPS profiles displayed an O-antigen of 11 bands when visualized *via* silver staining, their polysaccharide composition is different. Specifically, the O-antigen of *P. aeruginosa* PA01 consists of mannuronic acid, N-acetyl-D-fucosamine and rhamnose (Huszczynski *et al*., 2019), while that of *B. cenocepacia* K56-2 is composed of N-acetylgalactosamine and rhamnose (Ortega *et al*., 2005). Moreover, variations in the number of sugar residues in their O-antigen may further contribute to the observed differences in PDSTP antiadhesive properties.

As previously anticipated, PDSTP exhibited low antimicrobial activity when determining the MIC against *P. aeruginosa* PA01 and nine CF strains, with strain-specific susceptibilities. These differences likely arise from modifications of the LPS which will be extracted and analysed. Interestingly, the MIC values resulted to be increased in TSB compared to CAMHB. A similar effect was previously observed with aminoglycosides and was attributed to salt interfering with the electrostatic interactions between these antibiotics and the components of the outer membrane surface that mediate their uptake (Hancock, 1981). The positive charges of PDSTP may play a role in this specific biological activity.

The modest inhibitory effect on bacterial growth displayed by PDSTP is a characteristic of specific antibiotic adjuvants such as outer membrane permeabilizers (Douafer *et al*., 2019). Given this characteristic and also the interaction of PDSTP with the LPS, the putative adjuvant activity of PDSTP was investigated, revealing an overall increase in the effectiveness of the tested antibiotics against *P. aeruginosa* PA01 and multidrug-resistant CF isolates. Specifically, a combination of the compound with β-lactams showed the most significant reduction in the MIC and a durable efficacy over time for most strains.

The efficacy of PDSTP as an antibiotic adjuvant against *P. aeruginosa* is similar to that of natural polyamines, which can reduce the MIC of many β-lactams and other low molecular weight antibiotics against *P. aeruginosa*, although only at high concentrations (Kwon and Lu, 2006). These outer membrane permeabilizing molecules carry positively charged nitrogens and function by inhibiting efflux pumps (Cadelis *et al*., 2021; Wang *et al*., 2022; Li *et al*., 2019). Depolarization assay on *P. aeruginosa* PA01 demonstrated that PDSTP-mediated antibiotic potentiation relies on the same mechanism.

Besides the promising results achieved, the importance of developing PDSTP as an adjuvant compound is also highlighted by its exceptional efficacy against highly drug-resistant *P. aeruginosa*. Indeed, many adjuvants exhibit limited synergy with antibiotics against this bacterium (Vaara *et al*., 2010; Nikolaev *et al*., 2020; Stokes *et al*., 2017; Zhou *et al*., 2022).

Antibiotic potentiation was validated using a *Galleria mellonella* infection model, revealing that PDSTP enhanced the activity of ceftazidime also *in vivo*, highlighting its translational potential. Establishing the most suitable administration protocol in mammals requires further investigation with murine infection models, allowing for the testing of multiple administrations of the adjuvant, which is an option not available in *G. mellonella*. Antibiotic potentiation will be further investigated both *in vitro* and *in vivo* focusing on high molecular weight antibiotics. Additionally, other relevant CF bacteria will be employed.

Furthermore, the potential of PDSTP as a biofilm inhibitor was assessed, demonstrating a significant reduction in biofilm formation at sub-inhibitory concentrations using different *in vitro* and *ex vivo* models. The consistency in results across strains with structural differences in their biofilms suggests that PDSTP disrupts biofilm formation by targeting an essential mechanism shared by various *P. aeruginosa* strains. Specifically, since the compound is introduced only after the initial bacterial adhesion to the surface, it likely affects bacterial aggregation. Given that the LPS is involved in biofilm formation, its interaction with the compound may be involved in this specific biological process (Huszczynski *et al*., 2019).

This putative mechanism of action would distinguish PDSTP from most reported biofilm inhibitors which primarily function as quorum-sensing inhibitors (Wang *et al*., 2022; O'Loughlin *et al*., 2013; D'Angelo *et al*., 2018), lectin binding competitors (Bergmann *et al*., 2016) or repressors of exopolysaccharide production (van Tilburg Bernardes *et al*., 2017).

In conclusion, PDSTP showed a wide range of activities, especially against *P. aeruginosa*, being an effective inhibitor of bacterial adhesion to epithelial cells, enhancer of antibiotic activity and inhibitor of biofilm formation. These combined antivirulence and antibiotic potentiation properties may help addressing the growing threat of multidrug-resistant bacteria.

During my PhD, I spent six months in the laboratory of Prof. Sarah Vreugde at the University of Adelaide (Adelaide, South Australia), focusing on another alternative to fight *P. aeruginosa* infections: the phage therapy. Phages offers species-specific activity against not only bacteria resistant to antibiotics, but also biofilm-embedded and persister bacterial cells (Strathdee *et al*., 2023). Consequently, the aim of the second part of this work was to isolate and characterize novel *P. aeruginosa* phages and use them to select phage-resistant *P. aeruginosa* mutants.

Three *P. aeruginosa* phages, named PA48, PA49 and PA50, were isolated from wastewater. Interestingly, *P. aeruginosa* phages with high therapeutic potential are commonly found in this source (Martínez-Gallardo *et al*., 2023).

Genomic analysis demonstrated that PA49 is suitable for clinical applications. Indeed, the genome of PA49 was sequenced using the Nanopore platform and subsequently characterized, revealing its lytic nature and the absence of genes encoding virulence factors and antibiotic resistances.

Isolated phages were initially characterized in terms of stability and phage cycle dynamics. In fact, phages must remain active post-administration and during storage. Furthermore, the phage cycle should be short with a substantial phage progeny production for a rapid bacterial infection clearance. The three phages demonstrated stability across a wide range of pH values, temperatures and storage conditions. Considering that phages are generally administered by inhalation for treating bacterial infections at the lung level (Wang *et al*., 2021), the stability of the phage after nebulisation will be assessed. In terms of phage cycle, the results suggest a faster killing activity for PA49, compared to PA48 and PA50.

Subsequently, the phages were characterized from a microbiological perspective to investigate their killing properties both on planktonic and biofilm-embedded bacteria. They showed a similar broad host range, indicating that they may recognize a common receptor on bacterial surfaces. Nevertheless, they can be combined with other phages into phage cocktails to broaden the host range, besides overcoming phage resistance, thus enhancing treatment efficacy (Strathdee *et al*., 2023). Interestingly, three clinical isolates were resistant to all phages, suggesting the lack of the recognized receptor. When assessing the killing activity against planktonic *P. aeruginosa* PA01, PA48 and PA50 suppressed bacterial growth later compared to PA49. This is consistent with the rapid adsorption, shorter latent period and higher burst size of the myoviral phage, compared to the siphoviral phages. Finally, PA48, PA49 and PA50 were tested against mature biofilms of both *P. aeruginosa* PA01 reference strain and clinical isolates showing efficient biofilm eradication properties, especially for PA49.

It is worth highlighting that PA48 and PA50 produced highly similar results across all assays, suggesting that they might be the same phage. Considering the limitations of sequencing the genomes of these phages using the Nanopore platform, they will be sequenced using the Illumina platform. This approach should help overcome the Nanopore limitations, subsequently allowing to determine whether PA48 and PA50 are two different phages.

Earlier this year, several *P. aeruginosa* phages were described and primarily classified within the *Caudovirales* order. Indeed, phages belonging to this order are the majority of described phages, according to the literature (Dion *et al*., 2020), including the phages characterized in this study. Specifically, they fall into three categories which are myoviral (Wang *et al*., 2023b; Suchithra *et al*., 2023; Abdelghafar *et al*., 2023a), podoviral (Fei *et al*., 2023; Abdelghafar *et al*., 2023b) and schitoviral (Tsai *et al*., 2023; Kamyab *et al*., 2023) phages. The thermal stability of PA48, PA49 and PA50 aligns with those of the recently described phages. However, the phages described in this study exhibited a better stability under extreme pH conditions. PA48 and PA50 showed the lowest phage progeny productivity, even with their relatively long latent period. In contrast, PA49 displayed the highest burst size among the recently described myoviral phages (Wang *et al*., 2023b; Suchithra *et al*., 2023; Abdelghafar *et al*., 2023a), comparable to those of schitoviral phiPA1-3 (Tsai *et al*., 2023) and podoviral HZ2201 (Fei *et al*., 2023), but achieved within a shorter latent period. The host range of PA49 is comparable to those of the highly effective podoviral HZ2201 (Fei *et al*., 2023) and myoviral PseuPha1 (Suchithra *et al*., 2023). Finally, all these phages demonstrated efficient killing of both planktonic and biofilm-embedded *P. aeruginosa*, with some of them even showing promising *in vivo* activity in mouse (Wang *et al*., 2023b; Abdelghafar *et al*., 2023ab) and zebrafish (Tsai *et al*., 2023) infection models.

These findings highlight the therapeutic potential of PA48, PA49 and PA50, with a particular focus on PA49. Considering the promising antimicrobial activity observed in phage-antibiotic combinations (Martínez-Gallardo *et al*., 2022), the potential synergistic effects of these phages when used in conjunction with antibiotics will be evaluated. Finally, the efficacy of these phages will be tested in a mouse model of lung infections.

Phages exert strong selective pressure on bacteria, leading to the emergence of resistance. This resistance often results in physiological changes that may reduce bacterial fitness and increase antibiotic susceptibility. To counter phage resistance, one strategy is to drive bacterial evolution toward favourable trade-offs (Hasan and Ahn, 2022). In this work, two myoviral phages, PA49 and PA18 (previously characterized in the lab), were employed to select *P. aeruginosa* PA01 resistant mutants. The result of their sensitivity to PA18, PA48, PA49 and PA50 suggested that PA48, PA49 and PA50 share the same bacterial host receptor, while PA18 recognize a different one. In most cases, the growth of the BIMs was comparable to that of the parental *P. aeruginosa* PA01 strain. However, their ability to form biofilms was affected. Specifically, BIMs selected by PA18 exhibited increased biofilm formation, while PA49 BIMs displayed a defect in biofilm formation. Moreover, the BIMs resulted to be overall more susceptible to antibiotics commonly used in clinical setting, compared to the parental strain. Although most strains showed only a 2-fold MIC reduction, the MIC of colistin was significantly reduced, up to a 16-fold.

Some interesting favourable trade-offs associated with *P. aeruginosa* phage resistance were recently described, sharing similar characteristics with those characterized in this study. For instance, Li *et al*. described three phage-resistant bacteria: hipa2-R, phipa4-R and phipa10-R, selected by a podoviral, a siphoviral and a myoviral phage, respectively. hipa2-R and phipa4-R exhibited reduced biofilm production, similar to PA49 BIMs. In contrast, phipa10-R demonstrated increased biofilm formation, resembling PA18 BIMs. Moreover, hipa2-R and phipa10-R displayed different antibiotic profiles compared to the parental strain. However, there was no reduction in the MIC for colistin. On the other hand, phipa4-R exhibited an antibiotic profile identical to that of the parental strain (Li *et al*., 2022b). Interestingly, Wannasrichan *et al*. described three bacteria resistant to the myoviral phage JJ01 which not only exhibited reduced biofilm formation, but also showed a significant increase in susceptibility to colistin compared to the parental strain. These results align with the findings obtained for PA49 BIMs. Furthermore, this group demonstrated that the hypersensitivity to this antibiotic is due to perturbation of bacterial membranes (Wannasrichan *et al*., 2022). Further analyses will be performed to explore whether the BIMs isolated in this work share the same mechanism of action.

Finally, these phenotypes were attributed either to mutations in genes involved in the biosynthesis of the type IV pilus or large genomic deletion containing LPS-related genes (Li *et al*., 2022b; Xuan *et al*., 2022). Whole-genome sequencing will be performed to investigate whether mutations in type 4 pilus or LPS genes are involved.

These findings suggest that, although phage-resistant bacteria would emerge following phage administration, it will come at cost of bacterial fitness. These trade-offs could be beneficial for treatment, potentially impairing bacterial virulence and increasing the antibiotic susceptibility of these BIMs also *in vivo*. To further evaluate the impact on the virulence of these strains, their exoproteins will be collected and tested against air-liquid interface cultures of human nasal epithelial cells. Specifically, cytotoxicity, trans-epithelial electrical resistance and paracellular permeability will be explored. Finally, to determine whether the BIMs become more sensitive to antibiotics also when embedded into biofilm, minimum biofilm eradication concentration determination will be performed.

In summary, this research has been dedicated to the development of potential therapeutic strategies for combating bacterial infections, particularly those caused by antibiotic-resistant strains in cystic fibrosis patients. Overall, the alternative approaches described in this work provide a basis for further research and potential clinical applications, representing a valuable contribution for addressing the growing threat of antibiotic-resistant bacterial infections in contexts where conventional antibiotic therapy is often inefficient.

6. References

- Abdelghafar A, El-Ganiny A, Shaker G, Askoura M. 2023b. Isolation of a bacteriophage targeting *Pseudomonas aeruginosa* and exhibits a promising *in vivo* efficacy. *AMB Express*. 13(1):79. doi: 10.1186/s13568-023-01582-3.
- Abdelghafar A, El-Ganiny A, Shaker G. 2023a. A novel lytic phage exhibiting a remarkable *in vivo* therapeutic potential and higher antibiofilm activity against *Pseudomonas aeruginosa*. *Eur J Clin Microbiol Infect Dis*. doi: 10.1007/s10096-023-04649-y.
- Abedon ST, Danis-Wlodarczyk KM, Wozniak DJ. 2021. Phage cocktail development for bacteriophage therapy: toward improving spectrum of activity breadth and depth. *Pharmaceuticals*. 14(10):1019. doi: 10.3390/ph14101019.
- Ackermann HW. 2007. 5500 phages examined in the electron microscope. *Arch Virol*. 152(2):227-43. doi: 10.1007/s00705-006-0849-1.
- Ackermann H-W. *Bacteriophages*. Humana Press, 2009.
- Ahmed GF, Elkhatib WF, Noreddin AM. 2014. Inhibition of *Pseudomonas aeruginosa* PAO1 adhesion to and invasion of A549 lung epithelial cells by natural extracts. *J Infect Public Health*. 7(5):436-44. doi: 10.1016/j.jiph.2014.01.009.
- Akhoundsadegh N, Belanger CR, Hancock REW. 2019. Outer membrane interaction kinetics of new polymyxin B analogs in Gram-negative bacilli. *Antimicrob Agents Chemother*. 63(10):e00935-19. doi: 10.1128/AAC.00935-19.
- Akil N, Muhlebach MS. 2018. Biology and management of methicillin resistant *Staphylococcus aureus* in cystic fibrosis. *Pediatr Pulmonol*. 53(S3):S64-S74. doi: 10.1002/ppul.24139.
- Alcalá-Franco B, Montanari S, Cigana C, Bertoni G, Oliver A, Bragonzi A. 2012. Antibiotic pressure compensates the biological cost associated with *Pseudomonas aeruginosa* hypermutable phenotypes *in vitro* and in a murine model of chronic airways infection. *J Antimicrob Chemother*. 67(4):962-9. doi: 10.1093/jac/dkr587.

References

- Alcock BP, Raphenya AR, Lau TTY, Tsang KK, Bouchard M, Edalatmand A, Huynh W, Nguyen AV, Cheng AA, Liu S, Min SY, Miroshnichenko A, Tran HK, Werfalli RE, Nasir JA, Oloni M, Speicher DJ, Florescu A, Singh B, Faltyn M, Hernandez-Koutoucheva A, Sharma AN, Bordeleau E, Pawlowski AC, Zubyk HL, Dooley D, Griffiths E, Maguire F, Winsor GL, Beiko RG, Brinkman FSL, Hsiao WWL, Domselaar GV, McArthur AG. 2020. CARD 2020: antibiotic resistome surveillance with the comprehensive antibiotic resistance database. *Nucleic Acids Res*. 48(D1):D517-D525. doi: 10.1093/nar/gkz935.
- Alimbarova L, Egorova A, Riabova O, Monakhova N, Makarov V. 2022. A proof-of-concept study for the efficacy of dispirotripiperazine PDSTP in a rabbit model of herpes simplex epithelial keratitis. *Antiviral Res*. 202:105327. doi: 10.1016/j.antiviral.2022.105327.
- Arber W. 2014. Horizontal gene transfer among bacteria and its role in biological evolution. *Life*. 4(2):217-24. doi: 10.3390/life4020217.
- Aronoff SC. 1988. Outer membrane permeability in *Pseudomonas cepacia*: diminished porin content in a beta-lactam-resistant mutant and in resistant cystic fibrosis isolates. *Antimicrob Agents Chemother*. 32(11):1636-9. doi: 10.1128/AAC.32.11.1636.
- Askoura M, Mottawea W, Abujamel T, Taher I. 2011. Efflux pump inhibitors (EPIs) as new antimicrobial agents against *Pseudomonas aeruginosa*. *Libyan J Med*. doi: 10.3402/ljm.v6i0.5870.
- Ball G, Viarre V, Garvis S, Voulhoux R, Filloux A. 2012. Type II-dependent secretion of a *Pseudomonas aeruginosa* DING protein. *Res Microbiol.* 163(6-7):457-69. doi: 10.1016/j.resmic.2012.07.007.
- Bamford S, Ryley H, Jackson SK. 2007. Highly purified lipopolysaccharides from *Burkholderia cepacia* complex clinical isolates induce inflammatory cytokine responses via TLR4-mediated MAPK signalling pathways and activation of NFkappaB. *Cell Microbiol*. 9(2):532-43. doi: 10.1111/j.1462-5822.2006.00808.x.
- Barth H, Schafer C, Adah MI, Zhang F, Linhardt RJ, Toyoda H, Kinoshita-Toyoda A, Toida T, Van Kuppevelt TH, Depla E, Von Weizsacker F, Blum HE, Baumert TF. 2003. Cellular binding of hepatitis C virus envelope glycoprotein E2 requires cell surface heparan sulfate*. J Biol Chem*. 278(42):41003-12. doi: 10.1074/jbc.M302267200.
- Bartlett AH, Park PW. 2011. Heparan sulfate proteoglycans in infection. Glycans in diseases and therapeutics. 19:31–62. doi: 10.1007/978-3-642-16833-8_2.

- Benenson EV, Nemtsov BF, Krasnov SL. 1986. The new basic agent prospidin in the therapy of rheumatoid arthritis. An evaluation of the clinical effectiveness and the mechanism of action of prospidin. *Ter Arkh*. 58(12):103-8.
- Benthall G, Touzel RE, Hind CK, Titball RW, Sutton JM, Thomas RJ, Wand ME. 2015. Evaluation of antibiotic efficacy against infections caused by planktonic or biofilm cultures of *Pseudomonas aeruginosa* and *Klebsiella pneumoniae* in *Galleria mellonella*. *Int J Antimicrob Agents*. 46(5):538-45. doi: 10.1016/j.ijantimicag.2015.07.014.
- Bergmann M, Michaud G, Visini R, Jin X, Gillon E, Stocker A, Imberty A, Darbre T, Reymond JL. 2016. Multivalency effects on *Pseudomonas aeruginosa* biofilm inhibition and dispersal by glycopeptide dendrimers targeting lectin LecA. *Org Biomol Chem*. 14(1):138-48. doi: 10.1039/c5ob01682g.
- Berlutti F, Superti F, Nicoletti M, Morea C, Frioni A, Ammendolia MG, Battistoni A, Valenti P. 2008. Bovine lactoferrin inhibits the efficiency of invasion of respiratory A549 cells of different iron-regulated morphological forms of *Pseudomonas aeruginosa* and *Burkholderia cenocepacia*. *Int J Immunopathol Pharmacol*. 21(1):51-9. doi: 10.1177/039463200802100107.
- Bernheim A, Sorek R. 2020. The pan-immune system of bacteria: antiviral defence as a community resource. *Nat Rev Microbiol*. 18(2):113-119. doi: 10.1038/s41579-019-0278-2.
- Bishop JR, Schuksz M, Esko JD. 2007. Heparan sulphate proteoglycans fine-tune mammalian physiology. *Nature*. 446(7139):1030-7. doi: 10.1038/nature05817.
- Bland C, Ramsey TL, Sabree F, Lowe M, Brown K, Kyrpides NC, Hugenholtz P. 2007. CRISPR recognition tool (CRT): a tool for automatic detection of clustered regularly interspaced palindromic repeats. *BMC Bioinformatics*. 8:209. doi: 10.1186/1471-2105-8-209.
- Bleves S, Viarre V, Salacha R, Michel GP, Filloux A, Voulhoux R. 2010. Protein secretion systems in *Pseudomonas aeruginosa*: a wealth of pathogenic weapons. *Int J Med Microbiol*. 300(8):534-43. doi: 10.1016/j.ijmm.2010.08.005.
- Borin JM, Avrani S, Barrick JE, Petrie KL, Meyer JR. 2021. Coevolutionary phage training leads to greater bacterial suppression and delays the evolution of phage resistance. *Proc Natl Acad Sci U S A*. 118(23):e2104592118. doi: 10.1073/pnas.2104592118.

References

- Borselli D, Lieutaud A, Thefenne H, Garnotel E, Pagès JM, Brunel JM, Bolla JM. 2016. Polyamino-isoprenic derivatives block intrinsic resistance of *P. aeruginosa* to doxycycline and chloramphenicol *in vitro*. *PLoS One*. 11(5):e0154490. doi: 10.1371/journal.pone.0154490.
- Bouras G, Nepal R, Houtak G, Psaltis AJ, Wormald PJ, Vreugde S. 2023. Pharokka: a fast scalable bacteriophage annotation tool. *Bioinformatics*. 39(1):btac776. doi: 10.1093/bioinformatics/btac776.
- Bruchmann S, Dötsch A, Nouri B, Chaberny IF, Häussler S. 2013. Quantitative contributions of target alteration and decreased drug accumulation to *Pseudomonas aeruginosa* fluoroquinolone resistance. *Antimicrob Agents Chemother*. 57(3):1361-8. doi: 10.1128/AAC.01581-12.
- Bruscia E, Sangiuolo F, Sinibaldi P, Goncz KK, Novelli G, Gruenert DC. 2002. Isolation of CF cell lines corrected at DeltaF508-CFTR locus by SFHR-mediated targeting. *Gene Ther*. 9(11):683-5. doi: 10.1038/sj.gt.3301741.
- Bucior I, Pielage JF, Engel JN. 2012. *Pseudomonas aeruginosa* pili and flagella mediate distinct binding and signaling events at the apical and basolateral surface of airway epithelium. *PLoS Pathog*. 8(4):e1002616. doi: 10.1371/journal.ppat.1002616.
- Buroni S, Matthijs N, Spadaro F, Van Acker H, Scoffone VC, Pasca MR, Riccardi G, Coenye T. 2014. Differential roles of RND efflux pumps in antimicrobial drug resistance of sessile and planktonic *Burkholderia cenocepacia* cells. *Antimicrob Agents Chemother*. 58(12):7424-9. doi: 10.1128/AAC.03800-14.
- Burrows LL. 2012. *Pseudomonas aeruginosa* twitching motility: type IV pili in action. *Annu Rev Microbio*l. 66:493-520. doi: 10.1146/annurev-micro-092611-150055.
- Bush K, Fisher JF. 2011. Epidemiological expansion, structural studies, and clinical challenges of new β-lactamases from Gram-negative bacteria. *Annu Rev Microbiol*. 65:455-78. doi: 10.1146/annurev-micro-090110-102911.
- Buttress JA, Halte M, Te Winkel JD, Erhardt M, Popp PF, Strahl H. 2022. A guide for membrane potential measurements in Gram-negative bacteria using voltage-sensitive dyes. *Microbiology*. 168(9). doi: 10.1099/mic.0.001227.

- Cadelis MM, Li SA, Bourguet-Kondracki ML, Blanchet M, Douafer H, Brunel JM, Copp BR. 2021. Spermine derivatives of indole-3-carboxylic acid, indole-3-acetic acid and indole-3-acrylic acid as Gram-negative antibiotic adjuvants. *ChemMedChem*. 16(3):513-523. doi: 10.1002/cmdc.202000359.
- Camens S, Liu S, Hon K, Bouras GS, Psaltis AJ, Wormald PJ, Vreugde S. 2021. Preclinical development of a bacteriophage cocktail for treating multidrug resistant *Pseudomonas aeruginosa* infections. *Microorganisms*. 9(9):2001. doi: 10.3390/microorganisms9092001.
- Chambers HF. 1997. Methicillin resistance in staphylococci: molecular and biochemical basis and clinical implications. *Clin Microbiol Rev*. 10(4):781-91. doi: 10.1128/CMR.10.4.781.
- Chan BK, Sistrom M, Wertz JE, Kortright KE, Narayan D, Turner PE. 2016. Phage selection restores antibiotic sensitivity in MDR *Pseudomonas aeruginosa*. *Sci Rep*. 6:26717. doi: 10.1038/srep26717.
- Chan PP, Lin BY, Mak AJ, Lowe TM. 2021. tRNAscan-SE 2.0: improved detection and functional classification of transfer RNA genes. *Nucleic Acids Res*. 49(16):9077-9096. doi: 10.1093/nar/gkab688.
- Chen L, Yang J, Yu J, Yao Z, Sun L, Shen Y, Jin Q. 2005. VFDB: a reference database for bacterial virulence factors. *Nucleic Acids Res*. 33(Database issue):D325-8. doi: 10.1093/nar/gki008.
- Cheng SH, Gregory RJ, Marshall J, Paul S, Souza DW, White GA, O'Riordan CR, Smith AE. 1990. Defective intracellular transport and processing of CFTR is the molecular basis of most cystic fibrosis. *Cell*. 63(4):827-34. doi: 10.1016/0092-8674(90)90148-8.
- Cheung KJ Jr, Li G, Urban TA, Goldberg JB, Griffith A, Lu F, Burns JL. 2007. Pilus-mediated epithelial cell death in response to infection with *Burkholderia cenocepacia*. *Microbes Infect*. 9(7):829-37. doi: 10.1016/j.micinf.2007.03.001.
- Cho DY, Lim DJ, Mackey C, Skinner D, Zhang S, McCormick J, Woodworth BA. 2019. Ivacaftor, a cystic fibrosis transmembrane conductance regulator potentiator, enhances ciprofloxacin activity against *Pseudomonas aeruginosa*. *Am J Rhinol Allergy*. 33(2):129-136. doi: 10.1177/1945892418815615.
- Clokie MR, Millard AD, Letarov AV, Heaphy S. 2011. Phages in nature. *Bacteriophage*. 1(1):31-45. doi: 10.4161/bact.1.1.14942.
- CLSI. 1999. Methods for determining bactericidal activity of antimicrobial agents; approved guideline. CLSI document M26-A. Wayne, PA: Clinical and Laboratory Standards Institute.

References

- CLSI. 2020. Performance standards for antimicrobial susceptibility testing. 30th ed. CLSI supplement M100. Wayne, PA: Clinical and Laboratory Standards Institute.
- Connell BJ, Lortat-Jacob H. 2013. Human immunodeficiency virus and heparan sulfate: from attachment to entry inhibition. *Front Immunol*. 4:385. doi: 10.3389/fimmu.2013.00385.
- Conway BA, Chu KK, Bylund J, Altman E, Speert DP. 2004. Production of exopolysaccharide by *Burkholderia cenocepacia* results in altered cell-surface interactions and altered bacterial clearance in mice. *J Infect Dis*. 190(5):957-66. doi: 10.1086/423141.
- Cook R, Brown N, Redgwell T, Rihtman B, Barnes M, Clokie M, Stekel DJ, Hobman J, Jones MA, Millard A. 2021. INfrastructure for a PHAge REference Database: identification of large-scale biases in the current collection of cultured phage genomes. *Phage*. 2(4):214-223. doi: 10.1089/phage.2021.0007.
- Cornelis P. 2010. Iron uptake and metabolism in pseudomonads. *Appl Microbiol Biotechnol*. 86(6):1637-45. doi: 10.1007/s00253-010-2550-2.
- Cozens AL, Yezzi MJ, Kunzelmann K, Ohrui T, Chin L, Eng K, Finkbeiner WE, Widdicombe JH, Gruenert DC. 1994. CFTR expression and chloride secretion in polarized immortal human bronchial epithelial cells. *Am J Respir Cell Mol Biol*. 10(1):38-47. doi: 10.1165/ajrcmb.10.1.7507342.
- Crabbé A, Liu Y, Matthijs N, Rigole P, De La Fuente-Nùñez C, Davis R, Ledesma MA, Sarker S, Van Houdt R, Hancock RE, Coenye T, Nickerson CA. 2017. Antimicrobial efficacy against *Pseudomonas aeruginosa* biofilm formation in a three-dimensional lung epithelial model and the influence of fetal bovine serum. *Sci Rep*. 7:43321. doi: 10.1038/srep43321.
- Cystic Fibrosis Foundation. 2022. *CFFPR Annual Report 2021*.
- Dąbrowska K, Abedon ST. 2019. Pharmacologically aware phage therapy: pharmacodynamic and pharmacokinetic obstacles to phage antibacterial action in animal and human bodies. *Microbiol Mol Biol Rev*. 83(4):e00012-19. doi: 10.1128/MMBR.00012-19.
- Daccò V, Alicandro G, Consales A, Rosazza C, Sciarrabba CS, Cariani L, Colombo C. 2023. Cepacia syndrome in cystic fibrosis: a systematic review of the literature and possible new perspectives in treatment. *Pediatr Pulmonol*. 58(5):1337-1343. doi: 10.1002/ppul.26359.

- D'Angelo F, Baldelli V, Halliday N, Pantalone P, Polticelli F, Fiscarelli E, Williams P, Visca P, Leoni L, Rampioni G. 2018. Identification of FDA-approved drugs as antivirulence agents targeting the *pqs* quorum-sensing system of *Pseudomonas aeruginosa*. *Antimicrob Agents Chemother*. 62(11):e01296-18. doi: 10.1128/AAC.01296-18.
- Darby EM, Trampari E, Siasat P, Gaya MS, Alav I, Webber MA, Blair JMA. 2023. Molecular mechanisms of antibiotic resistance revisited. *Nat Rev Microbiol*. 21(5):280-295. doi: 10.1038/s41579-022-00820-y.
- Dasgupta N, Arora SK, Ramphal R. 2004. "The flagellar system of *Pseudomonas aeruginosa*" in "*Pseudomonas*: genomics, lifestyle and molecular architecture". Ed. JL Ramos (Boston, MA: *Springer US*). 675–698. doi: 10.1007/978-1-4419-9086-0_22.
- de Bentzmann S, Plotkowski C, Puchelle E. 1996. Receptors in the *Pseudomonas aeruginosa* adherence to injured and repairing airway epithelium. *Am J Respir Crit Care Med*. 154(4 Pt 2):S155-62. doi: 10.1164/ajrccm/154.4_Pt_2.S155.
- Dedrick RM, Guerrero-Bustamante CA, Garlena RA, Russell DA, Ford K, Harris K, Gilmour KC, Soothill J, Jacobs-Sera D, Schooley RT, Hatfull GF, Spencer H. 2019. Engineered bacteriophages for treatment of a patient with a disseminated drug-resistant *Mycobacterium abscessus*. *Nat Med*. 25(5):730-733. doi: 10.1038/s41591-019-0437-z.
- Deng Y, Boon C, Eberl L, Zhang LH. 2009. Differential modulation of *Burkholderia cenocepacia* virulence and energy metabolism by the quorum-sensing signal BDSF and its synthase. *J Bacteriol*. 191(23):7270-8. doi: 10.1128/JB.00681-09.
- Dion MB, Oechslin F, Moineau S. 2020. Phage diversity, genomics and phylogeny. *Nat Rev Microbiol*. 18(3):125-138. doi: 10.1038/s41579-019-0311-5.
- Dolce D, Neri S, Grisotto L, Campana S, Ravenni N, Miselli F, Camera E, Zavataro L, Braggion C, Fiscarelli EV, Lucidi V, Cariani L, Girelli D, Faelli N, Colombo C, Lucanto C, Lombardo M, Magazzù G, Tosco A, Raia V, Manara S, Pasolli E, Armanini F, Segata N, Biggeri A, Taccetti G. 2019. Methicillin-resistant *Staphylococcus aureus* eradication in cystic fibrosis patients: a randomized multicenter study. *PLoS One*. 14(3):e0213497. doi: 10.1371/journal.pone.0213497.
- Dong W, Lu W, McKeehan WL, Luo Y, Ye S. 2012. Structural basis of heparan sulfate-specific degradation by heparinase III. *Protein Cell*. 3(12):950-61. doi: 10.1007/s13238-012-2056-z.

References

- Douafer H, Andrieu V, Phanstiel O 4th, Brunel JM. 2019. Antibiotic adjuvants: make antibiotics great again! *J Med Chem*. 62(19):8665-8681. doi: 10.1021/acs.jmedchem.8b01781.
- Drawz SM, Bonomo RA. 2010. Three decades of beta-lactamase inhibitors. *Clin Microbiol Rev*. 23(1):160-201. doi: 10.1128/CMR.00037-09.
- Drevinek P, Holden MT, Ge Z, Jones AM, Ketchell I, Gill RT, Mahenthiralingam E. 2008. Gene expression changes linked to antimicrobial resistance, oxidative stress, iron depletion and retained motility are observed when *Burkholderia cenocepacia* grows in cystic fibrosis sputum. *BMC Infect Dis*. 8:121. doi: 10.1186/1471-2334-8-121.
- Drevinek P, Mahenthiralingam E. 2010. *Burkholderia cenocepacia* in cystic fibrosis: epidemiology and molecular mechanisms of virulence. *Clin Microbiol Infect*. 16(7):821-30. doi: 10.1111/j.1469-0691.2010.03237.x.
- Egorova A, Bogner E, Novoselova E, Zorn KM, Ekins S, Makarov V. 2021. Dispirotripiperazine-core compounds, their biological activity with a focus on broad antiviral property, and perspectives in drug design (mini-review). *Eur J Med Chem*. 211:113014. doi: 10.1016/j.ejmech.2020.113014.
- El'Garch F, Jeannot K, Hocquet D, Llanes-Barakat C, Plésiat P. 2007. Cumulative effects of several nonenzymatic mechanisms on the resistance of *Pseudomonas aeruginosa* to aminoglycosides. *Antimicrob Agents Chemother*. 51(3):1016-21. doi: 10.1128/AAC.00704-06.
- Engels W, Endert J, Kamps MA, van Boven CP. 1985. Role of lipopolysaccharide in opsonization and phagocytosis of *Pseudomonas aeruginosa*. *Infect Immun*. 49(1):182-9. doi: 10.1128/iai.49.1.182-189.1985.
- European Cystic Fibrosis Society. 2022. *ECFSPR Annual Report 2020*.
- Fei B, Li D, Liu X, You X, Guo M, Ren Y, Liu Y, Wang C, Zhu R, Li Y. 2023. Characterization and genomic analysis of a broad-spectrum lytic phage HZ2201 and its antibiofilm efficacy against *Pseudomonas aeruginosa*. *Virus Res*. 335:199184. doi: 10.1016/j.virusres.2023.199184.
- Feldman M, Bryan R, Rajan S, Scheffler L, Brunnert S, Tang H, Prince A. 1998. Role of flagella in pathogenesis of *Pseudomonas aeruginosa* pulmonary infection. *Infect Immun*. 66(1):43-51. doi: 10.1128/IAI.66.1.43-51.1998.

- Feuillet V, Medjane S, Mondor I, Demaria O, Pagni PP, Galán JE, Flavell RA, Alexopoulou L. 2006. Involvement of Toll-like receptor 5 in the recognition of flagellated bacteria. *Proc Natl Acad Sci USA*. 103(33):12487-92. doi: 10.1073/pnas.0605200103.
- Franklin MJ, Nivens DE, Weadge JT, Howell PL. 2011. Biosynthesis of the *Pseudomonas aeruginosa* extracellular polysaccharides, alginate, Pel, and Psl. *Front Microbiol*. 2:167. doi: 10.3389/fmicb.2011.00167.
- French S, Farha M, Ellis MJ, Sameer Z, Côté JP, Cotroneo N, Lister T, Rubio A, Brown ED. 2020. Potentiation of antibiotics against Gram-negative bacteria by polymyxin B analogue SPR741 from unique perturbation of the outer membrane. *ACS Infect Dis*. 6(6):1405-1412. doi: 10.1021/acsinfecdis.9b00159.
- Gautam V, Shafiq N, Singh M, Ray P, Singhal L, Jaiswal NP, Prasad A, Singh S, Agarwal A. 2015. Clinical and *in vitro* evidence for the antimicrobial therapy in *Burkholderia cepacia* complex infections. *Expert Rev Anti Infect Ther*. 13(5):629-63. doi: 10.1586/14787210.2015.1025056.
- Giard DJ, Aaronson SA, Todaro GJ, Arnstein P, Kersey JH, Dosik H, Parks WP. 1973. *In vitro* cultivation of human tumors: establishment of cell lines derived from a series of solid tumors. *J Natl Cancer Inst*. 51(5):1417-23. doi: 10.1093/jnci/51.5.1417.
- Giroglou T, Florin L, Schäfer F, Streeck RE, Sapp M. 2001. Human papillomavirus infection requires cell surface heparan sulfate. *J Virol*. 75(3):1565-70. doi: 10.1128/JVI.75.3.1565-1570.2001.
- Goltermann L, Tolker-Nielsen T. 2017. Importance of the exopolysaccharide matrix in antimicrobial tolerance of *Pseudomonas aeruginosa* aggregates. *Antimicrob Agents Chemother*. 61(4):e02696-16. doi: 10.1128/AAC.02696-16.
- Goss CH, Muhlebach MS. 2011. Review: *Staphylococcus aureus* and MRSA in cystic fibrosis. *J Cyst Fibros*. 10(5):298-306. doi: 10.1016/j.jcf.2011.06.002.
- Govan JR, Brown AR, Jones AM. 2007. Evolving epidemiology of *Pseudomonas aeruginosa* and the *Burkholderia cepacia* complex in cystic fibrosis lung infection. *Future Microbiol*. 2(2):153-64. doi: 10.2217/17460913.2.2.153.
- Hampton HG, Watson BNJ, Fineran PC. 2020. The arms race between bacteria and their phage foes. *Nature*. 577(7790):327-336. doi: 10.1038/s41586-019-1894-8.

- Hancock RE. 1981. Aminoglycoside uptake and mode of action - with special reference to streptomycin and gentamicin. Antagonists and mutants. *J Antimicrob Chemother*. 8(4):249-76. doi: 10.1093/jac/8.4.249.
- Hancock RE. 1997. Peptide antibiotics. *Lancet*. 349(9049):418-22. doi: 10.1016/S0140-6736(97)80051-7.
- Hanuszkiewicz A, Pittock P, Humphries F, Moll H, Rosales AR, Molinaro A, Moynagh PN, Lajoie GA, Valvano MA. 2014. Identification of the flagellin glycosylation system in *Burkholderia cenocepacia* and the contribution of glycosylated flagellin to evasion of human innate immune responses. *J Biol Chem*. 289(27):19231-44. doi: 10.1074/jbc.M114.562603.
- Harrington NE, Sweeney E, Alav I, Allen F, Moat J, Harrison F. 2021. Antibiotic efficacy testing in an *ex vivo* model of *Pseudomonas aeruginosa* and *Staphylococcus aureus* biofilms in the cystic fibrosis lung. *J Vis Exp*. (167). doi: 10.3791/62187.
- Harris JK, Wagner BD, Zemanick ET, Robertson CE, Stevens MJ, Heltshe SL, Rowe SM, Sagel SD. 2020. Changes in airway microbiome and inflammation with ivacaftor treatment in patients with cystic fibrosis and the G551D mutation. *Ann Am Thorac Soc*. 17(2):212-220. doi: 10.1513/AnnalsATS.201907-493OC.
- Hasan M, Ahn J. 2022. Evolutionary dynamics between phages and bacteria as a possible approach for designing effective phage therapies against antibiotic-resistant bacteria. *Antibiotics*. 11(7):915. doi: 10.3390/antibiotics11070915.
- Hawdon NA, Aval PS, Barnes RJ, Gravelle SK, Rosengren J, Khan S, Ciofu O, Johansen HK, Høiby N, Ulanova M. 2010. Cellular responses of A549 alveolar epithelial cells to serially collected *Pseudomonas aeruginosa* from cystic fibrosis patients at different stages of pulmonary infection. *FEMS Immunol Med Microbiol*. 59(2):207-20. doi: 10.1111/j.1574-695X.2010.00693.x.
- Helander IM, Mattila-Sandholm T. 2000. Fluorometric assessment of Gram-negative bacterial permeabilization. *J Appl Microbiol*. 88(2):213-9. doi: 10.1046/j.1365-2672.2000.00971.x.
- Henderson IR, Navarro-Garcia F, Desvaux M, Fernandez RC, Ala'Aldeen D. 2004. Type V protein secretion pathway: the autotransporter story. *Microbiol Mol Biol Rev*. 68(4):692-744. doi: 10.1128/MMBR.68.4.692-744.2004.
- Hendrix RW. 2002. Bacteriophages: evolution of the majority. *Theor Popul Biol*. 61(4):471-80. doi: 10.1006/tpbi.2002.1590.

- Heydorn A, Nielsen AT, Hentzer M, Sternberg C, Givskov M, Ersbøll BK, Molin S. 2000. Quantification of biofilm structures by the novel computer program COMSTAT. *Microbiology*. 146 (Pt 10):2395-2407. doi: 10.1099/00221287-146-10-2395.
- Hisert KB, Heltshe SL, Pope C, Jorth P, Wu X, Edwards RM, Radey M, Accurso FJ, Wolter DJ, Cooke G, Adam RJ, Carter S, Grogan B, Launspach JL, Donnelly SC, Gallagher CG, Bruce JE, Stoltz DA, Welsh MJ, Hoffman LR, McKone EF, Singh PK. 2017. Restoring cystic fibrosis transmembrane conductance regulator function reduces airway bacteria and inflammation in people with cystic fibrosis and chronic lung infections. *Am J Respir Crit Care Med*. 195(12):1617-1628. doi: 10.1164/rccm.201609-1954OC.
- Hon K, Liu S, Camens S, Bouras GS, Psaltis AJ, Wormald PJ, Vreugde S. 2022. APTC-EC-2A: a lytic phage targeting multidrug resistant *E. coli* planktonic cells and biofilms. *Microorganisms*. 10(1):102. doi: 10.3390/microorganisms10010102.
- Horna G, Ruiz J. 2021. Type 3 secretion system of *Pseudomonas aeruginosa*. *Microbiol Res*. 246:126719. doi: 10.1016/j.micres.2021.126719.
- Hryniewicz MM, Garbacz K. 2017. Borderline oxacillin-resistant *Staphylococcus aureus* (BORSA) - A more common problem than expected? *J Med Microbiol*. 66(10):1367-1373. doi: 10.1099/jmm.0.000585.
- Hunt TA, Kooi C, Sokol PA, Valvano MA. 2004. Identification of *Burkholderia cenocepacia* genes required for bacterial survival *in vivo*. *Infect Immun*. 72(7):4010-22. doi: 10.1128/IAI.72.7.4010-4022.2004.
- Huszczynski SM, Lam JS, Khursigara CM. 2019. The role of *Pseudomonas aeruginosa* lipopolysaccharide in bacterial pathogenesis and physiology. *Pathogens*. 9(1):6. doi: 10.3390/pathogens9010006.
- Iozzo RV, Schaefer L. 2015. Proteoglycan form and function: a comprehensive nomenclature of proteoglycans. *Matrix Biol*. 42:11-55. doi: 10.1016/j.matbio.2015.02.003.
- Jay Smith. 2023. https://hartfordcffund.org/
- Jayathilaka EHTT, Rajapaksha DC, Nikapitiya C, De Zoysa M, Whang I. 2021. Antimicrobial and anti-biofilm peptide octominin for controlling multidrug-resistant *Acinetobacter baumannii*. *Int J Mol Sci*. 22(10):5353. doi: 10.3390/ijms22105353.

- Jenul C, Sieber S, Daeppen C, Mathew A, Lardi M, Pessi G, Hoepfner D, Neuburger M, Linden A, Gademann K, Eberl L. 2018. Biosynthesis of fragin is controlled by a novel quorum sensing signal. *Nat Commun*. 9(1):1297. doi: 10.1038/s41467-018-03690-2.
- Jia S, Taylor-Cousar JL. 2023. Cystic fibrosis modulator therapies. *Annu Rev Med*. 74:413-426. doi: 10.1146/annurev-med-042921-021447.
- Jiang F, Waterfield NR, Yang J, Yang G, Jin Q. 2014. A *Pseudomonas aeruginosa* type VI secretion phospholipase D effector targets both prokaryotic and eukaryotic cells. *Cell Host Microbe*. 15(5):600-10. doi: 10.1016/j.chom.2014.04.010.
- Kalia M, Chandra V, Rahman SA, Sehgal D, Jameel S. 2009. Heparan sulfate proteoglycans are required for cellular binding of the hepatitis E virus ORF2 capsid protein and for viral infection. *J Virol*. 83(24):12714-24. doi: 10.1128/JVI.00717-09.
- Kamyab H, Torkashvand N, Shahverdi AR, Khoshayand MR, Sharifzadeh M, Sepehrizadeh Z. 2023. Isolation, characterization, and genomic analysis of vB_PaeS_TUMS_P81, a lytic bacteriophage against *Pseudomonas aeruginosa*. *Virus Genes*. 59(1):132-141. doi: 10.1007/s11262-022-01954-0.
- Kerem B, Rommens JM, Buchanan JA, Markiewicz D, Cox TK, Chakravarti A, Buchwald M, Tsui LC. 1989. Identification of the cystic fibrosis gene: genetic analysis. *Science*. 245(4922):1073-80. doi: 10.1126/science.2570460.
- Kessler E, Safrin M, Gustin JK, Ohman DE. 1998. Elastase and the LasA protease of *Pseudomonas aeruginosa* are secreted with their propeptides. *J Biol Chem*. 273(46):30225-31. doi: 10.1074/jbc.273.46.30225.
- Kintz E, Scarff JM, DiGiandomenico A, Goldberg JB. 2008. Lipopolysaccharide O-antigen chain length regulation in *Pseudomonas aeruginosa* serogroup O11 strain PA103. *J Bacteriol*. 190(8):2709-16. doi: 10.1128/JB.01646-07.
- Kitt H, Lenney W, Gilchrist FJ. 2016. Two case reports of the successful eradication of new isolates of *Burkholderia cepacia* complex in children with cystic fibrosis. *BMC Pharmacol Toxicol*. 17:14. doi: 10.1186/s40360-016-0054-0.
- Kolmogorov M, Yuan J, Lin Y, Pevzner PA. 2019. Assembly of long, error-prone reads using repeat graphs. *Nat Biotechnol*. 37(5):540-546. doi: 10.1038/s41587-019-0072-8.
- Kortright KE, Doss-Gollin S, Chan BK, Turner PE. 2021. Evolution of bacterial cross-resistance to lytic phages and albicidin antibiotic. *Front Microbiol*. 12:658374. doi: 10.3389/fmicb.2021.658374.

- Kwon DH, Lu CD. 2006. Polyamines increase antibiotic susceptibility in *Pseudomonas aeruginosa*. *Antimicrob Agents Chemother*. 50(5):1623-7. doi: 10.1128/AAC.50.5.1623-1627.2006.
- Labrie SJ, Samson JE, Moineau S. 2010. Bacteriophage resistance mechanisms. *Nat Rev Microbiol*. 8(5):317-27. doi: 10.1038/nrmicro2315.
- Lambert PA. 2002. Mechanisms of antibiotic resistance in *Pseudomonas aeruginosa*. *J R Soc Med*. 95 Suppl 41(Suppl 41):22-6.
- Langton Hewer SC, Smyth AR. 2014. Antibiotic strategies for eradicating *Pseudomonas aeruginosa* in people with cystic fibrosis. *Cochrane Database Syst Rev*. (11):CD004197. doi: 10.1002/14651858.CD004197.pub4.
- Laslett D, Canback B. 2004. ARAGORN, a program to detect tRNA genes and tmRNA genes in nucleotide sequences. *Nucleic Acids Res*. 32(1):11-6. doi: 10.1093/nar/gkh152.
- Lee J, Zhang L. 2015. The hierarchy quorum sensing network in *Pseudomonas aeruginosa*. *Protein Cell*. 6(1):26-41. doi: 10.1007/s13238-014-0100-x.
- Leid JG, Willson CJ, Shirtliff ME, Hassett DJ, Parsek MR, Jeffers AK. 2005. The exopolysaccharide alginate protects *Pseudomonas aeruginosa* biofilm bacteria from IFN-gamma-mediated macrophage killing. *J Immunol*. 175(11):7512-8. doi: 10.4049/jimmunol.175.11.7512.
- Leistner CM, Gruen-Bernhard S, Glebe D. 2008. Role of glycosaminoglycans for binding and infection of hepatitis B virus. *Cell Microbiol*. 10(1):122-33. doi: 10.1111/j.1462-5822.2007.01023.x.
- Lewenza S, Conway B, Greenberg EP, Sokol PA. 1999. Quorum sensing in *Burkholderia cepacia*: identification of the LuxRI homologs CepRI. *J Bacteriol*. 181(3):748-56. doi: 10.1128/JB.181.3.748-756.1999.
- Lewenza S, Visser MB, Sokol PA. 2002. Interspecies communication between *Burkholderia cepacia* and *Pseudomonas aeruginosa*. *Can J Microbiol*. 48(8):707-16. doi: 10.1139/w02-068.
- Li D, Schneider-Futschik EK. 2023. Current and emerging inhaled antibiotics for chronic pulmonary *Pseudomonas aeruginosa* and *Staphylococcus aureus* infections in cystic fibrosis. *Antibiotics*. 12(3):484. doi: 10.3390/antibiotics12030484.
- Li H, Luo YF, Williams BJ, Blackwell TS, Xie CM. 2012. Structure and function of OprD protein in *Pseudomonas aeruginosa*: from antibiotic resistance to novel therapies. *Int J Med Microbiol*. 302(2):63-8. doi: 10.1016/j.ijmm.2011.10.001.

- Li N, Zeng Y, Wang M, Bao R, Chen Y, Li X, Pan J, Zhu T, Hu B, Tan D. 2022b. Characterization of phage resistance and their impacts on bacterial fitness in *Pseudomonas aeruginosa*. *Microbiol Spectr*. 10(5):e0207222. doi: 10.1128/spectrum.02072-22.
- Li Q, Mao S, Wang H, Ye X. 2022a. The molecular architecture of *Pseudomonas aeruginosa* quorum-sensing inhibitors. *Mar Drugs*. 20(8):488. doi: 10.3390/md20080488.
- Li SA, Cadelis MM, Sue K, Blanchet M, Vidal N, Brunel JM, Bourguet-Kondracki ML, Copp BR. 2019. 6-Bromoindolglyoxylamido derivatives as antimicrobial agents and antibiotic enhancers. *Bioorg Med Chem*. 27(10):2090-2099. doi: 10.1016/j.bmc.2019.04.004.
- Li XZ, Nikaido H. 2009. Efflux-mediated drug resistance in bacteria: an update. *Drugs*. 69(12):1555-623. doi: 10.2165/11317030-000000000-00000.
- Liang OD, Ascencio F, Fransson LA, Wadstrom T. 1992. Binding of heparan sulfate to *Staphylococcus aureus*. *Infect Immun*. 60:899-906. doi: 10.1128/IAI.60.3.899-906.1992.
- Liao C, Huang X, Wang Q, Yao D, Lu W. 2022. Virulence factors of *Pseudomonas aeruginosa* and antivirulence strategies to combat its drug resistance. *Front Cell Infect Microbiol*. 12:926758. doi: 10.3389/fcimb.2022.926758.
- LiPuma JJ, Dasen SE, Nielson DW, Stern RC, Stull TL. 1990. Person-to-person transmission of *Pseudomonas cepacia* between patients with cystic fibrosis. *Lancet*. 336(8723):1094-6. doi: 10.1016/0140-6736(90)92571-x.
- Liu D, Van Belleghem JD, de Vries CR, Burgener E, Chen Q, Manasherob R, Aronson JR, Amanatullah DF, Tamma PD, Suh GA. 2021b. The safety and toxicity of phage therapy: a review of animal and clinical studies. *Viruses*. 13(7):1268. doi: 10.3390/v13071268.
- Liu D, Zeng YY, Shi MM, Qu JM. 2021a. Glucocorticoids elevate *Pseudomonas aeruginosa* binding to airway epithelium by upregulating syndecan-1 expression. *Front Microbiol*. 12:725483. doi: 10.3389/fmicb.2021.725483.
- Liu J, Thorp SC. 2002. Cell surface heparan sulfate and its roles in assisting viral infections. *Med Res Rev*. 22(1):1-25. doi: 10.1002/med.1026.
- Lo DK, Muhlebach MS, Smyth AR. 2022. Interventions for the eradication of meticillin-resistant *Staphylococcus aureus* (MRSA) in people with cystic fibrosis. *Cochrane Database Syst Rev*. 12(12):CD009650. doi: 10.1002/14651858.CD009650.pub5.

- Lopatina A, Tal N, Sorek R. 2020. Abortive infection: bacterial suicide as an antiviral immune strategy. *Annu Rev Virol*. 7(1):371-384. doi: 10.1146/annurev-virology-011620-040628.
- Lorusso AB, Carrara JA, Barroso CDN, Tuon FF, Faoro H. 2022. Role of efflux pumps on antimicrobial resistance in *Pseudomonas aeruginosa*. *Int J Mol Sci*. 23(24):15779. doi: 10.3390/ijms232415779.
- Loutet SA, Flannagan RS, Kooi C, Sokol PA, Valvano MA. 2006. A complete lipopolysaccharide inner core oligosaccharide is required for resistance of *Burkholderia cenocepacia* to antimicrobial peptides and bacterial survival *in vivo*. *J Bacteriol*. 188(6):2073-80. doi: 10.1128/JB.188.6.2073-2080.2006.
- Lu TK, Collins JJ. 2007. Dispersing biofilms with engineered enzymatic bacteriophage. *Proc Natl Acad Sci U S A*. 104(27):11197-202. doi: 10.1073/pnas.0704624104.
- Mahenthiralingam E, Campbell ME, Speert DP. 1994. Nonmotility and phagocytic resistance of *Pseudomonas aeruginosa* isolates from chronically colonized patients with cystic fibrosis. *Infect Immun. 62(2):596-605. doi: 10.1128/iai.62.2.596-605.1994.*
- Mahenthiralingam E, Coenye T, Chung JW, Speert DP, Govan JR, Taylor P, Vandamme P. 2000. Diagnostically and experimentally useful panel of strains from the *Burkholderia cepacia* complex. *J Clin Microbiol*. 38(2):910-3. doi: 10.1128/JCM.38.2.910-913.2000.
- Mahenthiralingam E, Urban TA, Goldberg JB. 2005. The multifarious, multireplicon *Burkholderia cepacia* complex. *Nat Rev Microbiol*. 3(2):144-56. doi: 10.1038/nrmicro1085.
- Maisonneuve E, Gerdes K. 2014. Molecular mechanisms underlying bacterial persisters. *Cell*. 157(3):539-48. doi: 10.1016/j.cell.2014.02.050.
- Makarov VA, Popov VO. 2022. PDSTP is the first drug in class to treat coronavirus infection. *Her Russ Acad Sci*. 92(4):488-490. doi: 10.1134/S1019331622040190.
- Malinovská L, Thai Le S, Herczeg M, Vašková M, Houser J, Fujdiarová E, Komárek J, Hodek P, Borbás A, Wimmerová M, Csávás M. 2019. Synthesis of β-d-galactopyranoside-presenting glycoclusters, investigation of their interactions with *Pseudomonas aeruginosa* lectin A (PA-IL) and evaluation of their anti-adhesion potential. *Biomolecules*. 9(11):686. doi: 10.3390/biom9110686.
- Mann EE, Wozniak DJ. 2012. *Pseudomonas* biofilm matrix composition and niche biology. *FEMS Microbiol Rev*. 36(4):893-916. doi: 10.1111/j.1574-6976.2011.00322.x.

References

- Marolda CL, Lahiry P, Vinés E, Saldías S, Valvano MA. 2006. Micromethods for the characterization of lipid A-core and O-antigen lipopolysaccharide. *Methods Mol Biol*. 347:237-52. doi: 10.1385/1-59745-167-3:237.
- Martin C, Lozano-Iturbe V, Girón RM, Vazquez-Espinosa E, Rodriguez D, Merayo-Lloves J, Vazquez F, Quirós LM, García B. 2019. Glycosaminoglycans are differentially involved in bacterial binding to healthy and cystic fibrosis lung cells. *J Cyst Fibros*. 18(3):e19-e25. doi: 10.1016/j.jcf.2018.10.017.
- Martínez-Gallardo MJ, Villicaña C, Yocupicio-Monroy M, Alcaraz-Estrada SL, León-Félix J. 2023. Current knowledge in the use of bacteriophages to combat infections caused by *Pseudomonas aeruginosa* in cystic fibrosis. *Folia Microbiol*. 68(1):1-16. doi: 10.1007/s12223-022-00990-5.
- Masuda N, Sakagawa E, Ohya S, Gotoh N, Tsujimoto H, Nishino T. 2000. Substrate specificities of MexAB-OprM, MexCD-OprJ, and MexXY-OprM efflux pumps in *Pseudomonas aeruginosa*. *Antimicrob Agents Chemother*. 44(12):3322-7. doi: 10.1128/AAC.44.12.3322-3327.2000.
- McNair K, Zhou C, Dinsdale EA, Souza B, Edwards RA. 2019. PHANOTATE: a novel approach to gene identification in phage genomes. *Bioinformatics*. 35(22):4537-4542. doi: 10.1093/bioinformatics/btz265.
- Mira NP, Madeira A, Moreira AS, Coutinho CP, Sá-Correia I. 2011. Genomic expression analysis reveals strategies of *Burkholderia cenocepacia* to adapt to cystic fibrosis patients' airways and antimicrobial therapy. *PLoS One*. 6(12):e28831. doi: 10.1371/journal.pone.0028831.
- Mitchell AB, Glanville AR. 2021. The impact of resistant bacterial pathogens including *Pseudomonas aeruginosa* and *Burkholderia* on lung transplant outcomes. *Semin Respir Crit Care Med*. 42(3):436-448. doi: 10.1055/s-0041-1728797.
- Mogayzel PJ Jr, Naureckas ET, Robinson KA, Brady C, Guill M, Lahiri T, Lubsch L, Matsui J, Oermann CM, Ratjen F, Rosenfeld M, Simon RH, Hazle L, Sabadosa K, Marshall BC; Cystic Fibrosis Foundation Pulmonary Clinical Practice Guidelines Committee. 2014. Cystic Fibrosis Foundation pulmonary guideline. Pharmacologic approaches to prevention and eradication of initial *Pseudomonas aeruginosa* infection. *Ann Am Thorac Soc*. 11(10):1640-50. doi: 10.1513/AnnalsATS.201404-166OC.

- Molina Bertrán SDC, Monzote L, Cappoen D, Escalona Arranz JC, Gordillo Pérez MJ, Rodríguez-Ferreiro AO, Chill Nuñez I, Novo CP, Méndez D, Cos P, Llauradó Maury G. 2022. Inhibition of bacterial adhesion and biofilm formation by seed-derived ethanol extracts from *Persea americana* Mill. *Molecules*. 27(15):5009. doi: 10.3390/molecules27155009.
- Moore RA, Bates NC, Hancock RE. 1986. Interaction of polycationic antibiotics with *Pseudomonas aeruginosa* lipopolysaccharide and lipid A studied by using dansyl-polymyxin. *Antimicrob Agents Chemother*. 29(3):496-500. doi: 10.1128/AAC.29.3.496.
- Morello E, Saussereau E, Maura D, Huerre M, Touqui L, Debarbieux L. 2011. Pulmonary bacteriophage therapy on *Pseudomonas aeruginosa* cystic fibrosis strains: first steps towards treatment and prevention. *PLoS One*. 6(2):e16963. doi: 10.1371/journal.pone.0016963.
- Moyá B, Beceiro A, Cabot G, Juan C, Zamorano L, Alberti S, Oliver A. 2012. Pan-β-lactam resistance development in *Pseudomonas aeruginosa* clinical strains: molecular mechanisms, penicillin-binding protein profiles, and binding affinities. *Antimicrob Agents Chemother*. 56(9):4771-8. doi: 10.1128/AAC.00680-12.
- Mulcahy LR, Burns JL, Lory S, Lewis K. 2010. Emergence of *Pseudomonas aeruginosa* strains producing high levels of persister cells in patients with cystic fibrosis. *J Bacteriol*. 192(23):6191-9. doi: 10.1128/JB.01651-09.
- Nemtsov BF, Benenson EV, Timina OV. 1998. Pulse therapy with prospidin and methotrexate: comparative efficacy in rheumatoid arthritis (12-month controlled study). *Klin Med (Mosk)*. 76(8):24-8.
- Nielsen TK, Forero-Junco LM, Kot W, Moineau S, Hansen LH, Riber L. 2023. Detection of nucleotide modifications in bacteria and bacteriophages: Strengths and limitations of current technologies and software. *Mol Ecol*. 32(6):1236-1247. doi: 10.1111/mec.16679.
- Nigro OD, Jungbluth SP, Lin HT, Hsieh CC, Miranda JA, Schvarcz CR, Rappé MS, Steward GF. 2017. Viruses in the oceanic basement. *mBio*. 8(2):e02129-16. doi: 10.1128/mBio.02129-16.
- Nikaido H. 2003. Molecular basis of bacterial outer membrane permeability revisited. *Microbiol Mol Biol Rev*. 67(4):593-656. doi: 10.1128/MMBR.67.4.593-656.2003.
- Nikolaev YA, Tutel'yan AV, Loiko NG, Buck J, Sidorenko SV, Lazareva I, Gostev V, Manzen'yuk OY, Shemyakin IG, Abramovich RA, Huwyler J, El'-Registan GI. 2020. The use of 4-Hexylresorcinol as antibiotic adjuvant. *PLoS One*. 15(9):e0239147. doi: 10.1371/journal.pone.0239147.

References

- Novoselova EA, Alimbarova LM, Monakhova NS, Lepioshkin AY, Ekins S, Makarov VA. 2020. *In vivo* activity of pyrimidine-dispirotripiperaziniumin in the male Guinea pig model of genital herpes. *J Virol Antivir Res*. doi: 10.37532/jva.2020.9(1).193.
- Novoselova EA, Riabova OB, Leneva IA, Nesterenko VG, Bolgarin RN, Makarov VA. 2017. Antiretroviral activity of a novel pyrimidyl-di(diazaspiroalkane) derivative. *Acta Naturae*. 9(1):105-107.
- Novoselova EA, Ryabova OB, Leneva IA, Makarov VA. 2019. Specific antiviral activity of pyrimidinedispirotripiperazinium alone and in combination with acyclovir on a herpes simplex virus infection model. *Pharm Chem J*. 781-785. doi.org/10.1007/s11094-019-02079-9.
- Oechslin F. 2018. Resistance development to bacteriophages occurring during bacteriophage therapy. *Viruses*. 10(7):351. doi: 10.3390/v10070351.
- O'Grady EP, Viteri DF, Malott RJ, Sokol PA. 2009. Reciprocal regulation by the CepIR and CciIR quorum sensing systems in *Burkholderia cenocepacia*. *BMC Genomics*. 10:441. doi: 10.1186/1471-2164-10-441.
- Olaitan AO, Morand S, Rolain JM. 2014. Mechanisms of polymyxin resistance: acquired and intrinsic resistance in bacteria. *Front Microbiol*. 5:643. doi: 10.3389/fmicb.2014.00643.
- O'Loughlin CT, Miller LC, Siryaporn A, Drescher K, Semmelhack MF, Bassler BL. 2013. A quorum-sensing inhibitor blocks *Pseudomonas aeruginosa* virulence and biofilm formation. *Proc Natl Acad Sci U S A*. 110(44):17981-6. doi: 10.1073/pnas.1316981110.
- Ondov BD, Treangen TJ, Melsted P, Mallonee AB, Bergman NH, Koren S, Phillippy AM. 2016. Mash: fast genome and metagenome distance estimation using MinHash. *Genome Biol*. 17(1):132. doi: 10.1186/s13059-016-0997-x. PMID: 27323842; PMCID: PMC4915045.
- Oromí-Bosch A, Antani JD, Turner PE. 2023. Developing phage therapy that overcomes the evolution of bacterial resistance. *Annu Rev Virol*. doi: 10.1146/annurev-virology-012423-110530.
- Ortega X, Hunt TA, Loutet S, Vinion-Dubiel AD, Datta A, Choudhury B, Goldberg JB, Carlson R, Valvano MA. 2005. Reconstitution of O-specific lipopolysaccharide expression in *Burkholderia cenocepacia* strain J2315, which is associated with transmissible infections in patients with cystic fibrosis. *J Bacteriol*. 187(4):1324-33. doi: 10.1128/JB.187.4.1324-1333.2005.

- Ortega X, Silipo A, Saldías MS, Bates CC, Molinaro A, Valvano MA. 2009. Biosynthesis and structure of the *Burkholderia cenocepacia* K56-2 lipopolysaccharide core oligosaccharide: truncation of the core oligosaccharide leads to increased binding and sensitivity to polymyxin B. *J Biol Chem*. 284(32):21738-51. doi: 10.1074/jbc.M109.008532.
- O'Shea R, Moser HE. 2008. Physicochemical properties of antibacterial compounds: implications for drug discovery. *J Med Chem*. 51(10):2871-8. doi: 10.1021/jm700967e.
- Pamukcu A, Bush A, Buchdahl R. 1995. Effects of *Pseudomonas aeruginosa* colonization on lung function and anthropometric variables in children with cystic fibrosis. *Pediatr Pulmonol*. 19(1):10-5. doi: 10.1002/ppul.1950190103.
- Pang Z, Raudonis R, Glick BR, Lin TJ, Cheng Z. 2019. Antibiotic resistance in *Pseudomonas aeruginosa*: mechanisms and alternative therapeutic strategies. *Biotechnol Adv*. 37(1):177-192. doi: 10.1016/j.biotechadv.2018.11.013.
- Payne JE, Dubois AV, Ingram RJ, Weldon S, Taggart CC, Elborn JS, Tunney MM. 2017. Activity of innate antimicrobial peptides and ivacaftor against clinical cystic fibrosis respiratory pathogens. *Int J Antimicrob Agents*. 50(3):427-435. doi: 10.1016/j.ijantimicag.2017.04.014.
- Pedersen SS. 1992. Lung infection with alginate-producing, mucoid *Pseudomonas aeruginosa* in cystic fibrosis. *APMIS Suppl*. 28:1-79.
- Pei R, Lamas-Samanamud GR. 2014. Inhibition of biofilm formation by T7 bacteriophages producing quorum-quenching enzymes. *Appl Environ Microbiol*. 80(17):5340-8. doi: 10.1128/AEM.01434-14.
- Pellegrini A, Lentini G, Famà A, Bonacorsi A, Scoffone VC, Buroni S, Trespidi G, Postiglione U, Sassera D, Manai F, Pietrocola G, Firon A, Biondo C, Teti G, Beninati C, Barbieri G. 2022. CodY is a global transcriptional regulator required for virulence in Group B *Streptococcus*. *Front Microbiol*. 13:881549. doi: 10.3389/fmicb.2022.881549.
- Philippe R and Urbach V. 2018. Specialized pro-resolving lipid mediators in cystic fibrosis. *Int J Mol Sci*. 19(10):2865. doi: 10.3390/ijms19102865.
- Philipson CW, Voegtly LJ, Lueder MR, Long KA, Rice GK, Frey KG, Biswas B, Cer RZ, Hamilton T, Bishop-Lilly KA. 2018. Characterizing phage genomes for therapeutic applications. *Viruses*. 10(4):188. doi: 10.3390/v10040188.

References

- Pires DP, Cleto S, Sillankorva S, Azeredo J, Lu TK. 2016. Genetically engineered phages: a review of advances over the last decade. *Microbiol Mol Biol Rev*. 80(3):523-43. doi: 10.1128/MMBR.00069-15.
- Pitt TL, Sparrow M, Warner M, Stefanidou M. 2003. Survey of resistance of *Pseudomonas aeruginosa* from UK patients with cystic fibrosis to six commonly prescribed antimicrobial agents. *Thorax*. 58(9):794-6. doi: 10.1136/thorax.58.9.794.
- Poirel L, Rodriguez-Martinez JM, Plésiat P, Nordmann P. 2009. Naturally occurring class A ss-lactamases from the *Burkholderia cepacia* complex. *Antimicrob Agents Chemother*. 53(3):876-82. doi: 10.1128/AAC.00946-08.
- Poole K. 2011. *Pseudomonas aeruginosa*: resistance to the max. *Front Microbiol*. 2:65. doi: 10.3389/fmicb.2011.00065.
- Poulain FE, Yost HJ. 2015. Heparan sulfate proteoglycans: a sugar code for vertebrate development? *Development*. 142(20):3456-67. doi: 10.1242/dev.098178.
- Qin S, Xiao W, Zhou C, Pu Q, Deng X, Lan L, Liang H, Song X, Wu M. 2022. *Pseudomonas aeruginosa*: pathogenesis, virulence factors, antibiotic resistance, interaction with host, technology advances and emerging therapeutics. *Signal Transduct Target Ther*. 7(1):199. doi: 10.1038/s41392-022-01056-1.
- Randell SH, Boucher RC. 2006. Effective mucus clearance is essential for respiratory health. *Am J Respir Cell Mol Biol*. 35(1):20-8. doi: 10.1165/rcmb.2006-0082SF.
- Ratjen F, Comes G, Paul K, Posselt HG, Wagner TO, Harms K; German Board of the European Registry for Cystic Fibrosis (ERCF). 2001. Effect of continuous antistaphylococcal therapy on the rate of *P. aeruginosa* acquisition in patients with cystic fibrosis. *Pediatr Pulmonol*. 31(1):13-6. doi: 10.1002/1099-0496(200101)31:1<13::aid-ppul1001>3.0.co;2-n.
- Rawat D, Nair D. 2010. Extended-spectrum β-lactamases in Gram-negative bacteria. *J Glob Infect Dis*. 2(3):263-74. doi: 10.4103/0974-777X.68531.
- Regan KH, Bhatt J. 2019. Eradication therapy for *Burkholderia cepacia* complex in people with cystic fibrosis. *Cochrane Database Syst Rev*. 4(4):CD009876. doi: 10.1002/14651858.CD009876.pub4.
- Reznikov LR, Abou Alaiwa MH, Dohrn CL, Gansemer ND, Diekema DJ, Stoltz DA, Welsh MJ. 2014. Antibacterial properties of the CFTR potentiator ivacaftor. *J Cyst Fibros*. 13(5):515-9. doi: 10.1016/j.jcf.2014.02.004.

- Ribeiro CMP, Higgs MG, Muhlebach MS, Wolfgang MC, Borgatti M, Lampronti I, Cabrini G. 2023. Revisiting host-pathogen interactions in cystic fibrosis lungs in the era of CFTR modulators. *Int J Mol Sci*. 24(5):5010. doi: 10.3390/ijms24055010.
- Rojas-Rojas FU, López-Sánchez D, Meza-Radilla G, Méndez-Canarios A, Ibarra JA, Estrada-de Los Santos P. 2019. The controversial *Burkholderia cepacia* complex, a group of plant growth promoting species and plant, animals and human pathogens. *Rev Argent Microbiol*. 51(1):84-92. doi: 10.1016/j.ram.2018.01.002.
- Rosenfeld M, Rayner O, Smyth AR. 2020. Prophylactic anti-staphylococcal antibiotics for cystic fibrosis. *Cochrane Database Syst Rev*. 9(9):CD001912. doi: 10.1002/14651858.CD001912.pub5.
- Rowe SM, Miller S, Sorscher EJ. 2005. Cystic fibrosis. *N Engl J Med*. 352(19):1992-2001. doi: 10.1056/NEJMra043184.
- Rumpf C, Lange J, Schwartbeck B, Kahl BC. 2021. *Staphylococcus aureus* and cystic fibrosis - A close relationship. What can we learn from sequencing studies? *Pathogens*. 10(9):1177. doi: 10.3390/pathogens10091177.
- Russell AB, Hood RD, Bui NK, LeRoux M, Vollmer W, Mougous JD. 2011. Type VI secretion delivers bacteriolytic effectors to target cells. *Nature*. 475(7356):343-7. doi: 10.1038/nature10244.
- Ryder C, Byrd M, Wozniak DJ. 2007. Role of polysaccharides in *Pseudomonas aeruginosa* biofilm development. *Curr Opin Microbiol*. 10(6):644-8. doi: 10.1016/j.mib.2007.09.010.
- Sadovskaya I, Brisson JR, Lam JS, Richards JC, Altman E. 1998. Structural elucidation of the lipopolysaccharide core regions of the wild-type strain PAO1 and O-chain-deficient mutant strains AK1401 and AK1012 from *Pseudomonas aeruginosa* serotype O5. *J Biochem*. 255(3):673-84. doi: 10.1046/j.1432-1327.1998.2550673.x.
- Sajjan SU, Carmody LA, Gonzalez CF, LiPuma JJ. 2008. A type IV secretion system contributes to intracellular survival and replication of *Burkholderia cenocepacia*. *Infect Immun*. 76(12):5447-55. doi: 10.1128/IAI.00451-08.
- Saldías MS, Ortega X, Valvano MA. 2009. *Burkholderia cenocepacia* O antigen lipopolysaccharide prevents phagocytosis by macrophages and adhesion to epithelial cells. *J Med Microbiol*. 58(Pt 12):1542-1548. doi: 10.1099/jmm.0.013235-0.

References

- Salsgiver EL, Fink AK, Knapp EA, LiPuma JJ, Olivier KN, Marshall BC, Saiman L. 2016. Changing epidemiology of the respiratory bacteriology of patients with cystic fibrosis. *Chest*. 149(2):390-400. doi: 10.1378/chest.15-0676.
- Sarrazin S, Lamanna WC, Esko JD. 2011. Heparan sulfate proteoglycans. *Cold Spring Harb Perspect Biol*. 3(7):a004952. doi: 10.1101/cshperspect.a004952.
- Schmidtke M, Riabova O, Dahse HM, Stelzner A, Makarov V. 2002. Synthesis, cytotoxicity and antiviral activity of N,N'-bis-5-nitropyrimidyl derivatives of dispirotripiperazine. *Antiviral Res*. 55(1):117-27. doi: 10.1016/s0166-3542(02)00014-1.
- Scoffone VC, Chiarelli LR, Trespidi G, Mentasti M, Riccardi G, Buroni S. 2017. *Burkholderia cenocepacia* infections in cystic fibrosis patients: drug resistance and therapeutic approaches. *Front Microbiol*. 8:1592. doi: 10.3389/fmicb.2017.01592.
- Scotet V, L'Hostis C, Férec C. The changing epidemiology of cystic fibrosis: incidence, survival and impact of the *CFTR* gene discovery. 2020. *Genes*. 11(6):589. doi: 10.3390/genes11060589.
- Sebastian-Valverde M, Pasinetti GM. 2020. The NLRP3 inflammasome as a critical actor in the inflammaging process. *Cells*. 9(6):1552. doi: 10.3390/cells9061552.
- Shkoporov AN, Ryan FJ, Draper LA, Forde A, Stockdale SR, Daly KM, McDonnell SA, Nolan JA, Sutton TDS, Dalmasso M, McCann A, Ross RP, Hill C. 2018. Reproducible protocols for metagenomic analysis of human faecal phageomes. *Microbiome*. 6(1):68. doi: 10.1186/s40168-018-0446-z.
- Shteinberg M, Haq IJ, Polineni D, Davies JC. 2021. Cystic fibrosis. *Lancet*. 397(10290):2195-2211. doi: 10.1016/S0140-6736(20)32542-3.
- Shukla D, Spear PG. 2001. Herpesviruses and heparan sulfate: an intimate relationship in aid of viral entry. *J Clin Invest*. 108(4):503-10. doi: 10.1172/JCI13799.
- Smith S, Rowbotham NJ, Regan KH. 2018. Inhaled anti-pseudomonal antibiotics for long-term therapy in cystic fibrosis. *Cochrane Database Syst Rev*. 3(3):CD001021. doi: 10.1002/14651858.CD001021.pub3.
- Sokol PA, Sajjan U, Visser MB, Gingues S, Forstner J, Kooi C. 2003. The CepIR quorum-sensing system contributes to the virulence of *Burkholderia cenocepacia* respiratory infections. *Microbiology*. 149(Pt 12):3649-3658. doi: 10.1099/mic.0.26540-0.

- Stapleton PJ, Izydorcyzk C, Clark S, Blanchard A, Wang PW, Yau Y, Waters V, Guttman DS. 2021. *Pseudomonas aeruginosa* strain-sharing in early infection among children with cystic fibrosis. *Clin Infect Dis*. 73(9):e2521-e2528. doi: 10.1093/cid/ciaa788.
- Steinegger M, Söding J. 2017. MMseqs2 enables sensitive protein sequence searching for the analysis of massive data sets. *Nat Biotechnol*. 35(11):1026-1028. doi: 10.1038/nbt.3988.
- Stites SW, Plautz MW, Bailey K, O'Brien-Ladner AR, Wesselius LJ. 1999. Increased concentrations of iron and isoferritins in the lower respiratory tract of patients with stable cystic fibrosis. *Am J Respir Crit Care Med*. 160(3):796-801. doi: 10.1164/ajrccm.160.3.9811018.
- Stokes JM, MacNair CR, Ilyas B, French S, Côté JP, Bouwman C, Farha MA, Sieron AO, Whitfield C, Coombes BK, Brown ED. 2017. Pentamidine sensitizes Gram-negative pathogens to antibiotics and overcomes acquired colistin resistance. *Nat Microbiol*. 2:17028. doi: 10.1038/nmicrobiol.2017.28.
- Strathdee SA, Hatfull GF, Mutalik VK, Schooley RT. 2023. Phage therapy: from biological mechanisms to future directions. *Cell*. 186(1):17-31. doi: 10.1016/j.cell.2022.11.017.
- Suchithra KV, Hameed A, Rekha PD, Arun AB. 2023. Description and host-range determination of phage PseuPha1, a new species of *Pakpunavirus* infecting multidrug-resistant clinical strains of *Pseudomonas aeruginosa*. *Virology*. 585:222-231. doi: 10.1016/j.virol.2023.06.009.
- Summers WC. 2012. The strange history of phage therapy. *Bacteriophage*. 2(2):130-133. doi: 10.4161/bact.20757.
- Taylor-Cousar JL, Mall MA, Ramsey BW, McKone EF, Tullis E, Marigowda G, McKee CM, Waltz D, Moskowitz SM, Savage J, Xuan F, Rowe SM. 2019. Clinical development of triple-combination CFTR modulators for cystic fibrosis patients with one or two F508del alleles. *ERJ Open Res*. 5(2):00082-2019. doi: 10.1183/23120541.00082-2019.
- Terzian P, Olo Ndela E, Galiez C, Lossouarn J, Pérez Bucio RE, Mom R, Toussaint A, Petit MA, Enault F. 2021. PHROG: families of prokaryotic virus proteins clustered using remote homology. *NAR Genom Bioinform*. 3(3):lqab067. doi: 10.1093/nargab/lqab067.
- Thomas MS. 2007. Iron acquisition mechanisms of the *Burkholderia cepacia* complex. *Biometals*. 20(3-4):431-52. doi: 10.1007/s10534-006-9065-4.
- Thornton CS, Parkins MD. 2023. Microbial epidemiology of the cystic fibrosis airways: past, present, and future. *Semin Respir Crit Care Med*. 44(2):269-286. doi: 10.1055/s-0042-1758732.

- Tomich M, Griffith A, Herfst CA, Burns JL, Mohr CD. 2003. Attenuated virulence of a *Burkholderia cepacia* type III secretion mutant in a murine model of infection. *Infect Immun*. 71(3):1405-15. doi: 10.1128/IAI.71.3.1405-1415.2003.
- Tomlin KL, Coll OP, Ceri H. 2001. Interspecies biofilms of *Pseudomonas aeruginosa* and *Burkholderia cepacia*. *Can J Microbiol*. 47(10):949-54.
- Tomlin KL, Malott RJ, Ramage G, Storey DG, Sokol PA, Ceri H. 2005. Quorum-sensing mutations affect attachment and stability of *Burkholderia cenocepacia* biofilms. *Appl Environ Microbiol*. 71(9):5208-18. doi: 10.1128/AEM.71.9.5208-5218.2005.
- Tsai YC, Lee YP, Lin NT, Yang HH, Teh SH, Lin LC. 2023. Therapeutic effect and anti-biofilm ability assessment of a novel phage, phiPA1-3, against carbapenem-resistant *Pseudomonas aeruginosa*. *Virus Res*. 335:199178. doi: 10.1016/j.virusres.2023.199178.
- Tseng SP, Tsai WC, Liang CY, Lin YS, Huang JW, Chang CY, Tyan YC, Lu PL. 2014. The contribution of antibiotic resistance mechanisms in clinical *Burkholderia cepacia* complex isolates: an emphasis on efflux pump activity. *PLoS One*. 9(8):e104986. doi: 10.1371/journal.pone.0104986.
- Ujmajuridze A, Chanishvili N, Goderdzishvili M, Leitner L, Mehnert U, Chkhotua A, Kessler TM, Sybesma W. 2018. Adapted bacteriophages for treating urinary tract infections. *Front Microbiol*. 9:1832. doi: 10.3389/fmicb.2018.01832.
- Urban TA, Griffith A, Torok AM, Smolkin ME, Burns JL, Goldberg JB. 2004. Contribution of *Burkholderia cenocepacia* flagella to infectivity and inflammation. *Infect Immun*. 72(9):5126-34. doi: 10.1128/IAI.72.9.5126-5134.2004.
- Vaara M, Siikanen O, Apajalahti J, Fox J, Frimodt-Møller N, He H, Poudyal A, Li J, Nation RL, Vaara T. 2010. A novel polymyxin derivative that lacks the fatty acid tail and carries only three positive charges has strong synergism with agents excluded by the intact outer membrane. *Antimicrob Agents Chemother*. 54(8):3341-6. doi: 10.1128/AAC.01439-09.
- Van Acker H, Sass A, Dhondt I, Nelis HJ, Coenye T. 2014. Involvement of toxin-antitoxin modules in *Burkholderia cenocepacia* biofilm persistence. *Pathog Dis*. 71(3):326-35. doi: 10.1111/2049-632X.12177.

- van Tilburg Bernardes E, Charron-Mazenod L, Reading DJ, Reckseidler-Zenteno SL, Lewenza S. 2017. Exopolysaccharide-repressing small molecules with antibiofilm and antivirulence activity against *Pseudomonas aeruginosa*. *Antimicrob Agents Chemother*. 61(5):e01997-16. doi: 10.1128/AAC.01997-16.
- Visser MB, Majumdar S, Hani E, Sokol PA. 2004. Importance of the ornibactin and pyochelin siderophore transport systems in *Burkholderia cenocepacia* lung infections. *Infect Immun*. 72(5):2850-7. doi: 10.1128/IAI.72.5.2850-2857.2004.
- Walters MC 3rd, Roe F, Bugnicourt A, Franklin MJ, Stewart PS. 2003. Contributions of antibiotic penetration, oxygen limitation, and low metabolic activity to tolerance of *Pseudomonas aeruginosa* biofilms to ciprofloxacin and tobramycin. *Antimicrob Agents Chemother*. 47(1):317-23. doi: 10.1128/AAC.47.1.317-323.2003.
- Wang CH, Hsieh YH, Powers ZM, Kao CY. 2020. Defeating antibiotic-resistant bacteria: exploring alternative therapies for a post-antibiotic era. *Int J Mol Sci*. 21(3):1061. doi: 10.3390/ijms21031061.
- Wang G, Brunel JM, Preusse M, Mozaheb N, Willger SD, Larrouy-Maumus G, Baatsen P, Häussler S, Bolla JM, Van Bambeke F. 2022. The membrane-active polyaminoisoprenyl compound NV716 re-sensitizes *Pseudomonas aeruginosa* to antibiotics and reduces bacterial virulence. *Commun Biol*. 5(1):871. doi: 10.1038/s42003-022-03836-5.
- Wang X, Tang J, Dang W, Xie Z, Zhang F, Hao X, Sun S, Liu X, Luo Y, Li M, Gu Y, Wang Y, Chen Q, Shen X, Xu L. 2023b. Isolation and characterization of three *Pseudomonas aeruginosa* viruses with therapeutic potential. *Microbiol Spectr*. 11(3):e0463622. doi: 10.1128/spectrum.04636-22.
- Wang X, Xie Z, Zhao J, Zhu Z, Yang C and Liu Y. 2021. Prospects of inhaled phage therapy for combatting pulmonary infections. *Front Cell Infect Microbiol*. 11:758392. doi: 10.3389/fcimb.2021.758392.
- Wang Y, Fan H, Tong Y. 2023a. Unveil the secret of the bacteria and phage arms race. *Int J Mol Sci*. 24(5):4363. doi: 10.3390/ijms24054363.
- Wannasrichan W, Htoo HH, Suwansaeng R, Pogliano J, Nonejuie P, Chaikeeratisak V. 2022. Phage-resistant *Pseudomonas aeruginosa* against a novel lytic phage JJ01 exhibits hypersensitivity to colistin and reduces biofilm production. *Front Microbiol*. 13:1004733. doi: 10.3389/fmicb.2022.1004733.

- Waters EM, Rowe SE, O'Gara JP, Conlon BP. 2016. Convergence of *Staphylococcus aureus* persister and biofilm research: can biofilms be defined as communities of adherent persister cells? *PLoS Pathog*. 12(12):e1006012. doi: 10.1371/journal.ppat.1006012.
- Weiss RJ, Esko JD, Tor Y. 2017. Targeting heparin and heparan sulfate protein interactions. *Org Biomol Chem*. 15(27):5656-5668. doi: 10.1039/c7ob01058c.
- Westra ER, Swarts DC, Staals RH, Jore MM, Brouns SJ, van der Oost J. 2012. The CRISPRs, they are a-changin': how prokaryotes generate adaptive immunity. *Annu Rev Genet*. 46:311-39. doi: 10.1146/annurev-genet-110711-155447.
- Whitby PW, VanWagoner TM, Springer JM, Morton DJ, Seale TW, Stull TL. 2006. *Burkholderia cenocepacia* utilizes ferritin as an iron source. *J Med Microbiol*. 55(Pt 6):661-668. doi: 10.1099/jmm.0.46199-0.
- Wiegand I, Hilpert K, Hancock RE. 2008. Agar and broth dilution methods to determine the minimal inhibitory concentration (MIC) of antimicrobial substances. *Nat Protoc*. 3(2):163-75. doi: 10.1038/nprot.2007.521.
- Wong GCL, Antani JD, Lele PP, Chen J, Nan B, Kühn MJ, Persat A, Bru JL, Høyland-Kroghsbo NM, Siryaporn A, Conrad JC, Carrara F, Yawata Y, Stocker R, V Brun Y, Whitfield GB, Lee CK, de Anda J, Schmidt WC, Golestanian R, O'Toole GA, Floyd KA, Yildiz FH, Yang S, Jin F, Toyofuku M, Eberl L, Nomura N, Zacharoff LA, El-Naggar MY, Yalcin SE, Malvankar NS, Rojas-Andrade MD, Hochbaum AI, Yan J, Stone HA, Wingreen NS, Bassler BL, Wu Y, Xu H, Drescher K, Dunkel J. 2021. Roadmap on emerging concepts in the physical biology of bacterial biofilms: from surface sensing to community formation. *Phys Biol*. 18(5):10.1088/1478-3975/abdc0e. doi: 10.1088/1478-3975/abdc0e.
- Wright GD. 2005. Bacterial resistance to antibiotics: enzymatic degradation and modification. *Adv Drug Deliv Rev*. 57(10):1451-70. doi: 10.1016/j.addr.2005.04.002.
- Xuan G, Lin H, Kong J, Wang J. 2022. Phage resistance evolution induces the sensitivity of specific antibiotics in *Pseudomonas aeruginosa* PAO1. *Microbiol Spectr*. 10(5):e0135622. doi: 10.1128/spectrum.01356-22.
- Yagci S, Hascelik G, Dogru D, Ozcelik U, Sener B. 2013. Prevalence and genetic diversity of *Staphylococcus aureus* small-colony variants in cystic fibrosis patients. *Clin Microbiol Infect*. 19(1):77-84. doi: 10.1111/j.1469-0691.2011.03742.x.

- Young JW, Locke JC, Altinok A, Rosenfeld N, Bacarian T, Swain PS, Mjolsness E, Elowitz MB. 2011. Measuring single-cell gene expression dynamics in bacteria using fluorescence time-lapse microscopy. *Nat Protoc*. 7(1):80-8. doi: 10.1038/nprot.2011.432.
- Zemanick ET, Hoffman LR. 2016. Cystic fibrosis: microbiology and host response. *Pediatr Clin North Am*. 63(4):617-36. doi: 10.1016/j.pcl.2016.04.003.
- Zhang R, LiPuma JJ, Gonzalez CF. 2009. Two type IV secretion systems with different functions in *Burkholderia cenocepacia* K56-2. *Microbiology*. 155(Pt 12):4005-4013. doi: 10.1099/mic.0.033043-0.
- Zhou Y, Huang W, Lei E, Yang A, Li Y, Wen K, Wang M, Li L, Chen Z, Zhou C, Bai S, Han J, Song W, Ren X, Zeng X, Pu H, Wan M, Feng X. 2022. Cooperative membrane damage as a mechanism for pentamidine-antibiotic mutual sensitization. *ACS Chem Biol*. 17(11):3178-3190. doi: 10.1021/acschembio.2c00613.
- Zlosnik JE, Hird TJ, Fraenkel MC, Moreira LM, Henry DA, Speert DP. 2008. Differential mucoid exopolysaccharide production by members of the *Burkholderia cepacia* complex. *J Clin Microbiol*. 46(4):1470-3. doi: 10.1128/JCM.02273-07.

List of original manuscripts

Full papers

Bonacorsi A, Trespidi G, Scoffone VC, Irudal S, Barbieri G, Riabova O, Monakhova N, Makarov V, Buroni S. Characterization of the dispirotripiperazine derivative PDSTP as antibiotic adjuvant and antivirulence compound against *Pseudomonas aeruginosa*. Under revision in PLOS Pathogens.

Panda SK, Buroni S, Swain SS, **Bonacorsi A**, da Fonseca Amorim EA, Kulshrestha M, da Silva LCN, Tiwari V. 2022. Recent advances to combat ESKAPE pathogens with special reference to essential oils. *Front Microbiol*. 13:1029098.

Pellegrini A, Lentini G, Famà A, **Bonacorsi A**, Scoffone VC, Buroni S, Trespidi G, Postiglione U, Sassera D, Manai F, Pietrocola G, Firon A, Biondo C, Teti G, Beninati C, Barbieri G. 2022. CodY is a global transcriptional regulator required for virulence in Group B *Streptococcus*. *Front Microbiol*. 13:881549.

Abstracts

Bonacorsi A, Trespidi G, Scoffone VC, Irudal S, Barbieri G, Makarov V, Pasca MR, Buroni S. Exploiting dispirotripiperazines as a novel strategy to fight *Pseudomonas aeruginosa* infections in cystic fibrosis. Poster presented at the 34th Società Italiana di Microbiologia Generale e Biotecnologie Microbiche congress in Cagliari (Italy), 21-24/09/2023.

Pellegrini A, Scoffone VC, Trespidi G, Irudal S, **Bonacorsi A**, Pietrocola G, Buroni S, Barbieri G. Interplay of CodY and CovR in regulating gene expression in Group B *Streptococcus*. Poster presented at the 34th Società Italiana di Microbiologia Generale e Biotecnologie Microbiche congress in Cagliari (Italy), 21-24/09/2023.

Bonacorsi A, Trespidi G, Scoffone VC, Buroni S. Exploring the activity of the dispirotripiperazine-based compound PDSTP on the cystic fibrosis pathogen *Pseudomonas aeruginosa*. This work was orally presented at the Cortona Procarioti congress in Cortona (Italy), 23-25/06/2022.

Pellegrini A, Lentini G, Famà A, **Bonacorsi A**, Scoffone VC, Buroni S, Trespidi G, Postiglione U, Sassera D, Manai F, Pietrocola G, Firon A, Biondo C, Teti G, Beninati C, Barbieri G. The global transcriptional regulator CodY is essential for *in vivo* virulence of Group B *Streptococcus*. Poster presented at the 21st Lancefield International Symposium on Streptococci and Streptococcal Diseases in Stockholm (Sweden), 07-10/06/2022.

Irudal S, Scoffone VC, Trespidi G, **Bonacorsi A**, Pellegrini A, Barbieri G, Buroni S. Reverse vaccinology as a tool to fight cystic fibrosis pathogens. Poster presented at the 32nd European Congress of Clinical Microbiology and Infectious Diseases in Lisbon (Portugal), 23-26/04/2022.

Pellegrini A, Lentini G, Famà A, **Bonacorsi A**, Scoffone VC, Buroni S, Trespidi G, Postiglione U, Sassera D, Manai F, Pietrocola G, Firon A, Biondo C, Teti G, Beninati C, Barbieri G. The CodY global regulator controls metabolism and virulence in Group B *Streptococcus*. Poster presented at the 32nd European Congress of Clinical Microbiology and Infectious Diseases in Lisbon (Portugal), 23-26/04/2022.

Pellegrini A, **Bonacorsi A**, Scoffone VC, Lentini G, Buroni S, Manai F, Postiglione U, Sassera D, Beninati C, Biondo C, Barbieri G. CodY is a global regulator of gene expression and controls virulence in Group B *Streptococcus*. Poster presented at the Associazione Genetica Italiana AGI2021 (online event), 22-24/09/2021.

frontiers | Frontiers in Microbiology

TYPE Review
PUBLISHED 06 December 2022
DOI 10.3389/fmicb.2022.1029098

Check for updates

OPEN ACCESS

EDITED BY
Amr H. Hashem,
Al-Azhar University, Egypt

REVIEWED BY
Salem S. Salem,
Al-Azhar University, Egypt
Rapee Thummeepak,
Naresuan University, Thailand

*CORRESPONDENCE
Vishvanath Tiwari
vishvanath@curaj.ac.in

SPECIALTY SECTION
This article was submitted to Antimicrobials, Resistance and Chemotherapy, a section of the journal Frontiers in Microbiology

RECEIVED 26 August 2022
ACCEPTED 01 November 2022
PUBLISHED 06 December 2022

CITATION
Panda SK, Buroni S, Swain SS, Bonacorsi A, da Fonseca Amorim EA, Kulshrestha M, da Silva LCN and Tiwari V (2022) Recent advances to combat ESKAPE pathogens with special reference to essential oils. *Front. Microbiol.* 13:1029098. doi: 10.3389/fmicb.2022.1029098

COPYRIGHT
© 2022 Panda, Buroni, Swain, Bonacorsi, da Fonseca Amorim, Kulshrestha, da Silva and Tiwari. This is an open-access article distributed under the terms of the Creative Commons Attribution License (CC BY). The use, distribution or reproduction in other forums is permitted, provided the original author(s) and the copyright owner(s) are credited and that the original publication in this journal is cited, in accordance with accepted academic practice. No use, distribution or reproduction is permitted which does not comply with these terms.

Recent advances to combat ESKAPE pathogens with special reference to essential oils

Sujogya Kumar Panda[1], Silvia Buroni[2], Shasank Sekhar Swain[3], Andrea Bonacorsi[2], Erika Alves da Fonseca Amorim[4], Mukta Kulshrestha[5], Luis Cláudio Nascimento da Silva[4] and Vishvanath Tiwari[5]*

[1]Centre of Environment Studies, Climate Change and Public Health, RUSA 2.0, Utkal University, Vani Vihar, Bhubaneswar, Odisha, India, [2]Department of Biology and Biotechnology, University of Pavia, Pavia, Italy, [3]Division of Microbiology and Noncommunicable Diseases (NCDs), Indian Council of Medical Research (ICMR)–Regional Medical Research Centre, Bhubaneswar, Odisha, India, [4]Laboratory of Microbial Pathogenesis, Universidade Ceuma, São Luís, Brazil, [5]Department of Biochemistry, Central University of Rajasthan, Ajmer, Rajasthan, India

Biofilm-associated bacteria, especially ESKAPE pathogens (*Enterococcus faecium*, *Staphylococcus aureus*, *Klebsiella pneumoniae*, *Acinetobacter baumannii*, *Pseudomonas aeruginosa*, and *Enterobacter* spp.), are a serious challenge worldwide. Due to the lack of discovery of novel antibiotics, in the past two decades, it has become necessary to search for new antibiotics or to study synergy with the existing antibiotics so as to counter life-threatening infections. Nature-derived compounds/based products are more efficient than the chemically synthesized ones with less resistance and lower side effects. In this descriptive review, we discuss the most promising therapeutics for the treatment of ESKAPE-related biofilms. The first aspect includes different types of natural agents [botanical drugs, essential oils (EOs), antimicrobial peptides, bacteriophages, and endolysins] effective against ESKAPE pathogens. The second part of the review deals with special references to EOs/essential oil components (EOCs) (with some exclusive examples), mode of action (via interfering in the quorum-sensing pathways, disruption of biofilm and their inhibitory concentrations, expression of genes that are involved, other virulence factors), existing in literature so far. Moreover, different essential oils and their major constituents were critically discussed using *in vivo* models to target ESKAPE pathogens along with the studies involving existing antibiotics.

KEYWORDS

antibiotics, biofilm, ESKAPE, essential oils, quorum-sensing, synergy, toxicity

Introduction

The ESKAPE bacteria are a group of opportunistic pathogens consisting of *Enterococcus faecium, Staphylococcus aureus*, *Klebsiella pneumoniae*, *Acinetobacter baumannii*, *Pseudomonas aeruginosa*, and *Enterobacter* species. These bacteria represent a global threat from a clinical point of view since they are generally multidrug-resistant (MDR), extensively drug-resistant (XDR), and pan drug-resistant (PDR). In particular, *E. faecium* is a Gram-positive generally inhabiting the human gastrointestinal tract which may lead to several diseases such as bacteremia, endocarditis, and neonatal meningitis. *S. aureus* is a Gram-positive bacterium colonizing humans at the level of the skin and the upper respiratory tract (nostrils) which maybe involved in skin infections, as well as pneumonia and sepsis. *K. pneumoniae* is a Gram-negative that is part of the normal microbiota of humans (skin and digestive system) which may cause respiratory and urinary infections, as well as bacteremia and liver abscess. *A. baumannii* is a ubiquitous Gram-negative bacterium which may lead to respiratory and urinary infections. *P. aeruginosa* is a ubiquitous Gram-negative causing several infections, including respiratory (especially in cystic fibrosis patients), urinary and skin infections (generally after a burn injury). Last, the genus *Enterobacter* comprises Gram-negative bacteria that may be natural commensals of the human gastrointestinal tract which may be involved in urinary, respiratory and soft skin infections. Due to the resistance of the ESKAPE bacteria to a broad range of antibiotics, there are severe challenges in the treatment of their infections, especially when biofilms are involved. In fact, bacteria inside the biofilms are about 1,000 times more resistant to antimicrobials as compared to planktonic cells (Patil et al., 2021). Consequently, there is an urgent need to develop new weapons to fight these pathogens, with particular emphasis on the eradication of their biofilms (Panda et al., 2021). Several strategies are being explored around the world in order to treat ESKAPE-related biofilms (Sahoo et al., 2021; **Figure 1**). A broad variety of proteins are involved in biofilm structuration, making them attractive targets to inhibit biofilm formation. For instance, the *Acinetobacter baumannii* outer membrane protein A (OmpA), involved in the virulence of this bacterium, plays a role in the formation of the biofilm: by down-regulating the expression of this protein through synthetic small compounds inhibiting the *ompA* promoter, the *in vitro* formation of biofilm is also affected (Na et al., 2021). Another example is the *Pseudomonas aeruginosa* carbohydrate-binding protein Lectin A (LecA) which is involved in the generation of the biofilm matrix: this molecule may be targeted by LecA synthetic inhibitors in order to impair the structure of the biofilm (Siebs et al., 2022).

For the establishment of biofilm, bacteria have to communicate among each other by means of quorum-sensing. The inhibition of quorum-sensing, i.e., quorum-quenching, is one of the promising strategies to impair biofilm formation. For instance, the *P. aeruginosa* acylase PvdQ is able to cleave the acyl homoserine lactones of *A. baumannii* which are the mediators of quorum-sensing in this pathogen, affecting bacterial communication and, as a consequence, impairing biofilm formation *in vitro* (Vogel et al., 2022).

Other strategies used to target biofilms involve immunotherapy. Besides vaccines (active immunotherapy), monoclonal antibodies (passive immunotherapy) may be exploited to fight the ESKAPE-related biofilms. For example, a monoclonal antibody which targets alginate produced by *P. aeruginosa*, an exopolysaccharide involved in biofilm structuration and protection of the bacterium from the host immune system, could be used. Indeed, when treated *in vitro* with this antibody, *P. aeruginosa* showed impairment in the formation of biofilm (Gao et al., 2020).

In general, it is important to consider both drug reuse/resensitization and drug repurposing. Belonging to the first category, carboxylic acid salts derived from the fluoroquinolone norfloxacin have a higher activity on the ESKAPE pathogens compared to the parent molecule and are active on their biofilms, particularly on the Gram-negative ones (Lowrence et al., 2018). Ethyl bromopyruvate, in spite of being a derivative of anticancer agent 3-bromo-pyruvic acid, can be used for drug repurposing (Kumar et al., 2019). In fact, it is effective on planktonic ESKAPE bacteria and on *Staphylococcus aureus* biofilms, and hence is a good example of drug repurposing (Kumar et al., 2019).

Some of the most promising therapeutics for the treatment of the ESKAPE-related biofilms are antimicrobial peptides, bacteriophages, bacteriophage-encoded products, and natural products such as essential oils (EOs) to eradicate them. It is crucial to consider the treatment of the biofilms of the ESKAPE pathogens on/inside of medical devices since they are sources of nosocomial infections, before implementing the treatment options. For instance, non-thermal plasma (NTP) is a partially ionized gas characterized by both antimicrobial and antibiofilm activity on the ESKAPE pathogens that can be used for the disinfection of medical devices as well as hospital surfaces. NTP

Abbreviations: AMPs, antimicrobial peptides; CBA, checkerboard assay; CFU, colony forming unit; CLA, cell lysis assay; EGCG, epigallocatechin gallate; EOs, essential oils; EOCs, essential oil components; ESKAPE, *Enterococcus faecium, Staphylococcus aureus, Klebsiella pneumoniae, Acinetobacter baumannii, Pseudomonas aeruginosa* and *Enterobacter* spp.; DEO, dill and its essential oil; DMSO, dimethyl sulfoxide; FICI, fractional inhibitory concentration index; HAI, hospital-acquired infections; IEPA/E, inhibition of efflux pumps activity/expression; IZGC, inhibition zone by EO gaseous contact; LecA, lectin A; LPS, lipopolysaccharide structure; OM, outer membrane; OmpA, outer membrane protein A; QS, quorum sensing; MBIC, minimum biofilm inhibitory concentration; MDM, microdilution method; MDR, multidrug-resistant; MIC, minimum inhibitory concentration; MSSA, methicillin susceptible *S. aureus*; MRSA, methicillin resistant *S. aureus*; NTP, non-thermal plasma; XDR, extensively drug-resistant.

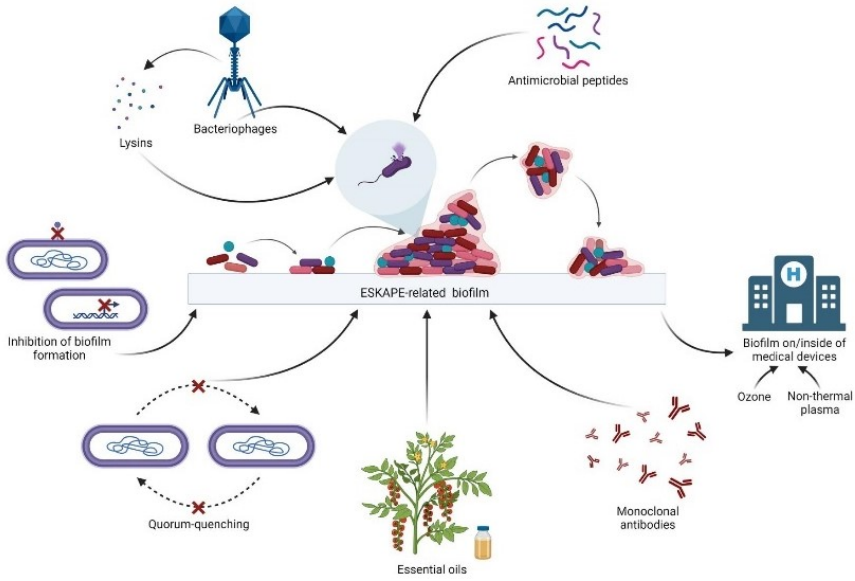

FIGURE 1
Therapeutic strategies for the treatment of the ESKAPE biofilms (adapted from "Biofilm Formation Cycle", by BioRender.com, 2022).

is more effective on Gram-negative bacteria compared to Gram-positive bacteria (Scholtz et al., 2021). Besides NTP, ozone can be used in order to eradicate ESKAPE-related biofilms from medical tools (Ibáñez-Cervantes et al., 2022).

This descriptive review includes the discussion of the most promising therapeutics for the treatment of ESKAPE-related biofilms. The first aspect covers different types of natural products effective against ESKAPE pathogens. The second part of the review deals with special references to EOs/essential oil components (EOCs) with some exclusive examples, mode of action, and synergy studies. Moreover, different EOs and their major constituents, as well as *in vivo* models to target ESKAPE pathogens were critically discussed.

Natural molecules against ESKAPE pathogens

Nature has provided a vast source of therapeutic agents along with a wide range of modern drugs which are in current use. These drugs are obtained from traditional medicinal plants as the diversity of biologically active molecules in these plants make them a potent source of medicines (Kothari et al., 2010; Tiwari et al., 2015). It has been reported that approximately 80% of the world's population, specifically in developing countries, depend on medicinal plants to fulfill their primary health care needs (Akinsulire et al., 2007). The plant secondary metabolites like alkaloids, flavonoids, terpenes, saponins, tannins, etc., possess different medicinal properties (Mors et al., 2000; Tiwari, 2016).

The prolonged hospital stays have resulted in increased risk of medical expenses and mortality due to hospital-acquired infections which majorly occur in immunocompromised patients because of the exposure to ESKAPE pathogens. Therefore, in order to combat the rapid evolution of disease-causing pathogens, finding new antimicrobials is essential. Numerous secondary metabolites, or phytochemicals, that have the ability to prevent disease are known to be produced by plants. The main benefits of plant-derived products make them viable options for medical treatments because of their potential efficacy and minimal to no negative side effects (Pal and Shukla, 2003). Therefore, the discussion of use of such chemicals and extracts produced from plants to combat ESKAPE pathogens is quite significant. Many efficacious drugs can be produced for disease eradication by using these bioactive compounds. About 80% of the total population which majorly includes developing nations is dependent on natural products. Synthetic drugs are gaining popularity these days due to their time effectiveness, refined quality, cost-effectiveness, and quick effect (Ekor, 2014). However, many natural products–derived compounds are in

various stages of drug development and have already highlighted the importance as well as the versatility of natural products as a future of novel drug development. Plants are a vital resource for novel drug development and other pharmacologically active compounds it has been observed that there are many drugs that are developed directly or indirectly from plants. According to World Health Organization (WHO), 11% of 252 drugs are considered basic and essential during the start of the 21st century and these drugs exclusively originated from the flowering plant (Veeresham, 2012). Some recent studies against biofilms provide the best example of natural products being effective and safe like synthetic halogenated furanone molecule, a secondary metabolite derivative, is generated from natural furanone produced by the Australian macroalga *Dilsea pulchra*. This substance can hinder bacterial signaling mechanisms and swarm cell movement. Additionally, it was proposed that *D. pulchra* furanones and AHL molecules' structural similarity affects how putative regulatory proteins interact with AHL molecules by binding competitively to the receptor. In ecologically relevant concentrations, furanone prevents the surface aggregation characteristics of relevant ecological microorganisms. Other common examples of plant-based drugs are Tannic acid, Endolysins (PlyC), and Epigallocatechin gallate (EGCG) which result in the cleavage of peptidoglycan (Payne et al., 2013).

Proteins including enzymes and transporters are the main target of the herbal compounds. Additionally, these active substances could attach to or block the location where the pathogenic elements bind. These herbal medicines can also impact the behavior of biomolecules, or even their expression in a disease-causing condition. By utilizing cutting-edge techniques, their target and method of action can also be determined, hence, lowering the chance of protein conformations that could cause diseases in the future. Plants can be metabolically engineered to produce more antimicrobial chemicals, which may pave the way for the discovery of new therapeutics. Active substances found in plants which change the expression or shape of proteins that cause illness are proved to be effective against drug-resistant microbes (**Table 1**). Consequently, they can be useful for creating a brand-new medicine to treat illnesses. To develop phytoconstituents as medicines targeting protein conformation, a thorough biochemical and biophysical investigation is required. Before being employed as medicines, phytoconstituents must be examined for their absorption, distribution, metabolism, excretion, and toxicity (ADMET) characteristics, pharmacophore mapping, effectiveness, and safety. However, for screening the antimicrobial compounds extracted from various plants against a wide range of Gram-positive as well as Gram-negative bacteria, the most commonly adopted methods are minimum inhibitory concentration (MIC), disk diffusion assay, and colony forming unit (CFU). According to the literature survey, it was found that few compounds were highly active against Gram-negative bacteria while some other compounds showed high activity against the Gram-positive bacteria.

Antimicrobial peptides

One of the most promising alternatives for the treatment of the ESKAPE-related biofilms are the antimicrobial peptides (AMPs). AMPs are positively-charged peptides generally made up of 10–15 amino acids. They are found in all the living organisms and are involved in the innate immunity (Patil et al., 2021). Generally, AMPs are broad-spectrum and cause the osmotic lysis of bacterial cells by permeabilizing their membranes, due to their amphipathic nature. Since this mechanism of action differs from that of antibiotics, resistance to AMPs can be more difficult to achieve (Panda et al., 2021).

Despite their potential, they rarely reach the market mostly due to problems such as low solubility, cytotoxicity, loss of activity (after administration), and susceptibility to proteolysis (Rodríguez et al., 2021; Sarkar et al., 2021). Synthetic molecular evolution can be exploited to evolve the AMPs that may overcome these limitations (Chen et al., 2022). The pipeline starts from parent peptides characterized by a strong antimicrobial activity on both Gram-positive and Gram-negative bacteria *in vitro* and, at the same time, ineffectiveness *in vivo* due to the impediments previously cited. These peptides are modified in order to construct a library of evolved peptides. Then, *In vitro* assays are performed to down-select candidate molecules based on solubility, cytotoxicity and peptide inactivation, besides their antimicrobial activity. Rational variation follows the down-selection step. As an example of an effective evolved AMP, D-CONGA showed a good activity on the ESKAPE pathogens in the planktonic form. Moreover, this peptide dramatically reduced *P. aeruginosa* viability within the biofilm *in vitro* (Starr et al., 2020).

In the context of synthetic AMPs, antimicrobial peptoids are synthetic oligomers that mimic AMPs and are resistant to proteolysis since their backbone is based on nitrogen atoms rather than carbon atoms. Not only their chemical structure is crucial to define the antimicrobial activity, but also their propensity to self-assemble in a physiological environment: among the most interesting therapeutic peptoids, TM peptoids that form bundled or ellipsoidal structures show better antimicrobial and antibiofilm activity against the ESKAPE pathogens compared to the TM peptoids which are not able to properly self-assemble or are characterized by worm-like assemblies. As an example of biologically active TM peptoids, the TM1 peptoid inhibits the growth of planktonic ESKAPE pathogens and affects the formation of their biofilms *in vitro* (Nielsen et al., 2022).

TABLE 1 Plant active compounds and their significant efficacy against various resistant pathogens.

Active compound	Plant (common name)	Botanical name	Active against	MIC (μg/ml)	References
Hexahydroxy diphenoyl ester vescalagin	Purple loosestrife	*Lythrum salicaria* L.	*Acinetobacter baumannii*, *Pseudomonas aeruginosa*, *Staphylococcus aureus*	NA NA 62	Becker et al., 2005; Guclu et al., 2014
Geraniol and terpinol-4-ol	Sugandhakokila	*Cinnamomum glaucescens*	MERSA	369	Panda et al., 2020
Diosgenin, smilagenin, β-sitosterol and hydroxy-tyrosol	Kumarika	*Smilax zeylanica*	MERSA	220	Panda et al., 2020
Propylene glycol	N/A	*Syzygium praecox*	MERSA	1,019	Panda et al., 2020
Tetradecanal and hexadecanoic aicid	Charcoal tree	*Trema orientalis*	MDR-S	369	Panda et al., 2020
β-Amyrine, acrosolic acid, Betulinic acid	Java cedar	*Bischofia javanica*	MDR-S	234	Panda et al., 2020
Myricitrin, mearnsatin-3-O-β-D gluco-pyrnoside	Ceylon olive	*Elaeocarpus serratus*	MDR-S	2,768	Panda et al., 2020
Methyl tridecanoate, arborinone, conferamide	Climbing acacia	*Acacia pennata*	MERSA	369	Panda et al., 2020
Terpenoids and steroids	Long-leaf varnish tree	*Holigarna caustica*	MERSA	369	Panda et al., 2020
α-pinene, methyl salicylate, β-cyclocitrol	Orange Jessamine	*Murraya Pennicula*	MERSA	406	Panda et al., 2020
Glycosides and saponins	Buddha coconut	*Plarygota alata*	MDR-S	550	Panda et al., 2020
No phytochemical reported till now	Lavender scallops	*Kalanchoe fedtschenkoi*	*Staphylococcus aureus*, *Acinetobacter baumannii*, *Pseudomonas areugenosa*	256	Richwagen et al., 2019
Saponins, polyphenols, tannins, anthrocynins, triterpines	Coastal golden leaf	*Bridelia mircrantha*	*Staphylococcus aureus*, *Klebsiella pneumoniae*, *Pseudomonas arugenosa*, MERSA,	128	Ngane, 2019
glucopyranoside	Bichoo	*Martynia annua*	*Klebsiella pneumoniae*, *Acinetobacter baumannii*, *Enterrococcus faecalis*, *Staphylococcus aureus*	256	Khan et al., 2018
Methanol	Stiff Bottlebrush	*Collistemon rigidus*	MERSA	N/A	Subramani et al., 2017
Aloe—emodine, coniine and lupeol	Bitter Aloe	*Aloe ferox*	*Staphylococcus aureus*, *Pseudomonas aeruginosa*, *Klebsiella pneumoniae*	310	Ghuman et al., 2016
Ellagic acid	Japanese rose	*Rosa rugosa* Thunb.	*A. baumannii*	250	Miyasaki et al., 2013
Terchebulin Chebulagic acid Chebulinic acid Corilagin	Black- or chebulic myrobalan	*Terminalia chebula* Retz.	*A. baumannii*	500 1,000 62.5 1,000	Miyasaki et al., 2013
Norwogonin Baicalin Baicalein	Chinese skullcap	*Scutellaria baicalensis* Georgi	*A. baumannii*	128 NA NA	Chan et al., 2007; Miyasaki et al., 2013
Eugenol	Clove	*Syzygium aromaticum* (L.) Merr. & L.M.Perry	*A. baumannii*	1,250	Johny et al., 2010; Pelletier, 2012
Trans-cinnamaldehyde	Cinnamon (Dalchini)	*Cinnamomum verum* J.Presl	*A. baumannii*	310	Johny et al., 2010; Pelletier, 2012
Carvacro	Oregano	*Origanum vulgare* L.	Biofilms of *S. aureus*, *A. baumannii*	0.015–0.031% v/v 310	Nostro et al., 2007; Johny et al., 2010; Pelletier, 2012
Thymol	Thyme	*Thymus adamovicii* Velen.	*A. baumannii*, *Staphylococcus epidermidis* biofilms	NA 0.031%, v/v 0.031–0.062%, V/V	Nostro et al., 2007; Johny et al., 2010; Pelletier, 2012

(Continued)

TABLE 1 (Continued)

Active compound	Plant (common name)	Botanical name	Active against	MIC (μg/ml)	References
Curcumin	Turmeric	*Curcuma longa* L.	*S. aureus,* *A. baumannii*	125–250 4 (while EGCG is present)	De et al., 2009; Mun et al., 2013; Betts and Wareham, 2014
Epigallocatechin gallate (EGCG)	Green tea	*Camellia sinensis* (L.) Kuntze	*S. aureus,* *A. baumannii*	100 312–625	Kono et al., 1997; Zhao et al., 2002; Osterburg et al., 2009; Gordon and Wareham, 2010; Betts and Wareham, 2014
Epicatechin	Green tea	*C. sinensis*	*A. baumannii*	NA	Betts et al., 2011
Theaflavin	Black tea	*C. sinensis*	*A.baumannii*	NA NA	Betts et al., 2011
(+)-Lyoniresinol-3 alpha-O-beta-D-glucopyranoside	Chinese boxthorn	*Lycium chinense* Mill.	*A. baumannii,* *S. aureus,* *Enterococcus faecalis*	NA NA NA	Chan et al., 2011
Paeonol	Moutan Peony	*Paeonia* × *suffruticosa* Andrews	*A. baumannii,* *S. aureus,* *E. faecalis*	NA NA NA	Chan et al., 2011
Berberine	Coptidis Rhizoma	*Coptis chinensis* Franch.	*A. baumannii,* *S. aureus,* *E. faecalis*	30	Chan et al., 2011
Berberine	Desert barberry	**Berberis fremontii*	*S. aureus*	NA	Stermitz et al., 2000
Honokiol, Magnolol	Cloudforest mangolia	*Magnolia macrophylla* var. *dealbata* (Zucc.) D.L.Johnson	*P. aeruginosa,* *A. baumannii*	NA	Jacobo-Salcedo et al., 2011
α-Elemene, δ-elemene, furanosesquiterpenes	Myrrh	*Commiphora myrrha* (Nees) Engl.	*Klebsiella pneumoniae,* *P. aeruginosa,* *A. baumannii*	6,250 6,250 2,500	Masoud and Gouda, 2012
p-Coumaric acid, ascorbic acid, pyrocatechol, cinnamic acid	Aloe vera	*Aloe barbadensis* Mill.	*S. aureus,* *Streptococcus* sp., *P. aeruginosa,* *K. pneumoniae*	NA	Lawrence et al., 2009
Allyl methyl disulfide, diallylsulfide, diallyltrisulfide, allyl methyl trisulfide, diallyldisulfide, diallyltetrasulfide	Garlic	*Allium sativum* L.	*P. aeruginosa,* *K. pneumoniae,* *A. baumannii*	3,120 1,250 3,120	Khadri et al., 2010
Stigmasterol, nimbiol, sugiol, 4-cymene, α-terpinene, terpinen-4-ol	Neem	*Azadirachta indica* A.Juss.	*S. aureus,* *Enterococci,* *Klebsiella* sp., *P. aeruginosa*	1,000 500 2,000 1,000	Fabry et al., 1998; Nand et al., 2012
Gossypetin, hibiscetin, quercetin, sabdaretin, delphinidin 3-O-sambubioside and cyanidin 3-O-sambubioside	(Indian sorrel/Rose mallow)	**Hibiscus subdarifa* Rottb.	*K. pneumoniae,* *Enterobacter aerogens,* *Enterobacter cloacae*	1,024 1,024 256	Djeussi et al., 2013; Rebelo, 2014
Quercetin-7-0-B-Dxylopyranoside, 7-baueren-3-acetate	Baobab/Gorakh imli	*Adansonia digitata* L.	*K. pneumoniae* *E. aerogens* *E. cloacae*	1,024 1,024 1,024	Djeussi et al., 2013

*Unresolved name, NA, MIC information is not available.

Bacteriophages and bacteriophage endolysins

Besides AMPs, bacteriophages (phages) and bacteriophage-encoded products can be employed as therapeutics for the treatment of the ESKAPE-related biofilms. Virulent phages are viruses that naturally infect bacterial hosts, eventually causing their lysis. As this interaction is specific, dysbiosis may be prevented. Importantly, they can be used to target antibiotic-resistant strains and are able to eradicate the biofilms of the

ESKAPE pathogens. Noteworthy, phages are able to degrade the biofilm matrix (including capsular polysaccharides) via specific enzymes that may promote the access of antibiotics to the deeper regions of the biofilms. Since bacteria can develop resistances against phages, phage cocktails may be used in order to overcome this problem, which also broadens the host range (targeting different strains of the target bacterium). In this context, PA4 is a recently described phage belonging to the *Myoviridae* family which reduces the biomass of *P. aeruginosa* biofilms, impairing the viability of the bacterium *in vitro* (Camens et al., 2021). Similarly, some of the recently characterized vB_SauM kayviruses are able to affect the vitality of *S. aureus* within the biofilm, reducing the pathogen biomass *in vitro* (Kaźmierczak et al., 2022).

During the lytic cycle of the bacteriophage within the bacterial host, lysins play a fundamental role, since they digest the peptidoglycan layer of the bacterial cell wall, causing the lysis of the cell and the release of the phage progeny. One of the features of lysins is that they are generally narrow-spectrum, which means that the beneficial bacteria belonging to the patient's microbiota are not compromised once administered. Not only lysins are active on planktonic bacteria, but also on biofilms. Efforts have been made in recent years specially to target Gram-negative bacteria. Due to the low permeability of the outer membrane of these bacteria, lysins are not able to reach their target. In this context, LysECD7 is a promising recombinant lysin that shows a promising activity on the Gram-negative ESKAPE pathogens, both in the planktonic form and in the biofilm state, even if a significantly higher lysin concentration is needed for a marked effect on the latter; this lysin is able to cross the outer membrane without any delivery system or additives (Vasina et al., 2021).

Interestingly, lysins encoded by phages infecting Gram-negative bacteria may be characterized by an amphipathic region able to permeabilize the outer membrane after administration, allowing the peptidoglycan layer to be affected. These amphipathic components may be isolated and employed as cationic peptides. PaP1 is a peptide derived from the PlyPa01 lysin (isolated from a phage infecting *P. aeruginosa*) characterized by membrane-acting properties and modified in order to increase the net charge of the peptide, as well as its antibacterial properties. When tested, PaP1 was found active on the ESKAPE pathogens in both monospecies and polymicrobial populations (*A. baumannii, P. aeruginosa* and *S. aureus*) and eradicates *P. aeruginosa* mature biofilms *in vitro* (Heselpoth et al., 2022).

Essential oils

Natural products can be a source of compounds which are active on both the planktonic and sessile forms of bacteria (Da Silva et al., 2017). Plant-derived EOs are a reservoir of volatile, hydrophobic secondary metabolites which may show a broad antimicrobial and antibiofilm activity against microbial pathogens, including the ESKAPE bacteria (El-Tarabily et al., 2021). The antimicrobial properties of these molecules are due to the fact that medicinal and aromatic plants naturally synthetize them in order to respond to various stresses, including microbial attacks. Noteworthy, EOs have a low potential for the development of microbial resistance due to their complex nature with multiple bioactive compounds, that leads to a multi-target activity which is not in the case of conventional antibiotics (Angane et al., 2022).

The mechanisms of action of these compounds are diverse and may be related to the target of either the bacterial virulence factors or the drug resistance mechanisms that characterize these pathogens (Vasconcelos et al., 2018). Belonging to the first category, these metabolites can inhibit biofilm formation and quorum-sensing while, in the second case, they can inhibit the function of efflux pumps and plasmid-mediated resistance (possibly by causing the loss of the plasmid carrying the resistance gene or by interfering with the transfer of the R-plasmid itself to a recipient cell). In the latter cases, EOs can be used in combination with known antibiotics since they mediate re-sensitization of the bacteria to the drug: in this way, the problem of antibiotic resistance can be addressed. It is important to highlight that these metabolites can also have bactericidal properties since they are lipophilic and can alter the membrane permeability, possibly causing membrane disruption (Álvarez-Martínez et al., 2021). An interesting application of EOs is related to their use in the disinfection of medical devices as well as hospital surfaces, preventing hospital-associated infections. As an example of EOs applications in the treatment of the ESKAPE biofilm, *P. aeruginosa* biofilm formation can be impaired *in vitro* by using EOs extracted from Mediterranean plants such as *Foeniculum vulgare* and *Ridolfia segetum* (Artini et al., 2018).

Anti-biofilm activities of essential oils and/or components

Biofilm-producing bacteria are typically resistant to antimicrobials and there is an urgent need for new approaches to fill the gap (Jouneghani et al., 2020; Sahoo et al., 2021). The formation of biofilm involves a complex mechanism with several targeted factors. There are several reports already published on the steps involved in development of biofilm (adhesion, microcolonies formation, and maturation) (**Figure 2**) and the targets starting with the adhesion to mature biofilm. The easiest way to prevent the formation is initiated by attachment, which involves the interaction between adhesive substances and receptors on the host surface. **Table 2**, provides a list of EOs and their components with anti-biofilm activity against ESKAPE pathogens. The list involves complex oils like Cassia,

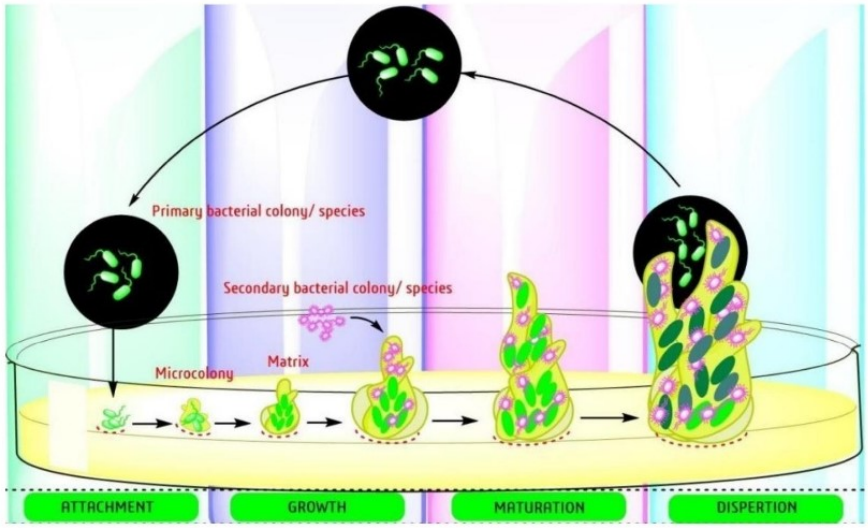

FIGURE 2
Steps involved in the development of bacterial biofilms (Sahoo et al., 2021).

cinnamon, clove, eucalyptol, lavender, lemon, marjoram, orange, oregano, peppermint, Peru balsam, rosemary, tea, and thyme oil. Moreover, several individual components were also reported including carvacrol, cinnamaldehyde, citral, citronellol, eugenol, Linalool, linalyl acetate, menthol, pulegone, thymol, α-terpineol, and terpinen-4-ol (**Table 2**). Most detailed studies involved the Gram-positive bacteria *S. aureus*, with genes [*icaD/icaA*, (intracellular gene)], biofilm-associated protein (*bap*), and several controlling genetic loci, e.g., *sarA luxS*, and *agr* quorum sensing (QS) (Yadav et al., 2015). Beside *S. aureus*, the Gram-negative bacteria *P. aeruginosa* is well studied with its mode of action.

Essential oil and quorum sensing—The language of bacteria

The two most studied bacteria are *S. aureus* and *P. aeruginosa*. Two most common oils, viz. clove oil (Husain et al., 2013) and peppermint oil (Husain et al., 2015), were tested to see their effects in reducing *P. aeruginosa* QS regulated biofilm formation. Authors observed a strong effect of both oils along with menthol as a constituent in inhibiting biofilm formation (84%), swarming migration (81%), production of virulence factors like LasB elastase activity (80%), protease activity (76%), chitinase activity (78%), and pyocyanin production (85%) (**Table 3**). A similar observation was also verified with eugenol on two MDR *P. aeruginosa*. Moreover, the authors found additional virulence factors such as rhamnolipid (57%), and pyoverdine (69%), which are responsible for microbial cell adhesion (Rathinam et al., 2017). Another report is also available by Al-Shabib et al. (2017) on the effect of eugenol to reduce the QS-regulated production of similar virulence factors in *P. aeruginosa* PAO1. In *P. aeruginosa*, curcumin (1 μg/ml) inhibits the formation of signaling molecules (Rudrappa and Bais, 2008). Tea oil was also observed to be effective in controlling biofilm formation in *S. aureus*, with interesting findings by transcriptome analysis as 104 genes downregulated while 200 genes were upregulated. Many of these genes are linked to biofilm formation, e.g., *sarA* gene (encodes the DNA-binding protein SarA) which is downregulated, and responsible for biofilm (Zhao et al., 2018).

Eugenol is also very effective in reducing the formation of biofilm in methicillin-resistant *S. aureus* (MRSA) (MIC: 0.04%) (Yadav et al., 2015). With the help of RT-qPCR tests, it was confirmed that eugenol (0.5 × MIC) reduced *sarA*, *seA* and *icaD* expression. Further, the gene expression studies showed why eugenol is strong enough to reduce the biofilm since these genes are related to biofilm e.g. regulatory gene (*sarA*), enterotoxin gene (*seA*), and adhesion gene (*icaD*) (Yadav et al., 2015). The authors also studied the effects of eugenol in *in vivo* experiments using an otitis media rat model. Eugenol (0.02%) bears a significant reduction of the bacterial colonization without any biofilms in comparison to the control tympanic bulla which was

TABLE 2 Antibacterial activities of essential oils/essential oil components against ESKAPE pathogen.

Essential oils and constituent(s)	Pathogenic bacteria	MIC values; (references)	MBIC; (references)
Cinnamomum cassia (L.) J.Presl.	*P. aeruginosa*	–; (Condò et al., 2020)	0.2%, v/v; (Kavanaugh and Ribbeck, 2012)
Coriandrum sativum L.	*A. baumannii*	1–4 μl/ml; (Duarte et al., 2013)	4 μl/ml; (Duarte et al., 2013)
Cymbopogon flexuosus (Nees ex Steud.) W.Watson	*S. aureus*, MRSA	0.5–4 mg/ml; (Piasecki et al., 2021)	0.06% v/v; (Adukwu et al., 2012)
Cymbopogon nardus (L.) Rendle	*S. aureus*	–	0.5 mg/ml; (Pontes et al., 2019)
Mentha piperita L.	28 clinic strains of *S. aureus*	64–256 μg/ml; (Li et al., 2011)	–
Origanum vulgare L.	*S. aureus*	–	10 μl/ml; (Dos Santos Rodrigues et al., 2018)
Perilla frutescens L. Britton	*S. aureus*, MRSA	0.4 μl/ml; (Qiu et al., 2011)	–
Plectranthus amboinicus (Lour.) Spreng.	*S. aureus*	0.25 mg/ml; (Vasconcelos et al., 2017)	0.5 mg/ml; (Vasconcelos et al., 2017)
Syzygium aromaticum (L.) Merr. & L.M.Perry	*S. aureus*	85.4 μl/ml; (Kačániová et al., 2021)	0.106 mg/ml; (Budri et al., 2015)
S. aromaticum	*P. aeruginosa*	223.3 μl/ml; (Kačániová et al., 2021)	1.3% v/v; (Kavanaugh and Ribbeck, 2012)
Cassia oil	*S. aureus*	0.3%, v/v; (Kavanaugh and Ribbeck, 2012)	0.6%, v/v; (Kavanaugh and Ribbeck, 2012)
Cassia oil	*P. aeruginosa*	0.2%, v/v; (Kavanaugh and Ribbeck, 2012)	0.4%, v/v; (Kavanaugh and Ribbeck, 2012)
Cinnamon oil	*K. pneumoniae*, *S. aureus*	>1.6 mg/ml 3.2 mg/ml; (Prabuseenivasan et al., 2006)	*S. aureus* (1 mg/ml) (Cui et al., 2016)
Clove oil	*P. aeruginosa*; *K. pneumoniae* and *S. aureus*	>1.6 mg/ml; >6.4 mg/ml; (Prabuseenivasan et al., 2006)	3.2%, sub MIC, biofilm of *P. aeruginosa*; (Husain et al., 2013)
Clove oil	*S. aureus*	1.2%, v/v; (Kavanaugh and Ribbeck, 2012)	1.6%, v/v; (Kavanaugh and Ribbeck, 2012)
Lavendor oil	*S. aureus*	0.8%, v/v; (Budzyńska et al., 2011)	1.6%, v/v; (Budzyńska et al., 2011)
Lavendor oil	*A. baumannii*	10.5–13.0 μl/ml; (Sienkiewicz et al., 2014)	>5%, v/v (*P. aeruginosa*); (Kavanaugh and Ribbeck, 2012)
Lemon oil	*K. pneumoniae*; *P. aeruginosa*, *S. aureus*	>12.8 mg/ml; (Prabuseenivasan et al., 2006)	*K. pneumoniae* (170 μl/L); (Sahal et al., 2016)
Lemon Balm oil	*S. aureus*	0.1%, v/v; (Budzyńska et al., 2011)	0.4%, v/v; (Budzyńska et al., 2011)
Orange oil	*K. pneumoniae*, *P. aeruginosa*; *S. aureus*	≥12.8 mg/ml >6.4 mg/ml; (Prabuseenivasan et al., 2006)	–
Oregano oil	*S. aureus*	0.062%, v/v; (Nostro et al., 2007)	0.5%, v/v; (Nostro et al., 2007)
Peru Balsam oil	*S. aureus*	2.5%, v/v; (Kavanaugh and Ribbeck, 2012)	3.5%, v/v; (Kavanaugh and Ribbeck, 2012)
Peru Balsam oil	*P. aeruginosa*	2.5%, v/v; (Kavanaugh and Ribbeck, 2012)	3.5%, v/v; (Kavanaugh and Ribbeck, 2012)
Rosemary oil	*K. pneumoniae*, *P. aeruginosa*; *S. aureus*	>6.4 mg/ml; >12.8 mg/ml; (Prabuseenivasan et al., 2006)	–
Tea tree oil	*S. aureus*	0.4%, v/v; (Budzyńska et al., 2011)	0.8%, v/v; (Budzyńska et al., 2011)

(Continued)

TABLE 2 (Continued)

Essential oils and constituent(s)	Pathogenic bacteria	MIC values; (references)	MBIC; (references)
Thyme oil	*S. aureus*	0.5%, v/v; (Kavanaugh and Ribbeck, 2012)	1.6%, v/v; (Kavanaugh and Ribbeck, 2012)
Allicin	MSSA and MRSA	32–64 μg/ml; (Leng et al., 2011)	80 μg/ml; (Zhang et al., 2022)
Carvacrol	*S. aureus*	0.35–2.80 mg/ml; (Rosato et al., 2010)	0.25 mg/ml; (Vasconcelos et al., 2017)
Carvacrol	*S. aureus*	0.02%, v/v; (Yadav et al., 2015)	0.04%, v/v; (Yadav et al., 2015)
Carvacrol	*S. aureus*	0.015%, v/v; (Nostro et al., 2007)	0.25%, v/v; (Nostro et al., 2007)
Carvacrol	*S. aureus*	0.3 μl/ml; (Souza et al., 2013)	200 μl/L; (Espina et al., 2017)
Carvacrol	Group A *Streptococci*	64–256 μg/ml; (Magi et al., 2015)	*E. faecalis* (0.01%, v/v); (Campana and Baffone, 2018)
Cinnamaldehyde	*P. aeruginosa*	0.1%, v/v; (Kavanaugh and Ribbeck, 2012)	0.2%, v/v; (Kavanaugh and Ribbeck, 2012)
Cinnamaldehyde	*P. aeruginosa*	–	11.8 mM; (Topa et al., 2018)
Cinnamaldehyde	*S. aureus*	–	0.199 mg/ml; (Budri et al., 2015)
Citral	*S. aureus*, MRSA	0.5 mg/ml; (Porfírio et al., 2017)	500 μl/L; (Espina et al., 2017)
Citronellol	*S. aureus*	0.35–1.40 mg/ml; (Rosato et al., 2007)	0.5 mg/ml; (Piasecki et al., 2021)
Curcumin	*P. aeruginosa*	62.5 μg/ml; (Adamczak et al., 2020)	100 μg/ml; (Packiavathy et al., 2014)
Eucalyptol	*S. aureus*	2.80–5.60 mg/ml; (Rosato et al., 2007)	256 μg/ml; (Hendry et al., 2009)
Eugenol	*S. aureus*	0.04%, v/v; (Yadav et al., 2015)	0.08%, v/v; (Yadav et al., 2015)
Eugenol	*S. aureus* (26 strains)	128–512 μg/ml; (Qiu et al., 2010)	0.237 mg/ml; (Budri et al., 2015)
Geraniol	*S. aureus*	0.08–1.40 mg/ml; (Rosato et al., 2007)	0.25 mg/ml; (Pontes et al., 2019)
Geranium	*K. pneumoniae*, *P. aeruginosa*, *S. aureus*	12.8 to >12.8 mg/ml; (Prabuseenivasan et al., 2006)	–
Limonene	MRSA	–	200 μl/L; (Espina et al., 2015)
Linalool	*S. aureus*	0.2–2.5 mg/ml; (Sonboli et al., 2005)	*A. baumannii* (8 μl/ml); (Alves et al., 2016)
Linalool	*S. aureus*	0.19%, v/v; (Budzyńska et al., 2011)	0.78%, v/v; (Budzyńska et al., 2011)
Linalyl acetate	*S. aureus*	0.19%, v/v; (Budzyńska et al., 2011)	0.19%, v/v; (Budzyńska et al., 2011)
Marjoram	*S. aureus*	0.125% v/v; (El-Shenawy et al., 2015)	Mixed biofilm (0.25 and 20 mg/ml); (Kerekes et al., 2019)
Menthol	*S. aureus*, MRSA	>2 mg/ml; (Qiu et al., 2010)	0.64–1.98 mg/ml; (Kifer et al., 2016)
Peppermint	*S. aureus*	0.5% (v/v); (Xiao et al., 2020)	0.5 mg/ml; (Kang et al., 2019)
Pulegone	*S. aureus*	3.75 to >15 mg/ml; (Sonboli et al., 2006)	–
Thymol	*S. aureus*	0.7–1.40 mg/ml; (Rosato et al., 2007)	0.5 μl/ml; (Ceylan and Ugur, 2015)

(Continued)

TABLE 2 (Continued)

Essential oils and constituent(s)	Pathogenic bacteria	MIC values; (references)	MBIC; (references)
Thymol	*S. aureus*	0.031%, v/v; (Nostro et al., 2007)	0.25%, v/v; (Nostro et al., 2007)
Triacetin	*S. aureus*	22.40 mg/ml; (Rosato et al., 2007)	–
α- terpineol	*S. aureus*	0.19%, v/v; (Budzyńska et al., 2011)	0.38%, v/v; (Budzyńska et al., 2011)
Terpinen-4-ol	*S. aureus*	0.19%, v/v; (Budzyńska et al., 2011)	0.19%, v/v; (Budzyńska et al., 2011)

–, data not available; MIC, minimum inhibitory concentration; MBIC, minimum biofilm inhibitory concentration; MSSA, methicillin susceptible *S. aureus*; MRSA, methicillin resistant *S. aureus*.

filled with cell debris and biofilm (Yadav et al., 2015). Another study also evidenced a significant reduction of biofilm in MRSA at sub-MIC concentration (Al-Shabib et al., 2017).

Several monoterpenes (citral, MIC = 500 μl/L; carvacrol, MIC = 200 μl/L; (+)-limonene, MIC = 5,000 μl/L), also showed reduction of biofilm formation in *S. aureus* at sub-MIC concentration. Among them, carvacrol is reported to be highly potent with the lowest concentration of 10 μl/L up to 80% reduction (Espina et al., 2015). In *P. aeruginosa*, cinnamaldehyde is able to reduce the production of AHLs probably due to hydrophobic interaction and strong bonding between cinnamaldehyde and LasI (Chang et al., 2014).

Eradication of established biofilms

Most of the biofilm studies are performed using spectrophotometer for absorption analysis performed using biofilm specific dyes. These assays indicate only the inhibition of biofilms and do not indicate the capability of the compound to eradicate an already established biofilm. All ESKAPE pathogens are biofilm-associated and, due to their intrinsic resistance, they are difficult to treat. **Table 2** shows a list of selected essential oils/essential oil components and their activity against ESKAPE pathogens in both planktonic (MIC values) and biofilm cells (Minimum Biofilm Inhibitory Concentration, MBIC). Most studies are found to be effective against *S. aureus* followed by *P. aeruginosa* while limited studies have been performed on *A. baumannii* and *K. pneumoniae*. In most cases, it is observed that the MIC value is not sufficient to inhibit biofilm, while in few cases even 100 fold could is not sufficient to treat established biofilm. Coelho and Pereira (2013) tested the three most common oils, e.g., cinnamon, tea, and palm rosa on established biofilm of *P. aeruginosa*. The authors noticed a sufficient reduction of the bacterial population (5 log10 to 2.5 log10 CFU/cm^2) and compared it with the standard antibiotic ciprofloxacin (Coelho and Pereira, 2013). Another interesting study by Lu et al. (2018) established the removal of preformed biofilm against both *S. aureus* and *P. aeruginosa* biofilms when treated with the oregano oil (carvacrol as a major constituent) (Lu et al., 2018). The experiment was further validated by an *in vivo* mouse model (third-degree burn wound infection) treated with the oregano oil (10 mg/ml for 3 days), resulting in a reduction of the 3 log10 steps population (Lu et al., 2018). Moreover, authors also detected changes in the cell structure, with disruption of biofilm under electron microscopy. This kind of study is highly valuable as it shows the direct effect of EOs/EOC and can distinguish the destruction or eradication of established biofilm.

Bactericidal toxic effects of essential oils and essential oil components on biofilms

Only limited oils/components were reported to be bactericidal. Eugenol is one of the major components that act very effectively at higher concentrations, at 12.8% (v/v), with 91.6% on the inhibitions of biofilms formed by MDR *S. aureus*. In comparison to eugenol, thyme oil also showed similar antibiofilm activity. The highest biofilm reduction (88% inhibition of *S. aureus* JSA10) was observed at 12.8% v/v (Jafri et al., 2014). Both *S. aureus* and *P. aeruginosa* were inhibited significantly when treated with cinnamaldehyde, a major constituent of *Cinnamomum zeylanicum* and *Cinnamomum cassia*. An interesting observation made by the authors is that the inhibition is not due to its anti-QS effect, but to its cytotoxic effects (Firmino et al., 2018).

Synergistic potentials of essential oils/essential oil components along with antibiotics against multidrug-resistant ESKAPE pathogens

In the past decade, there has been an increase in the research on the synergetic potentials of clinical antibiotics in

TABLE 3 Mode of action of select EOs/EOC against ESKAPE pathogen.

Essential oils	Pathogen	Mode of action	References
Chenopodium ambrosioides/α-Terpinene	*S. aureus* (IS-58)	Inhibition of EPs (*tetK*)	Limaverde et al., 2017
C. ambrosioides/α-Terpinene	*S. aureus* (1199B/1199)	Inhibition of EPs (*norA*)	Salehzadeh et al., 2018
C. verum	*K. pneumoniae*	Induction of oxidative stress and oxidation/DBM	Yang et al., 2019
C. cyminum	*K. pneumoniae*	Loss of plasmid integrity	Derakhshan et al., 2008
Dodartia orientalis	*S. aureus*	DBM	Wang et al., 2017
Dorema aucheri Bioss	*P. aeruginosa* PAO1	QS-inhibition, reduction on virulence factors (RVF) (pyoverdine and elastase production), and the transcription of *lasI*	Sepahi et al., 2015
Ferula asafoetida L.	*P. aeruginosa* PAO1	QS-inhibition, RVF (pyocyanin, pyoverdine, elastase production), and the transcription of lasI	Sepahi et al., 2015
Melaleuca alternifolia (tea tree oil)	*P. aeruginosa* NCTC 6749	DBM and metabolic events	Cox et al., 2001
Melaleuca alternifolia	Methicillin-resistant *S. aureus*, Carbapenem-resistant *K. pneumoniae, A. baumannii*, and *P. aeruginosa*	DBM (structural integrity and membrane permeabilization)	Oliva et al., 2018
Tea tree oil	*S. aureus*	Cell division inhibition	Reichling et al., 2002
Mentha piperita L.	*S. aureus*	Inhibition of α-toxin production (ITP)	Li et al., 2011
Mentha piperita L.	*P. aeruginosa* PAO1	QS-RVF (elastase, proteases, pyocyanin and chitinase)	Husain et al., 2015
Ocimum gratissimum	*P. aeruginosa* and *S. aureus*	Change in membrane permeability (CMP)	Hyldgaard et al., 2012
Origanum vulgare (oregano oil)	*P. aeruginosa* and *S. aureus*	Bacterial enzyme inhibition and reduce bacterial lipase and coagulase activity	Lambert et al., 2001
Rosmarinus officinalis/1,8-cineol	MDR *K. pneumoniae*	CMP	Moreno et al., 2015
Rosmarinus officinalis/Eucalyptol	MDR *A. baumannii* and *P. aeruginosa*	Inhibition of EPs	Saviuc et al., 2016
Origanum vulgare L.	*S. aureus*	ITP	De Souza et al., 2010
Perilla frutescens L. Britton	*S. aureus*, MRSA	ITP	Qiu et al., 2011
Syzygium aromaticum/Eugenol	MRSA	Anti-QS and anti-biofilm	Al-Shabib et al., 2017
Syzygium aromaticum	*P. aeruginosa*	QS- Inhibit swarming motility	Khan et al., 2009
Thymus vulgaris/thymol	*S. aureus*	Inhibition of EPs (norA)	Salehzadeh et al., 2018
Essential oil components			
Allicin	MSSA and MRSA	ITP	Leng et al., 2011
Carvacrol	*S. aureus*	DBM	Di Pasqua et al., 2007
Carvacrol	*S. aureus*	Inhibit enterotoxin production completely	Souza et al., 2013
Carvacrol	MRSA	Anti-QS and anti-biofilm	Sharifi et al., 2018
Carvacrol	*S. aureus*	Changes in fatty acid composition	Noumi et al., 2018
Carvacrol	*P. aeruginosa*	QS-Inhibition (pyocyanin production, biofilm)	Tapia-Rodriguez et al., 2017
Carvone	MRSA	Disruption and separation of the cytoplasmic contents by R-cat	Oosterhaven et al., 1995
Cinamoldehyde	Carbapenem resistant *A. baumannii*	Anti-biofilm	Mohamed et al., 2018
Cinamoldehyde	*P. aeruginosa* PA01	QS-Inhibition 7-fold of the lasR level, and pyocyanin production	Ahmed et al., 2019
Curcumin	*P. aeruginosa* PA01	QS-Inhibition 2-fold of elastase activity	Rudrappa and Bais, 2008
Curcumin	*P. aeruginosa* PA01	QS-Inhibition (alginate and prodigiosin production)	Packiavathy et al., 2014
Eugenol	*S. aureus*	Inhibit enterotoxin and α-hemolysin production significantly	Qiu et al., 2010

(Continued)

TABLE 3 (Continued)

Essential oils	Pathogen	Mode of action	References
Farnesol and nerolidol	*S. aureus*	Cytoplasm disruption (alteration of integrity and permeability, inhibition of cell respiration, K^+ leakage)	Cox et al., 2000; Inoue et al., 2004
6-Gingerol	*P. aeruginosa*	QS-Inhibition (biofilm formation, 53%), RVF (exoprotease, pyocyanin and rhamnolipid)	Kim et al., 2015
Linalyl acetate	*S. aureus*	DBM and leakage of intracellular materials	Trombetta et al., 2005; Mahizan et al., 2019
Linalyl anthranilate	Carbapenemase-producing *K. pneumoniae*	DBM and leakage of intracellular materials	Yang et al., 2021
Menthol	*S. aureus*	DBM and leakage of intracellular materials	Trombetta et al., 2005; Mahizan et al., 2019
Menthol	*S. aureus*, MRSA	ITP	Qiu et al., 2010
Menthol	*P. aeruginosa* PA01	QS-Inhibition, Anti-biofilm, RVF (protease activity, elastase activity, chitinase activity, pyocyanin production, swarming motility, EPS production)	Husain et al., 2015
β-pinene	*E. faecalis*	Anti-biofilm	Negreiros et al., 2016
Thymol	*S. aureus*	DBM and leakage of intracellular materials	Trombetta et al., 2005; Mahizan et al., 2019
Thymol	MRSA	Anti-biofilm and anti-quorum sensing	Sharifi et al., 2018
Thymol	*S. aureus*; MRSA	Inhibit α-hemolysin, enterotoxin production	Qiu et al., 2011
α- and γ-terpinene	*S. aureus*	DBM	Mahizan et al., 2019
Terpinene-4-ol	MRSA	Anti-QS and anti-biofilm	Perez et al., 2019
Terpinene-4-ol	*S. aureus*	Formation of multilamellar, mesosome-like structures	Carson et al., 2002; Reichling et al., 2002
Zingerone	*P. aeruginosa* PA01	QS-Inhibit protease production	Kumar et al., 2015

CMP, change in membrane permeability; DBM, disruption of bacterial membrane; Eps, extracellular polymeric substances; ITP, inhibition of α-toxin production; QS, quorum sensing.

combination with essential oils or individual components. We have reviewed various publications on the ESKAPE pathogens and summarized (**Table 4**) the synergistic effects of essential oils and antibiotics.

In combination with chloramphenicol, several essential oils viz. *Artemisia herba-alba, Cymbopogon citratus, Helichrysum italicum*, and *Thymus riatarum* showed synergistic effects against *Enterococcus aerogenes* EA27 (overexpressing the AcrAB-TolC efflux system) (Lorenzi et al., 2009; Fadli et al., 2014, 2016). Moreover, available literature suggests that *H. italicum* and *Thymus maroccanus* act synergetically against *A. baumannii* AP1 (reduced OprD expression) (Lorenzi et al., 2009; Fadli et al., 2011). Geraniol is the major constituent in most of these oils which in combination with chloramphenicol showed synergistic effects *E. aerogenes* EA27 with 256-fold reduction in MIC (Lorenzi et al., 2009). Authors also concluded that the mechanism of action is due to inhibition of efflux pumps activity/expression (AcrAB-TolC efflux system) (**Table 3**). Similarly, EOs- *Thymus broussonetii* and *Thymus riatarum,* showed synergistic effects when combined with ciprofloxacin, against MDR *P. aeruginosa,* MDR *S. aureus* and MDR *K. penumoniae* Fractional inhibitory Concentration Index (FICI < 0.5) (Fadli et al., 2012). The major constituents among both essential oils are carvacrol which was also observed to be in synergism with ciprofloxacin showing 8-fold reduction in MIC. The mechanism of action is due to the disruption of the bacterial membrane (Fadli et al., 2012). Moreover, carvacrol has also been observed to be synergistic with other antibiotics, such as nitrofurantoin against *Klebsiella oxytoca* (Zhang et al., 2011), and tetracycline against MDR *S. aureus* (Cirino et al., 2014; **Table 3**). Gentamicin is a commonly used antibacterial agent for synergy studies in several MDR bacteria, such as *A. baumannii, S. aureus, E. clocae, P. aeruginosa*, and *K. penumoniae*. Gentamicin in combination with EOs such as *Pelargonium graveolens, T. broussonetii*, and *T. riatarum* showed synergism by action on disruption of bacterial membrane (FICI < 0.5) (Fadli et al., 2012). Fadli et al. (2012), also studied the same essential oils in combination with the antibiotic Pristinamycin against *S. aureus, E. clocae, P. aeruginosa*, and *K. penumoniae* and recorded synergistic effects (FICI $= 0.5$). Other major components include thymol and eugenol, whose synergistic effects were tested in combination with tetracycline (Cirino et al., 2014) and vancomycin (Hemaiswarya and Doble, 2009), respectively.

Most studies focused on bacteria *S. aureus* and *P. aeruginosa* while few studies involved *A. baumannii, Enterobacter,* and *Klebsiella*. Most essential oils are complex in nature, but few studies also followed up on the major components,

TABLE 4 Synergistic effects of Essential oils and antibiotics against ESKAPE pathogens.

EOs/EOC	Antibiotics	Bacterial strains	Method(s)	Outcome	Mechanism of action	References
Artemisia herba-alba Asso	Chloramphenicol	*E. aerogenes* EA27	Microdilution method (MDM)	4-fold reduction in MIC	Alteration of outer membrane (OM), lipopolysaccharide structure (LPS)	Fadli et al., 2016
Aniba rosaeodora	Gentamicin	*A. baumannii*	Checkerboard assay (CBA)	FICI = 0.11	–	Rosato et al., 2007
Cymbopogon citratus (DC.) Stap	Chloramphenicol	*E. aerogenes* EA27	MDM	4-fold reduction in MIC	Alteration of OM-LPS	Fadli et al., 2016
Cinnamomum zeylanicum	Amikacin	*Acinetobacter* sp.,	CBA	Additive effect	–	Guerra et al., 2012
Coriandrum sativum	Chloramphenicol, Ciprofloxacin, Gentamicin	*A. baumannii*	CBA	FICI = 0.047 to 0.375	–	Duarte et al., 2012
Croton zehntneri Pax & K.Hoffm	Norfloxacin	*S. aureus* SA 1199B	Change in inhibition zone by EO gaseous contact (IZGC)	IZGC = 39.5%	Inhibition of efflux pumps activity/ expression (IEPA/E)	Coutinho et al., 2010
Helichrysum italicum (Roth) G.Don	Chloramphenicol	*E. aerogenes* EA27	MDM	8-fold reduction in MIC	IEPA/E	Lorenzi et al., 2009
Helichrysum italicum (Roth) G.Don	Chloramphenicol	*A. baumannii* AP1	MDM	8-fold reduction in MIC	IEPA/E	Lorenzi et al., 2009
Lippia microphylla Cham.	Norfloxacin	*S. aureus* SA 1199B	IZGC	IZGC = 39.5%	IEPA/E	Coutinho et al., 2011
Myrtus communis	Ciprofloxacine, polymixin B	*A. baumannii*	CBA	FICI = 0.047–0.375	–	Aleksic et al., 2014
Origanum vulgare L	Tetracycline	*S. aureus* I-58	MDM	4-fold reduction in MIC	IEPA/E	Cirino et al., 2014
Pelargonium graveolens	Gentamicin	*A. baumannii, S. aureus*	CBA	FICI = 0.11	–	Rosato et al., 2007
P. graveolens	Norfloxacin	*S. aureus*	CBA	FICI = 0.11	–	Rosato et al., 2007
Thymus broussonetii Bois	Cefixime	MDR *P. aeruginosa*	CBA, Cell lysis assay (CLA)	FICI = 0.5	Disruption of bacterial membrane (DBM)	Fadli et al., 2012
T. broussonetii	Cefixime	MDR *S. aureus*	CBA; CLA	FICI = 0.5	DBM	Fadli et al., 2012
T. broussonetii	Ciprofloxacin	MDR *P. aeruginosa*	CBA, CLA	FICI = 0.14	DBM	Fadli et al., 2012
T. broussonetii	Ciprofloxacin	MDR *S. aureus*	CBA, CLA	FICI = 0.5	DBM	Fadli et al., 2012
T. broussonetii	Gentamycin	MDR *E. clocae*	CBA, CLA	FICI = 0.5	DBM	Fadli et al., 2012
T. broussonetii	Gentamycin	MDR *P. aeruginosa*	CBA, CLA	FICI = 0.28	DBM	Fadli et al., 2012
T. broussonetii	Gentamycin	MDR *S. aureus*	CBA, CLA	FICI = 0.5	DBM	Fadli et al., 2012
T. broussonetii	Pristinamycin	MDR *K. pneumoniae*	CBA, CLA	FICI = 0.5	DBM	Fadli et al., 2012
T. broussonetii	Pristinamycin	MDR *S. aureus*	CBA, CLA	FICI = 0.5	DBM	Fadli et al., 2012
Thymus maroccanus Ball	Chloramphenicol	*A. baumannii* AP1	MDM	8 to 16 -fold reduction in MIC	Alteration of OM-LPS	Fadli et al., 2011
T. maroccanus	Chloramphenicol	*P. aeruginosa* PA124	MDM	4 to 8 -fold reduction in MIC	IEPA/E	Fadli et al., 2011
Thymus riatarum Humbert & Maire	Chloramphenicol	*E. aerogenes* EA27	MDM	16 -fold reduction in MIC	IEPA/E	Fadli et al., 2011
T.riatarum	Ciprofloxacin	MDR *E. clocae*	CBA, CLA	FICI = 0.37	DBM	Fadli et al., 2012
T. riatarum	Ciprofloxacin	MDR *K. penumoniae*	CBA, CLA	FICI = 0.5	DBM	Fadli et al., 2012
T. riatarum	Ciprofloxacin	MDR *P. aeruginosa*	CBA, CLA	FICI = 0.15	DBM	Fadli et al., 2012
T. riatarum	Ciprofloxacin	MDR *S. aureus*	CBA, CLA	FICI = 0.26	DBM	Fadli et al., 2012
T. riatarum	Gentamycin	MDR *E. clocae*	CBA, CLA	FICI = 0.19	DBM	Fadli et al., 2012
T. riatarum	Gentamycin	MDR *K. penumoniae*	CBA, CLA	FICI = 0.5	DBM	Fadli et al., 2012

(Continued)

TABLE 4 (Continued)

EOs/EOC	Antibiotics	Bacterial strains	Method(s)	Outcome	Mechanism of action	References
T. riatarum	Gentamycin	MDR *K. P. aeruginosa*	CBA, CLA	FICI = 0.18	DBM	Fadli et al., 2012
T. riatarum	Gentamycin	MDR *S. aureus*	CBA, CLA	FICI = 0.5	DBM	Fadli et al., 2012
T. riatarum	Pristinamycin	MDR *E. cloacae*	CBA, CLA	FICI = 0.5	DBM	Fadli et al., 2012
T. riatarum	Pristinamycin	MDR *S. aureus*	CBA, CLA	FICI = 0.5	DBM	Fadli et al., 2012
Zataria multiflora	Vancomycin	*S. aureus*	CBA	FICI = 0.32	–	Mahboubi and Bidgoli, 2010
Carvacrol	Ampicillin	*S. aureus*	CBA	FICI < 0.3	–	Palaniappan and Holley, 2010
Carvacrol	Bacitracin	*S. aureus*	CBA	FICI < 0.3	–	Palaniappan and Holley, 2010
Carvacrol	Nitrofurantoin	*K. oxytoca*	CBA	FICI ≤ 0.5	–	Zhang et al., 2011
Carvacrol	Ciprofloxacin	*S. aureus*	MDM, CLA	8-fold reduction in MIC	DBM	Fadli et al., 2012
Carvacrol	Ciprofloxacin	*K. pneumoniae*	MDM, CLA	4-fold reduction in MIC	DBM	Fadli et al., 2012
Carvacrol	Ciprofloxacin	*E. cloacae*	MDM, CLA	4-fold reduction in MIC	DBM	Fadli et al., 2012
Carvacrol	Tetracycline	*S. aureus* I-58	MDM	2-fold reduction in MIC	IEPA/E	Cirino et al., 2014
Eugenol	Vancomycin, β-lactams	*E. aerogenes, P. aeruginosa*	MDM, CBA	–	DBM	Hemaiswarya and Doble, 2009
Geraniol	Chloramphenicol	*E. aerogenes* EA27	MDM	256-fold reduction in MIC	IEPA/E	Lorenzi et al., 2009
Thymol	Tetracycline	*S. aureus* I-58	MDM	2-fold reduction in MIC	IEPA/E	Cirino et al., 2014

CBA, checkerboard assay; CLA, cell lysis assay; IZGC, change in inhibition zone by EO gaseous contact; OM, outer membrane, LPS, lipopolysaccharide structure; IEPA/E, inhibition of efflux pumps activity/expression; DBM, disruption of bacterial membrane.

e.g., carvacrol, eugenol, geraniol, and thymol. Owing to the complexity, it is important to know the mechanism of action that is responsible for synergistic effects. Table 3 describes the mechanism of actions in which mostly the disruption of bacterial membrane and inhibition of efflux pump activity/expression was observed to be the most common mode. Few studies also provide insights into the changes occuring in lipopolysaccharide structure and alteration of the outer membrane. Due to a complex mixture of components, most EOs exhibit antibacterial activities against both Gram-positive and Gram-negative pathogens. Moreover, the target bacteria and mode of action are different, as a result, the chances of resistance probability are less (Rai et al., 2017; Subramani et al., 2017). In most cases, the mode of mechanism acts as a membrane disruption, and as a result, leakage of cell content as well as coagulation of the cytoplasm. Moreover, other mechanisms involve their ability to inhibit the bacterial efflux pumps, metabolic pathways, antibiofilm, and anti-quorum sensing activity (Table 4). Moreover, due to the multiple bioactivities, such as antioxidant, anti-inflammatory, and wound healing properties, additional benefits may be observed during the treatment of ESKAPE pathogens (Subramani et al., 2017).

In vivo analysis of antimicrobial properties of essential oils against ESKAPE pathogens

Biofilm-forming bacteria are commonly involved in infection of skin wounds impairing the reparative process due to prolongation of inflammatory phase (Macedo et al., 2021). Thus, the microbial infection can lead to chronic wound development (Rahim et al., 2016). In this section we discuss the application of EOs and EOCs in the treatment of wound infections provoked by biofilm-forming bacteria (Table 5) (*A. baumannii*, *P. aeruginosa*, and *S. aureus*).

Acinetobacter baumannii

Some studies have examined the antimicrobial effects of EOs against *A. baumannii* using mammalian models. One study showed the evaluation of the EO extracted from *Origanum vulgare* (Lamiaceae) in *A. baumannii*-infected wounds in Wistar rats. The EO enhanced the healing and reduced the growth in tissue and wound secretions. The EO is mainly composed

TABLE 5 *In vivo* antimicrobial properties of essential oils against ESKAPE pathogens.

Bacteria	Essential oil/essential oil compound	Main compounds	Formulation	Model	References
A. baumannii	*Pimenta dioica* (L.) Merr. (Myrtaceae)	β-Myrcene (44.1%), 1,8-cineol (18.8%), Limonene (11.7%), Eugenol (8.6%)	EO was dissolved in sweet almond oil.	Excisional wounds in mice.	Ismail et al., 2020
	Pimenta racemose (Mill.) J.W.Moore (Myrtaceae)	β-Myrcene (39.6%), Eugenol (31%), Limonene (15.5%)	EO was dissolved in sweet almond oil.	Excisional wounds in mice.	Ismail et al., 2020
	Eugenol	–	Eugenol was dissolved in sweet almond oil.	Excisional wounds in mice.	Ismail et al., 2020
	Origanum vulgare (Lamiaceae)	α-Thujene, α-pinene, octanone, terpinene, p-cymene, carvacrol and thymol	–	Excisional wounds in Wistar rats.	Amini et al., 2019
P. aeruginosa	*Cinnamomum zeylanicum* Blume (Lauraceae)	Cinnamaldehyde (the main constituent), eugenol, coumarin, and O-methoxycinnamaldehyde.	Nanostructured lipid carrier gel containing the EO at 2% or 4%	Third-degree burn in male Sprague-Dawley rats.	Wen et al., 2021
	Cinnamaldehyde	–	–	Excisional wounds in female Swiss mice	Ferro et al., 2019
S. aureus	*Anethum graveolens* (Apiaceae)	α-Phellandrene (47.3%), p-cymene (18.5%) and carvone (14.1%)	Ointments containing the EO at 2 or 4%	Excisional wounds in BALB/c mice	
	Cymbopogon citratus (Poaceae)	Citral (38.66%), Myrcene (13.78%), Nerol (2.90%)	Carbopol gel with the EO 1%	Excisional wounds in Wistar rats	Oliveira et al., 2019
	Oliveria decumbens (Apiaceae)	Thymol (50.1%), γ -terpinene (20.7%), and p-cymene (17.6%)	Cream formulation containing *O. decumbens* and *P. graveolent*	Excisional wounds in BALB/c mice	Mahboubi et al., 2016
	Pelargonium graveolent (Geraniaceae)	β-Citronellol (39.3%) and geraniol (23.6%)			
	Trachyspermum ammi (L.) Sprague (Apiaceae).	Cymene (ρ) (36.64%), Terpinene (γ-) (35.98%), Thymol (18.14%)	Core-shell electrospun nanofibers containing the EO.	Excisional wounds in Sprague-Dawley male rats	Zare et al., 2021
S. aureus and *P. aeruginosa*	*T.carum carvi* L. (Apiaceae)	Carvone (56.9%), Limonene (36.1%)	EO encapsulated in nanostructured lipid carriers	Excisional wounds in BALB/c mice	Tazehjani et al., 2021
	Cinnamomum verum J.Presl (Lauraceae)	Cinnamic aldehyde (54.1%), α-copaene (12.3%), and styrene benzebe, ethenyle (7%)	Ointments containing the EO at 2 and 4%.	Excisional wounds in BALB/c mice	Seyed Ahmadi et al., 2019
	Mentha × *piperita* L. (Lamiaceae):	Menthol (39.80%), mentone (19.55%), neomenthol (8.82%)	Ointments containing the EO at 2, 4, or 8%	Excisional wounds in BALB/c mice	Modarresi et al., 2019
			EO encapsulated in nanostructured lipid carriers	Excisional wounds in BALB/c mice	Ghodrati et al., 2019
	Mentha pulegium L. (Lamiaceae)	Pulegone (72.18%), piperitenone (24.04%)	EO encapsulated in nanostructured lipid carriers	Excisional wounds in BALB/c mice	Khezri et al., 2019
	Rosmarinus officinalis L. (Lamiaceae)	1,8-Cineole and α-Pinene.	nanostructured lipid carrier gel containing the EO at 2% and 4%.	Excisional wounds in BALB/c mice	Khezri et al., 2019

(Continued)

TABLE 5 (Continued)

Bacteria	Essential oil/essential oil compound	Main compounds	Formulation	Model	References
	Salvia officinalis L. (Lamiaceae)	cis-Thujone (26.8%), camphor (16.4%), trans-thujone (14.1%) and 1,8-cineole (10.8%)	Ointments containing the EO at 2 and 4%.	Excisional wounds in BALB/c mice	Farahpour et al., 2020
	Satureja sahendica Bornm (Lamiaceae)	Carvacrol, thymol, γ-terpinene, p-cymene	Ointments containing the EO at 1, 2, and 4%.	Excisional wounds in BALB/c mice	Omarizadeh et al., 2021
	Zataria multiflora Boiss (Lamiaceae)	Thymol (52.90%), *p*-cymene (9.10), γ-terpinene (8.10%) and carvacrol (6.80%)	Ointments containing the EO.	Excisional wounds in BALB/c mice	Farahpour et al., 2020

of alpha thujene, alpha-pinene, octanone, terpinene, p-cymene, carvacrol, and thymol (Amini et al., 2019).

Other research examined the *in vitro* and *in vivo* antimicrobial effects of EOs from *Pimenta dioica* (L.) Merr. and *Pimenta racemose* (Mill.) J.W.Moore (Myrtaceae) against *A. baumannii* (Premachandran and Murthy, 2022). The EOs showed *in vitro* antimicrobial and antibiofilm actions against a range of *A. baumannii* strains. The authors selected the leaf oils for *in vivo* assay using male mice. The excisional wounds were infected by two successive additions of 10 μl of *A. baumannii* suspensions (10^7 and 10^8 CFU/ml). The animals were treated with the EOs and eugenol dissolved in sweet almond oil (5.2 and 2 μg/ml). Interestingly, the administration of *Pimenta* EOs had the highest action than eugenol. The authors did not report data about the wound repair (Ismail et al., 2020).

Pseudomonas aeruginosa

Trans-cinnamaldehyde is an EOC with reported antivirulence and antimicrobial action against *P. aeruginosa*. The *in vivo* antimicrobial effects of Trans-cinnamaldehyde were analyzed in wounds contaminated by *P. aeruginosa* (30 μl of 1.5×10^8 CFU/ml). Female Swiss mice (4 months old) were treated by the EOC solution in Dimethylsulfoxide (DMSO). The daily administration of trans-cinnamaldehyde modulated the host inflammatory response and inhibited the bacterial growth. Interestingly, the authors reported that the EOC actions were mediated by Transient Receptor Potential Ankyrin 1 (TRPA1) (Ferro et al., 2019).

The barks of *Cinnamomum zeylanicum* (Lauraceae) bear an EO mainly composed of Cinnamaldehyde, eugenol, coumarin, and *O*-methoxycinnamaldehyde (Alizadeh Behbahani et al., 2020). Wen et al. (2021) developed and characterized topical nanostructured lipid carrier (NLC) gel loaded with *C. zeylanicum* bark EO using thermosensitive Poloxamer 407 as a gelling agent. The effectiveness of this formulation was evaluated in a model of third-degree burn in male Sprague-Dawley rats. Each wound received an injection of *P. aeruginosa* suspension ($\sim 7.5 \times 10^5$ CFU/ml). The daily administration inhibited the growth of *P. aeruginosa* at the wound tissue and enhanced the skin repair (Wen et al., 2021).

Staphylococcus aureus

The EOs from *Oliveria Decumbens* (Apiaceae) and *Pelargonium Graveolens* (Geraniaceae) have been reported as effective against these bacteria (Mahboubi et al., 2011). These EOs were incorporated in a topical ointment and the antimicrobial effects were evaluated on MRSA-infected wounds in male Balb/c mice. In this model, the infection was established by the application of sutures containing MRSA strain. After 6 hour, the treatment was initiated and was provided three times a day. The treatment with the herbal formulation containing both EO reduced the bacterial load in the wound, with values similar to those observed in the positive control (mupirocin ointment). In addition, the EOs-incorporated ointment enhanced the healing process by collagen deposition. The major compounds detected in the EOs were thymol and β-citronellol for *O. decumbens* and *P. graveolent*, respectively (Mahboubi et al., 2016).

Anethum graveolens L. (Apiaceae) is popularly known as dill and its essential oil (DEO) is reported as an antimicrobial agent (Singh et al., 2005). The effects of ointments (90%, 5% hard paraffin and 5%) containing DEO at 2 or 4% were evaluated in excisional wounds infected by MRSA in male BALB/c mice (nine-weeks-old). The wounds were infected with 50 μl of MRSA suspension (5×10^7CFU/wound) and treated daily with the ointment. The topical administration of DEO-ointments promoted the wound contraction and reduced the bacterial burden. Histological analysis revealed that these effects were associated with the improvement of re-epithelialization, angiogenesis and collagen deposition. The animals treated with DEO-ointments also showed higher expressions of Bcl-2, p53, caspase-3, VEGF, and FGF-2 in comparison to the untreated

mice. The major compounds of DEO were α-phellandrene, p-cymene and carvone (Manzuoerh et al., 2019).

The EO from *Cymbopogon citratus* is another example of EO which reported *in vivo* anti-*S. aureus* activity. In this case, the EO was incorporated in carbopol at 1% and the formulation was applied in *S. aureus*-infected wounds (0.5×10^8 CFU/wound) performed in male Wistar mice (3–4 months). The EO used is mainly composed of Citral (38.66%), Myrcene (13.78%), and Nerol (2.90%). The treatment with *C. citratus* EO reduced the bacterial load with the same effectiveness as vancomycin (Oliveira et al., 2019).

Zare et al. (2021) developed Core-shell electrospun nanofibers containing the EO from *Trachyspermum ammi* (L.) Sprague (Apiaceae) and evaluated them in wounds contaminated by *S. aureus*. In this case, the author used Sprague-Dawley male rats (7–8 weeks old) and the wounds were infected with 1,000 μl of *S. aureus* suspension ($1–1.5 \times 10^8$ CFU/ml). The major compounds detected in the EO were Cymene (ρ) (36.64%), Terpinene (γ) (35.98%), Thymol (18.14%). The formulation showed high efficacy in reducing the growth of *S. aureus* in the wounds and promoted the healing process (Zare et al., 2021).

Staphylococcus aureus and *Pseudomonas aeruginosa*

Mentha × *piperita* L. (Lamiaceae) is source of an EO (known as PEO) with antibiofilm and antimicrobial actions against *S. aureus* and *P. aeruginosa* (Husain et al., 2015; Chraibi et al., 2021). The *in vivo* antimicrobial effects of ointments containing the PEO at 2, 4 and 8% were investigated. In this case, wounds in male BALB/c mice (12–14 weeks old) were infected by 25×10^7 units of *S. aureus* and *P. aeruginosa*. The topical treatment with PEO-containing ointments reduced the bacterial load and the expression of some inflammatory mediators (TNF-α, VEGF and FGF-2), while the genes for CCL2, CXCL1, IL-1β, TGF-β1, and IL-10 were upregulated. On the other hand, the PEO-treated wounds showed faster wound contraction than control animals, due to the increase in fibroblasts migration and collagen synthesis (Modarresi et al., 2019). PEO loaded in nanostructured lipid carriers also exhibited efficacy in this model (Ghodrati et al., 2019).

Similarly, the antimicrobial effects of ointments prepared with *Cinnamon verum* essential oil (2 and 4%) were tested in wounds infected by *S. aureus* and *P. aeruginosa*. The ointments were prepared using soft yellow paraffin. The excisional wounds were contaminated with 10^7 CFU of each bacterium. *C. verum* EO-containing ointment accelerated the tissue repair by inhibiting the inflammation and increasing the collagen deposition, keratin synthesis and the expression of key genes (IGF-1, FGF-2, and VEGF expression). The animals treated with *C. verum* EO exhibited higher antioxidant power. The major compounds presented in the used EO were Cinnamic aldehyde (54.1%), α-copaene (12.3%), and styrene benzebe, ethenyle (7%) (Seyed Ahmadi et al., 2019).

Other EOs that were efficient for the treatment of wounds with mixed infections by *S. aureus* and *P. aeruginosa* including those obtained from *Carum carvi* L. (Apiaceae) (Tazehjani et al., 2021), *Mentha pulegium* L. (Lamiaceae) (Khezri et al., 2019), *Rosmarinus officinalis* L. (Lamiaceae) (Khezri et al., 2019), *Salvia officinalis* L. (Lamiaceae) (Farahpour et al., 2020), *Satureja sahendica* Bornm (Lamiaceae) (Omarizadeh et al., 2021), *Zataria multiflora* Boiss (Lamiaceae) (Farahpour et al., 2020).

Mechanism of resistance, safety and application of essential oils

The present review deals with the recent development of EOs/EOCs targeting biofilm amongst ESKAPE pathogens. **Table 3** has elaborated the mode of action of selected EOs/EOCs but the gathered information is not sufficient and still, several efforts needed further studies on the mechanism of actions of individual EOs for a better understanding of the EO's anti-biofilm mechanisms. In general majority of EO's mechanisms of action to inhibit the formation of biofilm as well as to eradicate matured biofilm involves the action of EOs by inhibiting QS mechanisms, as well as interacting with the EPS matrix. Words and phrases like "all-natural" are safe, not correct that includes diffusing essential oils. Like other plant compounds safety of essential oils also depends largely on dosage. Many of the reported essential oils are reported to have allergic reactions to the skin as well as "hormone-related health complications" *https://www.cnet.com/health/are-essential-oils-actually-safe/*. Lu et al. (2018) studied the efficacy of oregano oil against several isolated bacteria with multidrug resistance as well as in *in vivo* burn infection model (*P. aeruginosa* PA01 and *S. aureus* USA 300). An interesting observation was found that MDR strains could not regain resistance even up to 20 passages when tested at sub-lethal concentrations. The effect of oregano oils on the skin of mice is prominent without any side effects (skin histologically or genotoxicity). Another experiment on mice model infected with *S. aureus* (ATCC #14775), aids in the survival of one-third treated population for thirty days compared to the control (all dead within 7 days) when treated with Origanum oil (Preuss et al., 2005). Yang et al. (2019), studied effects of *Artemisia vestita* oil on mice model infected with *Streptococcus pyogenes* and observed significant improvement on respiratory function of lungs as well as biochemical parameters of blood without any noticeable toxicity. **Table 5**, provides details of several *in vivo* studies infected with ESKAPE pathogens and most of these essential oils are effective without any side effects (Amini et al., 2019; Ferro et al., 2019; Oliveira et al., 2019; Tazehjani et al., 2021).

On the other hand, EOs are used for human kinds since ancient times. Many of the EOs are widely used in food and cosmetic as well as pharmaceutical industries without any toxicity. Indeed, it is necessary to study complete toxicity so as to make the best use of beneficial effects. The prime rewards of essential oil are its vast collection of aromatic plants (≈3000, of which 300) are known to be safe for humans by the U.S. FDA (Lu et al., 2018). Most of these essential oils are reported to possess antioxidant and antimicrobial activity, so as to consider green antimicrobials (economically low cost in crude form, biocompatible, less toxic without any harm to the environment and most importantly less resistance toward antibiotics). All these characteristics perfectly suit for an alternative effective solution for tackling antimicrobial resistance for ESKAPE pathogens. Moreover, certain limitation still needs to be addressed and more research needs to address including the "stability, selectivity, bio-availability, biocompatibility or any possible non-target or toxic effects on the human body or any type of allergy" (Yu et al., 2020).

Conclusions, challenges, and future perspectives

Compared to the planktonic form of the ESKAPE bacteria, those found within biofilms are estimated to be up to 1,000 times less sensitive to antimicrobials. To make this scenario worse, antibiotic resistance characterizing these pathogens is an ever-growing global threat. In order to address these problems, several strategies are being explored all over the globe especially to eradicate the biofilms of these bacteria. Some strategies include antimicrobial peptides and peptoids, bacteriophages and bacteriophage-encoded products such as endolysins, compounds able to impair biofilm formation (inhibiting either biofilm structuration or the quorum-sensing mechanisms regulating the formation of the biofilm) and immunotherapies (both active and passive), also drug reuse/resensitization and drug repurposing. Despite the potential of these strategies, the most important challenge that must be faced is the possible development of bacterial antibiotic resistance. This problem may be addressed by combining these strategies among each other, as well as with conventional antibiotics. For instance, one of the most promising alternative approaches is the use of EOs since their components naturally possess antimicrobial and antibiofilm activity. EOs can mediate resensitization of the bacteria to currently available antimicrobials by inhibiting antibiotic resistance mechanisms; another example is connected to the capability of phages to disrupt the matrix of the biofilm, making it permeable to antibiotics. New combinations of different approaches must be investigated as well, in order to broaden the therapeutic options for eradication of ESKAPE-biofilm mediated infections.

Author contributions

SP and VT: conceptualization and design and proofread of the final version. SP, SS, AB, EF, MK, LS, and VT: data curation. SP, LS, and VT: data analysis. SP, SB, SS, AB, EF, MK, LS, and VT: writing the manuscript. All authors contributed to the article and approved the submitted version.

Funding

SB was funded by the Italian Ministry of Education, University and Research (MIUR) (Dipartimenti di Eccellenza, Program 2018–2022) to Department of Biology and Biotechnology, "L. Spallanzani", University of Pavia (SB) and by the FWO Biofilm community (W000921N). EF receives a scholarship from Higher Education Personnel Improvement Coordination (CAPES-Brazil) and LS has research productivity grant from the National Council for Scientific and Technological Development (CNPq–Brazil). VT would like to thank the Indian Council of Medical Research, India (ICMR/AMR/*Adhoc*/291/2022-ECD-II) for funding.

Acknowledgments

SP was thankful to the RUSA 2.0 for supporting Centre of Excellence in Environment, Climate Change and Public Health (ECCPH), Utkal University, India.

Conflict of interest

The authors declare that the research was conducted in the absence of any commercial or financial relationships that could be construed as a potential conflict of interest.

Publisher's note

All claims expressed in this article are solely those of the authors and do not necessarily represent those of their affiliated organizations, or those of the publisher, the editors and the reviewers. Any product that may be evaluated in this article, or claim that may be made by its manufacturer, is not guaranteed or endorsed by the publisher.

References

Adamczak, A., Ożarowski, M., and Karpiński, T. M. (2020). Curcumin, a natural antimicrobial agent with strain-specific activity. *Pharmaceuticals* 13:153. doi: 10.3390/ph13070153

Adukwu, E., Allen, S. C., and Phillips, C. A. (2012). The anti-biofilm activity of lemongrass (*Cymbopogon flexuosus*) and grapefruit (*Citrus paradisi*) essential oils against five strains of *Staphylococcus aureus*. *J. Appl. Microbiol.* 113, 1217–1227. doi: 10.1111/j.1365-2672.2012.05418.x

Ahmed, S. A., Rudden, M., Smyth, T. J., Dooley, J. S., Marchant, R., and Banat, I. M. (2019). Natural quorum sensing inhibitors effectively downregulate gene expression of *Pseudomonas aeruginosa* virulence factors. *Appl. Microbiol. Biotechnol.* 103, 3521–3535. doi: 10.1007/s00253-019-09618-0

Akinsulire, O. R., Aibin, I., Adenipekun, T., Adelowotan, T., and Odugbemi, T. (2007). In vitro antimicrobial activity of crude extracts from plants *Bryophyllum pinnatum* and *Kalanchoe crenata*. *Afr. J. Tradit. Complement. Altern. Med.* 4, 338–344. doi: 10.4314/ajtcam.v4i3.31227

Aleksic, V., Mimica-Dukic, N., Simin, N., Nedeljkovic, N. S., and Knezevic, P. (2014). Synergistic effect of *Myrtus communis* L. essential oils and conventional antibiotics against multi-drug resistant *Acinetobacter baumannii* wound isolates. *Phytomedicine* 21, 1666–1674. doi: 10.1016/j.phymed.2014.08.013

Alizadeh Behbahani, B., Falah, F., Lavi Arab, F., Vasiee, M., and Tabatabaee Yazdi, F. (2020). Chemical composition and antioxidant, antimicrobial, and antiproliferative activities of *Cinnamomum zeylanicum* bark essential oil. *Evid. Based Complement. Alternat. Med.* 2020:5190603. doi: 10.1155/2020/5190603

Al-Shabib, N. A., Husain, F. M., Ahmad, I., and Baig, M. H. (2017). Eugenol inhibits quorum sensing and biofilm of toxigenic MRSA strains isolated from food handlers employed in Saudi Arabia. *Biotechnol. Biotechnol. Equip.* 31, 387–396. doi: 10.1080/13102818.2017.1281761

Álvarez-Martínez, F., Barrajón-Catalán, E., Herranz-López, M., and Micol, V. (2021). Antibacterial plant compounds, extracts and essential oils: An updated review on their effects and putative mechanisms of action. *Phytomedicine* 90:153626. doi: 10.1016/j.phymed.2021.153626

Alves, S., Duarte, A., Sousa, S., and Domingues, F. C. (2016). Study of the major essential oil compounds of *Coriandrum sativum* against *Acinetobacter baumannii* and the effect of linalool on adhesion, biofilms and quorum sensing. *Biofouling* 32, 155–165. doi: 10.1080/08927014.2015.1133810

Amini, M., Habibi, G., Rakei, S., Heidari, S., Taheri, H., Esfahani, R. B., et al. (2019). Growth Control of *Acinetobacter baumannii* in Infected wound by oregano essential oil in rats. *J. Res. Med. Dent. Sci.* 7, 136–139.

Angane, M., Swift, S., Huang, K., Butts, C. A., and Quek, S. Y. (2022). Essential oils and their major components: An updated review on antimicrobial activities, mechanism of action and their potential application in the food industry. *Foods* 11:464. doi: 10.3390/foods11030464

Artini, M., Patsilinakos, A., Papa, R., Božović, M., Sabatino, M., Garzoli, S., et al. (2018). Antimicrobial and antibiofilm activity and machine learning classification analysis of essential oils from different mediterranean plants against *Pseudomonas aeruginosa*. *Molecules* 23:482. doi: 10.3390/molecules23020482

Becker, H., Scher, J. M., Speakman, J.-B., and Zapp, J. (2005). Bioactivity guided isolation of antimicrobial compounds from *Lythrum salicaria*. *Fitoterapia* 76, 580–584. doi: 10.1016/j.fitote.2005.04.011

Betts, J. W., and Wareham, D. W. (2014). In vitro activity of curcumin in combination with epigallocatechin gallate (EGCG) versus multidrug-resistant *Acinetobacter baumannii*. *BMC Microbiol.* 14, 1–5. doi: 10.1186/1471-2180-14-172

Betts, J., Kelly, S., and Haswell, S. (2011). Antibacterial effects of theaflavin and synergy with epicatechin against clinical isolates of *Acinetobacter baumannii* and *Stenotrophomonas* maltophilia. *Int. J. Antimicrob. Agents* 38, 421–425. doi: 10.1016/j.ijantimicag.2011.07.006

Budri, P. E., Silva, N. C., Bonsaglia, E. C., Júnior, A. F., Júnior, J. A., Doyama, J. T., et al. (2015). Effect of essential oils of *Syzygium aromaticum* and *Cinnamomum zeylanicum* and their major components on biofilm production in *Staphylococcus aureus* strains isolated from milk of cows with mastitis. *J. Dairy Sci.* 98, 5899–5904. doi: 10.3168/jds.2015-9442

Budzyńska, A., Wickowska-Szakiel, M., Sadowska, B., Kalemba, D., and Różalska, B. (2011). Antibiofilm activity of selected plant essential oils and their major components. *Pol. J. Microbiol.* 60:35. doi: 10.33073/pjm-2011-005

Camens, S., Liu, S., Hon, K., Bouras, G. S., Psaltis, A. J., Wormald, P. J., et al. (2021). Preclinical development of a bacteriophage cocktail for treating multidrug resistant *Pseudomonas aeruginosa* Infections. *Microorganisms* 9:2001. doi: 10.3390/microorganisms9092001

Campana, R., and Baffone, W. (2018). Carvacrol efficacy in reducing microbial biofilms on stainless steel and in limiting re-growth of injured cells. *Food Control* 90, 10–17.

Carson, C. F., Mee, B. J., and Riley, T. V. (2002). Mechanism of action of *Melaleuca alternifolia* (tea tree) oil on Staphylococcus aureus determined by time-kill, lysis, leakage, and salt tolerance assays and electron microscopy. *Antimicrob. Agents Chemother.* 46, 1914–1920. doi: 10.1128/AAC.46.6.1914-1920.2002

Ceylan, O., and Ugur, A. (2015). Chemical composition and anti-biofilm activity of Thymus sipyleus BOISS. subsp. sipyleus BOISS. var. davisianus RONNIGER essential oil. *Arch. Pharm. Res.* 38, 957–965. doi: 10.1007/s12272-014-0516-0

Chan, B. C.-l., Lau, C., Jolivalt, C., Lui, S.-l., Ganem-Elbaz, C., Paris, J.-M., et al. (2011). Chinese medicinal herbs against antibiotic-resistant bacterial pathogens. *Sci. Against Microb. Pathog. Communica. Curr. Res. Technol. Adv.* 2, 773–781.

Chan, P.-C., Huang, L.-M., Lin, H.-C., Chang, L.-Y., Chen, M.-L., Lu, C.-Y., et al. (2007). Control of an outbreak of pandrug-resistant *Acinetobacter baumannii* colonization and infection in a neonatal intensive care unit. *Infect. Control Hosp. Epidemiol.* 28, 423–429. doi: 10.1086/513120

Chang, C.-Y., Krishnan, T., Wang, H., Chen, Y., Yin, W.-F., Chong, Y.-M., et al. (2014). Non-antibiotic quorum sensing inhibitors acting against N-acyl homoserine lactone synthase as druggable target. *Sci. Rep.* 4:7245. doi: 10.1038/srep07245

Chen, C. H., Bepler, T., Pepper, K., Fu, D., and Lu, T. K. (2022). Synthetic molecular evolution of antimicrobial peptides. *Curr. Opin. Biotechnol.* 75:102718. doi: 10.1016/j.copbio.2022.102718

Chraibi, M., Fadil, M., Farah, A., Lebrazi, S., and Fikri-Benbrahim, K. (2021). Antimicrobial combined action of *Mentha pulegium*, *Ormenis mixta* and *Mentha piperita* essential oils against *S. aureus*, *E. coli* and *C. tropicalis*: Application of mixture design methodology. *LWT* 145:111352. doi: 10.1016/j.lwt.2021.111352

Cirino, I. C. S., Menezes-Silva, S. M. P., Silva, H. T. D., De Souza, E. L., and Siqueira-Júnior, J. P. (2014). The essential oil from *Origanum vulgare L.* and its individual constituents carvacrol and thymol enhance the effect of tetracycline against *Staphylococcus aureus*. *Chemotherapy* 60, 290–293. doi: 10.1159/000381175

Coelho, F. A. B. L., and Pereira, M. O. (2013). "Exploring new treatment strategies for *Pseudomonas aeruginosa* biofilm infections based on plant essential oils," in *Microbial pathogens and strategies for combating them: Science, technology and education*, Vol. 1, ed. A. Méndez-Vilas (Badajoz: Formatex Research Center), 83–89.

Condò, C., Anacarso, I., Sabia, C., Iseppi, R., Anfelli, I., Forti, L., et al. (2020). Antimicrobial activity of spices essential oils and its effectiveness on mature biofilms of human pathogens. *Nat. Prod. Res.* 34, 567–574. doi: 10.1080/14786419.2018.1490904

Coutinho, H. D., Rodrigues, F. F., Nascimento, F. M., Costa, J. G., Falcão-Silva, V. S., and Siqueira-Júnior, J. P. (2011). Synergism of gentamicin and norfloxacin with the volatile compounds of *Lippia microphylla* Cham.(Verbenaceae). *J. Essent. Oil Res.* 23, 24–28. doi: 10.1080/10412905.2011.9700443

Coutinho, H., Matias, E., Santos, K., Tintino, S., Souza, C., Guedes, G., et al. (2010). Enhancement of the norfloxacin antibiotic activity by gaseous contact with the essential oil of *Croton zehntneri*. *J. Young Pharm.* 2, 362–364. doi: 10.4103/0975-1483.71625

Cox, S., Mann, C., and Markham, J. (2001). Interactions between components of the essential oil of *Melaleuca alternifolia*. *J. Appl. Microbiol.* 91, 492–497. doi: 10.1046/j.1365-2672.2001.01406.x

Cox, S., Mann, C., Markham, J., Bell, H. C., Gustafson, J., Warmington, J., et al. (2000). The mode of antimicrobial action of the essential oil of *Melaleuca alternifolia* (tea tree oil). *J. Appl. Microbiol.* 88, 170–175. doi: 10.1046/j.1365-2672.2000.00943.x

Cui, H., Li, W., Li, C., Vittayapadung, S., and Lin, L. (2016). Liposome containing cinnamon oil with antibacterial activity against methicillin-resistant *Staphylococcus aureus* biofilm. *Biofouling* 32, 215–225. doi: 10.1080/08927014.2015.1134516

Da Silva, L. C., Da Silva, M. V., and Correia, M. T. D. S. (2017). *New Frontiers in the search of antimicrobials agents from natural products*. Lausanne: Frontiers Media. doi: 10.3389/fmicb.2017.00210

De Souza, E. L., De Barros, J. C., De Oliveira, C. E. V., and Da Conceição, M. L. (2010). Influence of *Origanum vulgare* L. essential oil on enterotoxin production, membrane permeability and surface characteristics of *Staphylococcus aureus*. *Int. J. Food Microbiol.* 137, 308–311. doi: 10.1016/j.ijfoodmicro.2009.11.025

De, R., Kundu, P., Swarnakar, S., Ramamurthy, T., Chowdhury, A., Nair, G. B., et al. (2009). Antimicrobial activity of curcumin against *Helicobacter* pylori isolates from India and during infections in mice. *Antimicrob. Agents Chemother.* 53, 1592–1597. doi: 10.1128/AAC.01242-08

Derakhshan, S., Sattari, M., and Bigdeli, M. (2008). Effect of subinhibitory concentrations of cumin (*Cuminum cyminum* L.) seed essential oil and alcoholic extract on the morphology, capsule expression and urease activity of *Klebsiella pneumoniae*. *Int. J. Antimicrob. Agents* 32, 432–436. doi: 10.1016/j.ijantimicag.2008.05.009

Di Pasqua, R., Betts, G., Hoskins, N., Edwards, M., Ercolini, D., and Mauriello, G. (2007). Membrane toxicity of antimicrobial compounds from essential oils. *J. Agric. Food Chem.* 55, 4863–4870. doi: 10.1021/jf0636465

Djeussi, D. E., Noumedem, J. A., Seukep, J. A., Fankam, A. G., Voukeng, I. K., Tankeo, S. B., et al. (2013). Antibacterial activities of selected edible plants extracts against multidrug-resistant Gram-negative bacteria. *BMC Complement. Alterna. Med.* 13, 1–8. doi: 10.1186/1472-6882-13-164

Dos Santos Rodrigues, J. B., De Souza, N. T., Scarano, J. O. A., De Sousa, J. M., Lira, M. C., De Figueiredo, R. C. B. Q., et al. (2018). Efficacy of using oregano essential oil and carvacrol to remove young and mature *Staphylococcus aureus* biofilms on food-contact surfaces of stainless steel. *LWT* 93, 293–299. doi: 10.1016/j.lwt.2018.03.052

Duarte, A. F., Ferreira, S., Oliveira, R., and Domingues, F. C. (2013). Effect of coriander oil (*Coriandrum sativum*) on planktonic and biofilm cells of *Acinetobacter baumannii*. *Nat. Prod. Commun.* 8, 673–678. doi: 10.1177/1934578X1300800532

Duarte, A., Ferreira, S., Silva, F., and Domingues, F. (2012). Synergistic activity of coriander oil and conventional antibiotics against *Acinetobacter baumannii*. *Phytomedicine* 19, 236–238. doi: 10.1016/j.phymed.2011.11.010

Ekor, M. (2014). The growing use of herbal medicines: Issues relating to adverse reactions and challenges in monitoring safety. *Front. Pharmacol.* 4:177. doi: 10.3389/fphar.2013.00177

El-Shenawy, M. A., Baghdadi, H. H., and El-Hosseiny, L. S. (2015). Antibacterial activity of plants essential oils against some epidemiologically relevant food-borne pathogens. *Open Public Health J.* 8, 30–34. doi: 10.2174/1874944501508010030

El-Tarabily, K. A., El-Saadony, M. T., Alagawany, M., Arif, M., Batiha, G. E., Khafaga, A. F., et al. (2021). Using essential oils to overcome bacterial biofilm formation and their antimicrobial resistance. *Saudi J. Biol. Sci.* 28, 5145–5156.

Espina, L., Berdejo, D., Alfonso, P., García-Gonzalo, D., and Pagán, R. (2017). Potential use of carvacrol and citral to inactivate biofilm cells and eliminate biofouling. *Food Control* 82, 256–265. doi: 10.1016/j.foodcont.2017.07.007

Espina, L., Pagán, R., López, D., and García-Gonzalo, D. (2015). Individual constituents from essential oils inhibit biofilm mass production by multidrug resistant *Staphylococcus aureus*. *Molecules* 20, 11357–11372. doi: 10.3390/molecules200611357

Fabry, W., Okemo, P. O., and Ansorg, R. (1998). Antibacterial activity of East African medicinal plants. *J. Ethnopharmacol.* 60, 79–84.

Fadli, M., Bolla, J.-M., Mezrioui, N.-E., Pagès, J.-M., and Hassani, L. (2014). First evidence of antibacterial and synergistic effects of *Thymus riatarum* essential oil with conventional antibiotics. *Ind. Crops Prod.* 61, 370–376.

Fadli, M., Chevalier, J., Saad, A., Mezrioui, N.-E., Hassani, L., and Pages, J.-M. (2011). Essential oils from Moroccan plants as potential chemosensitisers restoring antibiotic activity in resistant Gram-negative bacteria. *Int. J. Antimicrob. Agents* 38, 325–330. doi: 10.1016/j.ijantimicag.2011.05.005

Fadli, M., Pagès, J.-M., Mezrioui, N.-E., Abbad, A., and Hassani, L. (2016). Artemisia herba-alba Asso and *Cymbopogon citratus* (DC.) Stapf essential oils and their capability to restore antibiotics efficacy. *Ind. Crops Prod.* 89, 399–404.

Fadli, M., Saad, A., Sayadi, S., Chevalier, J., Mezrioui, N.-E., Pagès, J.-M., et al. (2012). Antibacterial activity of *Thymus maroccanus* and *Thymus broussonetii* essential oils against nosocomial infection–bacteria and their synergistic potential with antibiotics. *Phytomedicine* 19, 464–471. doi: 10.1016/j.phymed.2011.12.003

Farahpour, M. R., Pirkhezr, E., Ashrafian, A., and Sonboli, A. (2020). Accelerated healing by topical administration of *Salvia officinalis* essential oil on *Pseudomonas aeruginosa* and *Staphylococcus aureus* infected wound model. *Biomed. Pharmacother.* 128:110120. doi: 10.1016/j.biopha.2020.110120

Ferro, T. A., Souza, E. B., Suarez, M. A., Rodrigues, J. F., Pereira, D. M., Mendes, S. J., et al. (2019). Topical application of cinnamaldehyde promotes faster healing of skin wounds infected with *pseudomonas aeruginosa*. *Molecules* 24:1627. doi: 10.3390/molecules24081627

Firmino, D. F., Cavalcante, T. T. A., Gomes, G. A., Firmino, N. C. S., Rosa, L. D., De Carvalho, M. G., et al. (2018). Antibacterial and antibiofilm activities of cinnamomum sp. essential oil and cinnamaldehyde: Antimicrobial activities. *Sci. World J.* 2018:7405736. doi: 10.1155/2018/7405736

Gao, F., Zhai, G., Wang, H., Lu, L., Xu, J., Zhu, J., et al. (2020). Protective effects of anti-alginate monoclonal antibody against *Pseudomonas aeruginosa* infection of HeLa cells. *Microb. Pathog.* 145:104240. doi: 10.1016/j.micpath.2020.104240

Ghodrati, M., Farahpour, M. R., and Hamishehkar, H. (2019). Encapsulation of peppermint essential oil in nanostructured lipid carriers: In-vitro antibacterial activity and accelerative effect on infected wound healing. *Colloids Surf. A Physicochem. Eng. Asp.* 564, 161–169.

Ghuman, S., Ncube, B., Finnie, J. F., Mcgaw, L. J., Coopoosamy, R. M., and Van Staden, J. (2016). Antimicrobial activity, phenolic content, and cytotoxicity of medicinal plant extracts used for treating dermatological diseases and wound healing in KwaZulu-Natal, South Africa. *Front. Pharmacol.* 7:320. doi: 10.3389/fphar.2016.00320

Gordon, N. C., and Wareham, D. W. (2010). Antimicrobial activity of the green tea polyphenol (−)-epigallocatechin-3-gallate (EGCG) against clinical isolates of *Stenotrophomonas* maltophilia. *Int. J. Antimicrob. Agents* 36, 129–131. doi: 10.1016/j.ijantimicag.2010.03.025

Guclu, E., Genc, H., Zengin, M., and Karabay, O. (2014). Antibacterial activity of *Lythrum salicaria* against multidrug-resistant *Acinetobacter baumannii* and *Pseudomonas aeruginosa*. *Annu. Res. Rev. Biol.* 4, 1099–1105.

Guerra, F. Q. S., Mendes, J. M., Sousa, J. P. D., Morais-Braga, M. F., Santos, B. H. C., Melo Coutinho, H. D., et al. (2012). Increasing antibiotic activity against a multidrug-resistant Acinetobacter spp by essential oils of *Citrus limon* and *Cinnamomum* zeylanicum. *Nat. Prod. Res.* 26, 2235–2238. doi: 10.1080/14786419.2011.647019

Hemaiswarya, S., and Doble, M. (2009). Synergistic interaction of eugenol with antibiotics against Gram negative bacteria. *Phytomedicine* 16, 997–1005.

Hendry, E., Worthington, T., Conway, B. R., and Lambert, P. (2009). Antimicrobial efficacy of eucalyptus oil and 1, 8-cineole alone and in combination with chlorhexidine digluconate against microorganisms grown in planktonic and biofilm cultures. *J. Antimicrob. Chemother.* 64, 1219–1225. doi: 10.1093/jac/dkp362

Heselpoth, R. D., Euler, C. W., and Fischetti, V. A. (2022). PaP1, a broad-spectrum lysin-derived cationic peptide to treat polymicrobial skin infections. *Front. Microbiol.* 13:817228. doi: 10.3389/fmicb.2022.817228

Husain, F. M., Ahmad, I., Asif, M., and Tahseen, Q. (2013). Influence of clove oil on certain quorum-sensing-regulated functions and biofilm of *Pseudomonas aeruginosa* and *Aeromonas hydrophila*. *J. Biosci.* 38, 835–844. doi: 10.1007/s12038-013-9385-9

Husain, F. M., Ahmad, I., Khan, M. S., Ahmad, E., Tahseen, Q., Khan, M. S., et al. (2015). Sub-MICs of Mentha piperita essential oil and menthol inhibits AHL mediated quorum sensing and biofilm of Gram-negative bacteria. *Front. Microbiol.* 6:420. doi: 10.3389/fmicb.2015.00420

Hyldgaard, M., Mygind, T., and Meyer, R. L. (2012). Essential oils in food preservation: Mode of action, synergies, and interactions with food matrix components. *Front. Microbiol.* 3:12. doi: 10.3389/fmicb.2012.00012

Ibáñez-Cervantes, G., Cruz-Cruz, C., Durán-Manuel, E. M., Loyola-Cruz, M. Á., Cureño-Díaz, M. A., Castro-Escarpulli, G., et al. (2022). Disinfection efficacy of ozone on ESKAPE bacteria biofilms: Potential use in difficult-to-access medical devices. *Am. J. Infect. Control.* doi: 10.1016/j.ajic.2022.03.037 [Epub ahead of print].

Inoue, Y., Shiraishi, A., Hada, T., Hirose, K., Hamashima, H., and Shimada, J. (2004). The antibacterial effects of terpene alcohols on *Staphylococcus aureus* and their mode of action. *FEMS Microbiol. Lett.* 237, 325–331. doi: 10.1016/j.femsle.2004.06.049

Ismail, M. M., Samir, R., Saber, F. R., Ahmed, S. R., and Farag, M. A. (2020). Pimenta oil as a potential treatment for *Acinetobacter baumannii* wound infection: In vitro and in vivo bioassays in relation to its chemical composition. *Antibiotics* 9:679. doi: 10.3390/antibiotics9100679

Jacobo-Salcedo, M. D. R., Gonzalez-Espindola, L. A., Alonso-Castro, A. J., Gonzalez-Martinez, M. D. R., Domínguez, F., and Garcia-Carranca, A. (2011). Antimicrobial activity and cytotoxic effects of *Magnolia dealbata* and its active compounds. *Nat. Prod. Commun.* 6, 1121–1124.

Jafri, H., Husain, F. M., and Ahmad, I. (2014). Antibacterial and antibiofilm activity of some essential oils and compounds against clinical strains of *Staphylococcus aureus*. *J. Biomed. Ther. Sci.* 1, 65–71.

Johny, A. K., Darre, M., Donoghue, A., Donoghue, D., and Venkitanarayanan, K. (2010). Antibacterial effect of trans-cinnamaldehyde, eugenol, carvacrol, and thymol on *Salmonella* Enteritidis and *Campylobacter jejuni* in chicken cecal contents in vitro. *J. Appl. Poult. Res.* 19, 237–244.

Jouneghani, R. S., Castro, A. H. F., Panda, S. K., Swennen, R., and Luyten, W. (2020). Antimicrobial activity of selected banana cultivars against important human pathogens, including candida biofilm. *Foods* 9:435. doi: 10.3390/foods9040435

Kačániová, M., Galovičová, L., Borotová, P., Valková, V., Ďuranová, H., Kowalczewski, P. Ł, et al. (2021). Chemical composition, in vitro and in situ antimicrobial and antibiofilm activities of *Syzygium aromaticum* (Clove) essential oil. *Plants* 10:2185.

Kang, J., Jin, W., Wang, J., Sun, Y., Wu, X., and Liu, L. (2019). Antibacterial and anti-biofilm activities of peppermint essential oil against *Staphylococcus aureus*. *Lwt* 101, 639–645.

Kavanaugh, N. L., and Ribbeck, K. (2012). Selected antimicrobial essential oils eradicate *Pseudomonas* spp. and *Staphylococcus aureus* biofilms. *Appl. Environ. Microbiol.* 78, 4057–4061. doi: 10.1128/AEM.07499-11

Kaźmierczak, N., Grygorcewicz, B., Roszak, M., Bochentyn, B., and Piechowicz, L. (2022). Comparative assessment of bacteriophage and antibiotic activity against multidrug-resistant *Staphylococcus aureus* biofilms. *Int. J. Mol. Sci.* 23:1274. doi: 10.3390/ijms23031274

Kerekes, E. B., Vidács, A., Takó, M., Petkovits, T., Vágvölgyi, C., Horváth, G., et al. (2019). Anti-biofilm effect of selected essential oils and main components on mono-and polymicrobic bacterial cultures. *Microorganisms* 7:345. doi: 10.3390/microorganisms7090345

Khadri, S., Boutefnouchet, N., and Dekhil, M. (2010). Antibacterial activity evaluation of *Allium sativum* essential oil compared to different *Pseudomonas Aeruginosa* strains in eastern Algeria. *Sci. Stud. Res. Chem. Chem. Eng. Biotechnol. Food Ind.* 11, 421–428.

Khan, M. F., Tang, H., Lyles, J. T., Pineau, R., Mashwani, Z.-U.-R., and Quave, C. L. (2018). Antibacterial properties of medicinal plants from Pakistan against multidrug-resistant ESKAPE pathogens. *Fronti. Pharmacol.* 9:815. doi: 10.3389/fphar.2018.00815

Khan, M. S. A., Zahin, M., Hasan, S., Husain, F. M., and Ahmad, I. (2009). Inhibition of quorum sensing regulated bacterial functions by plant essential oils with special reference to clove oil. *Lett. Appl. Microbiol.* 49, 354–360. doi: 10.1111/j.1472-765X.2009.02666.x

Khezri, K., Farahpour, M. R., and Mounesi Rad, S. (2019). Accelerated infected wound healing by topical application of encapsulated Rosemary essential oil into nanostructured lipid carriers. *Artif. Cells Nanomed. Biotechnol.* 47, 980–988. doi: 10.1080/21691401.2019.1582539

Kifer, D., Mužinić, V., and Klarić, M. Š (2016). Antimicrobial potency of single and combined mupirocin and monoterpenes, thymol, menthol and 1, 8-cineole against *Staphylococcus aureus* planktonic and biofilm growth. *J. Antibiot.* 69, 689–696. doi: 10.1038/ja.2016.10

Kim, H., Lee, S., Byun, Y., and Park, H. (2015). 6-Gingerol reduces *Pseudomonas aeruginosa* biofilm formation and virulence via quorum sensing inhibition. *Sci. Rep.* 5:8656. doi: 10.1038/srep08656

Kono, K., Tatara, I., Takeda, S., Arakawa, K., Shirotani, T., Okada, M., et al. (1997). Antibacterial activity of epigallocatechin gallate against *Helicobacter pylori*: Synergistic effect with Plaunotol. *J. Infect. Chemother.* 3, 170–172.

Kothari, V., Shah, A., Gupta, S., Punjabi, A., and Ranka, A. (2010). Revealing the antimicrobial potential of plants. *Int. J. Biosci. Technol.* 3, 1–20.

Kumar, A., Boradia, V. M., Thakare, R., Singh, A. K., Gani, Z., Das, S., et al. (2019). Repurposing ethyl bromopyruvate as a broad-spectrum antibacterial. *J. Antimicrob. Chemother.* 74, 912–920. doi: 10.1093/jac/dky555

Kumar, L., Chhibber, S., Kumar, R., Kumar, M., and Harjai, K. (2015). Zingerone silences quorum sensing and attenuates virulence of *Pseudomonas aeruginosa*. *Fitoterapia* 102, 84–95. doi: 10.1016/j.fitote.2015.02.002

Lambert, R., Skandamis, P. N., Coote, P. J., and Nychas, G. J. (2001). A study of the minimum inhibitory concentration and mode of action of oregano essential oil, thymol and carvacrol. *J. Appl. Microbiol.* 91, 453–462.

Lawrence, R., Tripathi, P., and Jeyakumar, E. (2009). Isolation, purification and evaluation of antibacterial agents from Aloe vera. *Braz. J. Microbiol.* 40, 906–915.

Leng, B.-F., Qiu, J.-Z., Dai, X.-H., Dong, J., Wang, J.-F., Luo, M.-J., et al. (2011). Allicin reduces the production of α-toxin by *Staphylococcus aureus*. *Molecules* 16, 7958–7968.

Li, J., Dong, J., Qiu, J.-Z., Wang, J.-F., Luo, M.-J., Li, H.-E., et al. (2011). Peppermint oil decreases the production of virulence-associated exoproteins by *Staphylococcus aureus*. *Molecules* 16, 1642–1654. doi: 10.3390/molecules16021642

Limaverde, P. W., Campina, F. F., Da Cunha, F. A., Crispim, F. D., Figueredo, F. G., Lima, L. F., et al. (2017). Inhibition of the TetK efflux-pump by the essential oil of *Chenopodium ambrosioides* L. and α-terpinene against *Staphylococcus aureus* IS-58. *Food Chem. Toxicol.* 109, 957–961. doi: 10.1016/j.fct.2017.02.031

Lorenzi, V., Muselli, A., Bernardini, A. F., Berti, L., Pagès, J.-M., Amaral, L., et al. (2009). Geraniol restores antibiotic activities against multidrug-resistant isolates from gram-negative species. *Antimicrob. Agents Chemother.* 53, 2209–2211. doi: 10.1128/AAC.00919-08

Lowrence, R., Ramakrishnan, A., Sundaramoorthy, N., Shyam, A., Mohan, V., Subbarao, H., et al. (2018). Norfloxacin salts of carboxylic acids curtail planktonic and biofilm mode of growth in ESKAPE pathogens. *J. Appl. Microbiol.* 124, 408–422. doi: 10.1111/jam.13651

Lu, M., Dai, T., Murray, C. K., and Wu, M. X. (2018). Bactericidal property of oregano oil against multidrug-resistant clinical isolates. *Front. Microbiol.* 9:2329. doi: 10.3389/fmicb.2018.02329

Macedo, D., Almeida, F., Wanderley, M., Ferraz, M., Santos, N., López, A., et al. (2021). Usnic acid: From an ancient lichen derivative to promising biological and nanotechnology applications. *Phytochem. Rev.* 20, 609–630.

Magi, G., Marini, E., and Facinelli, B. (2015). Antimicrobial activity of essential oils and carvacrol, and synergy of carvacrol and erythromycin, against clinical, erythromycin-resistant Group A Streptococci. *Front. Microbiol.* 6:165. doi: 10.3389/fmicb.2015.00165

Mahboubi, M., and Bidgoli, F. G. (2010). Antistaphylococcal activity of *Zataria multiflora* essential oil and its synergy with vancomycin. *Phytomedicine* 17, 548–550. doi: 10.1016/j.phymed.2009.11.004

Mahboubi, M., Feizabadi, M. M., Khamechian, T., Kazempour, N., Zadeh, M. R., Sasani, F., et al. (2016). The effect of *Oliveria decumbens* and *Pelargonium graveolens* on healing of infected skin wounds in mice. *World J. Plast. Surg.* 5:259.

Mahboubi, M., Kazempour, N., and Farzin, N. (2011). Antimicrobial activity of *Pelargonium graveolens* and *Oliveria decumbens* extracts against clinical isolates of *Staphylococcus aureus*. *J. Biol. Act. Prod. Nat.* 1, 105–111.

Mahizan, N. A., Yang, S.-K., Moo, C.-L., Song, A. A.-L., Chong, C.-M., Chong, C.-W., et al. (2019). Terpene derivatives as a potential agent against antimicrobial resistance (AMR) pathogens. *Molecules* 24, 2631.

Manzuoerh, R., Farahpour, M. R., Oryan, A., and Sonboli, A. (2019). Effectiveness of topical administration of *Anethum graveolens* essential oil on MRSA-infected wounds. *Biomed. Pharmacother.* 109, 1650–1658. doi: 10.1016/j.biopha.2018.10.117

Masoud, E., and Gouda, H. (2012). Effect of some natural plant extracts against gram negative bacteria in Njran Area, Saudi Arabia. *Egypt. Acad. J. Biol. Sci.* 4, 85–92.

Miyasaki, Y., Rabenstein, J. D., Rhea, J., Crouch, M.-L., Mocek, U. M., Kittell, P. E., et al. (2013). Isolation and characterization of antimicrobial compounds in plant extracts against multidrug-resistant *Acinetobacter baumannii*. *PLoS One* 8:e61594. doi: 10.1371/journal.pone.0061594

Modarresi, M., Farahpour, M.-R., and Baradaran, B. (2019). Topical application of *Mentha piperita* essential oil accelerates wound healing in infected mice model. *Inflammopharmacology* 27, 531–537. doi: 10.1007/s10787-018-0510-0

Mohamed, S. H., Salem, D., Azmy, M., and Fam, N. S. (2018). Antibacterial and antibiofilm activity of cinnamaldehyde against carbapenem-resistant *Acinetobacter baumannii* in Egypt: In vitro study. *J. Appl. Pharm. Sci.* 8, 151–156.

Moreno, S., Galván, E., Vázquez, N., Fiorilli, G., and Guido, P. C. (2015). "Antibacterial efficacy of Rosmarinus officinalis phytochemicals against nosocomial multidrug-resistant bacteria grown in planktonic culture and biofilm," in *The battle against microbial pathogens: Basic science, technological advances and educational programs. 1st edition*, (Badajoz: Formatex), 3–8.

Mors, W. B., Do Nascimento, M. C., Pereira, B. M. R., and Pereira, N. A. (2000). Plant natural products active against snake bite—the molecular approach. *Phytochemistry* 55, 627–642. doi: 10.1016/s0031-9422(00)00229-6

Mun, S.-H., Joung, D.-K., Kim, Y.-S., Kang, O.-H., Kim, S.-B., Seo, Y.-S., et al. (2013). Synergistic antibacterial effect of curcumin against methicillin-resistant *Staphylococcus aureus*. *Phytomedicine* 20, 714–718. doi: 10.1016/j.phymed.2013.02.006

Na, S.-H., Jeon, H., Oh, M.-H., Kim, Y.-J., Chu, M., Lee, I.-Y., et al. (2021). Therapeutic effects of inhibitor of ompA expression against carbapenem-resistant *Acinetobacter baumannii* strains. *Int. J. Mol. Sci.* 22:12257. doi: 10.3390/ijms222212257

Nand, P., Drabu, S., and Gupta, R. K. (2012). Insignificant anti-acne activity of *Azadirachta indica* leaves and bark. *J. Pharm. Negat. Results* 3, 29–33.

Negreiros, M. O., Pawlowski, Â, Zini, C. A., Soares, G. L., Motta, A. S., and Frazzon, A. P. (2016). Antimicrobial and antibiofilm activity of *Baccharis psiadioides* essential oil against antibiotic-resistant *Enterococcus faecalis* strains. *Pharm. Biol.* 54, 3272–3279. doi: 10.1080/13880209.2016.1223700

Ngane, R. A. N. (2019). Antibacterial activity of methanol extract and fractions from stem Bark of *Bridelia micrantha* (Hochst.) Baill.(Phyllanthaceae). *EC Pharmacol. Toxicol.* 7, 609–616.

Nielsen, J. E., Alford, M. A., Yung, D. B. Y., Molchanova, N., Fortkort, J. A., Lin, J. S., et al. (2022). Self-assembly of antimicrobial peptoids impacts their biological effects on ESKAPE bacterial pathogens. *ACS Infect. Dis.* 8, 533–545. doi: 10.1021/acsinfecdis.1c00536

Nostro, A., Roccaro, A. S., Bisignano, G., Marino, A., Cannatelli, M. A., Pizzimenti, F. C., et al. (2007). Effects of oregano, carvacrol and thymol on *Staphylococcus aureus* and *Staphylococcus epidermidis* biofilms. *J. Med. Microbiol.* 56, 519–523. doi: 10.1099/jmm.0.46804-0

Noumi, E., Merghni, A., Alreshidi, M. M., Haddad, O., Akmadar, G., De Martino, L., et al. (2018). *Chromobacterium violaceum* and *Pseudomonas aeruginosa* PAO1: Models for evaluating anti-quorum sensing activity of *Melaleuca alternifolia* essential oil and its main component terpinen-4-ol. *Molecules* 23:2672. doi: 10.3390/molecules23102672

Oliva, A., Costantini, S., De Angelis, M., Garzoli, S., Božović, M., Mascellino, M. T., et al. (2018). High potency of melaleuca alternifolia essential oil against multi-drug resistant gram-negative bacteria and methicillin-resistant *Staphylococcus aureus*. *Molecules* 23:2584. doi: 10.3390/molecules23102584

Oliveira, J. B., Teixeira, M. A., Paiva, L. F. D., Oliveira, R. F. D., Mendonça, A. R. D. A., and Brito, M. J. A. D. (2019). In vitro and in vivo antimicrobial activity of *Cymbopogon citratus* (DC.) Stapf. against *Staphylococcus* spp. isolated from newborn babies in an intensive care unit. *Microb. Drug Resist.* 25, 1490–1496. doi: 10.1089/mdr.2018.0047

Omarizadeh, K., Farahpour, M. R., and Alipour, M. (2021). Topical administration of an ointment prepared from *Satureja* sahendica essential oil accelerated infected full-thickness wound healing by modulating inflammatory response in a mouse model. *Wounds* 33, 321–328.

Oosterhaven, K., Poolman, B., and Smid, E. (1995). S-carvone as a natural potato sprout inhibiting, fungistatic and bacteristatic compound. *Ind. Crops Prod.* 4, 23–31.

Osterburg, A., Gardner, J., Hyon, S., Neely, A., and Babcock, G. (2009). Highly antibiotic-resistant *Acinetobacter baumannii* clinical isolates are killed by the green tea polyphenol (–)-epigallocatechin-3-gallate (EGCG). *Clin. Microbio. Infect.* 15, 341–346. doi: 10.1111/j.1469-0691.2009.02710.x

Packiavathy, I. A. S. V., Priya, S., Pandian, S. K., and Ravi, A. V. (2014). Inhibition of biofilm development of uropathogens by curcumin–an anti-quorum sensing agent from *Curcuma longa*. *Food Chem.* 148, 453–460. doi: 10.1016/j.foodchem.2012.08.002

Pal, S. K., and Shukla, Y. (2003). Herbal medicine: Current status and the future. *Asian Pac. J. Cancer Prev.* 4, 281–288.

Palaniappan, K., and Holley, R. A. (2010). Use of natural antimicrobials to increase antibiotic susceptibility of drug resistant bacteria. *Int. J. Food Microbiol.* 140, 164–168.

Panda, S. K., Buroni, S., Tiwari, V., and Da Silva, L. C. N. (2021). Insights into new strategies to combat biofilms. *Front. Microbiol.* 12:742647. doi: 10.3389/fmicb.2021.742647

Panda, S. K., Das, R., Lavigne, R., and Luyten, W. (2020). Indian medicinal plant extracts to control multidrug-resistant *S. aureus*, including in biofilms. *S. Afr. J. Bot.* 128, 283–291.

Patil, A., Banerji, R., Kanojiya, P., and Saroj, S. D. (2021). Foodborne ESKAPE biofilms and antimicrobial resistance: Lessons learned from clinical isolates. *Pathog. Glob. Health* 115, 339–356. doi: 10.1080/20477724.2021.1916158

Payne, D. E., Martin, N. R., Parzych, K. R., Rickard, A. H., Underwood, A., and Boles, B. R. (2013). Tannic acid inhibits *Staphylococcus aureus* surface colonization in an IsaA-dependent manner. *Infect. Immun.* 81, 496–504. doi: 10.1128/IAI.00877-12

Pelletier, R. P. (2012). Effect of plant-derived molecules on *Acinetobacter baumannii* biofilm on abiotic surfaces. *Honors Scholar Theses* 257. [Epub ahead of print].

Perez, A. P., Perez, N., Lozano, C. M. S., Altube, M. J., De Farias, M. A., Portugal, R. V., et al. (2019). The anti MRSA biofilm activity of *Thymus vulgaris* essential oil in nanovesicles. *Phytomedicine* 57, 339–351. doi: 10.1016/j.phymed.2018.12.025

Piasecki, B., Biernasiuk, A., Skiba, A., Skalicka-Woźniak, K., and Ludwiczuk, A. (2021). Composition, Anti-MRSA activity and toxicity of essential oils from *Cymbopogon* species. *Molecules* 26:7542. doi: 10.3390/molecules26247542

Pontes, E. K. U., Melo, H. M., Nogueira, J. W. A., Firmino, N. C. S., De Carvalho, M. G., Catunda Júnior, F. E. A., et al. (2019). Antibiofilm activity of the essential oil of citronella (*Cymbopogon nardus*) and its major component, geraniol, on the bacterial biofilms of *Staphylococcus aureus*. *Food Sci. Biotechnol.* 28, 633–639. doi: 10.1007/s10068-018-0502-2

Porfírio, E. M., Melo, H. M., Pereira, A. M. G., Cavalcante, T. T. A., Gomes, G. A., Carvalho, M. G. D., et al. (2017). In vitro antibacterial and antibiofilm activity of *Lippia alba* essential oil, citral, and carvone against *Staphylococcus aureus*. *Sci. World J.* 2017:4962707. doi: 10.1155/2017/4962707

Prabuseenivasan, S., Jayakumar, M., and Ignacimuthu, S. (2006). In vitro antibacterial activity of some plant essential oils. *BMC Complement. Altern. Med.* 6:39. doi: 10.1186/1472-6882-6-39

Premachandran, M. S., and Murthy, P. S. (2022). Ethnobotanical, phytochemical, pharmacological properties and applications of *Pimenta dioica* L. *J. Essent. Oil Res.* 34, 216–232. doi: 10.1080/10412905.2022.2032423

Preuss, H. G., Echard, B., Dadgar, A., Talpur, N., Manohar, V., Enig, M., et al. (2005). Effects of essential oils and monolaurin on *Staphylococcus aureus*: In vitro and in vivo studies. *Toxicol. Mech. Methods* 15, 279–285. doi: 10.1080/15376520590968833

Qiu, J., Feng, H., Lu, J., Xiang, H., Wang, D., Dong, J., et al. (2010). Eugenol reduces the expression of virulence-related exoproteins in *Staphylococcus aureus*. *Appl. Environ. Microbiol.* 76, 5846–5851. doi: 10.1128/AEM.00704-10

Qiu, J., Zhang, X., Luo, M., Li, H., Dong, J., Wang, J., et al. (2011). Subinhibitory concentrations of perilla oil affect the expression of secreted virulence factor genes in *Staphylococcus aureus*. *PLoS One* 6:e16160. doi: 10.1371/journal.pone.0016160

Rahim, K., Qasim, M., Rahman, H., Khan, T., Ahmad, I., Khan, N., et al. (2016). Antimicrobial resistance among aerobic biofilm producing bacteria isolated from chronic wounds in the tertiary care hospitals of Peshawar, Pakistan. *J. Wound Care* 25, 480–486. doi: 10.12968/jowc.2016.25.8.480

Rai, M., Paralikar, P., Jogee, P., Agarkar, G., Ingle, A. P., Derita, M., et al. (2017). Synergistic antimicrobial potential of essential oils in combination with nanoparticles: Emerging trends and future perspectives. *Int. J. Pharm.* 519, 67–78. doi: 10.1016/j.ijpharm.2017.01.013

Rathinam, P., Vijay Kumar, H., and Viswanathan, P. (2017). Eugenol exhibits anti-virulence properties by competitively binding to quorum sensing receptors. *Biofouling* 33, 624–639. doi: 10.1080/08927014.2017.1350655

Rebelo, J. M. D. C. C. (2014). *Pétalas da Flor de Açafrão (Crocus sativus L.): Valorização de um subproduto*. Ph.D. dissesrtation. Porto: Faculdade de Farmácia da Universidade do Porto.

Reichling, J., Harkenthal, M., Geiss, H., Hoppe-Tichy, T., and Saller, R. (2002). Electron microscopic and biochemical investigations on the antibacterial effects of Australian tea tree oil against *Staphylococcus aureus*. *Curr. Top. Phytochem.* 5, 77–84.

Richwagen, N., Lyles, J. T., Dale, B. L., and Quave, C. L. (2019). Antibacterial activity of *Kalanchoe mortagei* and *K. fedtschenkoi* against ESKAPE pathogens. *Front. Pharmacol.* 10:67. doi: 10.3389/fphar.2019.00067

Rodríguez, A. A., Otero-González, A., Ghattas, M., and Ständker, L. (2021). Discovery, optimization, and clinical application of natural antimicrobial peptides. *Biomedicines* 9:1381. doi: 10.3390/biomedicines9101381

Rosato, A., Piarulli, M., Corbo, F., Muraglia, M., Carone, A., Vitali, M., et al. (2010). In vitro synergistic action of certain combinations of gentamicin and essential oils. *Curr. Med. Chem.* 17, 3289–3295. doi: 10.2174/092986710792231996

Rosato, A., Vitali, C., De Laurentis, N., Armenise, D., and Milillo, M. A. (2007). Antibacterial effect of some essential oils administered alone or in combination with Norfloxacin. *Phytomedicine* 14, 727–732. doi: 10.1016/j.phymed.2007.01.005

Rudrappa, T., and Bais, H. P. (2008). Curcumin, a known phenolic from *Curcuma longa*, attenuates the virulence of *Pseudomonas aeruginosa* PAO1 in whole plant and animal pathogenicity models. *J. Agric. Food Chem.* 56, 1955–1962. doi: 10.1021/jf072591j

Sahal, G., Avcioglu, N. H., and Bilkay, I. S. (2016). Higher biofilm formation by multi-drug resistant *K. pneumoniae* and *K. rhinoscleromatis* strains and effects of lemon and ginger essential oils on biofilm formation. *Indian J. Pharm. Educ. Res.* 50, S82–S88.

Sahoo, A., Swain, S. S., Behera, A., Sahoo, G., Mahapatra, P. K., and Panda, S. K. (2021). Antimicrobial Peptides derived from insects offer a novel therapeutic option to combat biofilm: A review. *Front. Microbiol.* 12:661195. doi: 10.3389/fmicb.2021.661195

Salehzadeh, A., Hashemi Doulabi, M. S., Sohrabnia, B., and Jalali, A. (2018). The effect of thyme (*Thymus vulgaris*) extract on the expression of norA efflux pump gene in clinical strains of *Staphylococcus aureus*. *J. Genet. Resour.* 4, 26–36.

Sarkar, T., Chetia, M., and Chatterjee, S. (2021). Antimicrobial peptides and proteins: From nature's reservoir to the laboratory and beyond. *Front. Chem.* 9:432. doi: 10.3389/fchem.2021.691532

Saviuc, C., Gheorghe, I., Coban, S., Drumea, V., Chifiriuc, M.-C., Banu, O., et al. (2016). Rosmarinus officinalis essential oil and eucalyptol act as efflux pumps inhibitors and increase ciprofloxacin efficiency against *Pseudomonas aeruginosa* and *Acinetobacter baumannii* MDR strains. *Rom. Biotechnol. Lett.* 21:11783.

Scholtz, V., Vaňková, E., Kašparová, P., Premanath, R., Karunasagar, I., and Julák, J. (2021). Non-thermal plasma treatment of ESKAPE pathogens: A review. *Front. Microbiol.* 12:737635. doi: 10.3389/fmicb.2021.737635

Sepahi, E., Tarighi, S., Ahmadi, F. S., and Bagheri, A. (2015). Inhibition of quorum sensing in *Pseudomonas aeruginosa* by two herbal essential oils from Apiaceae family. *J. Microbiol.* 53, 176–180. doi: 10.1007/s12275-015-4203-8

Seyed Ahmadi, S. G., Farahpour, M. R., and Hamishehkar, H. (2019). Topical application of Cinnamon verum essential oil accelerates infected wound healing process by increasing tissue antioxidant capacity and keratin biosynthesis. *Kaohsiung J. Med. Sci.* 35, 686–694. doi: 10.1002/kjm2.12120

Sharifi, A., Mohammadzadeh, A., Zahraei Salehi, T., and Mahmoodi, P. (2018). Antibacterial, antibiofilm and antiquorum sensing effects of *Thymus daenensis* and Satureja hortensis essential oils against *Staphylococcus aureus* isolates. *J. Appl. Microbiol.* 124, 379–388. doi: 10.1111/jam.13639

Siebs, E., Shanina, E., Kuhaudomlarp, S., Da Silva Figueiredo Celestino Gomes, P., Fortin, C., Seeberger, P. H., et al. (2022). Targeting the central pocket of the *Pseudomonas aeruginosa* lectin LecA. *ChemBioChem.* 23:e202100563. doi: 10.1002/cbic.202100563

Sienkiewicz, M., Głowacka, A., Kowalczyk, E., Wiktorowska-Owczarek, A., Jóźwiak-Bębenista, M., and Łysakowska, M. (2014). The biological activities of cinnamon, geranium and lavender essential oils. *Molecules* 19, 20929–20940. doi: 10.3390/molecules191220929

Singh, G., Maurya, S., De Lampasona, M., and Catalan, C. (2005). Chemical constituents, antimicrobial investigations, and antioxidative potentials of *Anethum graveolens* L. essential oil and acetone extract: Part 52. *J. Food Sci.* 70, M208–M215. doi: 10.1111/j.1365-2621.2005.tb07190.x

Sonboli, A., Eftekhar, F., Yousefzadi, M., and Kanani, M. R. (2005). Antibacterial activity and chemical composition of the essential oil of *Grammosciadium platycarpum* Boiss. from Iran. *Zeitschrift für Naturforschung C* 60, 30–34. doi: 10.1515/znc-2005-1-206

Sonboli, A., Mirjalili, M. H., Hadian, J., Ebrahimi, S. N., and Yousefzadi, M. (2006). Antibacterial activity and composition of the essential oil of *Ziziphora clinopodioides* subsp. bungeana (Juz.) Rech. f. from Iran. *Zeitschrift für Naturforschung C* 61, 677–680. doi: 10.1515/znc-2006-9-1011

Souza, E., Oliveira, C., Stamford, T., Conceição, M., and Gomes Neto, N. (2013). Influence of carvacrol and thymol on the physiological attributes, enterotoxin production and surface characteristics of *Staphylococcus aureus* strains isolated from foods. *Braz. J. Microbiol.* 44, 29–36. doi: 10.1590/S1517-83822013005000001

Starr, C. G., Ghimire, J., Guha, S., Hoffmann, J. P., Wang, Y., Sun, L., et al. (2020). Synthetic molecular evolution of host cell-compatible, antimicrobial peptides effective against drug-resistant, biofilm-forming bacteria. *Proc. Natl. Acad. Sci. U.S.A.* 117, 8437–8448. doi: 10.1073/pnas.1918427117

Stermitz, F. R., Lorenz, P., Tawara, J. N., Zenewicz, L. A., and Lewis, K. (2000). Synergy in a medicinal plant: antimicrobial action of berberine potentiated by 5'-methoxyhydnocarpin, a multidrug pump inhibitor. *Proc. Natl. Acad. Sci. U.S.A.* 97, 1433–1437. doi: 10.1073/pnas.030540597

Subramani, R., Narayanasamy, M., and Feussner, K.-D. (2017). Plant-derived antimicrobials to fight against multi-drug-resistant human pathogens. *3 Biotech* 7, 1–15. doi: 10.1007/s13205-017-0848-9

Tapia-Rodriguez, M. R., Hernandez-Mendoza, A., Gonzalez-Aguilar, G. A., Martinez-Tellez, M. A., Martins, C. M., and Ayala-Zavala, J. F. (2017). Carvacrol as potential quorum sensing inhibitor of *Pseudomonas aeruginosa* and biofilm production on stainless steel surfaces. *Food Control* 75, 255–261. doi: 10.1016/j.foodcont.2016.12.014

Tazehjani, D. A. J., Farahpour, M. R., and Hamishehkar, H. (2021). Effectiveness of topical caraway essential oil loaded into nanostructured lipid carrier as a promising platform for the treatment of infected wounds. *Colloids Surf. A Physicochem. Eng. Asp.* 610:125748. doi: 10.1016/j.colsurfa.2020.125748

Tiwari, V. (2016). In vitro engineering of novel bioactivity in the natural enzymes. *Front. Chem.* 4:39. doi: 10.3389/fchem.2016.00039

Tiwari, V., Roy, R., and Tiwari, M. (2015). Antimicrobial active herbal compounds against *Acinetobacter baumannii* and other pathogens. *Front. Microbiol.* 6:618. doi: 10.3389/fmicb.2015.00618

Topa, S. H., Subramoni, S., Palombo, E. A., Kingshott, P., Rice, S. A., and Blackall, L. L. (2018). Cinnamaldehyde disrupts biofilm formation and swarming motility of *Pseudomonas aeruginosa*. *Microbiology* 164, 1087–1097. doi: 10.1099/mic.0.000692

Trombetta, D., Castelli, F., Sarpietro, M. G., Venuti, V., Cristani, M., Daniele, C., et al. (2005). Mechanisms of antibacterial action of three monoterpenes. *Antimicrob. Agents Chemother.* 49, 2474–2478. doi: 10.1128/AAC.49.6.2474-2478.2005

Vasconcelos, N., Croda, J., and Simionatto, S. (2018). Antibacterial mechanisms of cinnamon and its constituents: A review. *Microb. Pathog.* 120, 198–203. doi: 10.1016/j.micpath.2018.04.036

Vasconcelos, S. E. C. B., Melo, H. M., Cavalcante, T. T. A., Júnior, F. E. A. C., De Carvalho, M. G., Menezes, F. G. R., et al. (2017). *Plectranthus amboinicus* essential oil and carvacrol bioactive against planktonic and biofilm of oxacillin- and vancomycin-resistant *Staphylococcus aureus*. *BMC Complement. Altern. Med.* 17:462. doi: 10.1186/s12906-017-1968-9

Vasina, D. V., Antonova, N. P., Grigoriev, I. V., Yakimakha, V. S., Lendel, A. M., Nikiforova, M. A., et al. (2021). Discovering the potentials of four phage endolysins to combat Gram-negative infections. *Front. Microbiol.* 12:748718. doi: 10.3389/fmicb.2021.748718

Veeresham, C. (2012). Natural products derived from plants as a source of drugs. *J. Adv. Pharm. Technol. Res.* 3:200. doi: 10.4103/2231-4040.104709

Vogel, J., Jansen, I., Setroikromo, R., Cavallo, F. M., Van Dijl, J. M., and Quax, W. J. (2022). Fighting *Acinetobacter baumannii* infections with the acylase PvdQ. *Microbes Infect.* 24:104951. doi: 10.1016/j.micinf.2022.104951

Wang, F., Wei, F., Song, C., Jiang, B., Tian, S., Yi, J., et al. (2017). *Dodartia orientalis* L. essential oil exerts antibacterial activity by mechanisms of disrupting cell structure and resisting biofilm. *Ind. Crops Prod.* 109, 358–366.

Wen, M. M., Abdelwahab, I. A., Aly, R. G., and El-Zahaby, S. A. (2021). Nanophyto-gel against multi-drug resistant *Pseudomonas aeruginosa* burn wound infection. *Drug Deliv.* 28, 463–477. doi: 10.1080/10717544.2021.1889720

Xiao, S., Cui, P., Shi, W., and Zhang, Y. (2020). Identification of essential oils with activity against stationary phase *Staphylococcus aureus*. *BMC Complement. Med. Ther.* 20:99. doi: 10.1186/s12906-020-02898-4

Yadav, M. K., Chae, S.-W., Im, G. J., Chung, J.-W., and Song, J.-J. (2015). Eugenol: A phyto-compound effective against methicillin-resistant and methicillin-sensitive *Staphylococcus aureus* clinical strain biofilms. *PLoS One* 10:e0119564. doi: 10.1371/journal.pone.0119564

Yang, S.-K., Yusoff, K., Ajat, M., Thomas, W., Abushelaibi, A., Akseer, R., et al. (2019). Disruption of KPC-producing *Klebsiella pneumoniae* membrane via induction of oxidative stress by cinnamon bark (*Cinnamomum verum* J. Presl) essential oil. *PloS One* 14:e0214326. doi: 10.1371/journal.pone.0214326

Yang, S.-K., Yusoff, K., Ajat, M., Yap, W.-S., Lim, S.-H. E., and Lai, K.-S. (2021). Antimicrobial activity and mode of action of terpene linalyl anthranilate against carbapenemase-producing *Klebsiella pneumoniae*. *J. Pharm. Anal.* 11, 210–219. doi: 10.1016/j.jpha.2020.05.014

Yu, Z., Tang, J., Khare, T., and Kumar, V. (2020). The alarming antimicrobial resistance in ESKAPEE pathogens: Can essential oils come to the rescue? *Fitoterapia* 140:104433. doi: 10.1016/j.fitote.2019.104433

Zare, M. R., Khorram, M., Barzegar, S., Asadian, F., Zareshahrabadi, Z., Saharkhiz, M. J., et al. (2021). Antimicrobial core–shell electrospun nanofibers containing Ajwain essential oil for accelerating infected wound healing. *Int. J. Pharm.* 603:120698. doi: 10.1016/j.ijpharm.2021.120698

Zhang, D., Hu, H., Rao, Q., and Zhao, Z. (2011). Synergistic effects and physiological responses of selected bacterial isolates from animal feed to four natural antimicrobials and two antibiotics. *Foodborne Pathog. Dis.* 8, 1055–1062. doi: 10.1089/fpd.2010.0817

Zhang, H., Li, S., and Cheng, Y. (2022). Antibiofilm activity of allicin and quercetin in treating biofilm-associated orthopaedics infection. *Appl. Biochem. Biotechnol.* 1–7. doi: 10.1007/s12010-022-03845-4 [Epub ahead of print].

Zhao, W.-H., Hu, Z.-Q., Hara, Y., and Shimamura, T. (2002). Inhibition of penicillinase by epigallocatechin gallate resulting in restoration of antibacterial activity of penicillin against penicillinase-producing *Staphylococcus aureus*. *Antimicrob. Agents Chemother.* 46, 2266–2268. doi: 10.1128/AAC.46.7.2266-2268.2002

Zhao, X., Liu, Z., Liu, Z., Meng, R., Shi, C., Chen, X., et al. (2018). Phenotype and RNA-seq-Based transcriptome profiling of *Staphylococcus aureus* biofilms in response to tea tree oil. *Microb. Pathog.* 123, 304–313. doi: 10.1016/j.micpath.2018.07.027

frontiers | Frontiers in Microbiology

ORIGINAL RESEARCH
published: 28 April 2022
doi: 10.3389/fmicb.2022.881549

CodY Is a Global Transcriptional Regulator Required for Virulence in Group B *Streptococcus*

*Angelica Pellegrini[1], Germana Lentini[2], Agata Famà[2], Andrea Bonacorsi[1], Viola Camilla Scoffone[1], Silvia Buroni[1], Gabriele Trespidi[1], Umberto Postiglione[1], Davide Sassera[1], Federico Manai[1], Giampiero Pietrocola[3], Arnaud Firon[4], Carmelo Biondo[2], Giuseppe Teti[5], Concetta Beninati[2] and Giulia Barbieri[1]**

[1] Department of Biology and Biotechnology "Lazzaro Spallanzani," University of Pavia, Pavia, Italy, [2] Department of Human Pathology and Medicine, University of Messina, Messina, Italy, [3] Department of Molecular Medicine, University of Pavia, Pavia, Italy, [4] Institut Pasteur, Université de Paris, CNRS UMR 6047, Unité Biologie des Bactéries Pathogènes à Gram-positif, Paris, France, [5] Charybdis Vaccines Srl, Messina, Italy

OPEN ACCESS

Edited by:
Daniela De Biase, Sapienza University of Rome, Italy

Reviewed by:
Angela Tramonti, Institute of Molecular Biology and Pathology, Italian National Research Council, Italy
Vincenzo Scarlato, University of Bologna, Italy

***Correspondence:**
Giulia Barbieri
giulia.barbieri@unipv.it

Specialty section:
This article was submitted to Microbial Physiology and Metabolism, a section of the journal Frontiers in Microbiology

Received: *22 February 2022*
Accepted: *21 March 2022*
Published: *28 April 2022*

Citation:
Pellegrini A, Lentini G, Famà A, Bonacorsi A, Scoffone VC, Buroni S, Trespidi G, Postiglione U, Sassera D, Manai F, Pietrocola G, Firon A, Biondo C, Teti G, Beninati C and Barbieri G (2022) CodY Is a Global Transcriptional Regulator Required for Virulence in Group B Streptococcus. Front. Microbiol. 13:881549. doi: 10.3389/fmicb.2022.881549

Group B *Streptococcus* (GBS) is a Gram-positive bacterium able to switch from a harmless commensal of healthy adults to a pathogen responsible for invasive infections in neonates. The signals and regulatory mechanisms governing this transition are still largely unknown. CodY is a highly conserved global transcriptional regulator that links nutrient availability to the regulation of major metabolic and virulence pathways in low-G+C Gram-positive bacteria. In this work, we investigated the role of CodY in BM110, a GBS strain representative of a hypervirulent lineage associated with the majority of neonatal meningitis. Deletion of *codY* resulted in a reduced ability of the mutant strain to cause infections in neonatal and adult animal models. The observed decreased *in vivo* lethality was associated with an impaired ability of the mutant to persist in the blood, spread to distant organs, and cross the blood-brain barrier. Notably, the *codY* null mutant showed reduced adhesion to monolayers of human epithelial cells *in vitro* and an increased ability to form biofilms, a phenotype associated with strains able to asymptomatically colonize the host. RNA-seq analysis showed that CodY controls about 13% of the genome of GBS, acting mainly as a repressor of genes involved in amino acid transport and metabolism and encoding surface anchored proteins, including the virulence factor Srr2. CodY activity was shown to be dependent on the availability of branched-chain amino acids, which are the universal cofactors of this regulator. These results highlight a key role for CodY in the control of GBS virulence.

Keywords: group B *Streptococcus*, *Streptococcus agalactiae*, CodY, Srr2, bacterial meningitis, RNA-Seq, global regulation of gene expression, pathogenesis

INTRODUCTION

Group B *Streptococcus* (GBS, *Streptococcus agalactiae*) is the leading cause of sepsis and meningitis in neonates (Thigpen et al., 2011; Okike et al., 2014). Maternal vaginal colonization during pregnancy represents the principal risk factor for GBS transmission to the newborn through *in utero* ascending infections or aspiration of contaminated amniotic or vaginal fluids during

delivery. Vertically acquired neonatal infections lead to early-onset (0–7 days of life) invasive disease manifesting as pneumonia that rapidly progresses to sepsis (Edmond et al., 2012; Patras and Nizet, 2018). GBS can also cause late-onset disease that manifests between 7 and 90 days of life with bacteremia and a high complication rate of meningitis (Tazi et al., 2019).

Group B *Streptococcus* is capable of causing these diverse clinical manifestations thanks to its capacity to invade different host niches and adapt to various environmental conditions. This versatility is made possible by the activity of several transcriptional regulators which, in response to environmental signals, control the expression of proteins involved in nutrient acquisition, adhesion, virulence, and immune evasion (Rajagopal, 2009; Thomas and Cook, 2020).

CodY is a global transcriptional regulator highly conserved in nearly all low-G+C Gram-positive bacteria, including the genera *Bacillus*, *Lactococcus*, *Streptococcus*, *Listeria*, *Staphylococcus*, *Clostridium*, and *Clostridioides* (Guédon et al., 2005; Lemos et al., 2008; Dineen et al., 2010; Kreth et al., 2011; Lobel et al., 2012; Belitsky and Sonenshein, 2013; Brinsmade et al., 2014; Feng et al., 2016; Waters et al., 2016; Geng et al., 2018). In these organisms, CodY directly and indirectly controls the expression of hundreds of metabolic genes in response to nutrient availability (Sonenshein, 2005). In pathogens, CodY regulates also critical virulence determinants and, therefore, links nutrient availability and metabolism to pathogenesis in a species-specific manner. The nutritional status of the cell is monitored by CodY by its interaction with two ligands: branched-chain amino acids (BCAAs) (Guedon et al., 2001; Shivers and Sonenshein, 2004; Brinsmade et al., 2010) and GTP (Ratnayake-Lecamwasam et al., 2001; Handke et al., 2008). However, while BCAAs are universal cofactors of CodY, GTP was not found to be involved in CodY activation in *Lactococcus* (Petranovic et al., 2004) and *Streptococcus* species (Hendriksen et al., 2008). Once activated by binding to its cofactors, CodY binds DNA at sites characterized by a 15-nt canonical consensus binding motif "AATTTTCWGAAAATT" (den Hengst et al., 2005; Belitsky and Sonenshein, 2013; Biswas et al., 2020). As the intracellular pools of BCAAs change, the hundreds of genes whose expression is controlled by CodY are expressed in a hierarchical manner, reflecting the choice of turning on specific metabolic pathways ahead of others (Brinsmade et al., 2014; Waters et al., 2016). In many cases, the hierarchy of gene expression stems in part from the interplay between CodY and other transcriptional regulators. That is, many direct targets of CodY regulation are also controlled by other factors and the expression of several transcriptional regulators is CodY-regulated. Consequently, regulatory circuits interlinking different pathways are created (Belitsky et al., 2015; Barbieri et al., 2016).

In this work, we aimed at providing the first global analysis of the CodY regulon in GBS and at investigating the role of this regulator in controlling and coordinating metabolism and virulence in this bacterium. To this purpose, a capsular serotype III strain belonging to the hypervirulent clonal complex 17 (CC17, as defined by Multi Locus Sequence Typing analysis) was employed. This lineage is responsible for the vast majority of cases of neonatal GBS –elicited meningitis worldwide (Manning et al., 2009; Joubrel et al., 2015; Seale et al., 2016).

MATERIALS AND METHODS

Bacterial Strains, Plasmids, and Growth Conditions

Bacterial strains and plasmids used in this work are listed in **Table 1** and **Supplementary Table 1**, respectively. Employed primers are listed in **Supplementary Table 2**. GBS was cultured in Todd Hewitt (TH, Difco Laboratories) supplemented with 5 g/liter of yeast extract (THY) or in chemically defined medium (CDM, **Supplementary Table 3**) (Willett and Morse, 1966) at 37°C, 5% CO_2, steady state. *E. coli* strains were cultured in Luria Bertani (LB) broth at 37°C. Antibiotics were used at the appropriate concentrations. For *E. coli*: kanamycin 50 μg/ml; erythromycin 150 μg/ml. For GBS: kanamycin 1 mg/ml; erythromycin 10 μg/ml.

Strains Construction

The pG1-Δ*codY* vector used to create the Δ*codY* derivative of BM110 (Δ*codY*) was constructed by Gibson assembly (NEBuilder HiFi DNA Assembly Cloning Kit, New England Biolabs) with PCR amplified genomic regions located upstream and downstream of *codY*, using pG1_codYUpF + BM_codYFusR and BM_codYFusF + pG1_BM_codYDwR primers, and an inverse PCR fragment obtained with the pG1R and pG1F oligonucleotides on the temperature-sensitive pG1 plasmid

TABLE 1 | Bacterial strains used in this work.

S. agalactiae

Strain	Relevant genotype	Plasmid	Source or Reference
BM110	Serotype III, ST-17, human hypervirulent clinical isolate		Tazi et al., 2010
Δ*codY*	BM110 carrying an in-frame *codY* deletion		This work
BM1102	BM110	pTCVΩP_{tet}	This work
BM1103	BM110	pTCVΩP_{tet}_*codY*	This work
BM1104	Δ*codY*	pTCVΩP_{tet}	This work
BM1105	Δ*codY*	pTCVΩP_{tet}_*codY*	This work
BM1106	BM110	pTCVlacZ_*livKp220*	This work
BM1107	Δ*codY*	pTCVlacZ_*livKp220*	This work
BM1114	BM110	pTCVlacZ_*livKp1-220*	This work
BM1115	Δ*codY*	pTCVlacZ_*livKp1-220*	This work

E. coli

Strain	Genotype	Source or reference
XL-1 Blue	*recA1 endA1 gyrA96 thi-1 hsdR17 supE44 relA1 lac [F i proAB lacI^{q} ZΔM15 Tn10 (Tet^{r})]*	Agilent
BL21 DE3	*B F– ompT gal dcm lon hsdSB(rB–mB–) λ(DE3 [lacI lacUV5-T7p07 ind1 sam7 nin5]) [malB+]K-12(λS)*	

(Mistou et al., 2009). The three PCR fragments were fused by Gibson assembly and electroporated into *E. coli* XL1 blue. The obtained pG1-Δ*codY* plasmid was verified by sequencing and then electroporated in GBS. Transformants were selected at 30°C on TH plates supplemented with erythromycin. Plasmid integration and excision were performed as previously described (Biswas et al., 1993). The resulting in-frame deletion of *codY* on genomic DNA was verified by Sanger sequencing using external primers COH1_1525FUp and COH1_1527RDw.

To complement the *codY* deletion, the *codY* gene was amplified with oligonucleotides pTCV_codYF_Bam and pTCV_codYR_Pst, using BM110 chromosomal DNA as template. The obtained fragment was cloned between the *Bam*HI and *Pst*I sites of the pTCVΩP_{tet} vector (Buscetta et al., 2016). The resulting pTCVΩP_{tet}_*codY* plasmid was verified by sequencing and used to electroporate wild-type (WT) and Δ*codY* strains, thus obtaining BM1103 and BM1105, respectively (**Table 1**). Two control strains (BM1102 and BM1104) were prepared by electroporation of the empty pTCVΩP_{tet} plasmid into WT and Δ*codY* strains. Transformants were selected on TH agar plates supplemented with kanamycin.

Construction of *lacZ* Transcriptional Fusions and β-Galactosidase Assays

To prepare the pTCV-*lacZ*_*livK*p_{220} plasmid (**Supplementary Table 1**), a 269 bp fragment comprising the regulatory region and the first 27 nucleotides of the *livK* gene was amplified with primers livKp220F and livKp220R using the BM110 chromosomal DNA as template. The obtained amplicon was inserted by Gibson assembly between the *Eco*RI and *Bam*HI restriction sites of plasmid pTCV-*lacZ* (Poyart and Trieu-Cuot, 2006), upstream of the *lacZ* gene.

To create pTCVlacZ_*livKp1-220*, a 196 bp product containing the 5′ part of the *livK* regulatory region was amplified by using oligonucleotides livKp220F and mutagenic oligonucleotide livKp1R. A 125 bp fragment comprising the 3′ part of the regulatory region and the first 27 bp of the *livK* coding sequence was synthesized by using mutagenic oligonucleotide livKp1F and livKp220R as reverse primer. The two mutagenized, partially overlapping (52 bp overlap) PCR products and the *Eco*RI/*Bam*HI digested pTCV-*lacZ* plasmid were then fused by Gibson using the NEBuilder HiFi DNA Assembly Cloning Kit (New England Biolabs).

β-galactosidase specific activity was determined as previously described (Trespidi et al., 2020).

Time-Lapse Microscopy and Single-Cell Image Analysis

Agarose pads (Young et al., 2011) spotted with 5 μl of a 1:10 dilution of GBS cell cultures collected at mid-log phase of growth (OD600 0.5 in THY medium) were flipped and transferred to an imaging dish sealed with parafilm. Time-lapse imaging was performed using a Leica DMi8 widefield microscope, equipped with a 100× oil immersion objective (Leica HC PL Fluotar 100×/1.32 OIL PH3), a Leica DFC9000 sCMOS camera and driven by Leica LASX software. Experiments were performed using an environmental microscope incubator set at 37°C and bacteria were imaged in phase contrast, every 5-min and up to 6 h. Manual segmentation of individual cells and analysis of image stacks were performed using the ImageJ 1.52a software, as previously described (Manina et al., 2015). Data were analyzed using Prism 9.

RNA Preparation and Quantitative Real-Time-PCR

Group B *Streptococcus* total RNA was extracted from cells collected at mid-exponential phase of growth using the Quick-RNA Fungal/Bacterial Miniprep Kit (Zymo Research) as per the manufacturer's instructions. Traces of genomic DNA were removed from samples using the Turbo DNA-free DNase treatment and removal kit (Ambion). Reverse transcription and quantitative real-time PCR (qRT-PCR) experiments were performed in a single step using the iTaq Universal SYBR Green One-Step Kit (Bio-Rad). The reactions were performed in 20 μl volumes using 4 ng of DNAse I treated RNA and 400 nM primers targeting *livK*, *braB*, *brnQ*, and *gyrA* (used as reference gene).

RNA-Sequencing and Analysis

RNA-Seq was performed on four independent biological replicates for each strain. rRNA was depleted using the QIAseq FastSelect –5S/16S/23S Kit (QIAGEN). RNA was sequenced using Illumina sequencing technology (BMR-Genomics, Padua). For RNA-Seq data analysis, raw reads were quality checked using FASTQC[1] and processed by Trimmomatic (Bolger et al., 2014) to trim the adaptor sequences and remove low-quality reads. Clean reads were mapped onto the reference genome of *Streptococcus agalactiae* BM110 (Accession: NZ_LT714196.1) using Bowtie2 (Langmead, 2010). To quantify the known transcripts, the alignment results were input into featureCounts (Liao et al., 2014). Lastly, the R package DESeq2 (Love et al., 2014) was used to test for differential expression. We defined genes as differentially expressed using the following criteria: $|\text{Log2 Fold Change}| \geq 1$ and adjusted p-value FDR < 0.05. Prediction of orthologous groups was performed using COGnitor (Tatusov, 2000).

Mammalian Cell Culture and Epithelial Cell Adhesion Assays

A549 cells and HeLa cells were routinely grown in 75 cm^2 flasks in Dulbecco's modified Eagle's medium (DMEM) supplemented with 10% fetal bovine serum (FBS) at 37°C in 5% CO_2. Cells were seeded at 2×10^5 cell density per well in 24-well tissue culture plates and cultured in DMEM without antibiotics for 24 h. Bacteria grown to the mid-log phase were added to confluent monolayers at a multiplicity of infection of 10. After a 2-h incubation, monolayers were washed three times with PBS to remove the non-adherent bacteria, lysed, and serial dilutions of the cell lysates were plated to enumerate cell-associated bacteria. Percent of adhesion of each strain was calculated as follows (number of CFUs on plate)/(number of CFUs of initial

[1]https://qubeshub.org/resources/fastqc

inoculum) × 100. Percentage of adhesion was normalized to the WT strain, set at 100%.

Biofilm Formation Assay

For bacterial biofilm formation assays, a 1:20 dilution of an overnight culture grown in TH broth supplemented with 1% glucose and the appropriate antibiotic was used to inoculate (100 µl/well) a 96-well Tissue Culture Treated plate (16 technical replicates per strain). Non-adherent bacteria were removed by washing with PBS after 6 h of incubation at 37°C, 5% CO_2. Crystal violet staining was performed as previously described (Trespidi et al., 2021) after 19 h of incubation in TH + 1% glucose medium (37°C, 5% CO_2). Biofilm growth was evaluated by reading absorbance at 595 nm and normalizing the obtained value to the OD600 of the culture in the well.

For confocal microscopy analysis of biofilms, bacterial overnight cultures in TH broth supplemented with 1% glucose and the appropriate antibiotic were diluted in the same medium to an OD_{600} 0.05 (about 1 × 10^7 CFU/mL) before being added to a four-well Nunc Lab-Tek II Chambered Coverglass. Non-adherent cells were removed after 6 h. After overnight growth, biofilms were washed twice with PBS and stained with 5 µM Syto 9 (Invitrogen). Cells were imaged with a Leica TCS SP8 confocal microscope equipped with a Leica DMi8 inverted microscope, a tunable excitation laser source (White Light Laser, Leica Microsystems, Germany), and driven by Leica Application Suite X, ver. 3.5.6.21594, using a 63× oil immersion objective (Leica HC PL APO CS2 63X/1.40). Images were acquired using a 488 nm laser line as an excitation source, and the fluorescence emitted was collected in a 500–540 nm range for Syto 9 as previously described (Trespidi et al., 2020). Biofilm images were visualized and processed using ImageJ. Biofilm parameters were measured using the COMSTAT 2 software (Heydorn et al., 2000). All confocal

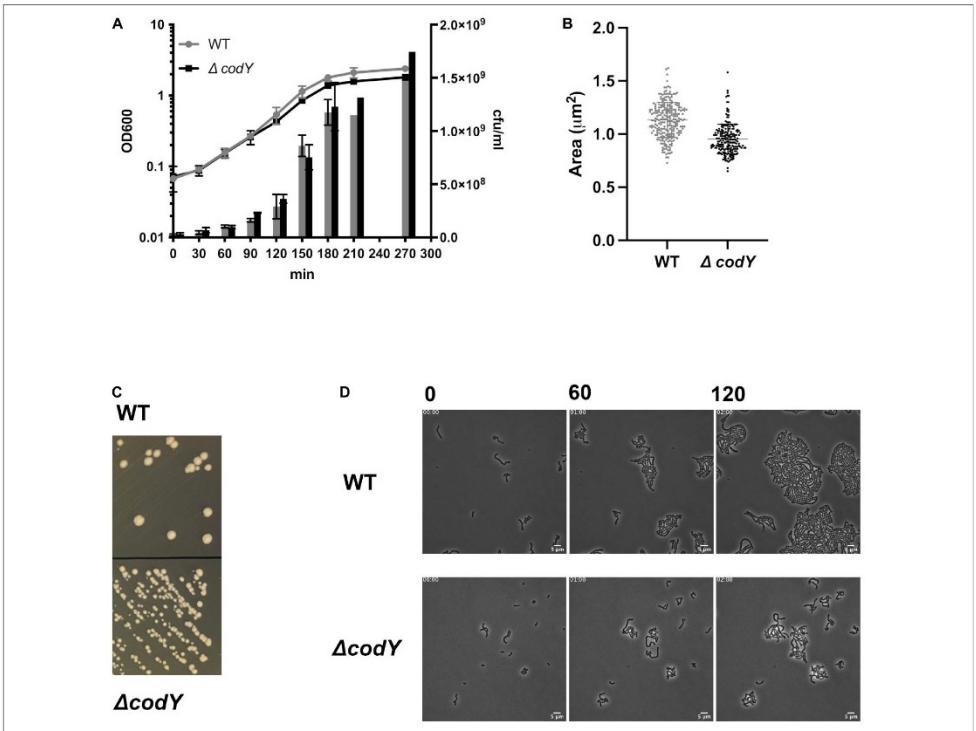

FIGURE 1 | Deletion of *codY* does not affect cell growth but is associated to a smaller cell size and colony morphology. **(A)** Growth of the BM110 strain (WT) and of the isogenic *codY* deletion mutant (Δ*codY*) in THY rich medium, evaluated as absorbance at OD_{600} (left axis) and cfu/ml (right axis). Data are the average ± SD of two independent experiments **(B)**. Single cell area measurements (µm²) of 50 cells of each strain. Reported data refer to two independent experiments. Statistically significant differences are indicated (Welch's *t*-test). **(C)** Colonies of the WT and Δ*codY* strains grown on THY agar plates. **(D)** Contrast-phase image stacks of BM110 and Δ*codY* cells during time-lapse microscopy. Scale bar is 5 µm.

scanning laser microscopy experiments were performed three times and standard deviations were measured.

Cloning, Overproduction, and Purification of CodY

The *codY* CDS was amplified with primers pET_GBS_codYF and pET_GBS_codYR. The obtained fragment was inserted by Gibson assembly between the *Eco*RI and *Bam*HI sites of plasmid pET28a. The CodY protein with an N-terminal 6X-His tag was produced in *E. coli* BL21 DE3 cells by IPTG (0.5 mM) induction at 28°C overnight. CodY protein was purified as previously described (Alfeo et al., 2021), and protein concentration was measured by Bradford protein assay (Bio-Rad).

Fragments Labeling and Electrophoretic Mobility Shift Assay

To be used as probes in gel-shift experiments, PCR products containing the regulatory region of the *livK* gene were amplified using the appropriate pTCV-*lacZ* derivative plasmid as template and the 5'FAM labeled, vector-specific primers Vlac1-FAM and Vlac2-FAM.

FAM-labeled fragments (50 nM) were incubated with increasing concentrations of CodY and electrophoretic mobility shift assays were performed as previously described (Barbieri et al., 2015). When indicated, BCAAs were added to the final concentration of 10 mM in the CodY-binding reaction mixture. Ten mM each isoleucine, leucine, and valine were also added to the 5% non-denaturing Tris-Glycine polyacrylamide gel and electrophoresis buffer.

Mouse Infection Models

In the neonatal model, 48-h-old mice of both sexes were inoculated subcutaneously with 8×10^4 CFU of the WT or the Δ*codY* strain, as previously described. Mice showing signs of irreversible disease, such as diffuse redness spreading from the infection site, were humanely euthanized. In the adult model of GBS sepsis, 8 week-old female mice were inoculated intraperitoneally with 5×10^8 CFU of the WT or the Δ*codY* strain, as previously described (Biondo et al., 2014). In the meningitis model, 8 week-old female mice were inoculated intravenously 1×10^9 CFU of WT or the Δ*codY* strain, as previously described (Lentini et al., 2018). Mice showing signs of irreversible disease, such as prolonged hunching, inactivity, or neurological symptoms were humanely euthanized. In further experiments, mice were euthanized at 16 h after challenge and bacterial burden was determined in organ homogenates, as previously described (Famà et al., 2020).

In vivo and *in vitro* Cytokine Induction

Female mice of 8 weeks of age were infected intraperitoneally with 1×10^9 CFU of the WT or the Δ*codY* strain. Mice were treated at 30 min post-challenge with penicillin (500 IU i.p.) to prevent bacterial overgrowth. Peritoneal lavage fluids were collected at the indicated times and analyzed for cytokine levels as previously described (Mohammadi et al., 2016). For *in vitro* cytokine induction, bone marrow-derived macrophages were obtained from 8-week-old female mice and cultured in the presence of M-CSF as previously described (Lentini et al., 2021). Macrophage cultures were then stimulated for 1 h with GBS grown to the late exponential phase at the indicated multiplicities of infection (MOI). Cultures were then treated with penicillin and gentamycin (100 IU and 50 μg/ml) to kill extracellular bacteria and supernatants were collected at 18 h after culture, as previously described (Lentini et al., 2021). Cytokine levels were measured in peritoneal lavage fluid samples or culture supernatants by ELISA, using Mouse TNF-alpha DuoSet ELISA DY410, Mouse IL-1 beta/IL-1F2 DuoSet ELISA DY401, Mouse CXCL2/MIP-2 DuoSet ELISA DY452, Mouse CXCL1/KC DuoSet ELISA DY453 (R&D Systems).

RESULTS

CodY Is Required for *in vivo* Virulence of Group B *Streptococcus*

A marker-free, in-frame deletion of the *codY* gene was created by allelic replacement in the CC17 wild-type strain BM110 (WT). The resulting Δ*codY* mutant showed no growth defects in rich THY liquid medium (**Figure 1A**). However, Δ*codY* cells showed a 10% reduced cell size and formed smaller colonies compared to the WT strain (**Figures 1B–D**), similarly to what was previously observed in *codY*-deleted mutants in other bacteria (Majerczyk et al., 2008; Geng et al., 2018).

To assess the *in vivo* impact of CodY on the ability of GBS to sustain infection, we determined the virulence properties of the Δ*codY* strain in several models of infection that closely mimic features of human infections (Magliani et al., 1998; Cusumano et al., 2004). In the first murine model of neonatal GBS sepsis, bacteria replicate at the inoculation site and spread systemically to the blood and distant organs. Newborn mice infected subcutaneously with the WT strain showed signs of irreversible infection within the first 24 h after challenge and were humanely euthanized. In contrast, nearly all neonates infected with the Δ*codY* strain survived and remained in good conditions until the end of the experiment (**Figure 2A**). In further studies, newborn mice were infected as above, and the organs were collected at 14 h after challenge. As shown in **Figures 2C,E,G**, considerable bacterial burden was detected in the blood, brain, and liver of all animals infected with WT GBS, while low bacterial numbers or no bacteria were present in the organs from mice infected with the *codY*-deleted strain. These data indicated that, in the absence of CodY, GBS is unable to replicate locally *in vivo* and to spread hematogenously to distant organs. Since GBS infections are being increasingly reported in adults, we sought to confirm the data obtained in newborn mice in an adult sepsis model. As shown in **Figure 2B** and **Supplementary Figures 1A–E**, all adult mice intraperitoneally inoculated with the *codY*-deleted strain survived while all mice infected with WT bacteria succumbed to overwhelming infection, confirming the results obtained in neonates. In view of the clinical importance of meningoencephalitis in the context of CC17 GBS infection, we also looked at the role of CodY in the ability of GBS to cross the blood-brain barrier using a meningoencephalitis

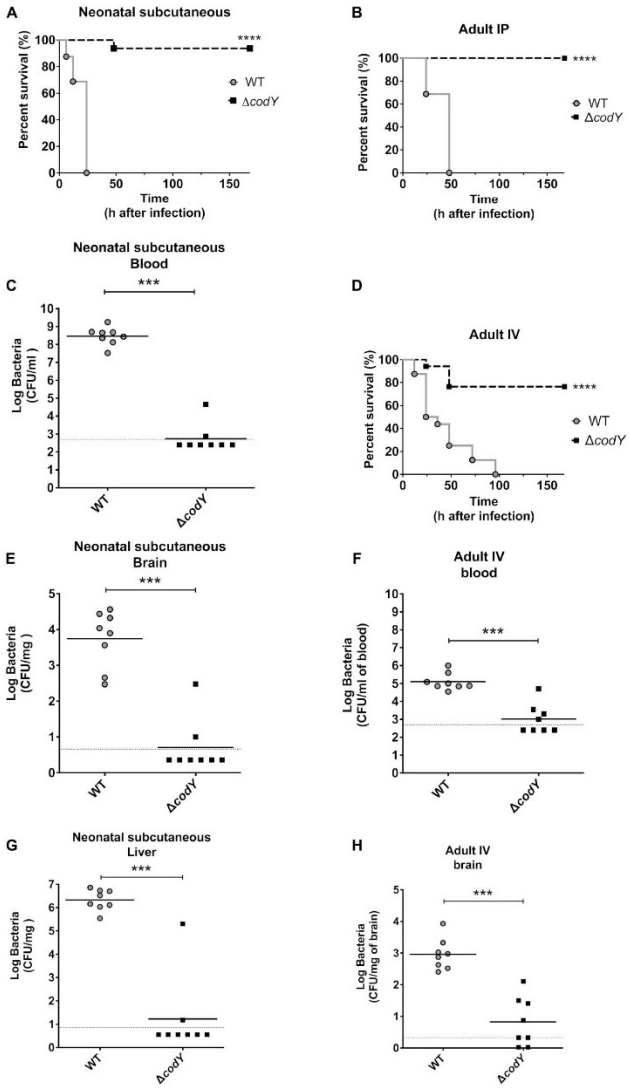

FIGURE 2 | *CodY* is necessary during neonatal and adult infections. **(A)** Lethality of newborn mice (8 per group) infected subcutaneously with 8×10^4 of the WT strain or the Δ*codY* mutant. **(C,E,G)** Bacterial burden in the indicated organs of newborn mice infected in the same experimental condition as in panel **(A)**; horizontal bars indicate mean log CFU values. **(B)** Lethality of adult mice (8 per group) infected intraperitoneally (IP) with 5×10^8 of the WT strain or Δ*codY* mutant. **(D)** Lethality of adult mice (8 per group) infected intravenously (IV) with 1×10^9 CFU. **(F,H)** Bacterial burden in the indicated organs of adult mice infected in the same experimental condition as in panel **(D)**; horizontal bars indicate mean log CFU values. $^{***}p < 0.001$; $^{****}p < 0.0001$ by the Kaplan Meier (panels **A,B,D**) or Mann Whitney test (panels **C, E–H**).

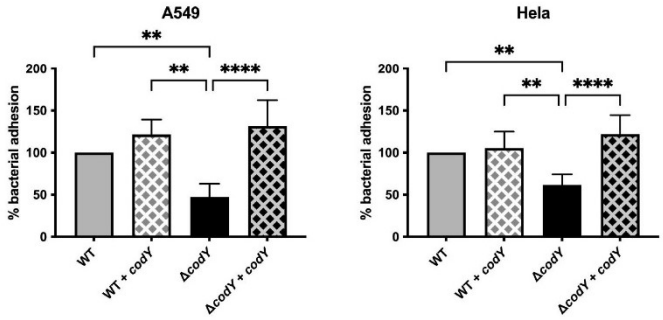

FIGURE 3 | CodY controls GBS adhesion to epithelial cells. Cell adhesion was quantified using HeLa and A549 immortalized cell lines. The WT and the Δ*codY* mutant contain the empty vector pTCVΩP_{tet} or the complementing vector pTCVΩP_{tet}_*codY* (+ *codY*). The percent of adhesion of each strain was calculated relative to the initial inoculum and was normalized to the adhesion of the WT strain, set as 100%. Represented data are the average ± SD of six independent experiments, each performed in duplicate. Statistically significant differences are indicated (One-way ANOVA). $^{**}p < 0.01$, $^{****}p < 0.0001$.

model in which bacteria are inoculated intravenously. Under these conditions, the Δ*codY* mutant displayed a considerably decreased ability to persist in the blood and to cause lethal encephalitis compared to WT bacteria (**Figures 2D,F,H**).

Deletion of CodY Does Not Impact the Host Cytokine Response to Group B *Streptococcus* Infection

To investigate whether the reduced virulence of GBS in the absence of CodY could be related to altered induction of pro-inflammatory cytokines, we used a sepsis model in which mice are infected intraperitoneally and cytokine levels are measured in peritoneal lavage fluid samples at different times after challenge. To avoid bacterial overgrowth, penicillin was administered at 30 min post-challenge. Under these conditions, TNF-α, IL-1β, Cxcl1, and Cxcl2 levels rapidly increased, to reach peak levels at 3 h after challenge with a WT strain (**Supplementary Figures 2A–D**). However, similar cytokine levels were detected in mice infected with the WT and Δ*codY* strains. Similarly, no differences were detected in TNF-α or IL-1β induction in peritoneal macrophages stimulated with the two strains (**Supplementary Figures 2E,F**).

CodY Contributes to Group B *Streptococcus* Adhesion to Epithelial Cells

Adhesion to host cells and tissue colonization are necessary for the establishment of a successful infection. Deletion of *codY* resulted in a 50% decrease in adherence to human epithelial cervix adenocarcinoma (HeLa) and human epithelial lung carcinoma (A549) cell lines compared to the WT strain (**Figure 3**). Complementation of *codY* deletion by plasmid-mediated expression of *codY* under the control of the constitutive Ptet promoter restored adhesion to levels similar to the WT strain. Plasmid-mediated CodY expression in the WT strain did not affect the adhesion ability of the parental strain.

CodY Controls the Ability of BM110 to Form Biofilms

The role of CodY in the ability of GBS to form biofilms was evaluated by crystal violet staining (**Figure 4A**) and confocal laser scanning microscopy (**Figure 4B**). While the WT strain formed a weak biofilm, the *codY*-deleted mutant formed a thicker, more compact biofilm able to completely cover the surface of the well and of the chambered coverglass (**Figures 4B–D**). The biofilm-forming ability was significantly reduced after complementation of the *codY* deletion. Eradication experiments revealed that biofilms formed by the Δ*codY* mutant were strongly reduced by treatment with proteinase K, while DNAse I was less effective against the biofilm biomass (**Figure 4A**). These results suggest that extracellular proteins are a major constituent of the Δ*codY* biofilm.

CodY Is a Global Regulator of Gene Expression in Group B *Streptococcus*

To determine the transcriptional changes associated with *codY* deletion, an RNA-Seq experiment was performed on WT and Δ*codY* bacteria during exponential growth in rich THY medium, i.e., under conditions of maximal CodY activity. A total of 277 genes (out of 2,128 analyzed genes) were differentially expressed at least twofold (adjusted *p*-value < 0.05) in the Δ*codY* strain, demonstrating a global regulatory role for CodY (**Supplementary Datasets 1A–C**). Among these, 256 genes were up-regulated (**Supplementary Dataset 1B**) and 21 genes were down-regulated (**Supplementary Dataset 1C**) in the mutant, supporting a role for CodY mainly as a repressor of gene expression (**Figure 5A**). Overall, fold changes associated with negative regulation were higher than those associated

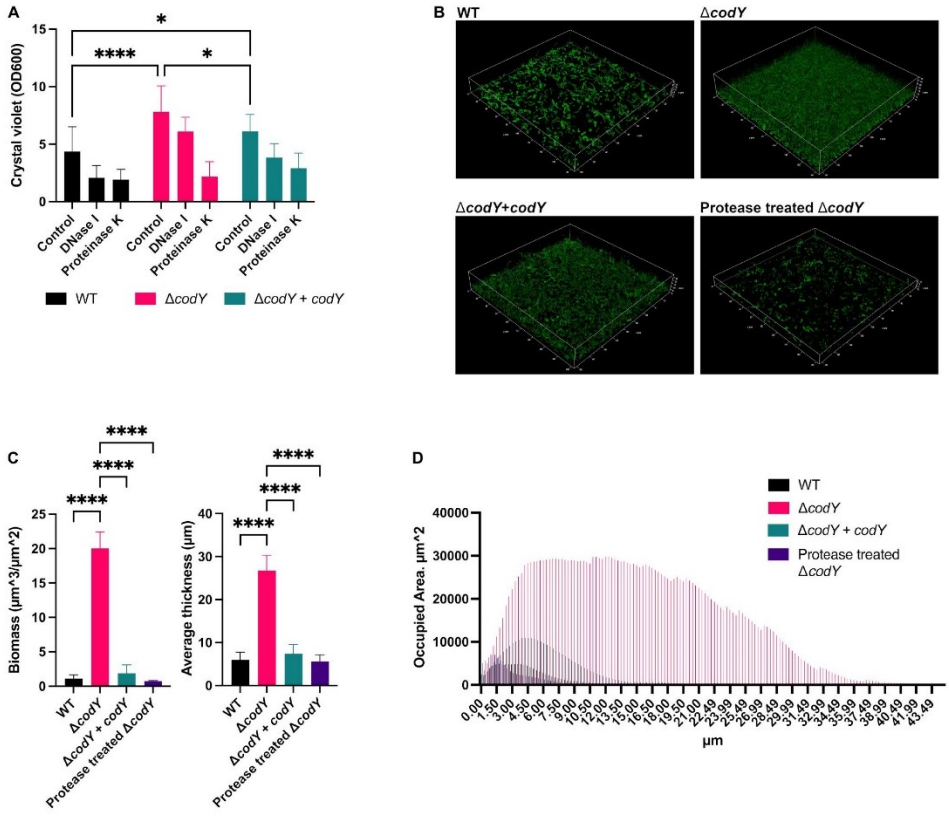

FIGURE 4 | CodY inhibits biofilm formation. **(A)** Biofilm biomass was measured by crystal violet staining after static culture for 19 h. The WT and the Δ*codY* strain contain the empty vector pTCVΩP_{tet} or the complementing vector pTCVΩP_{tet}_*codY* (+ *codY*). The role of eDNA and extracellular proteins as biofilm structural components was assessed by individual treatments with DNase I and proteinase K, respectively. Represented data are the average ± SD of two independent experiments, each performed in 8 replicates. Statistically significant differences are reported (two-way ANOVA). **(B)** Confocal laser scanning microscopic images of biofilms formed by WT, Δ*codY* and Δ*codY* + *codY* GBS strains grown for 19 h in Nunc™ Lab-Tek™ II Chambered Coverglass. The effect of treatment with proteinase K on the Δ*codY* biofilm is reported. **(C,D)** Analysis of biofilm properties by COMSTAT 2. Measures of total biomass, average thickness **(C)** and % of the area occupied by biofilm distribution **(D)**. Data are the average ± SD of the results from three independent replicates. : $*p < 0.05$, $****p < 0.0001$ (one-way ANOVA test).

with positive regulation. Notably, 55% (140/256) of the over-expressed genes were located in four prophages. The 98 genes whose expression was affected by *codY* deletion at least fourfold (94 up-regulated and 4 down-regulated genes) (**Supplementary Datasets 1D,E**) could be classified into seventeen categories by the Cluster of Orthologous Genes (COGs) analysis (**Supplementary Dataset 2** and **Figure 5B**). Among these, the most represented groups included genes involved in "amino acid transport and metabolism," "cell wall/membrane/envelope biogenesis," and "mobilome: prophages, transposons."

Specifically, CodY-repressed genes (**Supplementary Dataset 1D** and **Figure 5A**) included those encoding BCAAs transporters (*braB*, *brnQ*, all the genes belonging to the *livK-G* operon), the (oligo)peptide permease OppA1-F, adhesins, and serine peptidases anchored to the cell wall through the LPxTG motif, as well as proteins involved in DNA replication, recombination, and repair. Interestingly, the genes of the *cas* operon, involved in adaptive immunity, were among the ones more intensely up-regulated in the Δ*codY* mutant. Notably, the operon encoding for the CC17-specific virulence factor Srr2 was

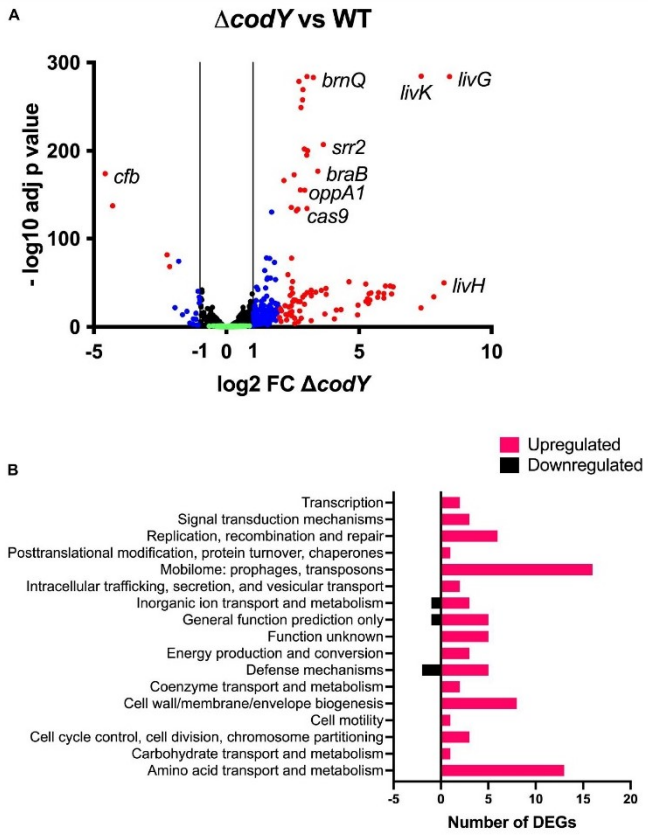

FIGURE 5 | (A) Volcano plot of the Δ*codY* transcriptome at mid-exponential phase in THY. Each dot represents a gene with its RNA-seq fold change and adjusted *p*-value calculated from four independent replicates. Genes showing a significant differential expression in the Δ*codY* strain (adjusted *p*-value < 0.05) are represented in blue (–2 ≤ log2FC ≤ –1 or 1 ≤ log2FC ≤ 2) and red (log2FC < –2 or log2FC > 2) according to their fold change relative to the WT strain. Black dots represent genes whose expression is not affected by *codY* deletion (–1 < log2FC < 1; adjusted *p*-value < 0.05). Green dots correspond to non-significant (adjusted *p*-value > 0.05) differentially transcribed genes. **(B)** COGs associated to downregulated and upregulated genes.

over-expressed in the absence of CodY. On the contrary, the gene encoding the CAMP factor pore-forming toxin Cfb was under positive regulation by CodY (**Supplementary Dataset 1E** and **Figure 5A**).

Using the FIMO Motif Search Tool (Grant et al., 2011), the genome of BM110 was scanned to search for sequences matching the conserved AATTTTCWGAAATT CodY binding motif. One hundred and one matches were retrieved from the genomic regions located upstream of the coding sequences of the genes, using a *p*-value lower than 0.0001. At least one of these sites was located in the proximity of the coding sequence of eighteen genes differentially expressed in the Δ*codY* strain (**Supplementary Datasets 1A–D** and **Supplementary Table 4**), predicting that these genes might be targets of direct CodY-mediated regulation.

Group B *Streptococcus* CodY Controls Gene Expression in Response to Branched-Chain Amino Acid Availability

As BCAAs (isoleucine, leucine, and valine, ILV) are universal positive cofactors of CodY (Richardson et al., 2015), the expression of CodY-dependent genes is expected to change in response to the availability of these amino acids. To test this hypothesis, the expression of CodY-regulated genes was analyzed

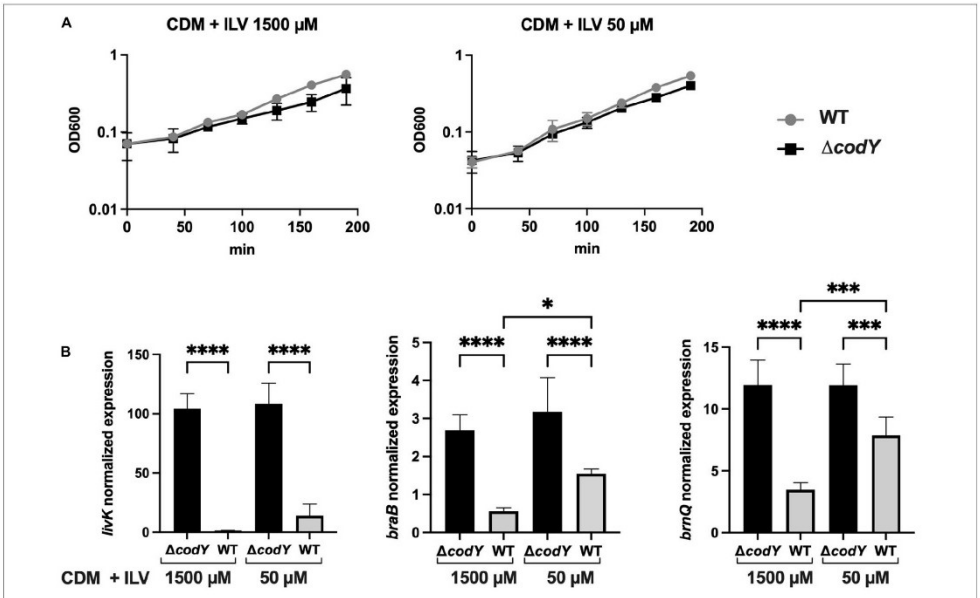

FIGURE 6 | CodY activity is dependent on branched-chain amino acids availability. **(A)** Growth of the WT (gray) and Δ*codY* mutant (black) in CDM supplemented with high (1500 μM) and low (50 μM) ILV concentrations. Reported data are the average ± SD of two independent experiments. **(B)** Expression analysis by qRT-PCR of the genes *livK*, *braB*, and *brnQ* in the WT and Δ*codY* mutant grown under high and low ILV concentrations. Gene expression is normalized to the expression of the housekeeping *gyrA* gene. Asterisks denote statistically significant differences as assessed by One-way ANOVA analysis $^{*}p < 0.05$, $^{***}p < 0.001$, $^{****}p < 0.0001$.

by qRT-PCR in WT and Δ*codY* cells grown to mid-log phase in CDM (Willett and Morse, 1966) containing a mix of all amino acids and supplemented with high (1,500 μM) or low (50 μM) concentrations of ILV. As GBS is unable to synthesize the precursors of most amino acids, including the BCAA (Glaser et al., 2002), ILV cannot be omitted from the growth medium. Under both conditions tested, the two strains showed similar growth kinetics, displaying approximately a two-fold increase in their doubling time compared to growth in rich, THY medium (**Figure 6A**). Three genes encoding BCAAs transporters and identified by RNA-Seq analysis (**Supplementary Dataset 1D** and **Figure 5A**) and qRT-PCR (**Supplementary Figure 3**) as subjected to different levels of CodY-mediated repression during growth in rich THY medium were included in the analysis. In the WT strain, transcription of all three genes increased when BCAA were less abundant in the defined medium, in accord with expected decrease in CodY activity. All three target genes were further and significantly over-expressed in the Δ*codY* mutant compared to the WT strain under both conditions tested, however, the extent of this overexpression was higher in *livK* (82-fold and 11-fold increase in CDM + 1500 μM and in CDM + 50 μM ILV, respectively) and lower in *braB* (3.4-fold and 2.3-fold increase in CDM + 1500 μM and in CDM + 50 μM ILV, respectively) and *brnQ* (4.8-fold and 2.8-fold increase in CDM + 1500 μM and in CDM + 50 μM ILV, respectively) (**Figure 6B** and **Supplementary Table 5**). The high level of gene expression in the Δ*codY* mutant was not affected by ILV levels. The obtained results in the WT strain suggest that, as the levels of BCAAs decrease, the expression of CodY-repressed genes increases in a gene-specific manner (**Figure 6B**).

Direct Transcriptional Repression of the *livK-G* Operon by CodY

The mechanism of CodY-mediated regulation of the *livK-G* operon, encoding an ABC-type BCAAs transporter, was investigated. Two putative CodY-binding motifs, with three and two mismatches to the consensus sequence, were identified by FIMO analysis at positions from −64 to −50 and from −31 to −17 respectively, with respect to the transcription start site (Mazzuoli et al., 2021) of the *livK* gene, the first gene of the operon (**Figure 7A**).

An electrophoretic-mobility shift assay (EMSA) was performed using purified CodY and a 6-carboxyfluorescein (FAM) labeled fragment encompassing the *livK* regulatory region from position −168 to +52 with respect to the transcription start site of the gene (**Figure 7A**). In the presence of 10 mM ILV, CodY bound the *livK* fragment with an apparent equilibrium

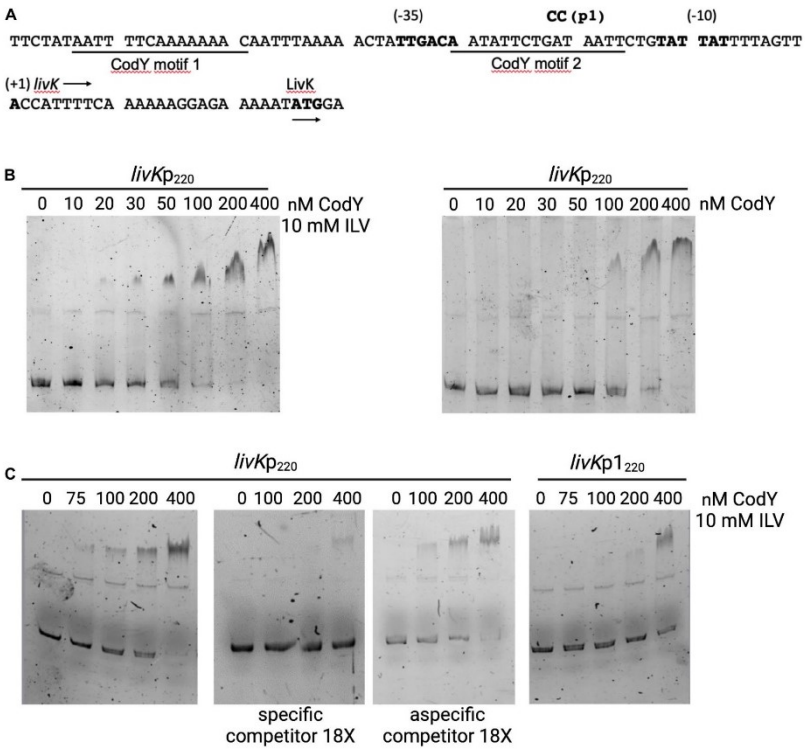

FIGURE 7 | CodY binds to the *livK* promoter. **(A)** Sequence (5' to 3') of the *livK* regulatory region. Coordinates are reported with respect to the transcription start point (Mazzuoli et al., 2021). The transcription start site, −10 and −35 promoter regions, and the starting codon of the *livK* CDS are in boldface. The directions of transcription and translation are indicated by the horizontal arrows. The sequences of the two CodY-binding motifs are underlined. The mutated nucleotides (p1) are shown above the sequence. **(B)** Electrophoretic mobility shift assays (EMSA) for binding of CodY to the *livK* regulatory region. CodY and the WT $livKp_{220}$ fragment were incubated in the presence or absence of 10 mM each isoleucine, leucine, and valine (ILV). When ILV were included in the reaction mixture, the non-denaturing polyacrylamide gel and the electrophoresis buffer were supplemented with 10 mM ILV. **(C)** EMSA performed with the WT $livKp_{220}$ and mutated $livKp1_{220}$ fragments. Specificity of binding was evaluated by performing the experiment with the WT fragment in the absence or presence of a specific (unlabeled $livKp_{220}$ fragment) or non-specific competitor. DNA-Protein mixtures were separated on 5% non-denaturing gel in presence of 10 mM ILV.

dissociation constant (K_D) of ≈50 nM (here, K_D reflects the concentration of CodY required to shift 50% of DNA fragments under conditions of vast protein excess over DNA) (**Figure 7B**). When ILV were omitted from the binding mixture, affinity of CodY for the *livK* regulatory region decreased (KD ≈150 nM), suggesting that BCAAs enhance CodY activity. Specificity of CodY binding was assessed by competitive and non-competitive binding assays in the presence of ILV and 18-fold excess of unlabeled specific or non-specific competitor DNA, respectively (**Figure 7C**).

A *lacZ* transcriptional fusion ($livKp_{220}$-*lacZ*) including the region spanning from position −168 to +52 with respect to the *livK* transcription start site was constructed using the pTCV-*lacZ* plasmid (Poyart and Trieu-Cuot, 2006). Under conditions of maximal CodY activity, during the exponential phase of growth in THY medium, expression of the $livKp_{220}$-*lacZ* fusion was about 400-fold higher in the *codY*-null mutant strain, BM1107, than in the WT strain, BM1106 (**Table 2**). A two-nucleotide substitution mutation was introduced at positions −22 and −23 with respect to the *livK* transcription start site, within the putative CodY-binding site located immediately upstream of the *livK* coding region ($livKp1_{220}$-*lacZ*). The p1 mutation, aimed at decreasing the similarity of the motif to the CodY-binding consensus sequence, strongly reduced the affinity of CodY for the

livK regulatory region (**Figure 7C**) and abolished CodY's ability to repress the *livK* promoter (**Table 2**).

DISCUSSION

In this study, we showed that the global transcriptional regulator CodY is essential for GBS virulence in several animal models of infection.

In low-G+C Gram-positive pathogens, this conserved transcriptional regulator coordinates metabolism and virulence in response to nutrient availability (Brinsmade, 2017). While CodY controls global metabolism in a generally conserved manner, genes involved in virulence are subjected to species-specific modes of regulation, depending on the occupied niche during infection and on the type of interaction that the bacterium establishes with the host. In *S. aureus* and *C. difficile* CodY strongly represses virulence genes, so that their expression is activated only when BCAA levels are low (Dineen et al., 2007, 2010; Majerczyk et al., 2008, 2010; Waters et al., 2016). On the contrary, in *Bacillus anthracis* and *Listeria monocytogenes* virulence is positively controlled by CodY (van Schaik et al., 2009; Château et al., 2011; Lobel et al., 2012, 2015). While understanding the function of CodY in *S. pneumoniae* is complicated by the *codY* essentiality in this important human pathogen (Caymaris et al., 2010), a role for this regulator in the control of virulence was demonstrated in other Streptococcal species (Malke et al., 2006; Lemos et al., 2008; Kreth et al., 2011; Feng et al., 2016; Geng et al., 2018).

Here, we confirmed that *codY* is not essential for the growth of GBS in complex or chemically defined liquid medium (Hooven et al., 2016) but is required *in vivo*. The reduced ability of the Δ*codY* mutant to cause infection is associated with a lower ability to disseminate, colonize host tissues, persist in blood and cause meningitis. This reduced virulence is not associated with an altered cytokine response in the host but is related to pleiotropic effects of the *codY* deletion, such as the decreased ability of the mutant strain to bind to human epithelial cells *in vitro* and the increased ability to form biofilm. Of note, while strains of the CC17, responsible for neonatal invasive infections, are generally weak biofilms formers, the ability to form strong biofilms is a common phenotype of strains able to asymptomatically colonize the host (Parker et al., 2016). As proteins appear to play a major role in promoting Δ*codY* biofilm structural stability, it is possible to speculate that surface proteins involved in bacterial adherence and encoded by genes that are repressed by CodY (e.g., Srr2, FbsB, and ScpB3) might be required for biofilm formation in GBS (Park et al., 2012).

The transcriptomic analysis in GBS strengthens the conserved role of CodY as a global regulator of metabolism, with genes encoding functions involved in the uptake of amino acids and oligopeptides subjected to the highest level of regulation. As genes required for the biosynthesis of precursors of most amino acids, including BCAAs, are missing in the genome of GBS, this bacterium relies on transporters and peptidases for amino acids metabolism (Milligan et al., 1978; Glaser et al., 2002). The capacity to take up exogenous oligopeptides is particularly important to support growth in amniotic fluid, which contains only low amounts of free amino acids (Mesavage et al., 1985; Samen et al., 2004). Notably, the majority of the genes involved in peptide and amino acid transport and metabolism that are upregulated during GBS growth in amniotic fluid (*oppA1-F* and *livK* operons, *braB*, *brnQ*, BQ8897_RS10635) are members of the CodY regulon identified in this work. As the *codY* gene itself is downregulated 11-fold during growth in amniotic fluid compared to a rich laboratory medium (Sitkiewicz et al., 2009), it might be hypothesized that the reduced levels of this repressor could be at the origin of the overexpression of peptides and amino acids transport systems in amniotic fluid.

We confirmed that the CodY response in GBS is dependent on the concentration of extracellular BCAAs which, besides being abundant amino acids in proteins, are precursors of branched-chain fatty acids, the predominant membrane fatty acids in Gram-positive bacteria (Richardson et al., 2015). CodY-mediated regulation of three genes involved in amino acid uptake (*livK*, *braB*, *brnQ*) is dependent on the level of BCAAs available in the growth medium. Therefore, as the abundance of its cofactors decreases, CodY-mediated repression of genes required for amino acid uptake is relieved. Among the analyzed genes, very low levels of *livK* expression were observed in a WT strain even under conditions of low BCAA-abundance. This result suggests that very few active molecules of CodY are sufficient to efficiently bind the regulatory region of the *livK* operon and repress its expression.

The CodY regulatory network links the metabolic status of several bacteria with the regulation of their virulence (Lobel et al., 2012; Waters et al., 2016). In GBS, CodY directly and indirectly regulates numerous genes involved in carbon and energy metabolism, cell wall and membrane biogenesis and virulence. The latter category includes surface-anchored proteins such as the Srr2 adhesin. This CC17-specific adhesin is a major virulence factor that supports the ability of GBS to cross the developing neonatal gastrointestinal epithelium and to adhere to and invade cerebral endothelial cells, thus leading to invasive infections and meningitis in neonates (Seifert et al., 2006; Six et al., 2015; Hays et al., 2019; Gori et al., 2020;

TABLE 2 | Expression of *livK-lacZ* fusions[a].

Strain	Relevant genotype[b]	Fusion genotype	β-galactosidase activity[c]		
			Miller Units[a]	%[b]	Repression[c] ratio
BM1106	wild-type	$livKp_{220}$-*lacZ*	0.47 ± 0.07	0.3	393.62
BM1107	Δ*codY*		185 ± 19.02	100.0	
BM1114	wild-type	$livKp1_{220}$-*lacZ*	157.6 ± 0.35	97.3	1.03
BM1115	Δ*codY*		161.9 ± 6.86	100.0	

[a] *β-galactosidase activity is reported in Miller Units. Data are the average ± SD of two independent experiments, each performed in duplicate.*
[b] *β-galactosidase activity of each fusion in the codY-deleted strain was normalized to 100%.*
[c] *The repression ratio is the ratio of expression values for the corresponding fusions in the codY null mutant in and wild-type strain.*

Deshayes de Cambronne et al., 2021). Importantly, the transcription of the *srr2* operon and of other genes included in the CodY regulon are directly repressed by the master regulator of virulence CovR (Mazzuoli et al., 2021). In the related pathogen *S. pyogenes*, CodY represses *covR* expression allowing to counterbalance CovRS activity according to the nutritional status of the cell (Kreth et al., 2011). Noteworthy, in GBS, CovR and CodY do not control each other's transcription (Mazzuoli et al., 2021), suggesting the existence of a different wiring between these two major regulatory pathways. A detailed investigation of the interplay between CodY and CovR regulations is necessary to define the mechanism(s) allowing a concerted regulation of virulence and metabolism in GBS.

Understanding how CodY activity is coordinated with the network of regulators controlling GBS adaptation and virulence will allow deciphering the signals and conditions governing host-pathogen interaction during colonization and infection.

DATA AVAILABILITY STATEMENT

The data presented in the study are deposited in the NCBI BioProject database (https://www.ncbi.nlm.nih.gov/bioproject/), BioProject accession number PRJNA808867.

ETHICS STATEMENT

The animal study was reviewed and approved by the Animal Welfare Committee of the University of Messina and the Ministero della Salute of Italy (Permit number 786/2018-PR prot. 5E567.10).

AUTHOR CONTRIBUTIONS

GB, GP, CBe, GTe, AFi, and CBi conceived the work and designed the experiments. AP, AB, VS, GTr, FM, and SB conducted the experiments. UP and DS performed the bioinformatic analyses. GL and AFa performed *in vivo* experiments. GB and AP wrote the manuscript. All authors contributed to the article and approved the submitted version.

FUNDING

This research was funded by Cariplo Foundation grant 2017-0785 to GB and by the Italian Ministry of Education, University and Research (MIUR) (Dipartimenti di Eccellenza, Program 2018–2022) to Department of Biology and Biotechnology, "L. Spallanzani," University of Pavia.

ACKNOWLEDGMENTS

We thank the PASS-BioMed Facility (Centro Grandi Strumenti) of the University of Pavia for the provision of confocal microscope infrastructure and the associated technical support provided by Amanda Oldani and Patrizia Vaghi. We thank Abraham L. Sonenshein and Boris R. Belitsky for helpful reading of the manuscript.

SUPPLEMENTARY MATERIAL

The Supplementary Material for this article can be found online at: https://www.frontiersin.org/articles/10.3389/fmicb.2022.881549/full#supplementary-material

REFERENCES

Alfeo, M. J., Pagotto, A., Barbieri, G., Foster, T. J., Vanhoorelbeke, K., De Filippis, V., et al. (2021). *Staphylococcus aureus* iron-regulated surface determinant B (IsdB) protein interacts with von Willebrand factor and promotes adherence to endothelial cells. *Sci. Rep.* 11:22799. doi: 10.1038/s41598-021-02065-w

Barbieri, G., Albertini, A. M., Ferrari, E., Sonenshein, A. L., and Belitsky, B. R. (2016). Interplay of CodY and ScoC in the regulation of major extracellular protease genes of *Bacillus subtilis*. *J. Bacteriol.* 198, 907–920. doi: 10.1128/JB.00894-15

Barbieri, G., Voigt, B., Albrecht, D., Hecker, M., Albertini, A. M., Sonenshein, A. L., et al. (2015). CodY regulates expression of the *Bacillus subtilis* extracellular proteases Vpr and Mpr. *J. Bacteriol.* 197, 1423–1432. doi: 10.1128/JB.02588-14

Belitsky, B. R., Barbieri, G., Albertini, A. M., Ferrari, E., Strauch, M. A., and Sonenshein, A. L. (2015). Interactive regulation by the *Bacillus subtilis* global regulators CodY and ScoC. *Mol. Microbiol.* 97, 698–716. doi: 10.1111/mmi.13056

Belitsky, B. R., and Sonenshein, A. L. (2013). Genome-wide identification of *Bacillus subtilis* CodY-binding sites at single-nucleotide resolution. *Proc. Natl. Acad. Sci. U.S.A.* 110, 7026–7031. doi: 10.1073/pnas.1300428110

Biondo, C., Mancuso, G., Midiri, A., Signorino, G., Domina, M., Lanza Cariccio, V., et al. (2014). Essential role of interleukin-1 signaling in host defenses against group B *Streptococcus*. *mBio*. 5:e1428-14. doi: 10.1128/mBio.01428-14

Biswas, I., Gruss, A., Ehrlich, S. D., and Maguin, E. (1993). High-efficiency gene inactivation and replacement system for gram-positive bacteria. *J. Bacteriol.* 175, 3628–3635. doi: 10.1128/jb.175.11.3628-3635.1993

Biswas, R., Sonenshein, A. L., and Belitsky, B. R. (2020). Genome-wide identification of *Listeria monocytogenes* CodY-binding sites. *Mol. Microbiol.* 113, 841–858. doi: 10.1111/mmi.14449

Bolger, A. M., Lohse, M., and Usadel, B. (2014). Trimmomatic: a flexible trimmer for Illumina sequence data. *Bioinformatics* 30, 2114–2120. doi: 10.1093/bioinformatics/btu170

Brinsmade, S. R. (2017). CodY, a master integrator of metabolism and virulence in Gram-positive bacteria. *Curr. Genet.* 63, 417–425. doi: 10.1007/s00294-016-0656-5

Brinsmade, S. R., Alexander, E. L., Livny, J., Stettner, A. I., Segre, D., Rhee, K. Y., et al. (2014). Hierarchical expression of genes controlled by the *Bacillus subtilis* global regulatory protein CodY. *Proc. Natl. Acad. Sci. U.S.A.* 111, 8227–8232. doi: 10.1073/pnas.1321308111

Brinsmade, S. R., Kleijn, R. J., Sauer, U., and Sonenshein, A. L. (2010). Regulation of CodY activity through modulation of intracellular branched-chain amino acid pools. *J. Bacteriol.* 192, 6357–6368. doi: 10.1128/JB.00937-10

Buscetta, M., Firon, A., Pietrocola, G., Biondo, C., Mancuso, G., Midiri, A., et al. (2016). PbsP, a cell wall-anchored protein that binds plasminogen to promote hematogenous dissemination of group B *Streptococcus*. *Mol. Microbiol.* 101, 27–41. doi: 10.1111/mmi.13357

Caymaris, S., Bootsma, H. J., Martin, B., Hermans, P. W. M., Prudhomme, M., and Claverys, J.-P. (2010). The global nutritional regulator CodY is an essential

protein in the human pathogen *Streptococcus pneumoniae*. *Mol. Microbiol.* 78, 344–360. doi: 10.1111/j.1365-2958.2010.07339.x

Château, A., Schaik, W., Six, A., Aucher, W., and Fouet, A. (2011). CodY regulation is required for full virulence and heme iron acquisition in *Bacillus anthracis*. *FASEB J.* 25, 4445–4456. doi: 10.1096/fj.11-188912

Cusumano, V., Midiri, A., Cusumano, V. V., Bellantoni, A., De Sossi, G., Teti, G., et al. (2004). Interleukin-18 is an essential element in host resistance to experimental group B streptococcal disease in neonates. *Infect. Immun.* 72, 295–300. doi: 10.1128/IAI.72.1.295-300.2004

den Hengst, C. D., van Hijum, S. A., Geurts, J. M., Nauta, A., Kok, J., and Kuipers, O. P. (2005). The *Lactococcus lactis* CodY regulon. *J. Biol. Chem.* 280, 34332–34342. doi: 10.1074/jbc.M502349200

Deshayes de Cambronne, R., Fouet, A., Picart, A., Bourrel, A.-S., Anjou, C., Bouvier, G., et al. (2021). CC17 group B *Streptococcus* exploits integrins for neonatal meningitis development. *J. Clin. Invest.* 131:e136737. doi: 10.1172/JCI136737

Dineen, S. S., McBride, S. M., and Sonenshein, A. L. (2010). Integration of metabolism and virulence by *Clostridium difficile* CodY. *J. Bacteriol.* 192, 5350–5362. doi: 10.1128/JB.00341-10

Dineen, S. S., Villapakkam, A. C., Nordman, J. T., and Sonenshein, A. L. (2007). Repression of *Clostridium difficile* toxin gene expression by CodY. *Mol. Microbiol.* 66, 206–219. doi: 10.1111/j.1365-2958.2007.05906.x

Edmond, K. M., Kortsalioudaki, C., Scott, S., Schrag, S. J., Zaidi, A. K., Cousens, S., et al. (2012). Group B streptococcal disease in infants aged younger than 3 months: systematic review and meta-analysis. *Lancet* 379, 547–556. doi: 10.1016/S0140-6736(11)61651-6

Famà, A., Midiri, A., Mancuso, G., Biondo, C., Lentini, G., Galbo, R., et al. (2020). Nucleic acid-sensing toll-like receptors play a dominant role in innate immune recognition of Pneumococci. *mBio* 11:e00415-20. doi: 10.1128/mBio.00415-20

Feng, L., Zhu, J., Chang, H., Gao, X., Gao, C., Wei, X., et al. (2016). The CodY regulator is essential for virulence in *Streptococcus suis* serotype 2. *Sci. Rep.* 6:21241. doi: 10.1038/srep21241

Geng, J., Huang, S.-C., Chen, Y.-Y., Chiu, C.-H., Hu, S., and Chen, Y.-Y. M. (2018). Impact of growth pH and glucose concentrations on the CodY regulatory network in *Streptococcus salivarius*. *BMC Genomics* 19:386. doi: 10.1186/s12864-018-4781-z

Glaser, P., Rusniok, C., Buchrieser, C., Chevalier, F., Frangeul, L., Msadek, T., et al. (2002). Genome sequence of *Streptococcus agalactiae*, a pathogen causing invasive neonatal disease. *Mol. Microbiol.* 45, 1499–1513. doi: 10.1046/j.1365-2958.2002.03126.x

Gori, A., Harrison, O. B., Mlia, E., Nishihara, Y., Chan, J. M., Msefula, J., et al. (2020). Pan-GWAS of *Streptococcus agalactiae* highlights lineage-specific genes associated with virulence and niche adaptation. *mBio* 11:e00728-20. doi: 10.1128/mBio.00728-20

Grant, C. E., Bailey, T. L., and Noble, W. S. (2011). FIMO: scanning for occurrences of a given motif. *Bioinformatics* 27, 1017–1018. doi: 10.1093/bioinformatics/btr064

Guedon, E., Serror, P., Ehrlich, S. D., Renault, P., and Delorme, C. (2001). Pleiotropic transcriptional repressor CodY senses the intracellular pool of branched-chain amino acids in *Lactococcus lactis*. *Mol. Microbiol.* 40, 1227–1239. doi: 10.1046/j.1365-2958.2001.02470.x

Guédon, E., Sperandio, B., Pons, N., Ehrlich, S. D., and Renault, P. (2005). Overall control of nitrogen metabolism in *Lactococcus lactis* by CodY, and possible models for CodY regulation in Firmicutes. *Microbiology* 151, 3895–3909. doi: 10.1099/mic.0.28186-0

Handke, L. D., Shivers, R. P., and Sonenshein, A. L. (2008). Interaction of *Bacillus subtilis* CodY with GTP. *J. Bacteriol.* 190, 798–806. doi: 10.1128/JB.01115-07

Hays, C., Touak, G., Bouaboud, A., Fouet, A., Guignot, J., Poyart, C., et al. (2019). Perinatal hormones favor CC17 group B *Streptococcus* intestinal translocation through M cells and hypervirulence in neonates. *eLife* 8:e48772. doi: 10.7554/eLife.48772

Hendriksen, W. T., Bootsma, H. J., Estevão, S., Hoogenboezem, T., de Jong, A., de Groot, R., et al. (2008). CodY of *Streptococcus pneumoniae* : link between nutritional gene regulation and colonization. *J. Bacteriol.* 190, 590–601. doi: 10.1128/JB.00917-07

Heydorn, A., Nielsen, A. T., Hentzer, M., Sternberg, C., Givskov, M., Ersbøll, B. K., et al. (2000). Quantification of biofilm structures by the novel computer program comstat. *Microbiology* 146, 2395–2407. doi: 10.1099/00221287-146-10-2395

Hooven, T. A., Catomeris, A. J., Akabas, L. H., Randis, T. M., Maskell, D. J., Peters, S. E., et al. (2016). The essential genome of *Streptococcus agalactiae*. *BMC Genomics* 17:406. doi: 10.1186/s12864-016-2741-z

Joubrel, C., Tazi, A., Six, A., Dmytruk, N., Touak, G., Bidet, P., et al. (2015). Group B *Streptococcus* neonatal invasive infections, France 2007–2012. *Clin. Microbiol. Infect.* 21, 910–916. doi: 10.1016/j.cmi.2015.05.039

Kreth, J., Chen, Z., Ferretti, J., and Malke, H. (2011). Counteractive balancing of transcriptome expression involving CodY and CovRS in *Streptococcus pyogenes*. *J. Bacteriol.* 193, 4153–4165. doi: 10.1128/JB.00061-11

Langmead, B. (2010). Aligning short sequencing reads with Bowtie. *Curr. Protoc. Bioinform.* 11:11.7. doi: 10.1002/0471250953.bi1107s32

Lemos, J. A., Nascimento, M. M., Lin, V. K., Abranches, J., and Burne, R. A. (2008). Global regulation by (p)ppGpp and CodY in *Streptococcus mutans*. *J. Bacteriol.* 190, 5291–5299. doi: 10.1128/JB.00288-08

Lentini, G., Famà, A., De Gaetano, G. V., Galbo, R., Coppolino, F., Venza, M., et al. (2021). Role of endosomal TLRs in *Staphylococcus aureus* infection. *J. Immunol.* 207, 1448–1455. doi: 10.4049/jimmunol.2100389

Lentini, G., Midiri, A., Firon, A., Galbo, R., Mancuso, G., Biondo, C., et al. (2018). The plasminogen binding protein PbsP is required for brain invasion by hypervirulent CC17 Group B streptococci. *Sci. Rep.* 8:14322. doi: 10.1038/s41598-018-32774-8

Liao, Y., Smyth, G. K., and Shi, W. (2014). FeatureCounts: an efficient general purpose program for assigning sequence reads to genomic features. *Bioinformatics* 30, 923–930. doi: 10.1093/bioinformatics/btt656

Lobel, L., Sigal, N., Borovok, I., Belitsky, B. R., Sonenshein, A. L., and Herskovits, A. A. (2015). The metabolic regulator CodY links *Listeria monocytogenes* metabolism to virulence by directly activating the virulence regulatory gene *prfA*. *Mol. Microbiol.* 95, 624–644. doi: 10.1111/mmi.12890

Lobel, L., Sigal, N., Borovok, I., Ruppin, E., and Herskovits, A. A. (2012). Integrative genomic analysis identifies isoleucine and CodY as regulators of *Listeria monocytogenes* virulence. *PLoS Genet.* 8:e1002887. doi: 10.1371/journal.pgen.1002887

Love, M. I., Huber, W., and Anders, S. (2014). Moderated estimation of fold change and dispersion for RNA-seq data with DESeq2. *Genome Biol.* 15:550. doi: 10.1186/s13059-014-0550-8

Magliani, W., Polonelli, L., Conti, S., Salati, A., Rocca, P. F., Cusumano, V., et al. (1998). Neonatal mouse immunity against group B streptococcal infection by maternal vaccination with recombinant anti-idiotypes. *Nat. Med.* 4, 705–709. doi: 10.1038/nm0698-705

Majerczyk, C. D., Dunman, P. M., Luong, T. T., Lee, C. Y., Sadykov, M. R., Somerville, G. A., et al. (2010). Direct Targets of CodY in *Staphylococcus aureus*. *J. Bacteriol.* 192, 2861–2877. doi: 10.1128/JB.00220-10

Majerczyk, C. D., Sadykov, M. R., Luong, T. T., Lee, C., Somerville, G. A., and Sonenshein, A. L. (2008). *Staphylococcus aureus* CodY negatively regulates virulence gene expression. *J. Bacteriol.* 190, 2257–2265. doi: 10.1128/JB.01545-07

Malke, H., Steiner, K., McShan, W. M., and Ferretti, J. J. (2006). Linking the nutritional status of *Streptococcus pyogenes* to alteration of transcriptional gene expression: the action of CodY and RelA. *Int. J. Med. Microbiol.* 296, 259–275. doi: 10.1016/j.ijmm.2005.11.008

Manina, G., Dhar, N., and McKinney, J. D. (2015). Stress and host immunity amplify *Mycobacterium tuberculosis* phenotypic heterogeneity and induce nongrowing metabolically active forms. *Cell Host Microbe* 17, 32–46. doi: 10.1016/j.chom.2014.11.016

Manning, S. D., Springman, A. C., Lehotzky, E., Lewis, M. A., Whittam, T. S., and Davies, H. D. (2009). Multilocus sequence types associated with neonatal group B streptococcal sepsis and meningitis in Canada. *J. Clin. Microbiol.* 47, 1143–1148. doi: 10.1128/JCM.01424-08

Mazzuoli, M.-V., Daunesse, M., Varet, H., Rosinski-Chupin, I., Legendre, R., Sismeiro, O., et al. (2021). The CovR regulatory network drives the evolution of Group B *Streptococcus* virulence. *PLoS Genet.* 17:e1009761. doi: 10.1371/journal.pgen.1009761

Mesavage, W. C., Suchy, S. F., Weiner, D. L., Nance, C. S., Flannery, D. B., and Wolf, B. (1985). Amino acids in amniotic fluid in the second trimester of gestation. *Pediatr. Res.* 19, 1021–1024. doi: 10.1203/00006450-198510000-00014

Milligan, T. W., Doran, T. I., Straus, D. C., and Mattingly, S. J. (1978). Growth and amino acid requirements of various strains of group B Streptococci. *J. Clin. Microbiol.* 7, 28–33. doi: 10.1128/jcm.7.1.28-33.1978

Mistou, M.-Y., Dramsi, S., Brega, S., Poyart, C., and Trieu-Cuot, P. (2009). Molecular dissection of the *secA2* locus of group B *Streptococcus* reveals that glycosylation of the Srr1 LPXTG protein is required for full virulence. *J. Bacteriol.* 191, 4195–4206. doi: 10.1128/JB.01673-08

Mohammadi, N., Midiri, A., Mancuso, G., Patanè, F., Venza, M., Venza, I., et al. (2016). Neutrophils directly recognize group B Streptococci and contribute to interleukin-1β production during infection. *PLoS One* 11:e0160249. doi: 10.1371/journal.pone.0160249

Okike, I. O., Johnson, A. P., Henderson, K. L., Blackburn, R. M., Muller-Pebody, B., Ladhani, S. N., et al. (2014). Incidence, etiology, and outcome of bacterial meningitis in infants aged <90 days in the United Kingdom and Republic of Ireland: prospective, enhanced, national population-based surveillance. *Clin. Infect. Dis.* 59, e150–e157. doi: 10.1093/cid/ciu514

Park, S. E., Jiang, S., and Wessels, M. R. (2012). CsrRS and environmental pH regulate group B *Streptococcus* adherence to human epithelial cells and extracellular matrix. *Infect. Immun.* 80, 3975–3984. doi: 10.1128/IAI.00699-12

Parker, R. E., Laut, C., Gaddy, J. A., Zadoks, R. N., Davies, H. D., and Manning, S. D. (2016). Association between genotypic diversity and biofilm production in group B *Streptococcus*. *BMC Microbiol.* 16:86. doi: 10.1186/s12866-016-0704-9

Patras, K. A., and Nizet, V. (2018). Group B Streptococcal maternal colonization and neonatal disease: molecular mechanisms and preventative approaches. *Front. Pediatr.* 6:27. doi: 10.3389/fped.2018.00027

Petranovic, D., Guédon, E., Sperandio, B., Delorme, C., Ehrlich, D., and Renault, P. (2004). Intracellular effectors regulating the activity of the *Lactococcus lactis* CodY pleiotropic transcription regulator. *Mol. Microbiol.* 53, 613–621. doi: 10.1111/j.1365-2958.2004.04136.x

Poyart, C., and Trieu-Cuot, P. (2006). A broad-host-range mobilizable shuttle vector for the construction of transcriptional fusions to β-galactosidase in Gram-positive bacteria. *FEMS Microbiol. Lett.* 156, 193–198. doi: 10.1111/j.1574-6968.1997.tb12726.x

Rajagopal, L. (2009). Understanding the regulation of Group B Streptococcal virulence factors. *Future Microbiol.* 4, 201–221. doi: 10.2217/17460913.4.2.201

Ratnayake-Lecamwasam, M., Serror, P., Wong, K.-W., and Sonenshein, A. L. (2001). *Bacillus subtilis* CodY represses early-stationary-phase genes by sensing GTP levels. *Genes Dev.* 15, 1093–1103. doi: 10.1101/gad.874201

Richardson, A. R., Somerville, G. A., and Sonenshein, A. L. (2015). Regulating the intersection of metabolism and pathogenesis in Gram-positive bacteria. *Microbiol. Spectr.* 3:MBP-0004-2014. doi: 10.1128/microbiolspec.MBP-0004-2014

Samen, U., Gottschalk, B., Eikmanns, B. J., and Reinscheid, D. J. (2004). Relevance of peptide uptake systems to the physiology and virulence of *Streptococcus agalactiae*. *J. Bacteriol.* 186, 1398–1408. doi: 10.1128/JB.186.5.1398-1408.2004

Seale, A. C., Koech, A. C., Sheppard, A. E., Barsosio, H. C., Langat, J., Anyango, E., et al. (2016). Maternal colonization with *Streptococcus agalactiae* and associated stillbirth and neonatal disease in coastal Kenya. *Nat. Microbiol.* 1:16067. doi: 10.1038/nmicrobiol.2016.67

Seifert, K. N., Adderson, E. E., Whiting, A. A., Bohnsack, J. F., Crowley, P. J., and Brady, L. J. (2006). A unique serine-rich repeat protein (Srr-2) and novel surface antigen (ε) associated with a virulent lineage of serotype III *Streptococcus agalactiae*. *Microbiology* 152, 1029–1040. doi: 10.1099/mic.0.28516-0

Shivers, R. P., and Sonenshein, A. L. (2004). Activation of the *Bacillus subtilis* global regulator CodY by direct interaction with branched-chain amino acids. *Mol. Microbiol.* 53, 599–611. doi: 10.1111/j.1365-2958.2004.04135.x

Sitkiewicz, I., Green, N. M., Guo, N., Bongiovanni, A. M., Witkin, S. S., and Musser, J. M. (2009). Transcriptome adaptation of Group B *Streptococcus* to growth in human amniotic fluid. *PLoS One* 4:e6114. doi: 10.1371/journal.pone.0006114

Six, A., Bellais, S., Bouaboud, A., Fouet, A., Gabriel, C., Tazi, A., et al. (2015). Srr2, a multifaceted adhesin expressed by ST-17 hypervirulent Group B *Streptococcus* involved in binding to both fibrinogen and plasminogen. *Mol. Microbiol.* 97, 1209–1222. doi: 10.1111/mmi.13097

Sonenshein, A. L. (2005). CodY, a global regulator of stationary phase and virulence in Gram-positive bacteria. *Curr. Opin. Microbiol.* 8, 203–207. doi: 10.1016/j.mib.2005.01.001

Tatusov, R. L. (2000). The COG database: a tool for genome-scale analysis of protein functions and evolution. *Nucleic Acids Res.* 28, 33–36. doi: 10.1093/nar/28.1.33

Tazi, A., Disson, O., Bellais, S., Bouaboud, A., Dmytruk, N., Dramsi, S., et al. (2010). The surface protein HvgA mediates group B *Streptococcus* hypervirulence and meningeal tropism in neonates. *J. Exp. Med.* 207, 2313–2322. doi: 10.1084/jem.20092594

Tazi, A., Plainvert, C., Anselem, O., Ballon, M., Marcou, V., Seco, A., et al. (2019). Risk factors for infant colonization by hypervirulent CC17 Group B *Streptococcus*: toward the understanding of late-onset disease. *Clin. Infect. Dis.* 69, 1740–1748. doi: 10.1093/cid/ciz033

Thigpen, M. C., Whitney, C. G., Messonnier, N. E., Zell, E. R., Lynfield, R., Hadler, J. L., et al. (2011). Bacterial meningitis in the United States, 1998–2007. *N. Engl. J. Med.* 364, 2016–2025. doi: 10.1056/NEJMoa1005384

Thomas, L., and Cook, L. (2020). Two-component signal transduction systems in the human pathogen *Streptococcus agalactiae*. *Infect. Immun.* 88:e931-9. doi: 10.1128/IAI.00931-19

Trespidi, G., Scoffone, V. C., Barbieri, G., Marchesini, F., Abualsha'ar, A., Coenye, T., et al. (2021). Antistaphylococcal activity of the FtsZ Inhibitor C109. *Pathogens* 10:886. doi: 10.3390/pathogens10070886

Trespidi, G., Scoffone, V. C., Barbieri, G., Riccardi, G., De Rossi, E., and Buroni, S. (2020). Molecular characterization of the *Burkholderia cenocepacia dcw* operon and FtsZ interactors as new targets for novel antimicrobial design. *Antibiotics* 9:841. doi: 10.3390/antibiotics9120841

van Schaik, W., Château, A., Dillies, M.-A., Coppée, J.-Y., Sonenshein, A. L., and Fouet, A. (2009). The global regulator CodY regulates toxin gene expression in *Bacillus anthracis* and Is required for full virulence. *Infect. Immun.* 77, 4437–4445. doi: 10.1128/IAI.00716-09

Waters, N. R., Samuels, D. J., Behera, R. K., Livny, J., Rhee, K. Y., Sadykov, M. R., et al. (2016). A spectrum of CodY activities drives metabolic reorganization and virulence gene expression in *Staphylococcus aureus*. *Mol. Microbiol.* 101, 495–514. doi: 10.1111/mmi.13404

Willett, N. P., and Morse, G. E. (1966). Long-chain fatty acid inhibition of growth of *Streptococcus agalactiae* in a chemically defined medium. *J. Bacteriol.* 91, 2245–2250. doi: 10.1128/jb.91.6.2245-2250.1966

Young, J. W., Locke, J. C. W., Altinok, A., Rosenfeld, N., Bacarian, T., Swain, P. S., et al. (2011). Measuring single-cell gene expression dynamics in bacteria using fluorescence time-lapse microscopy. *Nat. Protoc.* 7, 80–88. doi: 10.1038/nprot.2011.432

Conflict of Interest: The authors declare that the research was conducted in the absence of any commercial or financial relationships that could be construed as a potential conflict of interest.

Publisher's Note: All claims expressed in this article are solely those of the authors and do not necessarily represent those of their affiliated organizations, or those of the publisher, the editors and the reviewers. Any product that may be evaluated in this article, or claim that may be made by its manufacturer, is not guaranteed or endorsed by the publisher.

Copyright © 2022 Pellegrini, Lentini, Famà, Bonacorsi, Scoffone, Buroni, Trespidi, Postiglione, Sassera, Manai, Pietrocola, Firon, Biondo, Teti, Beninati and Barbieri. This is an open-access article distributed under the terms of the Creative Commons Attribution License (CC BY). The use, distribution or reproduction in other forums is permitted, provided the original author(s) and the copyright owner(s) are credited and that the original publication in this journal is cited, in accordance with accepted academic practice. No use, distribution or reproduction is permitted which does not comply with these terms.

Characterization of the dispirotripiperazine derivative PDSTP as antibiotic adjuvant and antivirulence compound against *Pseudomonas aeruginosa.*

Andrea Bonacorsi,[1¶] Gabriele Trespidi,[1¶] Viola C. Scoffone,[1] Samuele Irudal,[1] Giulia Barbieri,[1] Olga Riabova,[2] Natalia Monakhova,[2] Vadim Makarov,[2] Silvia Buroni.[1*]

[1]Department of Biology and Biotechnology "Lazzaro Spallanzani", University of Pavia, Pavia, Italy.

[2]Research Center of Biotechnology RAS, Moscow, Russia.

*Corresponding author

E-mail: silvia.buroni@unipv.it (SB)

¶These authors contributed equally to this work.

Abstract

Pseudomonas aeruginosa is a major human pathogen, able to establish difficult-to-treat infections in immunocompromised and cystic fibrosis (CF) patients. The high rate of antibiotic treatment failure is due to its notorious drug resistance, often mediated by the formation of persistent biofilms. Alternative strategies, capable of overcoming *P. aeruginosa* resistance, include antivirulence compounds which impair bacterial pathogenesis without exerting a strong selective pressure, besides the use of antimicrobial adjuvants that can resensitize drug-resistant bacteria to specific antibiotics. In this work, the dispirotripiperazine derivative PDSTP, already studied as antiviral, was characterized for its activity against *P. aeruginosa* adhesion to epithelial cells, its antibiotic adjuvant ability and its biofilm inhibitory potential. PDSTP resulted effective in impairing the adhesion of *P. aeruginosa* to various immortalized cell lines. Moreover, the combination of clinically relevant antibiotics with the compound led to a remarkable enhancement of the antibiotic efficacy towards multidrug-resistant CF clinical strains. PDSTP-ceftazidime combination maintained its efficacy *in vivo* in a *Galleria mellonella* infection model. Finally, the compound showed a promising biofilm inhibitory activity at low concentrations when tested both *in vitro* and using an *ex vivo* pig lung model.

Author Summary

The increasing number of deaths caused by infections with antibiotic-resistant bacteria poses a significant threat to global health and implies an urgent need to

45 develop new therapeutics. In this context, the ESKAPE bacterium *Pseudomonas*
46 *aeruginosa* represents a critical pathogen, especially for immunocompromised and
47 cystic fibrosis individuals. Indeed, infections caused by this pathogen are
48 increasingly difficult to treat due to its remarkable ability to rapidly develop
49 resistance towards standard antibiotic treatments. In this work, we investigate the
50 efficacy of the dispirotripiperazine derivative PDSTP as antivirulence compound
51 and antibiotic adjuvant against *P. aeruginosa*. This molecule resulted devoid of
52 antibacterial activity but showed a promising anti-adhesive and anti-biofilm
53 properties, beside a great antibiotic-enhancing efficacy towards antibiotic-resistant
54 clinical strains. Our data describe PDSTP as a compound combining different
55 characteristics that together they will help preventing or successfully treating
56 infections due to antibiotic-resistant *P. aeruginosa*.
57
58

59 Introduction

60 Epidemiological studies have shown that about 1.27 million people died from
61 infections caused by antibiotic-resistant bacteria in 2019 [1], a number that could
62 grow to 10 million by 2050 [2]. Among these threatening bacteria, *Pseudomonas*
63 *aeruginosa* plays an important role, especially when carbapenem-resistant strains
64 are involved. Indeed, this bacterium is listed among the “critical” pathogen by the
65 World Health Organization [3].
66 *P. aeruginosa* is involved in upper and lower airway infections in cystic fibrosis
67 (CF) patients, that ultimately lead to respiratory failure [4]. This is particularly

68 relevant as the prevalence of this pathogen in CF adults can reach 80-90% in some
69 European countries [5]. Also, this bacterium belongs to the ESKAPE pathogens
70 and is generally associated with nosocomial infections characterized by a broad
71 antibiotic resistance [4].
72 Having a large versatile genome, *P. aeruginosa* can adapt to several hostile niches
73 within the human body, being also equipped with many virulence factors [4]. One
74 of the main challenges in the treatment of this pathogen is connected to its ability
75 to form biofilms, generally associated with the establishment of chronic infections
76 difficult to eradicate: it is estimated that bacteria within biofilms can exhibit a 10 to
77 1000-fold increased antibiotic resistance compared to their planktonic form [6].
78 Nowadays, the treatment of *P. aeruginosa* infections primarily involves the
79 administration of ceftazidime, ciprofloxacin, tobramycin and colistin [7]. However,
80 these compounds are becoming ineffective because of intrinsic, acquired and
81 adaptive antibiotic resistance.
82 Given the limited progress in the development of new antibiotics and the threat of
83 infections with emerging antibiotic-resistant strains, there is an urgent need to
84 develop alternative therapeutic strategies, including the repurposing of existing
85 drugs [8, 9]. Among the various approaches, antivirulence strategies are
86 particularly promising due to their ability to impair bacterial pathogenesis, without
87 killing the bacteria, so exerting lower selective pressure and reducing resistance
88 development compared to conventional antibiotics [10]. Moreover, it is worth
89 considering combination therapies which involve the use of existing and novel

antimicrobials with compounds that increase membrane permeability, inhibit efflux pumps or impair signalling pathways connected to antibiotic resistance [11].

PDSTP is a non-toxic dispirotripiperazine-based compound characterized by four quaternary positively charged nitrogen atoms (Fig 1). It has been investigated as antiviral since it impairs viral adsorption to negatively charged heparan-sulphate glycosaminoglycans (HSGAGs) expressed at the surface of human cells by saturating them through electrostatic interactions [12]. In particular, PDSTP exhibits a good antiviral activity *in vitro* when tested on herpes simplex virus type 1 [12] and on human immunodeficiency virus type 1 and 2 [13]. In addition, this compound prevents the death of a herpetic encephalitis mouse model when utilized in combination with acyclovir [14], is more effective compared to acyclovir when used to treat a guinea pig model of genital herpes [15], reduces both corneal lesions and viral infection course in a rabbit model of herpes simplex epithelial keratitis [16] and prevents severe viral pneumonia induced by SARS-CoV-2 in a Syrian hamster infection model [17].

Besides viruses, bacteria have evolved to use HSGAGs as receptors [18]. Specifically, *P. aeruginosa* interacts with HS chains through bacterial adhesins [19]. The probability of this interaction increases when epithelia are injured: for instance, when the respiratory epithelium is damaged, polarized epithelial cells dedifferentiate and increase the expression of HS proteoglycans at their apical surface, promoting bacterial adhesion [20]. In this context, PDSTP may be active not only on viruses, but also on bacteria, preventing their interaction with HSGAGs and, possibly, their adhesion to human cells.

The aim of this work was to investigate the putative anti-adhesive properties of PDSTP on *P. aeruginosa* by adhesion assay and imaging flow cytometry, testing the compound on different human cell lines challenged with *P. aeruginosa* clinical isolates. In addition, antimicrobial combination susceptibility testing and time-killing assays were performed on a panel of *P. aeruginosa* clinical isolates to determine whether PDSTP potentiates the activity of antibiotics currently utilized in clinics. Antibiotic potentiation was then evaluated *in vivo* employing a *Galleria mellonella* infection model. Finally, the ability of the compound to impair biofilm formation was determined both *in vitro* and *ex vivo*.

Results

PDSTP shows a negligible inhibitory effect on *P. aeruginosa* growth

The activity of PDSTP was tested by broth microdilution method in MHB and TSB against the reference strain *P. aeruginosa* PA01 and a panel of 9 *P. aeruginosa* CF clinical isolates [21], showing a negligible effect on their growth (Table 1).

Table 1. Minimum inhibitory concentrations of PDSTP for *P. aeruginosa* PA01 and a panel of 9 *P. aeruginosa* CF clinical isolates in MHB and TSB.

		PA01	BST44	SG2	NN2	NN83	NN84	RP73	RP74	BT2	BT72
MIC (µg/mL)	MHB	64	256	128	64	32	64	512	512	64	32
	TSB	256	512	256	256	128	256	>512	512	256	128

PDSTP impairs *P. aeruginosa* adhesion to human pulmonary epithelial cells

To investigate the putative anti-adhesive properties of PDSTP, adhesion assays were performed by plate counting. The MIC of PDSTP against *P. aeruginosa* PA01 in human cells growth medium corresponded to 64 µg/mL in DMEM and 128 µg/mL in MEM; in fact, bacterial growth was partially affected when adhesion assays were performed at 37°C. Consequently, infected monolayers were incubated at 4°C to prevent bacterial growth during the assay [22], thus completely avoiding the observed growth impairment, even at high concentrations of the compound (data not shown). *P. aeruginosa* PA01 adhesion to the A549 lung epithelial cell line was impaired in a dose-dependent manner when treated with increasing concentrations of PDSTP (from 1 to 400 µg/mL). A statistically significant decrease in bacterial adhesion was already appreciated by treating cells with 10 µg/mL of PDSTP (41.4% reduction compared to the control), while it was almost completely abolished with a treatment of 400 µg/mL (95.9% reduction compared to the control) (Fig 2).

PDSTP (50 µg/mL) also affected the adhesion of *P. aeruginosa* PA01 to the 16HBE (WT-CFTR) and CFBE (ΔF508-CFTR) bronchial cell lines, reducing bacterial adhesion of 60.6 and 54.3%, respectively (Fig 3).

The anti-adhesive properties of PDSTP were then tested against hypermucoid *P. aeruginosa* strains. The activity of PDSTP was analysed on a *P. aeruginosa* clone, specifically BT2 (early isolate) and BT72 (late isolate) strains, isolated from the

155 same CF patient 15 years apart. Interestingly, *P. aeruginosa* BT2 adhered more
156 to A549 cells compared to the BT72 strain (data not shown), a phenotype that has
157 previously been described in longitudinal studies [23]. In this experiment, two
158 concentrations of PDSTP were assayed. As shown in figure 4, *P. aeruginosa* BT2
159 adhesion was 22.5 and 7.5% that of the control when treated with 50 and 200
160 µg/mL of the compound, respectively. On the other hand, 50 µg/mL of PDSTP
161 were not able to affect *P. aeruginosa* BT72 adhesion, but increasing the compound
162 to 200 µg/mL caused a reduction of 65.8% in bacterial adhesion compared to the
163 control (Fig 4).
164 Heparin is a structural analogue of heparan-sulphates [24]. Since PDSTP binds to
165 heparan-sulphates [12], an excess of heparin should scavenge the compound,
166 allowing bacteria to interact with HSGAGs and consequently to adhere to human
167 cells. To test this hypothesis, A549 cell monolayers were treated with PDSTP (50
168 µg/mL), heparin (50 µg/mL) and an equal combination of these two compounds
169 (50 µg/mL each). As a result, heparin alone did not impair *P. aeruginosa* PA01
170 adhesion to human cells, while the combination of PDSTP and heparin re-
171 established the normal adhesive properties of the bacterium to the A549 cell line
172 (Fig 5).
173 To validate these results, adhesion was quantified by imaging flow cytometry.
174 GFP-expressing *P. aeruginosa* PA01 adhesion to the A549 cell line showed a
175 reduction of 68% when treated with 50 µg/mL of PDSTP, compared to the control
176 (Fig 6). This is consistent with the adhesion reduction reported in figure 2 using the
177 same concentration of the compound (66% reduction).

178 Imaging flow cytometry can also provide a software-based analysis of the
179 fluorescent spots within single-cell images (S1 Fig), allowing a more detailed
180 characterization of the PDSTP anti-adhesive effect. The number of adhered GFP-
181 expressing *P. aeruginosa* PA01 bacteria for each A549 cell was counted and data
182 were represented in terms of number of events, i.e., the number of human cells
183 with 1, 2-3, 4-6 or more than 7 adhered bacteria, on 10.000 acquisition (S2 Fig).
184 As shown in figure 7A, most of the control human cells interacted with only one
185 bacterium, while the number of events involving a larger number of bacteria
186 decreased proportionally. The same pattern was observed in samples treated with
187 50 µg/mL of PDSTP, but with fewer events due to impaired bacterial adhesion.
188 Interestingly, when the numbers of events were normalized on the total number of
189 cells with adhered bacteria, it was evident that PDSTP especially affected multiple
190 bacterial adhesion (Fig 7B).
191

192 PDSTP potentiates the activity of antibiotics currently
193 used in clinics

194 Combination therapy involves the combination of antibiotics with compounds that
195 increase their intracellular concentration or allow to overcome antibiotic resistance
196 [11]. To determine whether PDSTP could potentiate the activity of antibiotics
197 currently used to treat *P. aeruginosa* infections, antibiotic combination
198 susceptibility tests were performed. Antibiotics with different mechanisms of action
199 were chosen, specifically amikacin, ceftazidime, ciprofloxacin, colistin,
200 meropenem and tobramycin. This panel of antibiotics was combined with PDSTP

and tested against *P. aeruginosa* PA01. Specifically, PDSTP was used at a concentration of 25 µg/mL, which corresponds to about half of the MIC in MHB (Table 1).

As reported in Table 2, the MICs of the tested antibiotics showed a reduction ranging from 2 to 128-fold when combined with PDSTP. In particular, the presence of PDSTP did not cause a great increase in tobramycin efficacy (2-fold decrease in the MIC), while for all the other antimicrobials, especially for ceftazidime (128-fold decrease in the MIC), an adjuvant effect was observed.

Table 2. Minimum inhibitory concentrations in MHB of a panel of antibiotics and those of their combinations with PDSTP against *P. aeruginosa* PA01 and respective fold reduction.

***P. aeruginosa* PA01**	**Susceptible (S)**	**Intermediate (I)**	**Resistant (R)**	**MIC**	**MIC antibiotic + PDSTP**	**Fold reduction**
Amikacin	≤ 16 µg/mL	32 µg/mL	≥ 64 µg/mL	4 µg/mL (S)	1 µg/mL (S)	4x
Tobramycin	≤ 4 µg/mL	8 µg/mL	≥ 16 µg/mL	0.5 µg/mL (S)	0.25 µg/mL (S)	2x
Ceftazidime	≤ 8 µg/mL	16 µg/mL	≥ 32 µg/mL	2 µg/mL (S)	0.0156 µg/mL (S)	128x
Meropenem	≤ 2 µg/mL	4 µg/mL	≥ 8 µg/mL	1 µg/mL (S)	0.0625 µg/mL (S)	16x
Ciprofloxacin	≤ 0.5 µg/mL	1 µg/mL	≥ 2 µg/mL	0.125 µg/mL (S)	0.0078 µg/mL (S)	16x
Colistin	-	≤ 2 µg/mL	≥ 4 µg/mL	1 µg/mL (I)	0.0625 µg/mL (S)	16x

213 MIC breakpoints used to categorize *P. aeruginosa* as susceptible, intermediate or resistant to
214 antibiotics are shown. Susceptible (S), intermediate (I) and resistant (R) antibiotic profile are
215 indicated below the respective MIC value.
216
217 Subsequently, combination efficacy was tested on multidrug-resistant *P.*
218 *aeruginosa* CF clinical strains (BST44, SG2, NN2, NN83, NN84, RP73, RP74, BT2
219 and BT72) only for those antibiotics that showed, according to the Clinical and
220 Laboratory Standard Institute (CLSI) guidelines [25], an intermediate or resistant
221 profile (Table 3). Also in this case, the concentration of PDSTP in the combination
222 was around half of the MIC determined for each bacterium in MHB (Table 1), i.e.,
223 100 µg/mL for BST44, 50 µg/mL for SG2, 25 µg/mL for NN2,15 µg/mL for NN83,
224 25 µg/mL for NN84, 200 µg/mL for RP73 and 200 µg/mL for RP74. As indicated in
225 Table 3, there was an overall increased activity when antibiotics were combined
226 with PDSTP.
227
228
229
230
231
232
233
234

Table 3. Minimum inhibitory concentrations in MHB of a panel of antibiotics and of their combinations with PDSTP against *P. aeruginosa* CF clinical isolates, along with the respective fold reduction.

		BST44	SG2	NN2	NN83	NN84	RP73	RP74
Amikacin	**MIC**		64 µg/mL (R)	32 µg/mL (I)	256 µg/mL (R)	32 µg/mL (I)	64 µg/mL (R)	32 µg/mL (I)
	MIC antibiotic + PDSTP		16 µg/mL (S)	16 µg/mL (S)	128 µg/mL (R)	16 µg/mL (S)	32 µg/mL (I)	16 µg/mL (S)
	Fold reduction		4x	2x	2x	2x	2x	2x
Tobramycin	**MIC**		8 µg/mL (I)	>256 µg/mL (R)	>256 µg/mL (R)			
	MIC antibiotic + PDSTP		4 µg/mL (S)	>256 µg/mL (R)	>256 µg/mL (R)			
	Fold reduction		2x					
Ceftazidime	**MIC**	16 µg/mL (I)	128 µg/mL (R)	16 µg/mL (I)	32 µg/mL (R)	16 µg/mL (I)	32 µg/mL (R)	128 µg/mL (R)
	MIC antibiotic + PDSTP	1 µg/mL (S)	2 µg/mL (S)	0.125 µg/mL (S)	4 µg/mL (S)	0.5 µg/mL (S)	4 µg/mL (S)	32 µg/mL (R)
	Fold reduction	16x	64x	128x	8x	32x	8x	4x
Meropenem	**MIC**	16 µg/mL (R)				32 µg/mL (R)	16 µg/mL (R)	16 µg/mL (R)
	MIC antibiotic + PDSTP	1 µg/mL (S)				1 µg/mL (S)	1 µg/mL (S)	2 µg/mL (S)
	Fold reduction	16x				32x	16x	8x
Ciprofloxacin	**MIC**					4 µg/mL (R)		16 µg/mL (R)
	MIC antibiotic + PDSTP					2 µg/mL (R)		8 µg/mL (R)
	Fold reduction					2x		2x

238 Susceptible (S), intermediate (I) and resistant (R) antibiotic profile are indicated below the
239 respective MIC value.
240
241 Only for tobramycin and ciprofloxacin, MIC reduction did not exceed 2-fold for each
242 strain, while amikacin MIC decreased 4-fold only against SG2 strain (Table 3). As
243 reported for PA01 strain, the combination with ceftazidime showed the most
244 remarkable effect, leading to a significant reduction in the MICs of all isolates, up
245 to 128-fold (Table 3). Moreover, meropenem confirmed the promising activity of
246 PDSTP-β-lactam combination, being its efficacy significantly increased in each
247 strain tested, up to 32-fold (Table 3). Generally, all the clinical isolates tested
248 showed resistance to at least two antibiotics. Two strains were even resistant to
249 four antimicrobials (NN84 and RP74). In most cases, PDSTP was able to
250 resensitize the clinical isolates showing a resistant antibiotic profile, especially to
251 meropenem (4/4 strains), ceftazidime (6/7 strains) and amikacin (4/6 strains), while
252 one strain was only partially resensitized, i.e., from resistant to intermediate
253 antibiotic profile (Table 3).
254 To better characterize the activity of the combinations, *P. aeruginosa* PA01 time-
255 killing assays in TSB were performed. As reported in figure 8, combination of
256 tobramycin (1 µg/mL), ciprofloxacin (0.0625 µg/mL), ceftazidime (1 µg/mL) and
257 colistin (1 µg/mL), at a concentration equivalent to half of the respective MIC in
258 TSB (data not shown), with either 50 or 200 µg/mL of PDSTP, showed a significant
259 reduction in bacterial viability respect to the best treatment with the only antibiotic
260 or PDSTP, especially during the first hours of treatment. As expected,
261 combinations with 200 µg/mL of PDSTP had a greater activity compared to those

262 with 50 µg/mL. In particular, combination of tobramycin with 50 and 200 µg/mL of
263 PDSTP (Fig 8A) showed a bacterial viability reduction up to 3.48 and 4.45 log_{10} in
264 the CFU/mL. On the other hand, 50 and 200 µg/mL of the PDSTP combined with
265 ciprofloxacin (Fig 8B) reduced bacterial viability up to 2.78 and 4.54 logs,
266 respectively. Since reductions in the CFU/mL after 5 hours of treatment were
267 greater than 2 log_{10} compared to the respective most active compound,
268 combinations were defined as synergistic at the lowest tested concentration of
269 PDSTP. On the other hand, combination of PDSTP with either ceftazidime (Fig
270 8C) and colistin (Fig 8D) did not show synergy (up to 0.72/1.89 log_{10} CFU/mL
271 reduction for ceftazidime and 1.43/1.42 log_{10} CFU/mL reduction for colistin).
272 Interestingly, with the administration of 50 µg/mL of PDSTP in combination with
273 the antibiotics, bacterial viability after 24 hours was comparable with the control
274 growth for tobramycin, ciprofloxacin and colistin, and with the antibiotic treatment
275 alone for ceftazidime. In contrast, when antimicrobials were combined with 200
276 µg/mL of PDSTP, the number of CFU/mL after 24 hours was, for each antibiotic
277 but colistin, significantly lower compared to the other conditions, especially for
278 ceftazidime (Fig 8).
279 To confirm the results obtained with PA01 strain, the efficacy of the same PDSTP-
280 antibiotic combinations was also tested against the 9 *P. aeruginosa* CF clinical
281 isolates by time-killing assays in TSB using a plate reader. In this case, considering
282 the fair correlation between CFU reduction and the OD_{600} variations seen in time-
283 killing experiments with PA01 strain (S3 Fig), bacterial growth was monitored for
284 24 hours by measuring the OD_{600}. The concentrations of PDSTP and antibiotic

285 employed differ for each strain (Tables 4-7) since they were chosen to avoid the
286 complete inhibition of the growth with the monotherapy. With a few exceptions,
287 these concentrations corresponded to about half of the MIC value of ceftazidime,
288 tobramycin and ciprofloxacin, while the concentrations of colistin were equal to the
289 MIC (S1 Table). In this assay, bacterial growth was considered completely
290 inhibited after the treatment when the increase in OD_{600} did not exceed 0.3.
291 In general, combination therapies caused a significant inhibition of the bacterial
292 growth, although this was not the case for RP73 and RP74 strains, against which
293 PDSTP was unable to synergize with any of the four antibiotics (Tables 4-7, S4-
294 S7 Figs) and so they were considered resistant to the PDSTP antibiotic-enhancing
295 activity under these experimental conditions.
296
297 **Table 4.** Efficacy of the PDSTP-ceftazidime combination treatment against 9 *P.*
298 *aeruginosa* CF clinical strains, expressed in hours of bacterial growth inhibition.

	BST44	SG2	NN2	NN83	NN84	RP73	RP74	BT2	BT72
Ceftazidime (µg/mL)	4	32	2	8	12	16	32	1	0.5
PDSTP (µg/mL)	200	200	200	100	200	200	200	200	150
Growth inhibition (hours)	24	24	24	24	24	None	None	24	24

299
300
301
302

Table 5. Efficacy of the PDSTP-tobramycin combination treatment against 9 *P. aeruginosa* CF clinical strains, expressed in hours of bacterial growth inhibition.

	BST44	SG2	NN2	NN83	NN84	RP73	RP74	BT2	BT72
Tobramycin (µg/mL)	2	16	32	32	8	8	1	0.75	4
PDSTP (µg/mL)	200	200	200	100	200	200	200	200	150
Growth inhibition (hours)	6	24	None	None	24	None	None	24	24

Table 6. Efficacy of the PDSTP-ciprofloxacin combination treatment against 9 *P. aeruginosa* CF clinical strains, expressed in hours of bacterial growth inhibition.

	BST44	SG2	NN2	NN83	NN84	RP73	RP74	BT2	BT72
Ciprofloxacin (µg/mL)	0.0156	0.125	0.25	0.25	2	0.25	1	0.0312	0.0312
PDSTP (µg/mL)	200	200	200	100	200	200	200	200	150
Growth inhibition (hours)	24*	24*	24	24*	24	None	None	24	24

* OD_{600} of the combination treatment remained stably lower than the other conditions for 24h but a modest increase of the OD_{600} occurred within the first hours of treatment.

Table 7. Efficacy of the PDSTP-colistin combination treatment against 9 *P. aeruginosa* CF clinical strains, expressed in hours of bacterial growth inhibition.

	BST44	SG2	NN2	NN83	NN84	RP73	RP74	BT2	BT72
Colistin (µg/mL)	2	0.125	0.5	1	2	2	0.0625	2	1
PDSTP (µg/mL)	200	200	200	100	200	200	200	200	150
Growth inhibition (hours)	12	None	10	12	24	None	None	10	10

The most promising results were obtained with the PDSTP-ceftazidime combination. Indeed, this combination induced complete inhibition of bacterial growth for 24 hours for each *P. aeruginosa* strain, including the highly resistant SG2 strain (Table 4, S4 Fig). Instead, the combination with tobramycin showed a more variable efficacy, resulting in a 24 hours growth inhibition of SG2, NN84, BT2 and BT72 strains, and only a 6 hours inhibition for the BST44 strain (Table 5, S5 Fig). Moreover, PDSTP could not revert the tobramycin resistant phenotype of NN2 and NN83 strains (Table 5), as already highlighted by antibiotic combination susceptibility testing (Table 3, S5 Fig). PDSTP-ciprofloxacin combination showed a long-term inhibitory effect against each strain, although a complete growth inhibition was observed only for NN2, NN84, BT2 and BT72 (Table 6, S6 Fig). Finally, as reported for PA01, colistin resulted the least effective antibiotic against *P. aeruginosa*. Indeed, even using a concentration equal to the MIC, its combination with PDSTP led to a long-term inhibition only against NN84 strain, while a 10 hours inhibition was observed for BST44, NN2, NN83, BT2 and BT72 (Table 7, S7 Fig). SG2 strain was insensitive to this combination (Table 7, S7 Fig). Overall, time-killing assays confirmed the results obtained by antibiotic combination susceptibility testing, validating the efficacy of PDSTP as enhancer of the activity of different classes of clinically relevant antibiotics against *P. aeruginosa*.

PDSTP increases ceftazidime efficacy *in vivo*

337 The *in vitro* efficacy of the PDSTP-ceftazidime combination was validated *in vivo*
338 by *Galleria mellonella* infection experiments. Ceftazidime (5 mg/kg) and PDSTP
339 (6.25 mg/kg) concentrations employed in this assay resulted non-toxic to *G.*
340 *mellonella* (data not shown). Infection with 10^4 CFU of *P. aeruginosa* PA01 caused
341 100% larval mortality in the non-treated (data not shown), physiological saline and
342 PDSTP treated groups (Fig 9) 24 hours post-inoculation. On the contrary,
343 treatment with ceftazidime alone resulted in 25% survival after 48 hours. Of note,
344 the combination treatment with PDSTP gave a statistically significant increase in
345 larval viability compared with the antibiotic alone up to 47% at 48 hours (Fig 9).
346 This confirms the *in vitro* activity observed for the PDSTP-ceftazidime combination.
347

348 PDSTP inhibits biofilm formation *in vitro* and in an *ex vivo* 349 pig lung model

350 To evaluate whether PDSTP affects biofilm formation of *P. aeruginosa* PA01 and
351 two clinical isolates, *in vitro* biofilm inhibition assays were performed in TSB. PA01,
352 NN2 and SG2 strains were employed due to their differences in biofilm formation
353 abilities. First, crystal violet assays showed that 50 µg/mL of PDSTP (or 25 µg/mL
354 for SG2 since 50 µg/mL inhibited the growth in the experimental conditions
355 described in Materials and Methods) significantly decreased the quantity of biofilm
356 formed after 24 hours compared to the respective untreated controls (Fig 10A).
357 PDSTP antibiofilm activity was then evaluated using confocal laser scanning
358 microscopy (CLSM). In particular, PA01 strain formed a thick and homogeneous
359 biofilm. Compared to PA01, NN2 biofilm was thicker, while that of SG2 was more

heterogeneous and characterized by bacterial aggregates (Fig 10B). For all the strains, PDSTP impaired biofilm formation, i.e. the quantity of biofilm was visibly decreased and SG2 biofilm was less structured (Fig 10B). Subsequent COMSTAT2 analysis showed that the compound significantly reduced both the average biofilm thickness and biomass (Figs 10C and D), while it significantly increases the roughness, an indicator of altered biofilm structure (Fig 10E).

To validate PDSTP antibiofilm activity, an *ex vivo* pig lung (EVPL) tissue model, embedded in synthetic cystic fibrosis medium (SCFM) [26] to further mimic the CF lung environment, was employed. The pig lung structure and immunology resemble those of humans, making this model particularly relevant. Similarly to the previous analyses, biofilm formation was impaired by the compound for all the strains. Indeed, the numbers of CFU/mL recovered from biofilms were significantly lower when treated with PDSTP, compared to untreated controls. CFU/mL reduction was similar to that of ciprofloxacin treatment (0.06 µg/mL), used as positive control (Fig 11A). Finally, CLSM was used to visualize *P. aeruginosa* PA01 biofilm, stained with Syto9, on lung tissue fragments. Also in this case, PDSTP (50 µg/mL) impaired biofilm formation (Fig 11B), while COMSTAT2 analysis showed the significant reduction in biofilm biomass due to PDSTP treatment, compared to the control, which is in line with ciprofloxacin (0.06 µg/mL) treatment (Fig 11C).

Discussion

The antiviral dispirotripiperazine-based compound PDSTP was tested *in vitro* against *P. aeruginosa* PA01 adhesion on different pulmonary epithelial cell lines,

383 including a CF cell line, resulting effective at very low concentrations. Noteworthy,
384 these concentrations are more than 50 times lower than the 50% cytotoxic
385 concentration [12]. PDSTP anti-adhesive activity was maintained also when tested
386 against hypermucoid *P. aeruginosa* BT2 and BT72 clinical isolates, although a
387 higher concentration was required to impair the adhesion of BT72. This difference
388 may be attributed to their distinct levels of interaction with human cells.
389 A preliminary study of the mechanism involved in PDSTP impairment of bacterial
390 adhesion was carried out analysing PA01 strain adhesion by imaging flow
391 cytometry. Interestingly, PDSTP treatment particularly affected the adhesion of
392 multiple bacteria to human cells, probably reducing the accessibility of the human
393 cell surface receptors to bacteria. Indeed, the presence of heparin in adhesion
394 experiments re-established the normal adhesive capabilities of PA01 strain by
395 scavenging PDSTP. This result highlights the high affinity of the compound
396 towards HSGAGs and a possible involvement of these surface receptors in PDSTP
397 anti-adhesive activity as in the case of viral adsorption. Further studies are ongoing
398 in our laboratory to clarify this molecular mechanism.
399 Considering the current research on anti-adhesive molecules against *P.*
400 *aeruginosa*, PDSTP shows some advantages compared to other approaches such
401 as natural extracts [27, 28] and glycoclusters [29]. Indeed, PDSTP has been
402 extensively tested *in vivo* as antiviral, showing to be non-cytotoxic, effective at low
403 concentrations and characterized by a broad therapeutic index. On the contrary,
404 natural extracts and glycoclusters generally require very high concentrations to be
405 effective *in vitro*, often in the range of mg/mL, which limits their use *in vivo*.

406 Moreover, by targeting HSGAGs on cell surface, PDSTP shows a novel anti-
407 adhesive mechanism, different from the inhibition of the lectin-glycan interaction
408 exerted by glycoclusters [30]. It is worth noting that the compound may have broad-
409 spectrum anti-adhesive properties since other relevant pathogens adhere to
410 HSGAGs, including *Mycobacterium tuberculosis*, Gram-positive streptococci and
411 species belonging to ESKAPE group [18].
412 By determining the MIC against PA01 and different CF strains, the compound
413 showed a low inherent antimicrobial activity with strain-specific susceptibilities.
414 These differences are probably due to modifications of the molecular target which
415 is likely localized on the bacterial surface. This hypothesis is supported by the high
416 molecular weight of the compound, which prevents its diffusion *via* porins, as well
417 as its high polarity, which makes its entry across the lipid bilayer unlikely [31]. A
418 differential effect of PDSTP was also found when MICs were determined using
419 different microbial culture media, with a systematic increase in the MIC values in
420 TSB compared to MHB. A similar culture medium-dependent activity was already
421 reported for aminoglycosides which showed a decreased efficacy in media with
422 high ionic strength, such as TSB. In fact, salt interferes with the electrostatic
423 interactions between aminoglycosides and components of the outer membrane
424 surface that mediate antibiotic uptake [32]. Being the positively charged nitrogen
425 atoms of PDSTP the mediators of the antiviral activity of dispirotripiperazines [33],
426 it is plausible to hypothesize that these charges may also play a role in this specific
427 biological activity.

The slight inhibitory effect on bacterial growth showed by PDSTP is a peculiar characteristic of antibiotic adjuvants [34]. The PDSTP adjuvant activity was proven against the *P. aeruginosa* PA01 and a panel of multidrug-resistant CF isolates, showing an overall increase in the efficacy of the tested antibiotics. Specifically, β-lactams showed the highest MIC fold reduction and a durable efficacy of the combination over time for most strains. Aminoglycosides and ciprofloxacin, instead, had a great efficacy in combination with PDSTP, particularly during the first hours of treatment, but with a narrower spectrum of activity. Finally, PDSTP-colistin combination had the least durable inhibitory effect on bacterial growth. The PDSTP efficacy profile as antibiotic adjuvant against *P. aeruginosa* can be compared with that of natural polyamines. Indeed, these molecules significantly decreased the MIC of many β-lactams and other low molecular weight antibiotics against *P. aeruginosa*, although only at high concentrations [35]. The mechanism of action of these molecules was characterized in optimized spermine derivatives, demonstrating to be mediated by inhibition of efflux pumps and increased permeability of the outer membrane [36, 37]. Given the similarities in the spectrum of activity of spermine and PDSTP, besides being both characterized by reactive positively charged nitrogens [33, 38], it is plausible to speculate that PDSTP may share a similar mechanism of action against *P. aeruginosa*. We are currently performing experiments to verify this hypothesis. In addition to the promising results obtained, the importance of developing PDSTP as adjuvant compound is also underlined by its uncommon efficacy against this extremely drug-resistant

pathogen. In fact, many adjuvants show a limited synergy with the antibiotics against *P. aeruginosa* [39-42].

To validate the *in vitro* results, antibiotic potentiation was evaluated using a *Galleria mellonella* infection model, showing that PDSTP enhanced ceftazidime activity and highlighting its translational potential *in vivo*. To establish the most appropriate administration protocol in mammals, further investigations with murine infection models are necessary, allowing to test multiple administration of the adjuvant, an option not available in *G. mellonella*.

The ability to form biofilm is a major virulence factor in *P. aeruginosa* and new molecules able to impair its formation are highly desirable, thus PDSTP biofilm inhibitory potential was assessed. Using different *in vitro* models, PDSTP was demonstrated to significantly decrease biofilm formation at sub-inhibitory concentrations. Confocal microscopy analysis allowed the visualization of the biofilm perturbation in the presence of the compound, highlighting a substantial decrease in the average biofilm thickness and biomass, besides an overall alteration of the structure. Furthermore, PDSTP efficacy was validated in an *ex vivo* pig lung biofilm model, essentially confirming its efficacy as biofilm inhibitor and showing an activity comparable with the antibiotic ciprofloxacin. The coherence in the results obtained against strains showing macroscopic structural differences in their biofilms suggests that PDSTP impairs biofilm formation by targeting an essential mechanism shared by different *P. aeruginosa* strains. In particular, since the compound is added only after the initial adhesion to the surface, it probably affects bacterial aggregation. Indeed, PDSTP could interact

473 with bacterial surface, as hypothesized for its bacterial growth inhibitory activity,
474 and disrupt the cell-cell interaction fundamental for this process. This putative
475 mechanism of action is unique among the currently reported biofilm inhibitors that
476 mainly act as quorum-sensing inhibitors [37, 43, 44], competitors of the lectin
477 binding [45] or repressors of exopolysaccharide production [46].
478 To conclude, PDSTP showed a remarkable spectrum of activities against *P.*
479 *aeruginosa*, being effective in inhibiting bacterial adhesion to epithelial cells,
480 increasing antibiotic efficacy and impairing biofilm formation. In light of these
481 results, the combined antivirulence and antibiotic potentiation properties of PDSTP
482 may help addressing the emerging threat of multidrug-resistant bacterial
483 infections.
484

485 Materials and Methods

486 Bacterial strains, human pulmonary epithelial cell
487 cultures, growth conditions, antibiotics and compounds

488 The *P. aeruginosa* reference strain PA01 (laboratory collection) and 9 *P.*
489 *aeruginosa* CF clinical isolates (BST44, SG2, NN2, NN83, NN84, RP73, RP74,
490 BT2 and BT72) [21] were grown in tryptic soy broth (TSB; BD) or cation-adjusted
491 Mueller-Hinton broth (MHB; BD) at 37°C. The synthetic cystic fibrosis sputum
492 medium (SCFM) was prepared with 0.1% casamino acids [47].
493 PDSTP, short for 3,3'-(2-methyl-5-nitropyrimidine-4,6-diyl)bis-3,12-diaza-6,9-
494 diazonia-dispiro[5.2.5.2]hexadecane tetrachloride dihydrochloride nonahydrate,

was synthesized at the Research Centre of Biotechnology RAS (Moscow, Russia) as described previously [12] and its purity was determined by high-performance liquid chromatography analysis (S8 Fig).

Tested antibiotics were amikacin (Sigma-Aldrich), ceftazidime (Sigma-Aldrich), ciprofloxacin (Sigma-Aldrich), colistin (Sigma-Aldrich), meropenem (Venus Pharma GmbH) and tobramycin (Sigma-Aldrich); ciprofloxacin was dissolved in 0.1N NaOH, while the other antibiotics were dissolved in water. PDSTP and heparin (Sigma-Aldrich) were dissolved in water.

Human pulmonary epithelial cell cultures

Human pulmonary epithelial cells were routinely cultured in 75 cm^2 flasks either in Dulbecco's modified Eagle's medium (DMEM; Euroclone) supplemented with 10% foetal bovine serum (FBS; Euroclone), 0.1 mM MEM non-essential amino acids (Euroclone), 100 U/mL penicillin and 0.1 mg/mL streptomycin (Euroclone) or minimal essential medium (MEM; Euroclone) supplemented with 10% FBS, 2 mM glutamine (Euroclone), 100 U/mL penicillin and 0.1 mg/mL streptomycin, at 37°C in 5% CO_2. Specifically, A549 cells [48] were cultured in DMEM, while 16HBE14o- [49] and CFBE41o-, carrying the biallelic ΔF508 mutation [50], were grown in MEM.

Quantification of the adhesion to epithelial cells

Quantification of the adhesion by plate counting

518 Adhesion assays by plating adhered bacteria were performed as previously
519 described [22], with appropriate modifications. Briefly, 1.5 x 10^5 cells per well were
520 seeded in 24-well tissue culture plates and cultured in medium without antibiotics
521 for 48 hours. Two-day old confluent monolayers were infected with bacteria
522 collected during the mid-log phase of growth and resuspended in medium without
523 antibiotics at a multiplicity of infection (MOI) of 10 bacteria per human cell. At the
524 time of the infection, PDSTP and/or heparin were added at the desired
525 concentration in duplicate, while two wells were not treated (control wells). After 2
526 hours of incubation at 4°C, cell monolayers were gently washed three times with
527 phosphate-buffered saline (PBS; Sigma-Aldrich) to remove non-adherent bacteria,
528 lysed with 1% Triton (Riedel-de Haën) and appropriate dilutions of the cell lysates
529 were plated to enumerate adhered bacteria. The percentage of bacterial adhesion
530 to human cells was calculated as:

531 $$\frac{Number\ of\ CFUs\ of\ adhered\ bacteria}{Number\ of\ CFUs\ of\ inoculated\ bacteria}\ x\ 100$$

532 The percentage of bacterial adhesion was then normalized on the untreated
533 sample, set at 100%.

534

535 **Quantification of the adhesion by ImageStream Flow Cytometry**
536 **analysis**

537 After incubating the infected monolayers (MOI = 100) with an isogenic *P.*
538 *aeruginosa* PA01 strain constitutively expressing GFP [51] for 2 hours at 4°C and
539 washing them four times with ice-cold PBS to remove non-adherent bacteria,
540 quantification of the adhesion by ImageStream Flow Cytometry was performed as

follows. Human cells were gently detached from the 24-well tissue culture plate with a cell scraper, washed by centrifugation at 4°C with 1 mL of Dulbecco's PBS (Sigma-Aldrich) and resuspended in 50 µL of the same buffer to obtain a final concentration of 2 x 10^7 cells/mL. Samples were kept on ice until the analysis at the Amnis ImageStreamX MkII instrument (Cytek).

For each sample, 10.000 events were acquired at 40X magnification (NA = 0.75; core size = 10 µm) with 488 nm laser excitation (100 mW). Brightfield images were collected in channel 4, cell-bacteria complexes in channel 2 (480-560 nm channel width, 528/65 bandpass) and channel 6 (745-800 nm width, 762/35 bandpass) was used for scatterplot (SSC) detection. Sheath fluid without Mg^{2+} and Ca^{2+} (D-PBS, ThermoFisher) was used in all measurements.

Acquisition was performed by Inspire software (Amnis, version 1.3) with the following gating strategy: focused cells linear gate G1 (GradientRMS_Ch04) and selecting single cells square gate G2 (AspectRatio_Ch04/Area_Ch04).

Data analysis was made using Amnis IDEAS software (version 6.2): focused cells gate ("GradientRMS_Ch04" feature), single cells gate ("AspectRatio_Ch04"/"Area_Ch04" features) and finally the custom "BactCount" features were applied for quantification (S6 Fig). "BactCount" feature was created as follows: a custom "BactCount" mask was created (PeakM02,Ch02,Bright24.5) and the "SpotCount" feature was applied on this mask.

Minimum inhibitory concentration (MIC) determination of the PDSTP-antibiotic combinations

564 The MICs of the antibiotics alone and in combination with PDSTP were determined
565 in MHB using the broth microdilution method, according to the EUCAST guidelines
566 [52]. Two-fold serial dilutions of antibiotics were prepared into a U-bottom 96-well
567 plate. Bacteria were collected during the mid-log phase of growth and diluted to
568 have about 5 x 10^5 CFU/mL. The culture was split in two subcultures and PDSTP
569 was added to one of them. Subcultures were inoculated into the 96-well plate
570 which was then incubated at 37°C for 24 hours. After the incubation, 30 µL of
571 0.01% resazurin (Sigma-Aldrich) were added to each well and the plate was further
572 incubated at 37°C for 4 hours. Blue to purple resazurin is reduced to pink resorufin
573 by aerobic respiration of metabolically active bacterial cells, allowing visual
574 determination of the MICs.

575

576 Time-killing assays

577 Time-killing assay by plate counting

578 Time-killing assays were performed in TSB to evaluate the activity of PDSTP in
579 combination with different antibiotics against *P. aeruginosa* PA01 overtime, using
580 the broth microdilution method [53]. An overnight liquid bacterial culture was
581 diluted 1:100 and incubated as a shaking culture (200 rpm) at 37°C. Bacterial
582 growth was followed by monitoring the OD_{600} and, once the culture reached an
583 optical density of 0.35 (corresponding to about 1 x 10^8 CFU/mL), it was divided into
584 four subcultures. One subculture was not treated (control), the second one was
585 supplemented with sub-inhibitory concentrations of PDSTP, the antibiotic was
586 added to the third subculture at a concentration equivalent to a half of the MIC,

and the last one was treated with both PDSTP and the antibiotic. Subcultures were further incubated under the same conditions. At each time point (0, 1, 2, 3, 4, 5 and 24 hours), the OD_{600} was measured and bacterial viable count was evaluated by plating appropriate dilutions of the collected aliquots to calculate the respective number of CFU/mL.

Synergy was defined as a ≥ 2 $\log_{10}$ decrease in the CFU/mL of the culture treated with the antibiotic-PDSTP combination after 5 hours compared with its most active component [54].

High-throughput time-killing assay using the plate reader

The time-killing assay experimental procedure was modified, obtaining a high-throughput protocol to test the activity of PDSTP combinations with antibiotics against the CF clinical isolates at once. Overnight bacterial cultures were diluted 1:100 in TSB and incubated as shaking cultures (200 rpm) at 37°C, until an OD_{600} of 0.35 was reached. 200 µL/well of bacterial cultures were transferred into a U-bottom 96-well plate and supplemented with sub-inhibitory concentrations of PDSTP, antibiotic or their combination, in duplicate. One well was left untreated as growth control. Assays were carried out using a CLARIOstar microplate reader (BMG Labtech), measuring the OD_{600} of the cultures every 15 minutes for 24 hours at 37°C. To perform these experiments, a custom plate mode program was set up, including 90 cycles with shaking for 900 seconds (orbital shaking at 300 rpm, with 3 mm of diameter) before each reading, to increase the oxygenation and maintain bacteria in suspension.

Analysis of the PDSTP-antibiotic combination *in vivo*

Combination therapy of PDSTP and ceftazidime was tested *in vivo* by *G. mellonella* infection experiments [55]. Larvae were purchased from a local provider in Pavia and grouped in petri dishes (at least 10 larvae/group) according to their weight. Subsequently, inoculation with a lethal dose (10^4 CFU) of mid-exponential phase *P. aeruginosa* PA01, or physiological saline (control), was carried out with an injection volume of 10 µL. After 2 hours of incubation at 30°C in the dark, mock and PA01 infected larvae were administered with 10 µL of physiological saline (control), ceftazidime (5 mg/kg), PDSTP (6.25 mg/kg) or a combination of ceftazidime (5mg/kg) and PDSTP (6.25 mg/kg), and re-incubated in the same conditions for 3 days. Larval viability was registered after 24, 48 and 72 hours, considering the lack of movement after tactile stimulus, suggestive of larval death. Data from four independent experiments were analysed using log-rank (Mantell-Cox) test.

In vitro biofilm inhibition assays

Biofilm inhibition assay using crystal violet staining

The biofilm inhibitory activity of PDSTP was tested on *P. aeruginosa* strains using the crystal violet staining method [56]. An overnight bacterial culture in TSB was diluted to an OD_{600} of about 0.05 (corresponding to approximately 1×10^8 CFU/mL) in fresh medium. 200 µL of the culture were inoculated into the microtiter plate and

632 incubated for 2 hours at 37°C. After the incubation, the supernatant was removed
633 and replaced with 200 µL of fresh medium with or without 50 µg/mL of PDSTP.
634 The plate was further incubated for 20 hours at 37 °C. Biofilm biomass was then
635 quantified by crystal violet staining.
636

637 **Biofilm inhibition assay using confocal laser scanning**
638 **microscopy**

639 For the confocal laser scanning microscopy biofilm visualization, an overnight
640 bacterial culture in TSB was diluted to an OD_{600} of about 0.05 in fresh medium.
641 The bacterial suspension was inoculated into the four-well chambered coverslip µ-
642 Slide Glass Bottom (Ibidi) for 2 hours at 37 °C. After the incubation, the supernatant
643 was removed and replaced with fresh TSB medium with or without 25-50 µg/mL of
644 PDSTP. After overnight incubation, the medium was removed, biofilms were
645 washed twice with PBS and stained with Syto 9 (Invitrogen) at a final concentration
646 of 1 µM. Samples were visualized with a Leica TCS SP8 confocal microscope
647 equipped with a 63× oil immersion objective (HC PI Apo CS2 63x oil/1.4, Leica). A
648 488nm laser line was used to excite Syto9 fluorescence and the emission was
649 collected between 500nm and 550nm. Three snapshots were acquired randomly
650 at different positions in the confocal field of each chamber. The Z-slices were
651 obtained every 0.3 microns. For visualization and processing of biofilm images,
652 ImageJ was used. Thickness, biomass, roughness coefficient and biofilm
653 distribution were analyzed using the COMSTAT2 software [57]. All confocal
654 scanning laser microscopy experiments were performed three times.

655

656 *Ex vivo* pig lung tissue biofilm model

657 *Ex vivo* pig lung dissection and infection

658 All pig lungs used were supplied by a commercial butcher and dissected on the
659 day of arrival. *Ex vivo* pig lung (EVPL) tissue was dissected to extract the
660 bronchioles as previously described [47]. Following UV light sterilization, square
661 bronchiolar tissue pieces were placed into a 24-well plate with a 400 µL, 0.8%
662 agarose pad (UV sterilized).
663 To infect the tissue, 2 µL of an overnight *P. aeruginosa* culture diluted to an OD_{600}
664 of about 0.05 were spotted onto the tissue, while 2 µL of SCFM were spotted as
665 negative control. To better mimic the CF lung environment, 500 µL SCFM were
666 added to each well and the plate was incubated statically for the 2 hours at 37°C.
667 After the incubation, medium was removed and replaced with 500 µL of fresh
668 SCFM with or without 25-50 µg/mL of PDSTP. 0.06 µg/mL of ciprofloxacin were
669 used as positive control. The plate was incubated overnight at 37°C.

670

671 Bacterial recovery from the EVPL model and count determination

672 To recover bacteria, tissues were removed from the wells and washed with 500 µL
673 of PBS. Tissue sections were then transferred in sterile homogenization tubes
674 (Fisherbrand) with 5 mm glass beads (Merck) and 500 µL of PBS. Samples were
675 homogenized using a Minilys Homogenizer (Bertin) for 20 seconds at 15 m/s.
676 Tissue homogenates were serially diluted in PBS and plated on LB agar. Colony
677 counts were performed after 24 hours at 37°C.

678

679 **Biofilm staining on the EVPL model**

680 After overnight incubation, tissues were washed with 500 µL of PBS and placed
681 into four-well chambered coverslip µ-Slide Glass Bottom (Ibidi). Tissues were
682 stained with 5 µM Syto9 (Invitrogen), washed twice with PBS and turned upside
683 down onto the cover glass. Samples were visualized with a Leica TCS SP8
684 confocal microscope equipped with a 63x oil immersion objective (HC Pl Apo CS2
685 63x oil/1.4, Leica). A 488nm laser line was used to excite Syto9 fluorescence and
686 the emission was collected between 500nm and 550nm. The scaffold surface was
687 acquired using a 561nm laser in reflection mode. Three z-stacks randomly chosen
688 at different positions in each chamber were acquired with a z step of 0.7 microns.

689

690 **Statistical Methods**

691 Analyses were performed using Prism 10.0 (GraphPad). Comparison of more than
692 two groups was performed with the unpaired *t*-test, one-way or two-way ANOVA.
693 For *in vivo* analysis, log rank (Mantel-Cox) test was used.

694

695 **Acknowledgments**

696 The authors are grateful to Dr. Alessandra Bragonzi (IRCCS San Raffaele
697 Scientific Institute, Milan) for providing the *P. aeruginosa* clinical isolates; to Dr.
698 Alberto Azzalin (Dept. of Biology and Biotechnology, University of Pavia) for
699 ImageStream Flow Cytometry analysis; to Dr. Amanda Oldani and Dr. Patrizia

700 Vaghi (Centro Grandi Strumenti, University of Pavia) for technical assistance with
701 confocal microscopy; to Mr. Edoardo Alessi (Tenuta Alessi s.a.s.) for providing pig
702 lungs. The funders had no role in study design, data collection and analysis,
703 decision to publish, or preparation of the manuscript.

704

705

706 References

707 1. Antimicrobial Resistance Collaborators. Global burden of bacterial
708 antimicrobial resistance in 2019: a systematic analysis. Lancet. 2022;
709 399:629-655.
710 2. de Kraker ME, Stewardson AJ, Harbarth S. Will 10 million people die a
711 year due to antimicrobial resistance by 2050? PLoS Med. 2016; 13:
712 e1002184.
713 3. Tacconelli E, Carrara E, Savoldi A, Harbarth S, Mendelson M, Monnet
714 DL, Pulcini C, Kahlmeter G, Kluytmans J, Carmeli Y, Ouellette M, Outterson
715 K, Patel J, Cavaleri M, Cox EM, Houchens CR, Grayson ML, Hansen P,
716 Singh N, Theuretzbacher U, Magrini N. WHO pathogens priority list working
717 group. Discovery, research, and development of new antibiotics: the WHO
718 priority list of antibiotic-resistant bacteria and tuberculosis. Lancet Infect Dis.
719 2018; 18:318-327.
720 4. Qin S, Xiao W, Zhou C, Pu Q, Deng X, Lan L, Liang H, Song X, Wu M.
721 *Pseudomonas aeruginosa*: pathogenesis, virulence factors, antibiotic

722 resistance, interaction with host, technology advances and emerging
723 therapeutics. Signal Transduct Target Ther. 2022; 7:199.
724 5. Orenti A, Zolin A, Jung A, van Rens J et al. ECFSPR Annual Report 2020.
725 2022.
726 6. Tuon FF, Dantas LR, Suss PH, Tasca Ribeiro VS. Pathogenesis of
727 the *Pseudomonas aeruginosa* biofilm: a review. Pathogens. 2022; 11:300.
728 7. Wood SJ, Kuzel TM, Shafikhani SH. *Pseudomonas aeruginosa*:
729 infections, animal modeling, and therapeutics. Cells. 2023; 12:199.
730 8. Sanya DRA, Onésime D, Vizzarro G, Jacquier N. Recent advances in
731 therapeutic targets identification and development of treatment strategies
732 towards *Pseudomonas aeruginosa* infections. BMC Microbiol. 2023; 23:86.
733 9. Panda SK, Buroni S, Swain SS, Bonacorsi A, da Fonseca Amorim EA,
734 Kulshrestha M, da Silva LCN, Tiwari V. Recent advances to combat
735 ESKAPE pathogens with special reference to essential oils. Front Microbiol.
736 2022; 13:1029098.
737 10. Liao C, Huang X, Wang Q, Yao D, Lu W. Virulence factors
738 of *Pseudomonas aeruginosa* and antivirulence strategies to combat its drug
739 resistance. Front Cell Infect Microbiol. 2022; 12:926758.
740 11. Wang CH, Hsieh YH, Powers ZM, Kao CY. Defeating antibiotic-resistant
741 bacteria: exploring alternative therapies for a post-antibiotic era. Int J Mol
742 Sci. 2020; 2:1061.

35

743 12. Schmidtke M, Riabova O, Dahse HM, Stelzner A, Makarov V. Synthesis,
744 cytotoxicity and antiviral activity of N,N'-bis-5-nitropyrimidyl derivatives of
745 dispirotripiperazine. Antiviral Res. 2002; 55:117-127.
746 13. Novoselova EA, Riabova OB, Leneva IA, Nesterenko VG, Bolgarin RN,
747 Makarov VA. Antiretroviral activity of a novel pyrimidyl-di(diazaspiroalkane)
748 derivative. Acta Naturae. 2017; 9:105-107.
749 14. Novoselova EA, Ryabova OB, Leneva IA, Makarov VA. Specific antiviral
750 activity of pyrimidinedispirotripiperazinium alone and in combination with
751 acyclovir on a herpes simplex virus infection model. Pharm Chem J. 2019;
752 53:781-785.
753 15. Novoselova EA, Alimbarova LM, Monakhova NS, Lepioshkin AY, Ekins
754 S, Makarov VA. *In vivo* activity of pyrimidine-dispirotripiperaziniumin in the
755 male Guinea pig model of genital herpes. J Virol Antivir Res. 2020; 9:1.
756 16. Alimbarova L, Egorova A, Riabova O, Monakhova N, Makarov V. A
757 proof-of-concept study for the efficacy of dispirotripiperazine PDSTP in a
758 rabbit model of herpes simplex epithelial keratitis. Antiviral Res. 2022;
759 202:105327.
760 17. Makarov VA, Popov VO. PDSTP is the first drug in class to treat
761 coronavirus infection. Her Russ Acad Sci. 2022; 92:488-490.
762 18. García B, Merayo-Lloves J, Martin C, Alcalde I, Quirós LM, Vazquez F.
763 Surface proteoglycans as mediators in bacterial pathogens infections. Front
764 Microbiol. 2016; 7:220.

765 19. Bucior I, Pielage JF, Engel JN. *Pseudomonas aeruginosa* pili and
766 flagella mediate distinct binding and signaling events at the apical and
767 basolateral surface of airway epithelium. PLoS Pathog. 2012; 8:e1002616.
768 20. Bartlett AH, Park PW. Heparan sulfate proteoglycans in infection. *In*
769 Mauro S.G. Pavão (ed), Glycans in diseases and therapeutics, 1st ed, vol
770 1. Springer Berlin, Heidelberg; 2011. pp. 31-62.
771 21. Alcalá-Franco B, Montanari S, Cigana C, Bertoni G, Oliver A, Bragonzi
772 A. Antibiotic pressure compensates the biological cost associated with
773 *Pseudomonas aeruginosa* hypermutable phenotypes *in vitro* and in a
774 murine model of chronic airways infection. J Antimicrob Chemother. 2012;
775 67:962-969.
776 22. Berlutti F, Superti F, Nicoletti M, Morea C, Frioni A, Ammendolia MG,
777 Battistoni A, Valenti P. Bovine lactoferrin inhibits the efficiency of invasion
778 of respiratory A549 cells of different iron-regulated morphological forms of
779 *Pseudomonas aeruginosa* and *Burkholderia cenocepacia*. Int J
780 Immunopathol Pharmacol. 2008; 21:51-59.
781 23. Hawdon NA, Aval PS, Barnes RJ, Gravelle SK, Rosengren J, Khan S,
782 Ciofu O, Johansen HK, Høiby N, Ulanova M. Cellular responses of A549
783 alveolar epithelial cells to serially collected *Pseudomonas aeruginosa* from
784 cystic fibrosis patients at different stages of pulmonary infection. FEMS
785 Immunol Med Microbiol. 2010; 59:207-220.
786 24. Liu J, Thorp SC. Cell surface heparan sulfate and its roles in assisting
787 viral infections. Med Res Rev. 2002; 22:1-25.

788 25. CLSI. Performance standards for antimicrobial susceptibility testing.
789 30th ed. CLSI supplement M100. Wayne, PA: Clinical and Laboratory
790 Standards Institute; 2020.
791 26. Palmer KL, Brown SA, Whiteley M. Membrane-bound nitrate reductase
792 is required for anaerobic growth in cystic fibrosis sputum. J Bacteriol. 2007;
793 189:4449-4455.
794 27. Ahmed GF, Elkhatib WF, Noreddin AM. Inhibition of *Pseudomonas*
795 *aeruginosa* PAO1 adhesion to and invasion of A549 lung epithelial cells by
796 natural extracts. J Infect Public Health. 2014; 7:436-444.
797 28. Molina Bertrán SDC, Monzote L, Cappoen D, Escalona Arranz JC,
798 Gordillo Pérez MJ, Rodríguez-Ferreiro AO, Chill Nuñez I, Novo CP, Méndez
799 D, Cos P, Llauradó Maury G. Inhibition of bacterial adhesion and biofilm
800 formation by seed-derived ethanol extracts from *Persea americana* Mill.
801 Molecules. 2022; 27:5009.
802 29. Malinovská L, Thai Le S, Herczeg M, Vašková M, Houser J, Fujdiarová
803 E, Komárek J, Hodek P, Borbás A, Wimmerová M, Csávás M. Synthesis of
804 β-d-galactopyranoside-presenting glycoclusters, investigation of their
805 interactions with *Pseudomonas aeruginosa* lectin A (PA-IL) and evaluation
806 of their anti-adhesion potential. Biomolecules. 2019; 9:686.
807 30. Wojtczak K, Byrne JP. Structural considerations for building synthetic
808 glycoconjugates as inhibitors for *Pseudomonas aeruginosa* lectins.
809 ChemMedChem. 2022; 17:e202200081.

38

31. O'Shea R, Moser HE. Physicochemical properties of antibacterial compounds: implications for drug discovery. J Med Chem. 2008; 51:2871-2878.

32. Hancock RE. Aminoglycoside uptake and mode of action with special reference to streptomycin and gentamicin. Antagonists and mutants. J Antimicrob Chemother. 1981; 8:249-276.

33. Egorova A, Bogner E, Novoselova E, Zorn KM, Ekins S, Makarov V. Dispirotripiperazine-core compounds, their biological activity with a focus on broad antiviral property, and perspectives in drug design (mini-review). Eur J Med Chem. 2021; 211:113014.

34. Douafer H, Andrieu V, Phanstiel O 4th, Brunel JM. Antibiotic adjuvants: make antibiotics great again! J Med Chem. 2019; 62:8665-8681.

35. Kwon DH, Lu CD. Polyamines increase antibiotic susceptibility in *Pseudomonas aeruginosa*. Antimicrob Agents Chemother. 2006 50:1623-1627.

36. Cadelis MM, Li SA, Bourguet-Kondracki ML, Blanchet M, Douafer H, Brunel JM, Copp BR. Spermine derivatives of indole-3-carboxylic acid, indole-3-acetic acid and indole-3-acrylic acid as Gram-negative antibiotic adjuvants. ChemMedChem. 2021; 16:513-523.

37. Wang G, Brunel JM, Preusse M, Mozaheb N, Willger SD, Larrouy-Maumus G, Baatsen P, Häussler S, Bolla JM, Van Bambeke F. The membrane-active polyaminoisoprenyl compound NV716 re-sensitizes

Pseudomonas aeruginosa to antibiotics and reduces bacterial virulence. Commun Biol. 2022; 5:871.

38. Li SA, Cadelis MM, Sue K, Blanchet M, Vidal N, Brunel JM, Bourguet-Kondracki ML, Copp BR. 6-Bromoindolglyoxylamido derivatives as antimicrobial agents and antibiotic enhancers. Bioorg Med Chem. 2019; 27:2090-2099.

39. Vaara M, Siikanen O, Apajalahti J, Fox J, Frimodt-Møller N, He H, Poudyal A, Li J, Nation RL, Vaara T. A novel polymyxin derivative that lacks the fatty acid tail and carries only three positive charges has strong synergism with agents excluded by the intact outer membrane. Antimicrob Agents Chemother. 2010; 54:3341-3346.

40. Nikolaev YA, Tutel'yan AV, Loiko NG, Buck J, Sidorenko SV, Lazareva I, Gostev V, Manzen'yuk OY, Shemyakin IG, Abramovich RA, Huwyler J, El'-Registan GI. The use of 4-Hexylresorcinol as antibiotic adjuvant. PLoS One. 2020; 15:e0239147.

41. Stokes JM, MacNair CR, Ilyas B, French S, Côté JP, Bouwman C, Farha MA, Sieron AO, Whitfield C, Coombes BK, Brown ED. Pentamidine sensitizes Gram-negative pathogens to antibiotics and overcomes acquired colistin resistance. Nat Microbiol. 2017; 2:17028.

42. Zhou Y, Huang W, Lei E, Yang A, Li Y, Wen K, Wang M, Li L, Chen Z, Zhou C, Bai S, Han J, Song W, Ren X, Zeng X, Pu H, Wan M, Feng X. Cooperative membrane damage as a mechanism for pentamidine-antibiotic mutual sensitization. ACS Chem Biol. 2022; 17:3178-3190.

43. O'Loughlin CT, Miller LC, Siryaporn A, Drescher K, Semmelhack MF, Bassler BL. A quorum-sensing inhibitor blocks *Pseudomonas aeruginosa* virulence and biofilm formation. Proc Natl Acad Sci U S A. 2013; 110:17981-17986.

44. D'Angelo F, Baldelli V, Halliday N, Pantalone P, Polticelli F, Fiscarelli E, Williams P, Visca P, Leoni L, Rampioni G. Identification of FDA-approved drugs as antivirulence agents targeting the *pqs* quorum-sensing system of *Pseudomonas aeruginosa*. Antimicrob Agents Chemother. 2018; 62:e01296-18.

45. Bergmann M, Michaud G, Visini R, Jin X, Gillon E, Stocker A, Imberty A, Darbre T, Reymond JL. Multivalency effects on *Pseudomonas aeruginosa* biofilm inhibition and dispersal by glycopeptide dendrimers targeting lectin LecA. Org Biomol Chem. 2016; 14:138-148.

46. van Tilburg Bernardes E, Charron-Mazenod L, Reading DJ, Reckseidler-Zenteno SL, Lewenza S. Exopolysaccharide-repressing small molecules with antibiofilm and antivirulence activity against *Pseudomonas aeruginosa*. Antimicrob Agents Chemother. 2017; 61:e01997-16.

47. Harrington NE, Sweeney E, Alav I, Allen F, Moat J, Harrison F. Antibiotic efficacy testing in an *ex vivo* model of *Pseudomonas aeruginosa* and *Staphylococcus aureus* biofilms in the cystic fibrosis lung. J Vis Exp. 2021; e62187.

48. Giard DJ, Aaronson SA, Todaro GJ, Arnstein P, Kersey JH, Dosik H, Parks WP. *In vitro* cultivation of human tumors: establishment of cell lines

878 derived from a series of solid tumors. J Natl Cancer Inst. 1973; 51:1417-
879 1423.
880 49. Cozens AL, Yezzi MJ, Kunzelmann K, Ohrui T, Chin L, Eng K,
881 Finkbeiner WE, Widdicombe JH, Gruenert DC. CFTR expression and
882 chloride secretion in polarized immortal human bronchial epithelial cells. Am
883 J Respir Cell Mol Biol. 1994; 10:38-47.
884 50. Bruscia E, Sangiuolo F, Sinibaldi P, Goncz KK, Novelli G, Gruenert DC.
885 Isolation of CF cell lines corrected at DeltaF508-CFTR locus by SFHR-
886 mediated targeting. Gene Ther. 2002; 9:683-685.
887 51. Crabbé A, Liu Y, Matthijs N, Rigole P, De La Fuente-Nùñez C, Davis R,
888 Ledesma MA, Sarker S, Van Houdt R, Hancock RE, Coenye T, Nickerson
889 CA. Antimicrobial efficacy against *Pseudomonas aeruginosa* biofilm
890 formation in a three-dimensional lung epithelial model and the influence of
891 fetal bovine serum. Sci Rep. 2017; 7:43321.
892 52. Wiegand I, Hilpert K, Hancock RE. Agar and broth dilution methods to
893 determine the minimal inhibitory concentration (MIC) of antimicrobial
894 substances. Nat Protoc. 2008; 3:163-175.
895 53. Scoffone VC, Ryabova O, Makarov V, Iadarola P, Fumagalli M, Fondi
896 M, Fani R, De Rossi E, Riccardi G, Buroni S. Efflux-mediated resistance to
897 a benzothiadiazol derivative effective against *Burkholderia cenocepacia*.
898 Front Microbiol. 2015; 6:815.

42

54. CLSI. Methods for determining bactericidal activity of antimicrobial agents; approved guideline. CLSI document M26-A. Wayne, PA: Clinical and Laboratory Standards Institute; 1999.

55. Benthall G, Touzel RE, Hind CK, Titball RW, Sutton JM, Thomas RJ, Wand ME. Evaluation of antibiotic efficacy against infections caused by planktonic or biofilm cultures of *Pseudomonas aeruginosa* and *Klebsiella pneumoniae* in *Galleria mellonella*. Int J Antimicrob Agents. 2015; 46:538-545.

56. Vandecandelaere I, Van Acker H, Coenye T. A microplate-based system as *in vitro* model of biofilm growth and quantification. Methods Mol Biol. 2016; 1333:53-66.

57. Heydorn A, Nielsen AT, Hentzer M, Sternberg C, Givskov M, Ersbøll BK, Molin S. Quantification of biofilm structures by the novel computer program COMSTAT. Microbiology (Reading). 2000; 146:2395-2407.

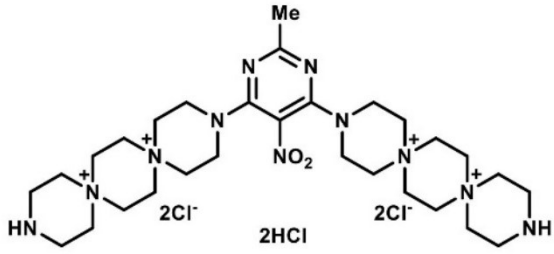

Fig 1. Chemical structure of the compound PDSTP.

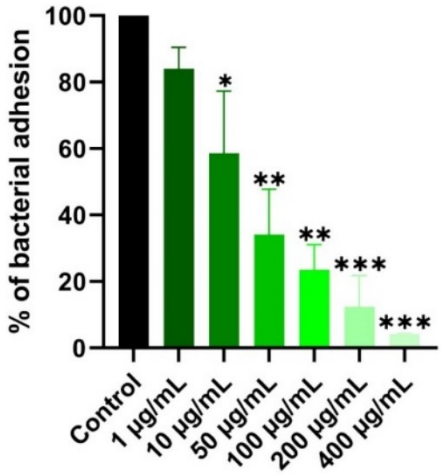

Fig 2. PDSTP decreases the adhesion of *P. aeruginosa* PA01 to A549 cell line. Differential adhesion abilities to the A549 cell line of *P. aeruginosa* PA01 treated with increasing concentrations of PDSTP (from 1 to 400 µg/mL). The experiment was performed twice, each time in duplicate. Statistically significant differences are indicated (One-way ANOVA test; ns, not significant; *, $p < 0.05$; **, $p < 0.005$; ***, $p < 0.0005$).

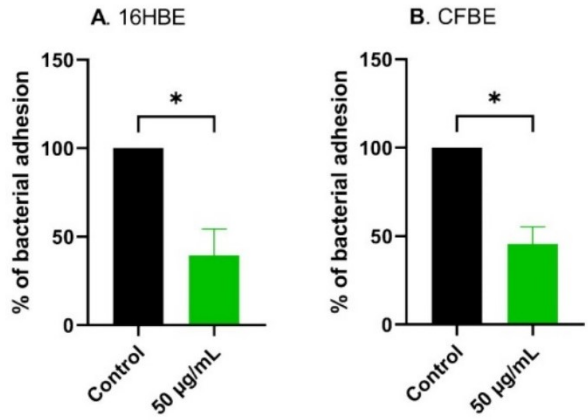

931 **Fig 3. PDSTP decreases the adhesion of *P. aeruginosa* PA01 to 16HBE and**
932 **CFBE cell lines.** Differential adhesion abilities to the 16HBE (A) and CFBE (B)
933 cell lines of *P. aeruginosa* PA01 treated with 50 µg/mL of PDSTP. The experiment
934 was performed twice, each time in duplicate. Statistically significant differences are
935 indicated (Student's *t* test; *, $p < 0.05$).
936

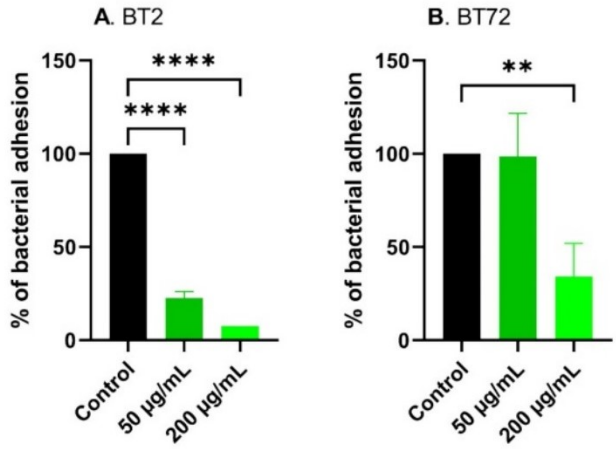

937 **Fig 4. PDSTP decreases the adhesion of *P. aeruginosa* BT2 and BT72 to A549**
938 **cell line.** Differential adhesion abilities to the A549 cell line of *P. aeruginosa* BT2

45

939 (A) and BT72 (B) treated with two concentrations of PDSTP (50 and 200 µg/mL).
940 The experiment was performed twice, each time in duplicate. Statistically
941 significant differences are indicated (One-way ANOVA test; **, $p < 0.01$; ****, $p <$
942 0.0001).
943

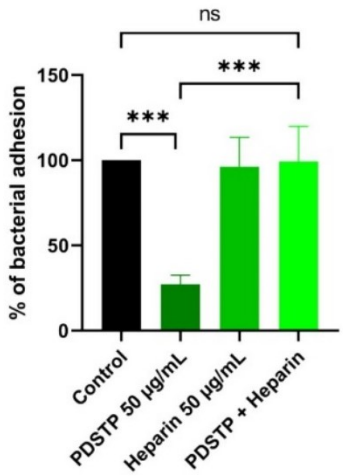

944 **Fig 5. Heparin binds PDSTP abolishing its activity against *P. aeruginosa***
945 **PA01 adhesion.** Differential adhesion abilities to the A549 cell line of *P.*
946 *aeruginosa* PA01 treated with 50 µg/mL of PDSTP, 50 µg/mL heparin and a
947 mixture of PDSTP and heparin (at the previously used concentrations). The
948 experiment was performed three times, each time in duplicate. Statistically
949 significant differences are indicated (One-way ANOVA test; ns, not significant; ***,
950 $p < 0.001$).
951
952
953

954

955

956

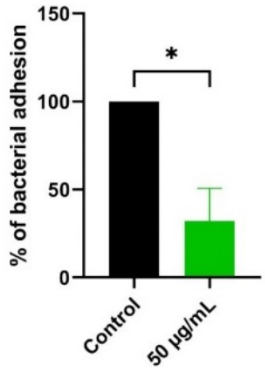

957 **Fig 6. PDSTP decreases the adhesion of *P. aeruginosa* PA01 to A549 cell line**
958 **(quantification by imaging flow cytometry).** Differential adhesion abilities to the
959 A549 cell line of GFP-expressing *P. aeruginosa* PA01 treated with 50 µg/mL of
960 PDSTP. The experiment was performed twice, each time in duplicate. Statistically
961 significant differences are indicated (Student's *t* test; *, $p < 0.05$).

47

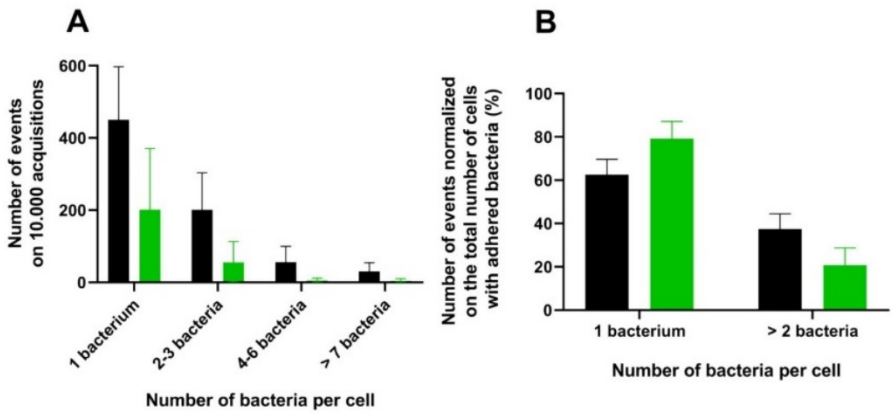

Fig 7. PDSTP prevents multiple bacterial adhesion to the single cell. Events showing the number of adhered GFP-expressing *P. aeruginosa* PA01 per A549 cell on 10.000 acquisitions of the control (black column) and samples treated with 50 µg/mL of PDSTP (green column) (A), and number of events normalized on the total number of cells with adhered bacteria, expressed in percentage, of the control (black column) and cells treated with 50 µg/mL of the compound (green column) (B).

970

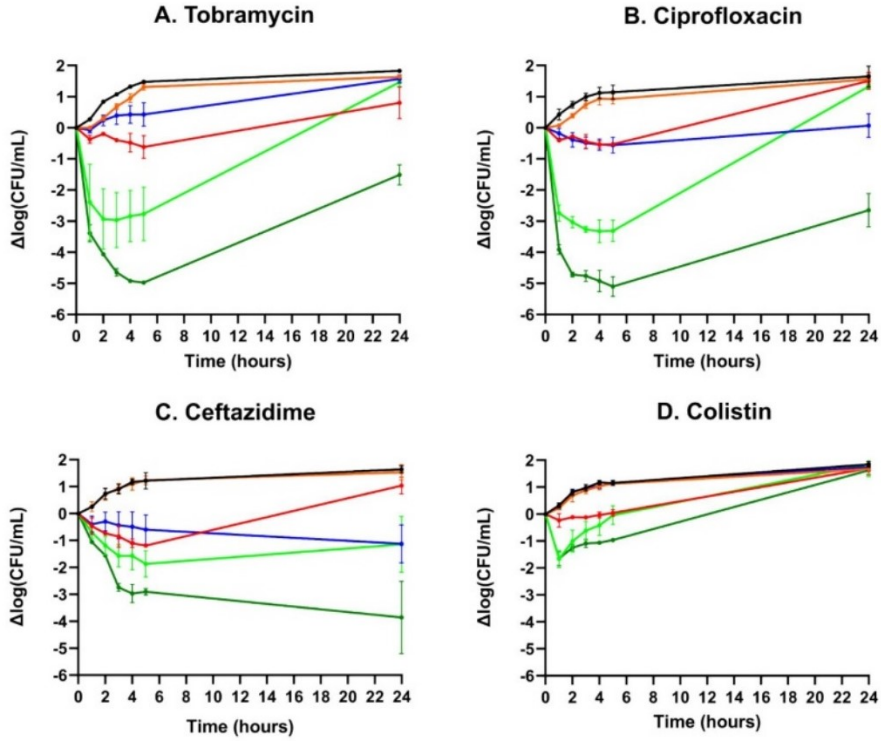

971 **Fig 8. PDSTP increases the efficacy of different antibiotics against *P.***
972 ***aeruginosa* PA01.** *P. aeruginosa* PA01 time-killing assays of tobramycin (A),
973 ciprofloxacin (B), ceftazidime (C) and colistin (D) combined with either 50 or 200
974 µg/mL of PDSTP, represented as the difference in the number of CFU/mL on a
975 logarithmic scale. Black line, untreated sample; orange line, treatment with 50
976 µg/mL of PDSTP; red line, treatment with 200 µg/mL of PDSTP; blue line,
977 treatment with a concentration equal to ½ MIC of the antibiotic; light green line,
978 combination of 50 µg/mL of PDSTP with the antibiotic; dark green line, combination
979 of 200 µg/mL of PDSTP with the antimicrobial.

49

980

981

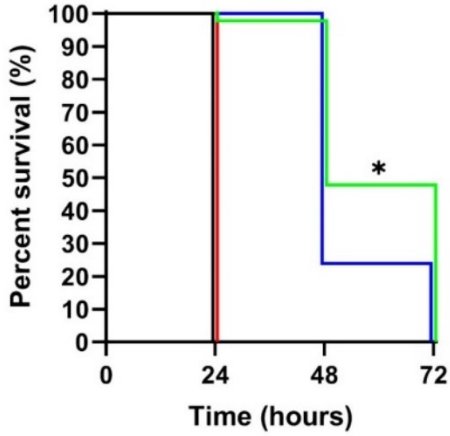

982 **Fig 9. PDSTP increases ceftazidime efficacy *in vivo*.** Kaplan-Meier survival
983 curve of *G. mellonella* larvae infected with *P. aeruginosa* PA01 and treated with
984 physiological saline (black), PDSTP (red), ceftazidime (blue) or the combination of
985 PDSTP and ceftazidime (green) (Log-rank test; *, $p < 0.05$).

50

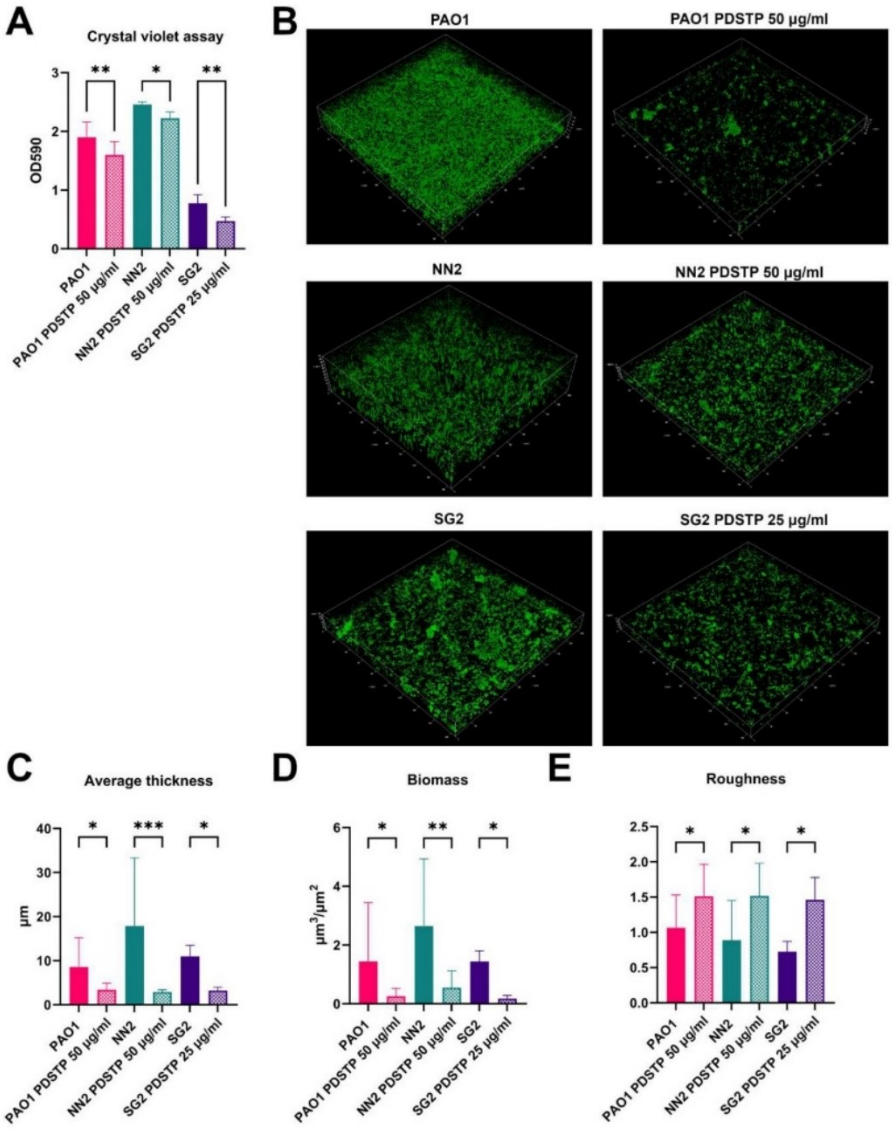

986

987 **Fig 10. PDSTP impairs biofilm formation of *P. aeruginosa* strains *in vitro*.**

988 Effect of PDSTP against biofilm formation in *P. aeruginosa* PA01, NN2 and SG2

51

989 strains using crystal violet assay (A). CLSM images (400x magnification) of *P.*
990 *aeruginosa* biofilms formed with or without PDSTP (B). 2D images acquired at
991 equal distances along the Z-axis were stacked to reconstruct the 3D biofilm
992 images. Analysis of biofilm properties by COMSTAT2 (C-E). Experiments were
993 performed three times. Statistically significant differences are indicated (One-way
994 ANOVA test; *, $p < 0.05$; **, $p < 0.01$).
995

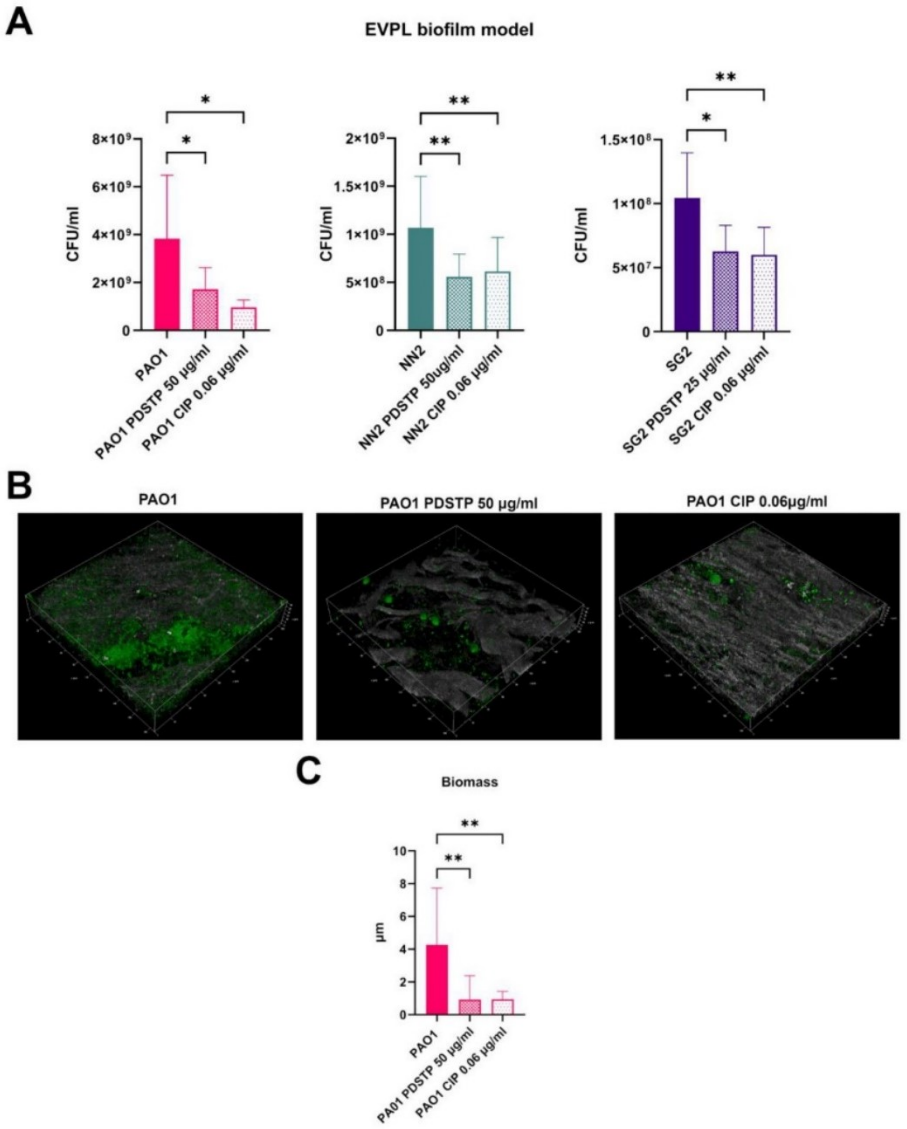

996

997 **Fig 11. PDSTP impairs biofilm formation of *P. aeruginosa* strains in *ex vivo***

998 **pig lung tissue model.** Effect of PDSTP on *P. aeruginosa* PA01, NN2 and SG2

53

999 strains biofilm formation in an *ex vivo* pig lung model (EVPL), represented as the
1000 number of CFU/mL recovered from treated and untreated tissues (A). CLSM
1001 images (400x magnification) of *P. aeruginosa* PA01 biofilms formed on EVPL with
1002 or without PDSTP (B). 2D images acquired at equal distances along the Z-axis
1003 were stacked to reconstruct the 3D biofilm images. Analysis of biofilm properties
1004 by COMSTAT2 (C). Experiments were performed three times. Statistically
1005 significant differences are indicated (One-way ANOVA test; *, $p < 0.05$; **, $p <$
1006 0.01).
1007

1008 Supporting information

1009

1010 **S1 Fig. Representative image galleries of A549 cells infected with GFP-**
1011 **expressing *P. aeruginosa* PA01.** Ch04: bright field. Ch02: GFP fluorescence
1012 (λex/λem = 480-560 nm). Ch04/Ch02: superimposition of bright field and
1013 fluorescence channels. Ch06: dark field side scatter. Pictures were acquired at 40x
1014 magnification using Amnis® ImageStream®X Mk II (Cytek).
1015

1016 **S2 Fig. Counting of GFP-expressing *P. aeruginosa* PA01 cells using Spot**
1017 **Count feature.** On focus-cells population defined by GradientRMS feature
1018 histogram (A). Single cells population (gated on focus-cells) defined by
1019 Area/Aspect ratio features dot plot (B). Untreated sample: histogram of bacteria
1020 count using the custom "BactCount" feature (applied to focused, single cells) (C).

1021 Treatment with 50 µg/mL of PDSTP sample: histogram of bacteria count using the
1022 custom "BactCount" feature (applied to focused, single cells) (D).
1023
1024 **S3 Fig. PDSTP increases the efficacy of different antibiotics against *P.***
1025 ***aeruginosa* PA01.** *P. aeruginosa* PA01 time-killing assays of tobramycin (A),
1026 ciprofloxacin (B), ceftazidime (C) and colistin (D) combined with either 50 or 200
1027 µg/mL of PDSTP, represented as variation of optical density at 600 nm. Black line,
1028 untreated sample; orange line, treatment with 50 µg/mL of PDSTP; red line,
1029 treatment with 200 µg/mL of PDSTP; blue line, treatment with a concentration
1030 equal to ½ MIC of the antibiotic; light green line, combination of 50 µg/mL of
1031 PDSTP with the antibiotic; dark green line, combination of 200 µg/mL of PDSTP
1032 with the antimicrobial.
1033
1034 **S4 Fig. Ceftazidime-PDSTP combination inhibits *P. aeruginosa* strains**
1035 **growth.** *P. aeruginosa* CF clinical isolates time-killing assays of ceftazidime
1036 combined with PDSTP, represented as variation of optical density at 600 nm. Black
1037 line, untreated sample; red line, treatment with sub-inhibitory concentrations of
1038 PDSTP; blue line, treatment with sub-inhibitory concentrations of ceftazidime; light
1039 green line, combination of PDSTP with the antibiotic.
1040
1041 **S5 Fig. Tobramycin-PDSTP combination inhibits *P. aeruginosa* strains**
1042 **growth.** *P. aeruginosa* CF clinical isolates time-killing assays of tobramycin
1043 combined with PDSTP, represented as variation of optical density at 600 nm. Black

1044 line, untreated sample; red line, treatment with sub-inhibitory concentrations of
1045 PDSTP; blue line, treatment with sub-inhibitory concentrations of tobramycin; light
1046 green line, combination of PDSTP with the antibiotic.
1047
1048 **S6 Fig. Ciprofloxacin-PDSTP combination inhibits *P. aeruginosa* strains**
1049 **growth.** *P. aeruginosa* CF clinical isolates time-killing assays of ciprofloxacin
1050 combined with PDSTP, represented as variation of optical density at 600 nm. Black
1051 line, untreated sample; red line, treatment with sub-inhibitory concentrations of
1052 PDSTP; blue line, treatment with sub-inhibitory concentrations of ciprofloxacin;
1053 light green line, combination of PDSTP with the antibiotic.
1054
1055 **S7 Fig. Colistin-PDSTP combination inhibits *P. aeruginosa* strains growth.**
1056 *P. aeruginosa* CF clinical isolates time-killing assays of colistin combined with
1057 PDSTP, represented as variation of optical density at 600 nm. Black line, untreated
1058 sample; red line, treatment with sub-inhibitory concentrations of PDSTP; blue line,
1059 treatment with a concentration equal to the MIC of colistin; light green line,
1060 combination of PDSTP with the antibiotic.
1061
1062 **S8 Fig. HPLC traces for PDSTP.** Purity of PDSTP was analyzed by analytical
1063 high-performance liquid chromatography (HPLC) on a LC-20 Prominence HPLC
1064 system (Shimadzu, Kyoto, Japan) equipped with a SPD-20A Prominence UV
1065 detector at 254 nm. Chromatographic separation was carried out on a Kromasil
1066 60-Diol HPLC column (4.6 × 250 mm, 5 µm; Nouryon, Göteborg, Sweden) at 30

°C, with a sample injection volume of 20 µL. A mobile phase consisting of methanol and DMSO (90:10 v/v), and heptafluorobutyric acid in methanol (0.5:95.5 v/v) was programmed with gradient elution at a flow rate of 1300 µL/min. Data were processed with a LC solution software version 1.25 (Shimadzu).

S1 Table. Minimum inhibitory concentrations in TSB of ceftazidime, tobramycin, ciprofloxacin and colistin against *P. aeruginosa* CF clinical isolates.